General Disclaimer

One or more of the Following Statements may affect this Document

- This document has been reproduced from the best copy furnished by the organizational source. It is being released in the interest of making available as much information as possible.

- This document may contain data, which exceeds the sheet parameters. It was furnished in this condition by the organizational source and is the best copy available.

- This document may contain tone-on-tone or color graphs, charts and/or pictures, which have been reproduced in black and white.

- This document is paginated as submitted by the original source.

- Portions of this document are not fully legible due to the historical nature of some of the material. However, it is the best reproduction available from the original submission.

Produced by the NASA Center for Aerospace Information (CASI)



FACILITY FORM 602

N 69-23384 (ACCESSION NUMBER) (THRU)
248 (PAGES) (CODE)
CR-100658 (NASA CR OR TMX OR AD NUMBER) 03 (CATEGORY)

THERMO ELECTRON

CORPORATION

RQT-53563

THERMO ELECTRON
ENGINEERING CORPORATION

Report No. TE 4072-49-68

Thermo Electron Corporation, 85 First Avenue, Waltham, Massachusetts 02154

FINAL REPORT

RESEARCH IN
THERMIONIC CONVERSION

Contract NAS7-508

September 1966 to September 1967

Prepared for

National Aeronautics and Space Administration
Pasadena Office
4800 Oak Park Drive
Pasadena, California

ACKNOWLEDGMENTS

This work was performed under the supervision of O. S. Merrill of the Jet Propulsion Laboratory, California Institute of Technology.

The authors would also like to acknowledge the assistance of S. J. Pechinski in the taking and reduction of data, K. Wong in design, and F. J. Compagna, E. Ameen and C. Yassemedis in construction of the converters.

TABLE OF CONTENTS

Chapter		Page
	Acknowledgments	ii
I	Introduction and Summary	I-1
II	Plasma Analysis D. LIEB and W. BORNHORST	II-1
	A. Introduction	II-1
	B. Description of Approach	II-3
	C. Analytical Statement of the Problem	II-5
	D. Results	II-11
	E. Discussion	II-12
	F. Conclusions	II-26
	References for Chapter II	II-27
III	Parametric Data F. RUFEH, D. LIEB, C. WANG, and L. VAN SOMEREN	III-1
	A. Rhenium Emitter	III-1
	B. Tungsten Emitter	III-27
	References for Chapter III	III-78
IV	Electronegative Additives Formed in Situ F. RUFEH D. LIEB and F. FRAIM	IV-1
	A. Oxides Formed on the Collector and Guard Surfaces	IV-1
	B. Oxides Formed in the Additive Reservoir	IV-19
	C. Discussion	IV-27
	D. Converter Performance with Cesium Oxide Only	IV-30
	E. Other Experiences with Cesium-Oxygen Systems	IV-42
	References for Chapter IV	IV-52

TABLE OF CONTENTS (continued)

Chapter		Page
V	Molybdenum Trioxide as an Oxygen Source F. FRAIM, F. HOLLY, and L. VAN SOMEREN	V-1
	A. Introduction	V-1
	B. Analysis of MoO_3 as an Oxygen Source	V-3
	C. Reactions of MoO_3 with Diode Materials	V-16
	D. Compatibility Test	V-26
	E. Differential Thermal Analysis	V-27
	F. Diode Experiments	V-30
	G. Conclusions	V-54
	References for Chapter V	V-56
VI	Electropositive Additives	VI-1
	References for Chapter VI	VI-10
Appendix - Converter Performance With and Without Additives		A-1

CHAPTER I

INTRODUCTION AND SUMMARY

This report presents the work performed under Contract NAS7-508 for NASA/JPL during the one-year period ending September 30, 1967. This work is a continuation of an applied research program which has been in progress for several years. The primary objective of the program is the improvement of converter performance by a continuous interplay between theoretical analyses and experimental results.

During the past year, detailed theoretical analysis of the plasma properties of thermionic converters was initiated (Chapter II). A digital computer program was written for the study of the sensitivity of the plasma properties with respect to the variation of different plasma parameters. In particular, the influence of electron thermal conductivity and ionization rate on the spatial distributions of various plasma properties was examined. The electron thermal conductivity was shown to be significant in determining the electron temperature variation in the plasma and to greatly affect the establishment of local thermodynamic equilibrium. The influence of ionization was examined for an ion-rich emitter, and it was shown that this ionization gives rise to an upper mode through its effects on the ion density and on the electrostatic potential distributions. These results will be important in understanding the variations in performance produced by changes in spacing, pressure, and emitter ion-richness.

Parametric data obtained from several variable-spacing converters are presented in Chapter III. Performance data obtained from an electroetched rhenium emitter were compared with previous data from a similar emitter. This comparison showed that the technique

of electroetching and heat-treating is quite reproducible. Emitter work function was measured as a function of cesium temperature for emitter temperatures of 1560, 1660, 1760, and 1860° K. These four sets of data are useful for determining the extent of validity of the T_E / T_R correlation and for finding other correlations. Variable-spacing families of volt-ampere characteristics were obtained covering a wide range of operating conditions. The interelectrode spacings, cesium pressures and emitter temperatures were selected to yield the I-V characteristics at several values of cesium pressure for a given Pd* and ion-richness.

Performance data were also obtained from a variable-spacing converter with a single-crystal tungsten emitter and a polycrystalline tungsten collector. The power output of this converter was not so high as that from a converter with a similar emitter but a molybdenum collector.

The effect of oxygen on converter performance was studied in a variable-spacing research converter and is discussed in Chapter IV. Parametric data in the presence of oxygen was obtained over the emitter temperature range of 1650 to 1850° K. and the interelectrode spacing range of 5 to 20 mils. Under certain conditions, the addition of oxygen to the converter resulted in the same output power and voltage as that from a cesium-only converter with an emitter temperature 100° K higher, or alternately, with one-fourth the interelectrode spacing, a significant improvement in either case. Performance was stable for the period of a 300-hour test. Experimental results showed that the source of oxygen must be placed close to the emitter surface to avoid transport difficulties.

---

* The product of cesium pressure and interelectrode spacing.

Collector surfaces appear to be a promising location for the oxygen source.

The possibility of using cesium oxides as a source of both cesium and oxygen was investigated in a fixed-spacing converter, and the following preliminary data was obtained: Cesium oxides released enough cesium and oxygen to operate the converter. The performance with cesium oxide only was superior to that with cesium only and was stable for the period of a 400-hour test. The temperature range of the cesium oxide reservoir was about 100° K higher than the usual temperature range for a cesium reservoir. There is a possibility that the temperature difference may be increased by further experimental investigations. This feature is significant in most thermionic applications, where special cooling must be provided to keep the reservoir cold.

The behavior of molybdenum trioxide as an oxygen additive is discussed in Chapter V. Both thermodynamic calculations and experimental studies with thermionic converters were undertaken. The calculations were needed because of the conflicting information which resulted from an intensive literature survey. These calculations were performed with reference to the thermal decomposition of MoO_3 both in the solid and in the vapor phases, and with reference to the compatibility of solid MoO_3 and the gaseous trimer with various converter materials. Preliminary calculations were also performed concerning the possible molybdenum oxide-cesium reactions. The experimental program consisted of a series of four thermionic converter experiments, differential thermal analysis studies of molybdenum oxides and their reactions with various materials, and compatibility studies of molybdenum trioxide with converter materials. The four

converters included both planar converters and filamentary emitter diodes. The former were used to measure performance characteristics, while the latter were used to measure work functions. The results of the converter experiments indicated that molybdenum trioxide did release oxygen but not in the amounts expected.

The use of electropositive additives to improve the performance of low-pressure cesium converters is discussed in Chapter VI. It was shown theoretically that multi-valent electropositive additives modify the emitter work function, but that improvement in converter performance is doubtful because of the effect of these additives on the collector work function. Preliminary experiments were performed with ytterbium to verify the theoretical conclusions. Outgassing was performed for a period of 50 hours in the temperature range of 400 to 700° K. The converter experiments indicated that the emitter work function was reduced by the additive. No performance data were obtained because of a short which developed between the electrodes. The analysis of the disassembled converter showed a chemical reaction between ytterbium and its copper reservoir.

CHAPTER II

PLASMA ANALYSIS

D. Lieb and W. Bornhorst

A. INTRODUCTION

Thermionic converter plasmas have been analyzed many times, using various assumptions to reduce the complication of the problem.[1,2] The assumptions were such that closed-form expressions for the volt-ampere characteristic of the converter can be derived. It turns out that the derived I-V relations depend primarily on the overall energy balance for the plasma rather than its detailed characteristic properties. Thus, agreement between theory and experiment can be established for a variety of assumed values for such plasma properties as electron mobility, collision probability, etc. This agreement does not imply that the plasma conditions have been accurately represented.

Recently, detailed experimental data[3,4] on the plasma in actual and simulated converters have become available. These results make it possible to compare actual internal plasma conditions with those predicted theoretically. The object of the present study is to calculate the plasma conditions in a converter without the assumptions required for explicit solutions. To this end, the equations describing the plasma are solved numerically by means of a digital computer. Thus particle density, electron temperature, field etc., are obtained as functions of position in the plasma. Solutions are found for a variety of plasma parameters. These results can be compared with the experimental data available. In the work described in this report, the analysis has been carried to the point where a J-V curve has been obtained assuming certain electrode work functions, but no attempt has been made to correlate the results with experimental data.

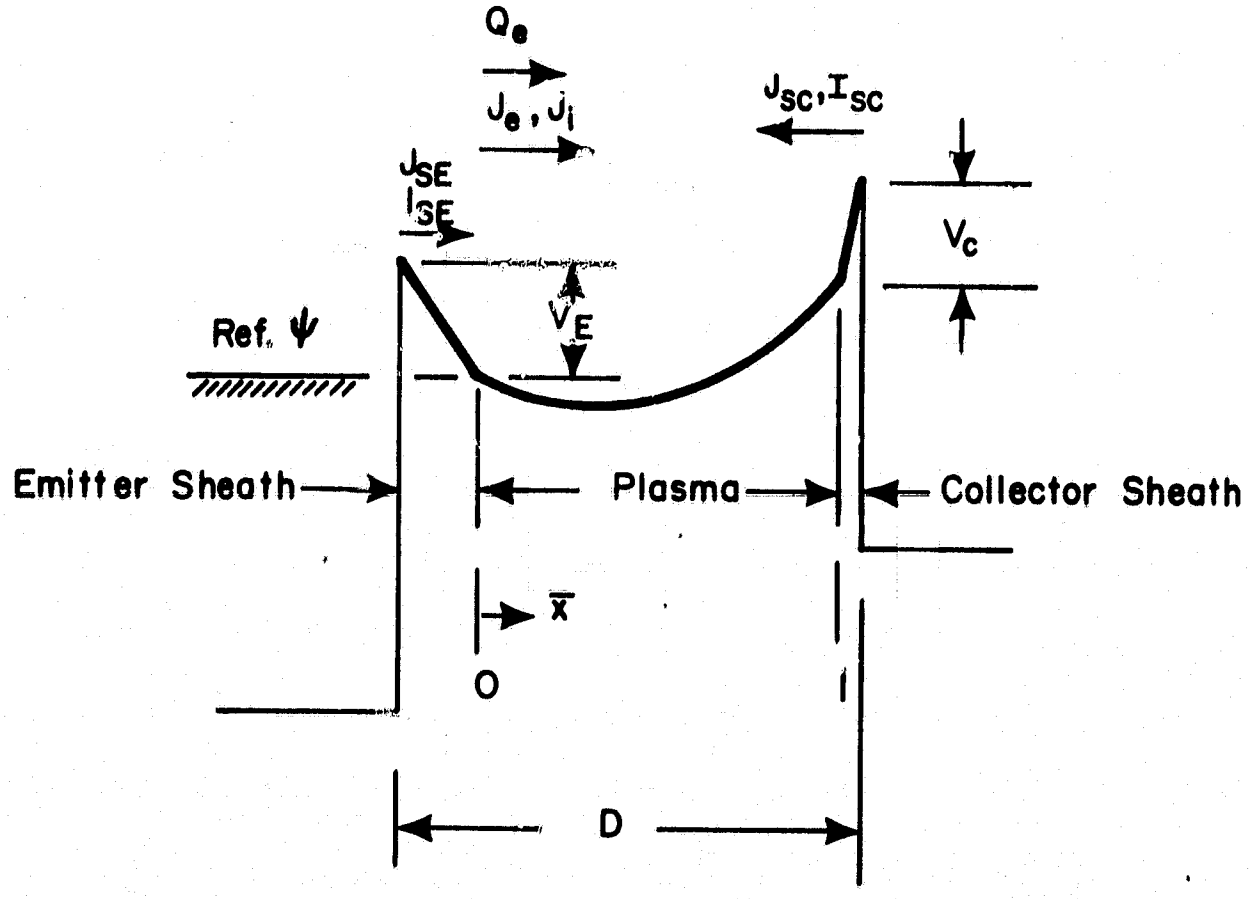


Figure II-1. Potential Diagram for Plasma.

B. DESCRIPTION OF APPROACH

For simplicity in the analysis of the problem, the interelectrode space in a converter can be divided into three regions: emitter sheath, collector sheath, and plasma. The sheaths, which allow for the transition between the plasma and the electrodes, are assumed to have a negligible thickness compared with that of the plasma (see Figure II-1), and to be collisionless. These conditions apply for spacings large compared to a Debye length.

The equations describing the plasma and the sheaths for the converter are written in a form suitable for numerical solution on a digital computer. The technique used is to choose a set of initial values for the plasma variables at the emitter edge of the plasma and then to calculate values for all the required derivatives at the same point. By using the derivatives, the values of the variables at an adjacent plasma point can be determined, and the process can be repeated with these new values. The solution is thus advanced through the plasma until conditions which satisfy a collector sheath are reached. Thus a plasma thickness is obtained.

If the conditions at the emitter edge of the plasma are chosen to be consistent with a particular current density and emitter temperature, the solution obtained above is characteristic of this current density and the spacing reached in the step-by-step process. To obtain a solution for a specific spacing, the initial conditions must be selected so as to be consistent with the spacing, and in practice, several trial calculations have to be made to determine the proper initial conditions. The equations and assumptions used in the study and the results obtained so far are described below.

TABLE II-1

θ	-	temperature multiplied by Boltzmann's constant, i.e., kT
J	-	current
J_r , J_s	-	electron random and saturation currents
I_r , I_s	-	ion random and saturation currents
P	-	potential
n	-	particle density
μ	-	particle mobility
D	-	spacing
K	-	coefficient of thermal conductivity
V_i	-	ionization energy of cesium
V	-	potential difference
e	-	electronic charge
n_s	-	Saha equilibrium particle density
$\dot{\xi}$	-	net ionization rate
Q	-	energy
x	-	distance from emitter edge of plasma
$\overline{x}$	-	normalized distance = $\frac{x}{D}$
α	-	parameter describing generation and recombination rates
N_o	-	neutral particle density

Primes refer to differentiation with respect to $\overline{x}$.

Subscripts:

e, i	-	electron and ion components
o, 1	-	values at emitter and collector edges of plasma, respectively
ε, c	-	values for emitter and collector side of sheath

C. ANALYTICAL STATEMENT OF THE PROBLEM

1. Plasma Transport Equations

The differential equations which describe the particle transport in the plasma can be stated in terms of particle currents and energies. If neutrality is assumed throughout the plasma region (the number density of electrons and ions is equal at each point) and ion energy transport neglected, the transport equations are:

$$J_e = \mu_e(\theta_e)\left[\theta_e \frac{dn}{dx} + en\frac{d\psi}{dx}\right] \tag{1.1}$$

$$J_i = \mu_i(\theta_i)\left[\theta_i \frac{dn}{dx} - en\frac{d\psi}{dx}\right] \tag{1.2}$$

$$\left(\frac{5}{2}\theta_e + e\psi\right) J_e - K_e \frac{d\theta_e}{dx} = Q_e \tag{1.3}$$

where all symbols are defined in Table II-1. The divergence of energy at each point is related to the net ionization rate, which in turn is related to the continuity equation for the electron and ion currents. Specifically,

$$\frac{dQ_e}{dx} = -V_i \dot{\xi} \tag{1.4}$$

and

$$\dot{\xi} = \frac{dJ_e}{dx} \tag{1.5}$$

$$\frac{dJ_e}{dx} = \frac{dJ_i}{dx} \tag{1.6}$$

There are six equations with eight unknowns: θ_e, J_e, J_i, ψ, θ_i, n, $\dot{\xi}$ and Q_e. Therefore two more equations are needed. One of these

two equations is the relation between particle density, electron temperature and ionization rate:

$$\dot{\xi} = \alpha (n_e^2 n - n^3) \qquad (1.7)$$

The constants α and n_e define the recombination rate and the Saha equilibrium concentration.[2] A second equation can be introduced; the ion energy transport is neglected and the ion temperature is assumed to be constant at the average of the emitter and collector values:

$$\theta_i = \frac{\theta_E + \theta_C}{2} \qquad (1.8)$$

These eight equations form a complete system for the description of the plasma region of the converter. Solutions can be obtained when a sufficient number of boundary conditions are specified.

For programming purposes, a normalized distance, $\bar{x}$, was used to represent fractional spacing, and equations (1.1) through (1.7) were rewritten. Specifically, the density and field terms are separated in the current equations, and thus these equations become:

$$n' = -\left(\frac{J_e}{e\mu_e} + \frac{J_i}{e\mu_i}\right) \frac{D}{\theta_e + \theta_i} \qquad (2.1)$$

$$\psi' = \frac{1}{n} \left(\frac{J_i}{\theta_i (e\mu_i)} - \frac{J_e}{\theta_e (e\mu_e)}\right) \frac{D}{\frac{1}{\theta_e} + \frac{1}{\theta_i}} \qquad (2.2)$$

Equation (1. 3) was differentiated and combined with (1. 4) and (1. 5) to give an expression for the derivative of the electron temperature:

$$\theta_e' = -\frac{J_e'}{J_e}\left(\theta_e + \frac{2}{5}\psi + \frac{2}{5}V_i\right) - \frac{2}{5}\psi' + \frac{2}{5}\frac{K_e}{J_e}\theta_e'' + \frac{2}{5}\frac{K_e'}{J_e}\theta_e' \qquad (2.3)$$

The ion and electron current derivatives are obtained by combining equations (1. 5) and (1. 6) with (1. 7):

$$J_e' = eD\alpha n\left(n_i^2 - n^2\right) \qquad (2.4)$$

$$J_i' = J_e' \qquad (2.5)$$

At the sheaths, the energy flux in the plasma becomes

$$\left(\frac{5}{2}\theta_e + \psi\right) J_e - K_e\theta_e' = Q_e \qquad (2.6)$$

Each of the five equations (2. 1) through (2. 5), with the five variables n, ψ, θ_e, J_e and J_i, can be simply written as difference equations of the form

$$F(\bar{x} + h) = F(\bar{x}) + h\,F'(\bar{x}) \qquad (3)$$

The contribution due to the thermal conductivity of the electrons is represented by the terms involving K_e in equation (2. 3). Solutions were investigated both for K_e equal to zero and for K_e different from zero.

2. Boundary Conditions

A completely determined solution to equations (2. 1) through (2. 6) requires six boundary conditions[5,6] (five if K_e is zero in

equations (2. 3) and (2. 6)). These may be derived from particle and energy balance equations plus the conditions specifying an operating point for the converter.

At the emitter there are the relations for electron flux, ion flux and energy flux. For an accelerating emitter sheath (Figure II-1) these relations are:

$$J_{eo} = J_{SE} - J_{ro} \exp(-V_E/\theta_{eo}) \quad (4.1)$$

$$J_{io} = I_{SE} \exp(-V_E/\theta_E) - I_{ro} \quad (4.2)$$

$$Q_{eo} = J_{SE}(2\theta_E + V_E) - (J_{SE} - J_{eo})(2\theta_{eo} + V_E) \quad (4.3)$$

Equations (4. 1) through (4. 3) represent only two boundary conditions, since an additional new variable, V_E, has been introduced (emitter work function and temperature are known).

At the collector, relations similar to those at the emitter are applicable. For an accelerating sheath, these are:

$$J_{e1} = J_{r1} - J_{sc} \exp(-V_C/\theta_C) \quad (5.1)$$

$$J_{i1} = I_{r1} \exp(-V_C/\theta_{e1}) - I_{sc} \quad (5.2)$$

$$Q_{e1} = 2J_{r1}\theta_{e1} - 2J_{sc}\theta_C \exp(-V_C/\theta_C) \quad (5.3)$$

and for a retarding sheath they are:

$$J_{e1} = J_{r1} \exp(-V_C/\theta_{e1}) - J_{sc} \quad (6.1)$$

$$J_{i1} = I_{r1} - I_{sc} \exp(V_C/\theta_C) \quad (6.2)$$

$$Q_{e1} = J_{sc}(2\theta_C + V_C) + (J_{sc} + J_{e1})(2\theta_{e1} + V_C) \quad (6.3)$$

Again a new variable, V_c, has been introduced so the three equations (5.1) through (5.3) or (6.1) through (6.3) actually furnish only two boundary conditions.

The two remaining conditions are determined by the operating point on the J-V curve and an arbitrary reference value for voltage. In this work J_{e_0} was selected as defining the operating point, i.e., approximately the output current density. The voltage reference was taken as $\psi = 0$ at the emitter edge of the plasma. In the case where K_e is zero, there is now a redundant boundary condition which cannot be matched. The collector energy flux relation had to be neglected when K_e was taken as zero.

3. Parameters

Before the equations can be solved, the various plasma coefficients, such as mobility and electron thermal conductivity, which are functions of position, must be expressed in terms of the six variables or their derivatives. At the present stage of the study simplified relations were chosen. The coefficients to be defined are: μ_e, μ_i, K_e, and α. Electron-ion scattering was neglected for the mobility relations, and the expressions[7] used were:

$$\mu_e = 0.98\, e^2/m_e \nu_{en} \tag{7.1}$$

$$\mu_i = 0.90\, e^2/m_i \nu_{in} \tag{7.2}$$

where m is particle mass and ν_{-n} is the collision frequency with neutrals.

$$\nu_{en} = \frac{3\sqrt{\pi}\, N_o\, \sigma_{en}\, (\theta_e/k)^{\frac{1}{2}}}{2^{3/2}\, (m_e)^{1/2}} \tag{8.1}$$

$$\nu_{in} = \frac{3\sqrt{\pi}\, N_o\, \sigma_{in}\, (\theta_i / k)^{\frac{1}{2}}}{4\, (m_i)^{\frac{1}{2}}} \qquad (8.2)$$

where N_o is the neutral density and σ_{-n} the hard-sphere cross section with neutrals.

The electron thermal conductivity was based on the electron-neutral mean free path, and the expression[7] used was:

$$K_e = \frac{1.88\, N_o\, \mu_e\, \theta_e}{0.98\, D} \qquad (9.1)$$

The recombination rate parameter was defined by the form used by Wilkins.[5]

$$\alpha = k_r \left[5.6 \times 10^{-17}\, \theta_e^{-4.5} \right] \qquad (9.2)$$

where k_r is an input parameter, and θ_e is in electron volts.

The parameters σ_{in}, σ_{en} and k_r were specified for each run and can be used to investigate the sensitivity of the solutions to the various parameters.

4. Integration Procedure

The plasma equations, (2.1) through (2.5), were solved by selecting a set of six initial values (n_o, ψ_o, θ_{eo}, θ''_{eo}, J_{eo}, J_{io}), and then advancing step by step across the plasma using equation (3). From the emitter boundary equations, the initial electron current density, and the reference value of ψ, four of the initial conditions are determined. The remaining two must be chosen arbitrarily and their correctness evaluated from the collector sheath relations when the solution reaches that sheath.

D. RESULTS

The first attempts were made assuming that K_e was zero in equations (1.3), (2.3) and (2.6). Thus only five initial values are required, of which only one, say n_o, cannot be determined at the emitter. Different values were chosen for n_o, and the solution advanced until either equation (5.1) or equation (6.2) could be satisfied for a collector sheath. If this condition had occurred at $\bar{x} = 1$, it would have represented a valid solution for the particular operating point chosen. However, no value for n_o could be found which would extend $\bar{x}$ to greater than 0.2. The difficulty was traced to the energy boundary relation, equation (4.3), which caused the electron temperature to approach infinity as larger values of n_o were selected.

Solutions extended to $\bar{x} = 1$ could be found if the emitter energy equation, (4.3), was omitted, and the two parameters, θ_{ec} and n_o, were arbitrarity chosen to start the computation. The results showed that n_o and θ_{ec} indeed had to have values incompatible with the emitter energy equation, (4.3), for such solutions to be obtained. Figure II-2 shows a plot of the required n_o as a function of normalized current density for two values of T_{ec}.

It would have been possible at this stage to re-introduce the collector energy balance equation and to attempt to define θ_{ec} by requiring (5.3) or (6.3) to be satisfied. Because the emitter energy balance was felt to be much more significant in determining θ_{ec}, this was not done. Instead, solutions for K_e different from zero were studied.

Values of K_e were calculated by assuming that electron-neutral collisions were dominant. These values were used in equation (2.6) at

the emitter, but not in equation (2-3), where the K_e - dependent terms were neglected. A typical solution is shown in Figures II-3 and II-4. Note that for such solutions the collector energy balance relation, (5.3) or (6.3), is redundant since the $K_e \theta_e''$ is neglected from equation (2.3). This implies that only one initial value had to be guessed, say n_o, to initially replace the collector boundary relations. Of course, eventually the correct value of n_o is determined by satisfying the collector sheath relations at the desired spacing.

It is seen from Figure II-3 that θ_e versus x has a large curvature near the emitter and collector edges of the plasma. This implies that the $K_e \theta_e''$ term in the plasma equation, (2.3), is significant, and therefore should not be neglected from this equation. Introduction of this factor eliminates the redundancy of the collector energy balance equations and requires that two parameters be guessed at the emitter. For such calculations, n_o and θ_{eo}'' were selected.

Integrations performed with K_e finite produced results which were quite sensitive to the particular value of θ_{eo}'' chosen, too high a value causing the temperature to curve suddenly upwards, and, conversely, too low a value causing it to curve suddenly downwards. Typical results are shown in Figure II-5.

E. DISCUSSION

As discussed in the previous section, the plasma distributions are fully determined by the five differential equations (2.1) through (2.5). These five differential equations are strongly coupled. The following interpretation of the equations, however, has been useful in understanding the character of the solutions.

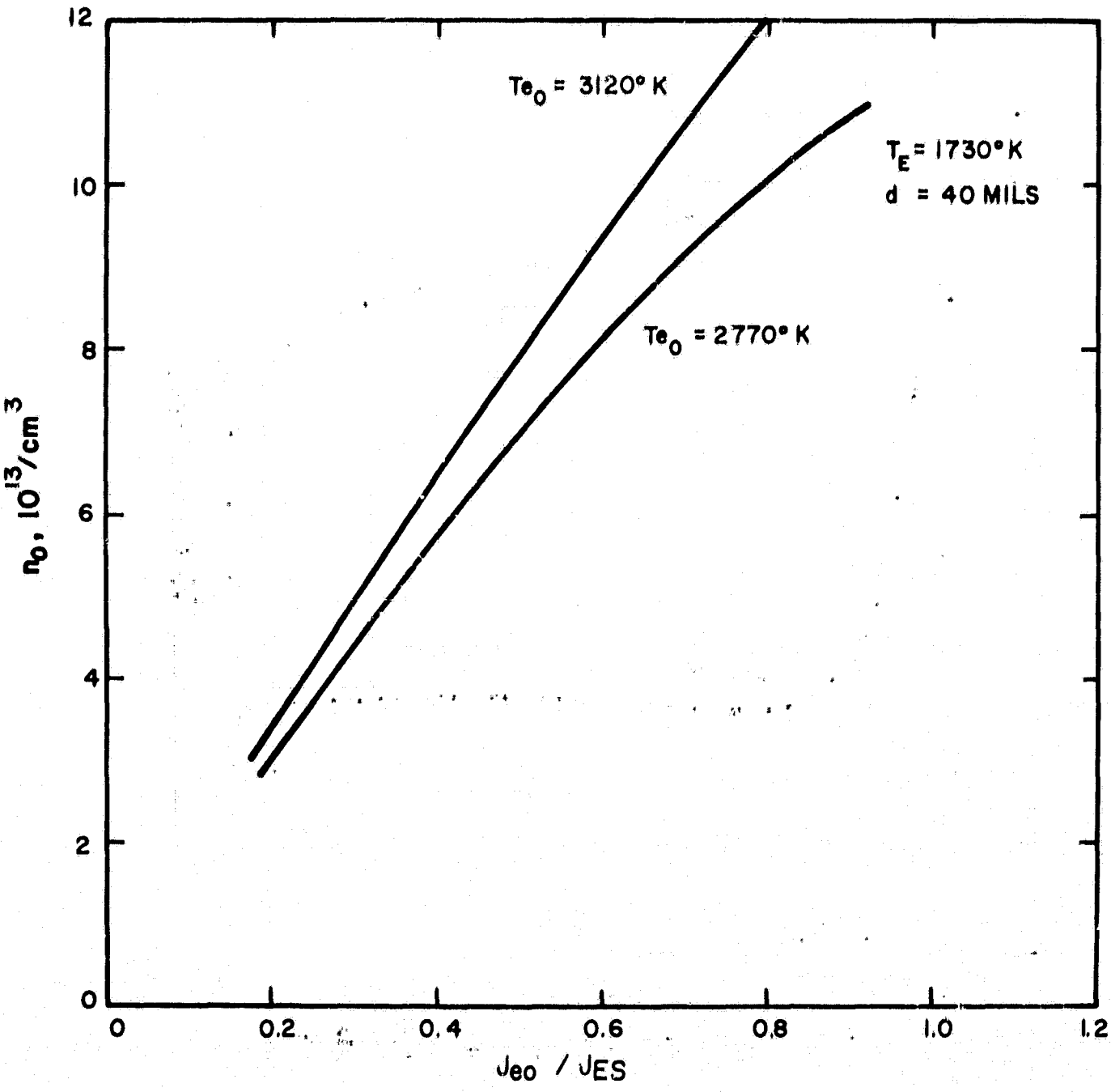


Figure II-2. Initial Conditions as a Function of Current.

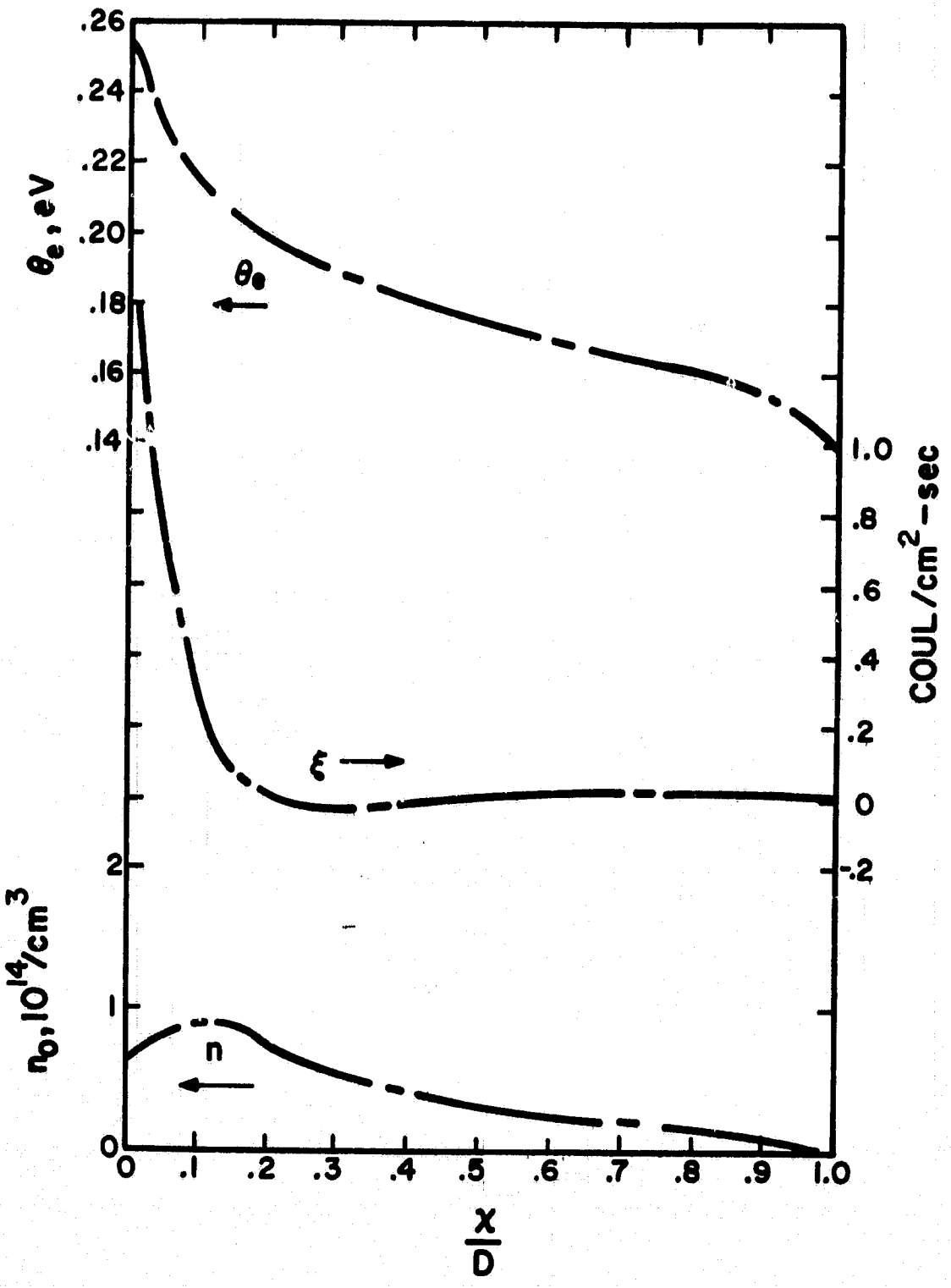


Figure II-3. Plasma Distributions with $K_e = 0$.

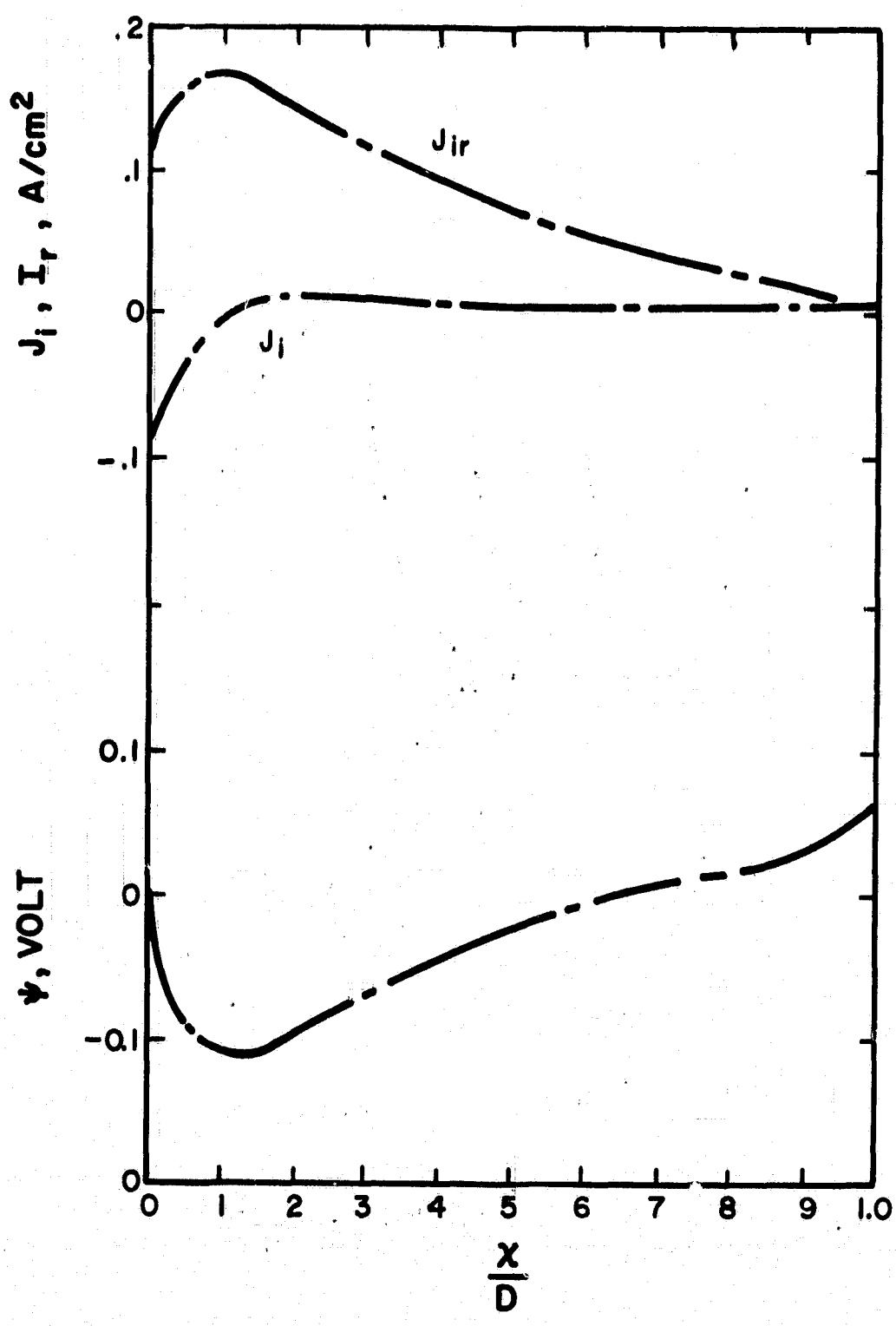


Figure II-4. Plasma Distributions with $K_e = 0$.

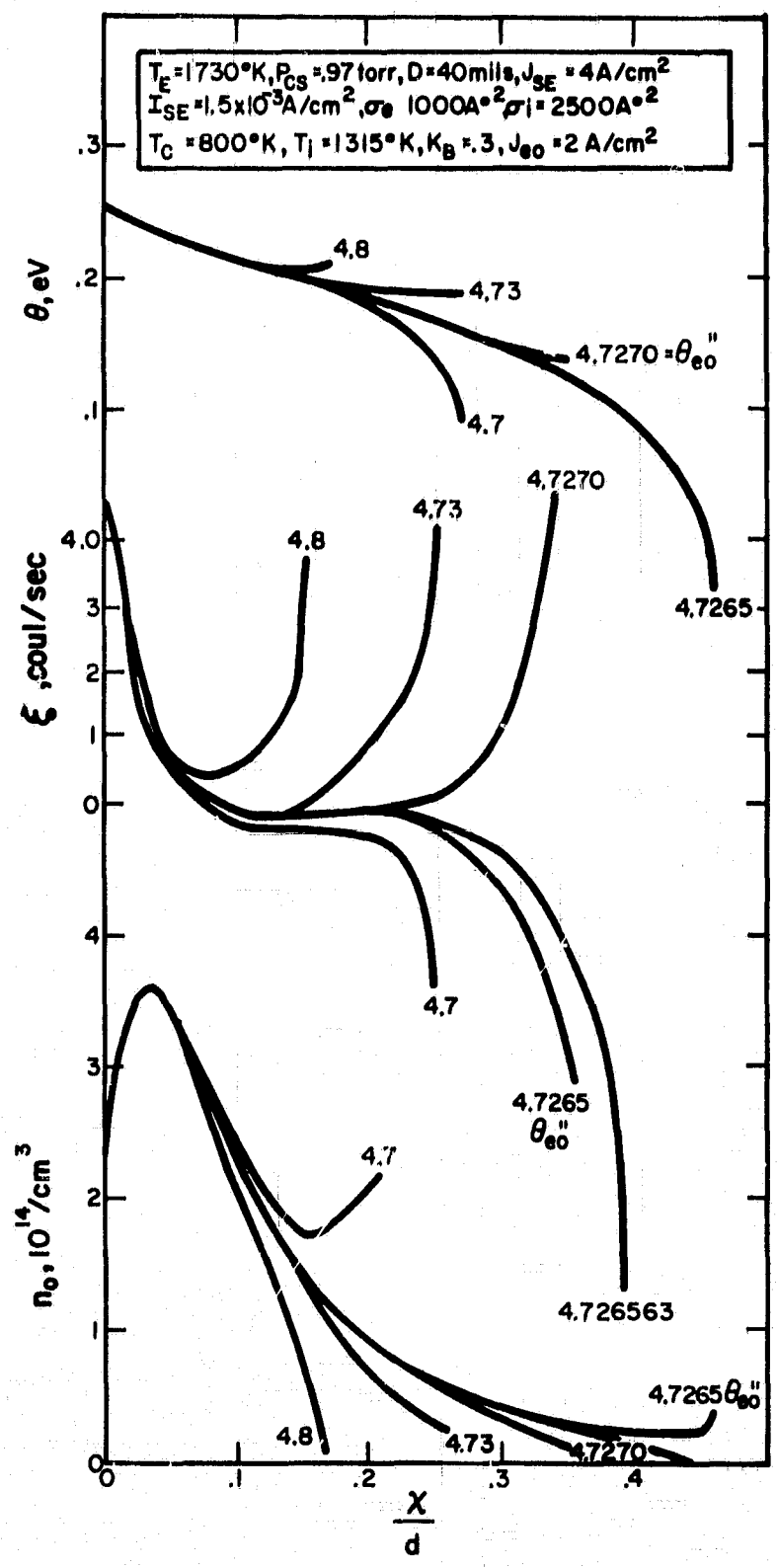


Figure II-5. Plasma Distributions Showing Effects of Initial Values when K_e is Finite.

Starting with the ionization and particle conservation equations, (2. 4) and (2. 5), we see that the net ionization rate is a function of electron temperature and number density. The effect of the ionization rate, $\dot{\xi}$, on the electron current, J_e, is usually very small compared with that of J_{e_0}. On the other hand, the effect of the ion current, J_i, is large compared with that of $\dot{\xi}$ on J_{i_0}. Thus it is reasonable to view the electron current as essentially constant.

For given values of J_e and J_i, the gradients of n and ψ are essentially determined from equations (2. 1) and (2. 2). Since the ratio of the mobilities of electrons and ions is about 500 to 1, the importance of the ion current in equations (2. 1) and (2. 2) is comparable with that of the electron current when their ratio is 1/500 or greater. Thus we conclude that n' will be positive for relatively large negative values of J_i and negative for small values of J_i.

An approximate relation for the second derivative of n is easily obtained by differentiating equation (2. 1) and disregarding small terms. The result is

$$n'' = -\left(\frac{1}{e\mu_e} + \frac{1}{e\mu_i}\right) \frac{D}{(\sigma_e + \sigma_i)} \dot{\xi} \qquad (10.1)$$

Thus we see that n'' is negative in regions where net ionization is predominant and positive where net recombination is predominant. Also, we conclude that n must be approximately linear with distance when the ionization rate is small.

The energy equation, (2 3), essentially relates the change in electron temperature to the net ionization rate, the electric field, and the conduction term. If we take the case for very small electron thermal

conductivity, K_e, and consider zones in the plasma where ψ' is relatively small, we see that the electron temperature will tend to the Saha value. Because of the exponential dependence of the ionization rates on electron temperature, a relatively hot plasma has a very strong tendency to cool to its Saha temperature. It appears, however, that for the types of plasma existing in a converter, the conduction term in equation (2.3) is very large and is the controlling factor for the temperature distribution.

1. Results for No Electron Thermal Conductivity in the Plasma

We shall first discuss the results for thermal conductivity zero in the plasma region but finite at the emitter edge (see Figures II-3 and II-4.

With the guessed value for n_o, the choice for J_{eo}, and the arbitrary reference value for ψ_o, the two emitter boundary conditions (mass balance and energy balance) determine the initial ion current (J_{io}) and the initial electron temperature (θ_{eo}). The result of this calculation for reasonable values of n_o is a relatively large negative ion current (J_{io}) and a high θ_{eo} compared with the Saha temperature corresponding to n_o.

Because of the high initial temperature, the ionization rate is high, and therefore the temperature drops rapidly to nearly the Saha value, thereby causing the ionization to fall to almost zero. Saha equilibrium is nearly established by the time $\bar{x}$ is 0.2. Because of the large negative ion current and the positive ionization rate, the initial slope of n is positive (see equation (2.1)) and n'' is negative. The second derivative, n'', remains negative (see equation (10.1)) until the ionization goes to zero, at which point n'' changes sign. Notice that the slope of n goes through

zero near the point where the ion current is 1/500 of the electron current (see equation 2.1)). Near the collector side of the plasma, where the ion current and ionization rate are very small, the slope of n is constant and equal to that required to carry the current J_e. The variations in ψ are very similar to those in n, as is expected from equation (2.2).

The solutions were terminated at a value $\bar{x} = 0.95$ because at this point the random ion current, I_r, was equal to the ion current, J_i, a condition satisfying the collector particle balance. Higher values of n_o terminated at larger values of $\bar{x}$, and lower values of n_o terminated at smaller values of $\bar{x}$.

2. Effect of Electron Thermal Conductivity on Plasma Distributions

With electron thermal conductivity included, the electron temperature is forced to maintain nearly a constant slope (see solid line Figure II-6). As a result, the region of new ionization extends further into the plasma (to $\bar{x} = 0.4$ compared with $\bar{x} = 0.2$). The increased ionization means that a larger value of n is required before Saha equilibrium can be established. These effects are shown in Figure II-6 for the solutions having the same energy flux and electron current into the plasma at the emitter.

3. Calculated J-V Curve and Effects of Ionization

The points on the J-V curve shown in Figure II-7 were calculated with the thermal conductivity term included. In order to assure an electron-accelerating emitter sheath and thus eliminate any double sheath effects, the emission was set to be ion-rich ($\beta = 3$).

The curve shows a knee at point "C," indicating a division between upper and lower modes. Points "A" and "B" were calculated with the ionization artificially suppressed (i. e. , $k_r = 0$ in equation (9. 1)). Ionizations are thus seen to be the significant factor in producing the upper mode.

Figure II-8 compares the plasma distributions with and without ionizations. Points "A" and "C" from Figure II-7 are examined. Consider first the ion and electron currents with $\dot{\xi} = 0$ (i. e. , point "A"). Since J_e' and J_i' are zero, J_e and J_i must be constant. From the current equations, (1. 1) and (1. 2), n' and $n\psi'$ must also be constant. Therefore the particle density decreases linearly with distance, and ψ falls very rapidly to allow the field, ψ', to compensate for the small particle density near the collector. The electron temperature, θ_e, rises toward the collector as the electrons gain energy falling through the potential drop in the plasma.

When ionization is permitted (point "C"), it peaks mainly near the center of the plasma. The total integrated net ionization is indicated on the J_i curve and is seen to be almost five times the ion current for point "A." Thus, even though the ionization is nearly an order of magnitude less than the surface ion current, it is significant compared with the plasma ion current. The ion generation produces an increased ion density near the center of the plasma, thereby increasing the gradient of n towards the collector and decreasing it towards the emitter. However, since the initial electron current has been held constant, the electric field must react to maintain a constant sum of the field and concentration terms in the J_e equation, (1. 1). The gradient of ψ is thus increased towards the emitter and decreased towards the collector, and because n is much smaller near the collector, the total potential drop across the plasma decreases. The electron temperature again responds to the potential variation, although there is a slight effect

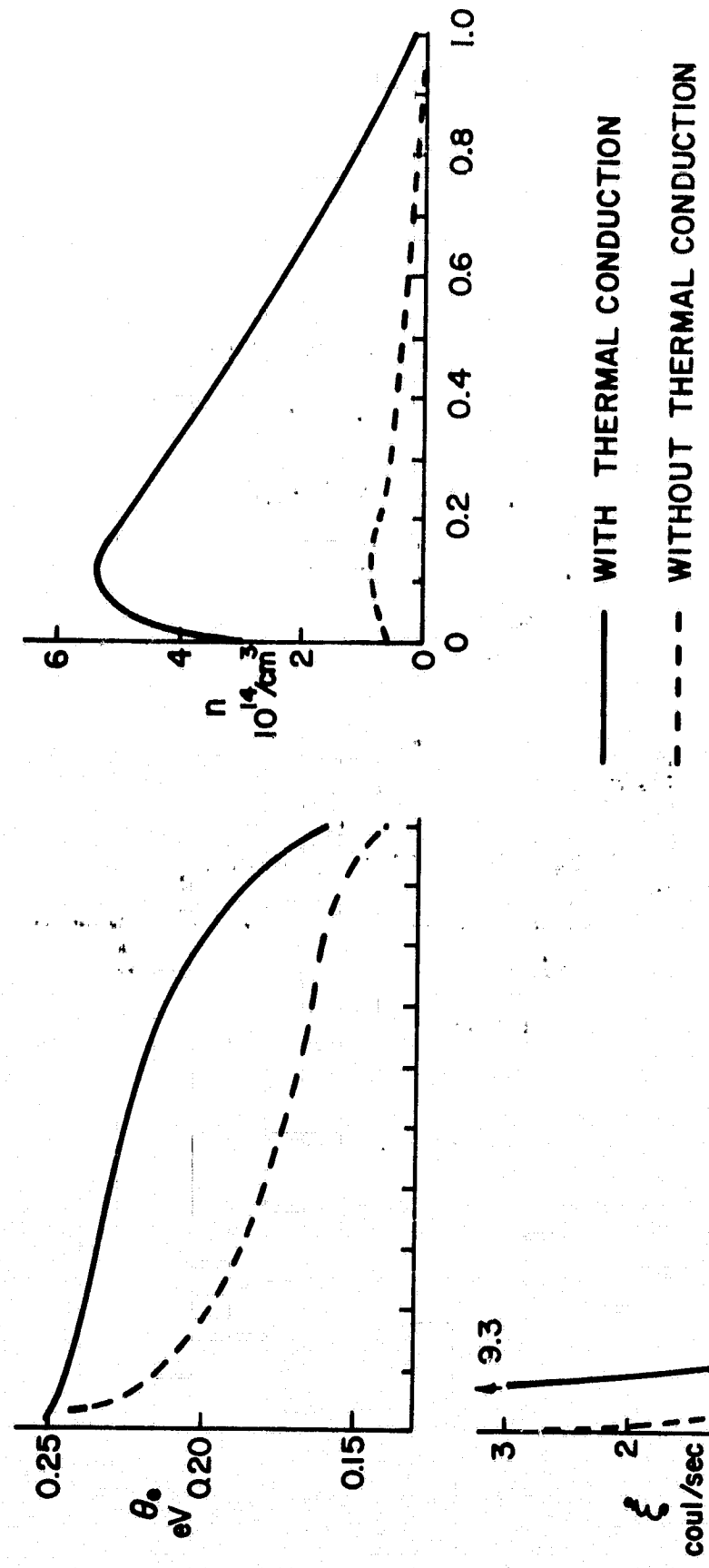


Figure II-6. Comparison of Distributions With and Without Electron Thermal Conductivity Effects.

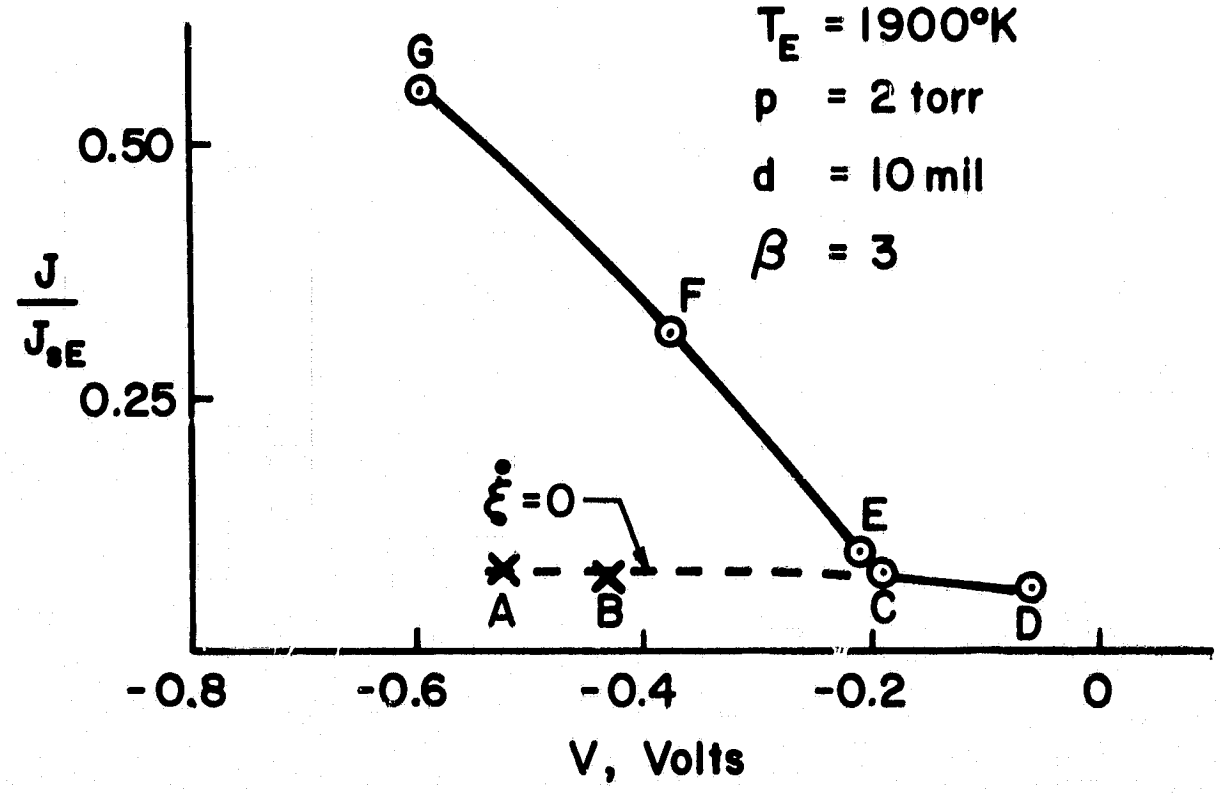


Figure II-7. Calculated J-V Curve.

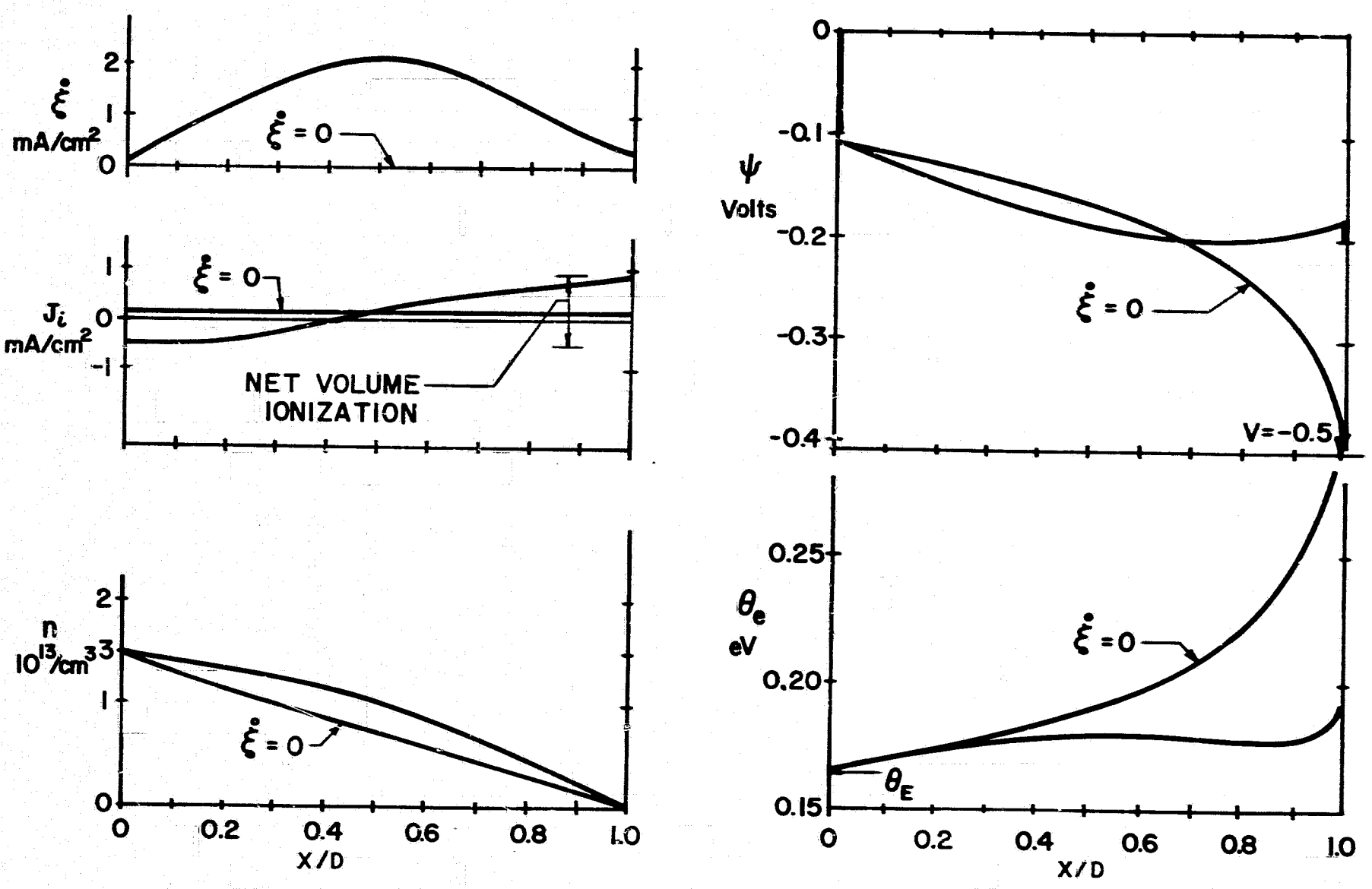


Figure II-8. Comparison of Plasma Distributions With and Without Ionization.

due to the energy used in the ionization. The turn-up in temperature near the collector was observed in electron-accelerating collector sheath cases and is due to the additional $1/2\,\theta_e$ appearing in the energy of transport ($5/2\theta_e$) and not in the half-Maxwellian distribution ($2\theta_e$) of the electrons leaving the plasma. This effect has been observed with gases* as they enter a fine porous plug. Together with the temperature rise associated with the fall in potential, this turn-up could be responsible for the anode-glow mode of the converter.

Figure II-9 shows the distributions obtained at several points on the J-V curve. Both emitter and collector sheaths are indicated by tick marks on the potential diagram. As the current density increases, the region of peak net ionization moves towards the emitter, and the amount of ionization increases.

Similar effects are observed with the ion density; the hump moves towards the emitter and becomes more pronounced. With the increasing ion density, the electron thermal conductivity becomes active, and the temperature falls almost linearly from higher and higher initial values as saturation is approached. The potential diagrams show that the emitter sheath becomes much larger in the upper mode and that the field becomes retarding for electrons through most of the plasma away from the emitter edge. Near the emitter in the upper mode the field is accelerating, since the concentration gradient is in the wrong direction. There are thus relatively large ion currents into both emitter and collector.

*Knudsen effect.

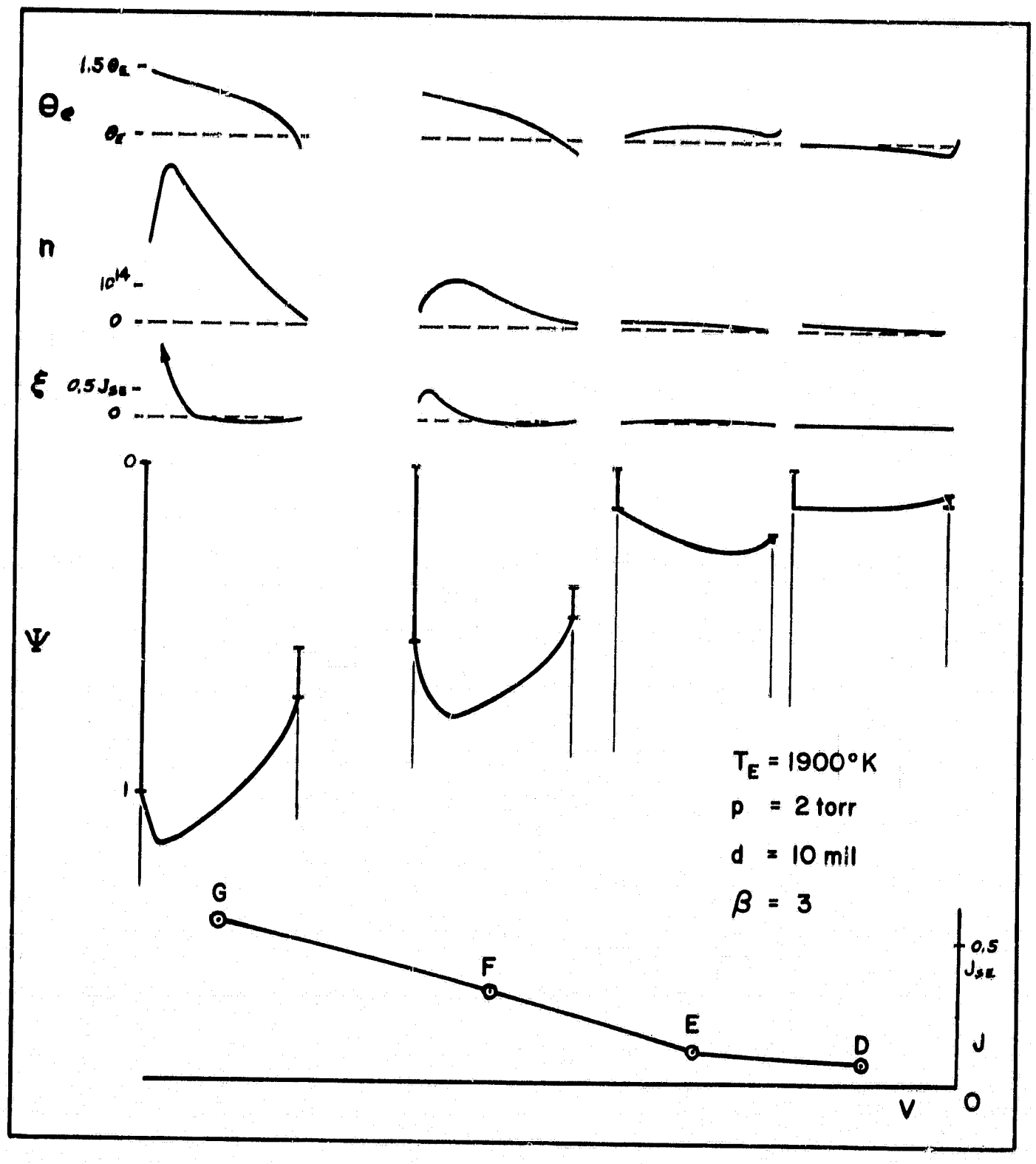


Figure II-9. Plasma Distributions at Points on the J-V Curve.

E. CONCLUSIONS

The plasma analysis program has examined the influence of electron thermal conductivity and of ionization on the plasma distributions. The thermal conductivity has been shown to maintain a much more uniform temperature gradient through the plasma, to cause more ionization, to delay the onset of local thermodynamic equilibrium, and to require higher ion and electron concentrations for the same emitter conditions when compared with formulations neglecting this factor. The effect of net ionization in the plasma becomes significant when its magnitude is comparable with that of the plasma ion current rather than with that of the surface ion current. From this point ionization increases with current, ion concentration becomes peaked, a large electron-accelerating emitter sheath is formed, and the electric field becomes retarding outside the region of net ionization. Both of these factors become important in the upper-mode portion of the J-V curve, and their effects must be considered in examining the converter characteristics under various operating conditions.

REFERENCES FOR CHAPTER II

1. R. H. Bullis et al., "The Plasma Physics of Thermionic Converters," Report on the Thermionic Conversion Specialist Conference, San Diego, California, October 1965, pp. 9-29.

2. Daniel R. Wilkins and Elias P. Gyftopoulos, "Thermionic Converters Operating in the Ignited Mode, Part II, Theoretical Output Current Characteristics," Report on the Thermionic Conversion Specialist Conference, San Diego, California, October 1965.

3. W. H. Reichelt and L. Agnew, " Identification of the Ionic Species in a Cesium Plasma Diode," 1966 IEEE Conference Record of the Thermionic Conversion Specialist Conference, Houston, Texas, pp. 70-74.

4. G. A. Dyuzhev et al., "Investigations of Plasma in High-Pressure Cesium Converters, Part III, Distribution of Density, Electron Temperature, and Space Potential in the Interelectrode Space of Thermionic Converters," Soviet Physics-Technical Physics, Vol. 11, No. 9, March 1967.

5. D. R. Wilkins, "Theoretical Description of Thermionic Converter Output Performance Characteristics," 1966 IEEE Conference Record of the Thermionic Conversion Specialist Conference, Houston, Texas, pp. 259-268.

6. Hansen and Warner, Journal of Applied Physics, February 1967.

7. D. R. Wilkins and E. P. Gyftopoulos, "Transport Phenomena in Low Energy Plasmas," International Conference on Thermionic Electrical Power Generation, London, September 1965.

CHAPTER III

PARAMETRIC DATA

F. Rufeh, D. Lieb, C. Wang, L. van Someren

A. RHENIUM EMITTER

1. Introduction

In a program carried out during the fiscal year 1965-1966,[1] a new technique was developed for the preparation of emitter surfaces, involving electroetching and heat treatment. A rhenium emitter was prepared by this technique and incorporated into a variable-spacing converter in order to determine its electrical performance characteristics. The data obtained showed a remarkable improvement in performance compared with that of other rhenium emitter surfaces. The same emitter was incorporated into a second variable-spacing converter. Its performance was in good agreement with that observed in the first converter.

In the current program the electroetching and heat treatment technique was used to prepare another rhenium emitter surface. This emitter was incorporated into a variable-spacing converter. The converter performance was tested to determine the reproducibility of the emitter preparation and to obtain additional parametric data.

2. Variable-Spacing Converter

The variable-spacing converter used for this experiment is equipped with an active collector guard ring which is maintained at the same temperature and electrical potential as the collector (Figure III-1). Flexible bellows allow the interelectrode spacing to be varied from zero to 100 mils. The diode is continuously pumped during the operation

through a tubulation in the cesium reservoir. Any cesium that escapes toward the ion pump is condensed by the baffles and returned to the reservoir. The design of this converter originally included a molybdenum collector[2], but it was modified to use a rhenium collector and guard assembly. Two rhenium sheets of 20-mil thickness were machined and brazed to the collector and guard assembly. The collector and guard were assembled with a sapphire spacer, and the surfaces were ground for flatness and parallelism.

3. Performance Data

Families of volt-ampere characteristics were recorded for various cesium reservoir temperatures while the other parameters were held constant. Figures III-2 through III-4 show three families at T_e = 1660° K, interelectrode spacings of 5, 10, and 20 mils, respectively, and at a constant collector temperature of 770°K. This collector temperature is optimum for the 1660°K emitter temperature. Each family defines an envelope which represents the optimized performance with respect to cesium reservoir and collector temperatures. The cesium reservoir envelopes at T_e = 1660°K are summarized in Figure III-5 to determine the optimized performance with respect to interelectrode spacing. The output voltage is not corrected for emitter sleeve voltage loss. A correction of 3 mV/amp is required to convert to electrode voltage.

Another set of temperature families, taken at T_e = 1760°K, are presented in Figures III-6 through III-9. The optimum collector temperature at T_e = 1760°K was 820°K. A summary of the cesium temperature envelopes at various spacings is shown in Figure III-10. Finally, similar data recorded at the emitter temperature of 1860°K are shown in Figures III-11 through III-15.

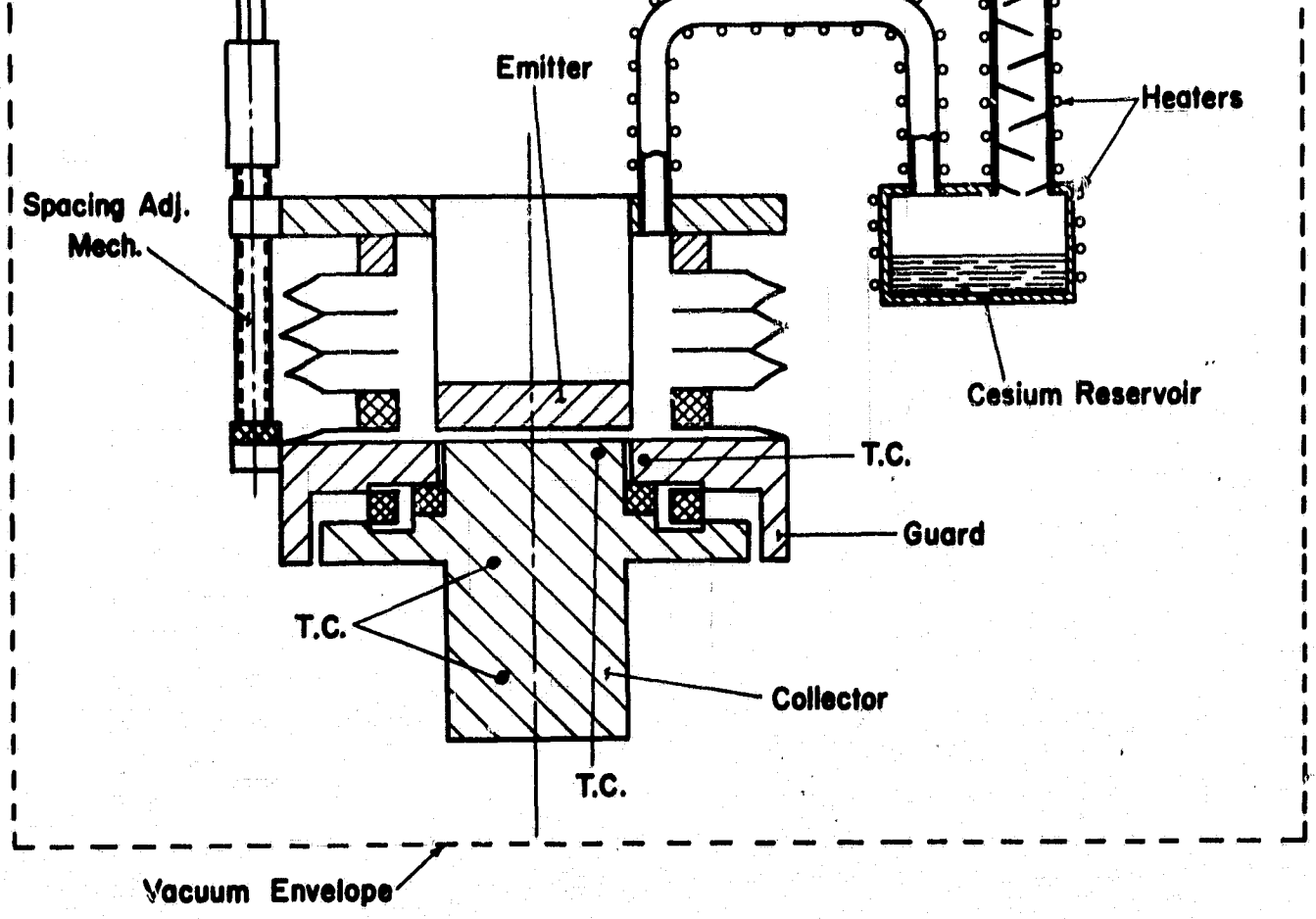


Figure III-1. Schematic of the Variable-Spacing Converter.

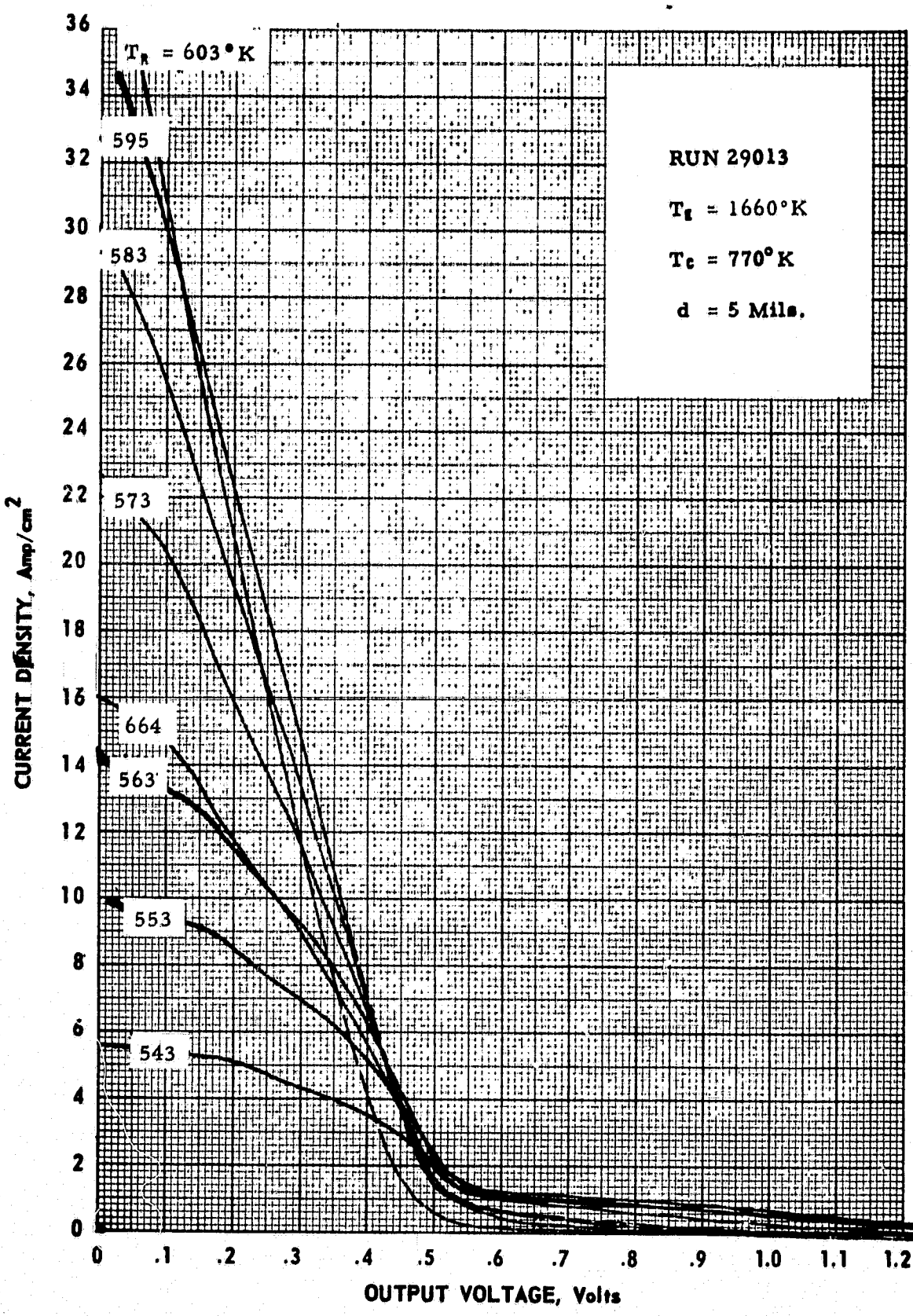


Figure III-2. Cesium-Temperature Family at T_E = 1660°K and d = 5 mils.

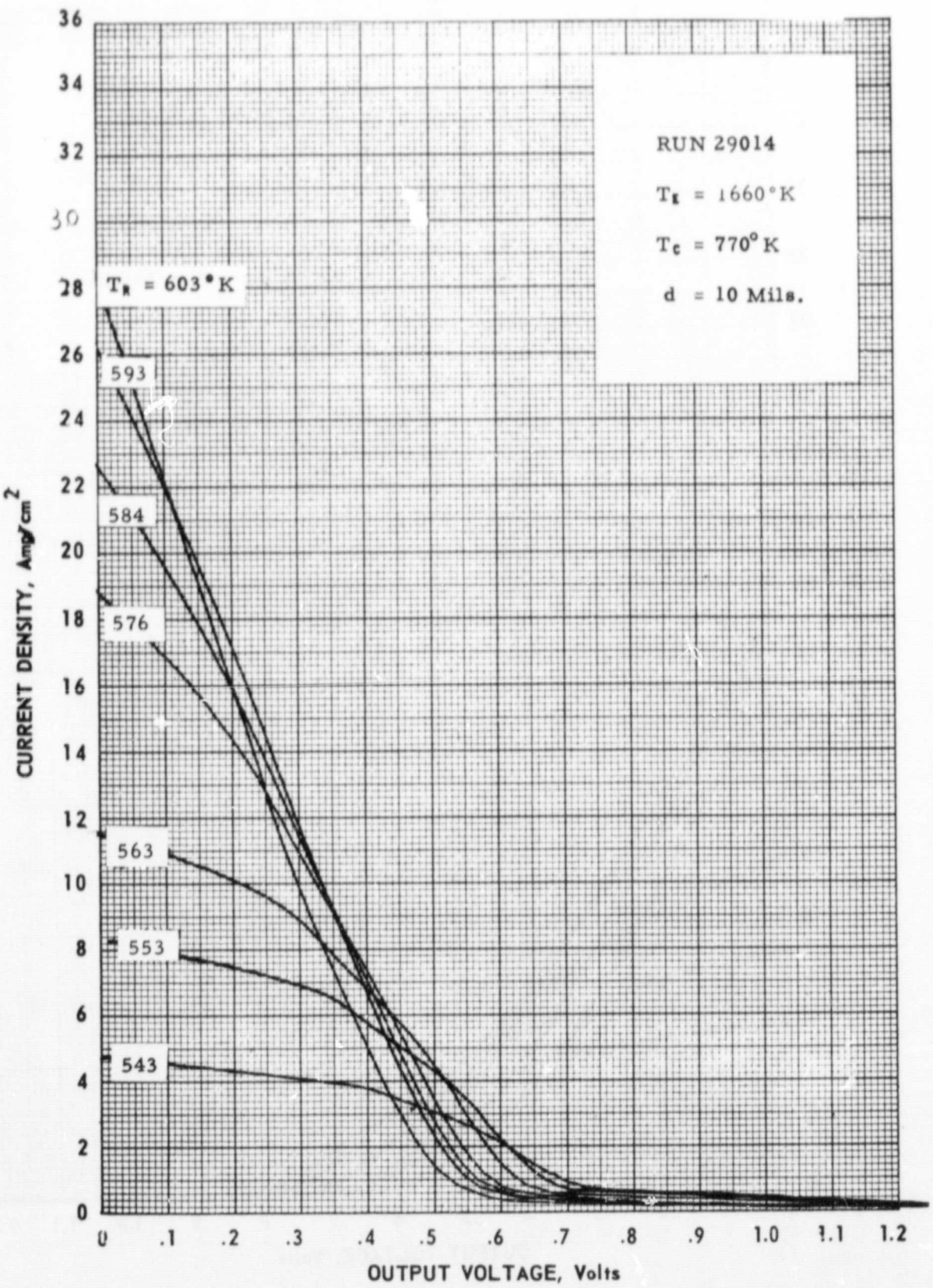


Figure III-3. Cesium-Temperature Famiiy at T_E = 1660°K and d = 10 mils.

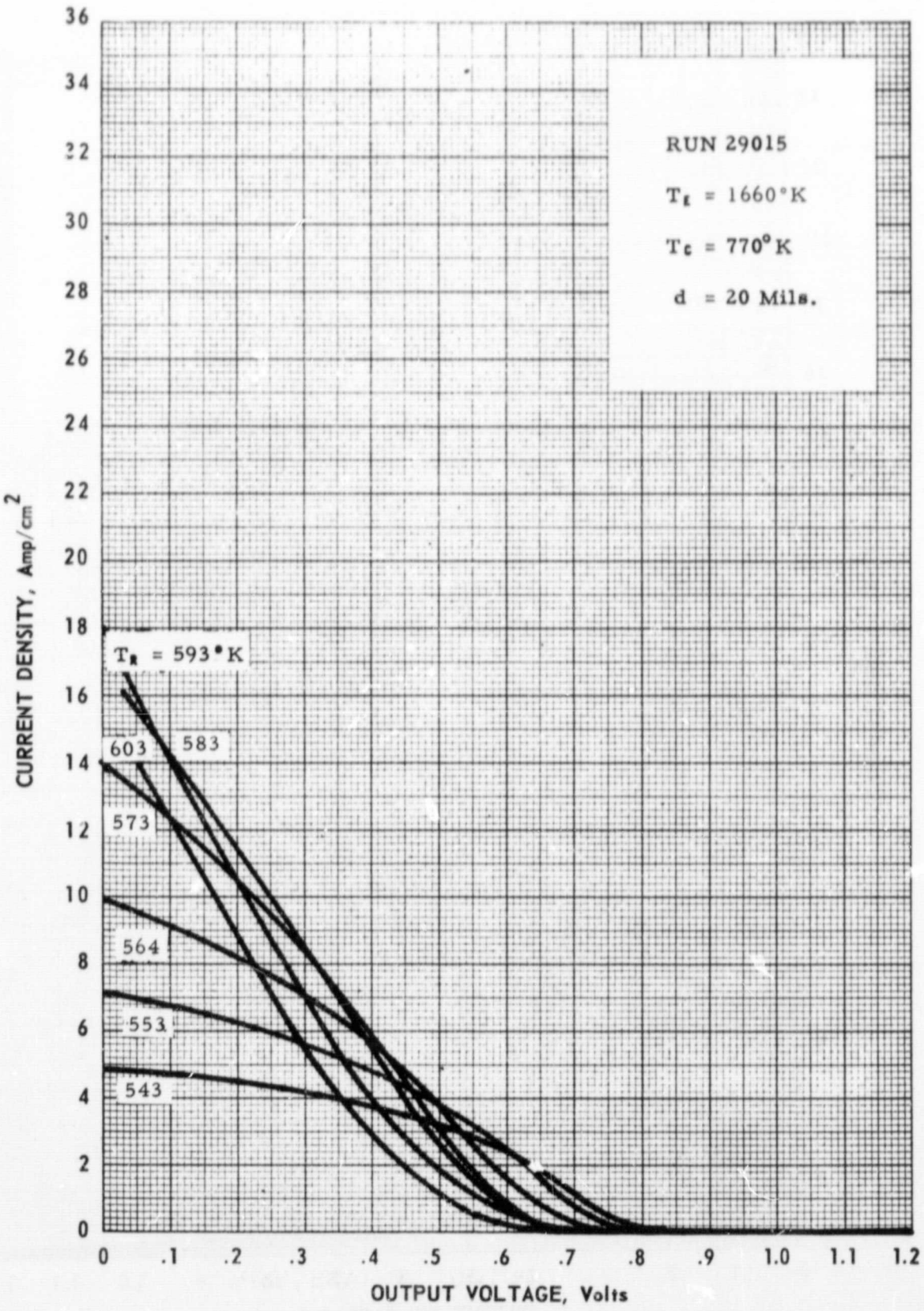


Figure III-4. Cesium-Temperature Family at T_E = 1660°K and d = 20 mils.

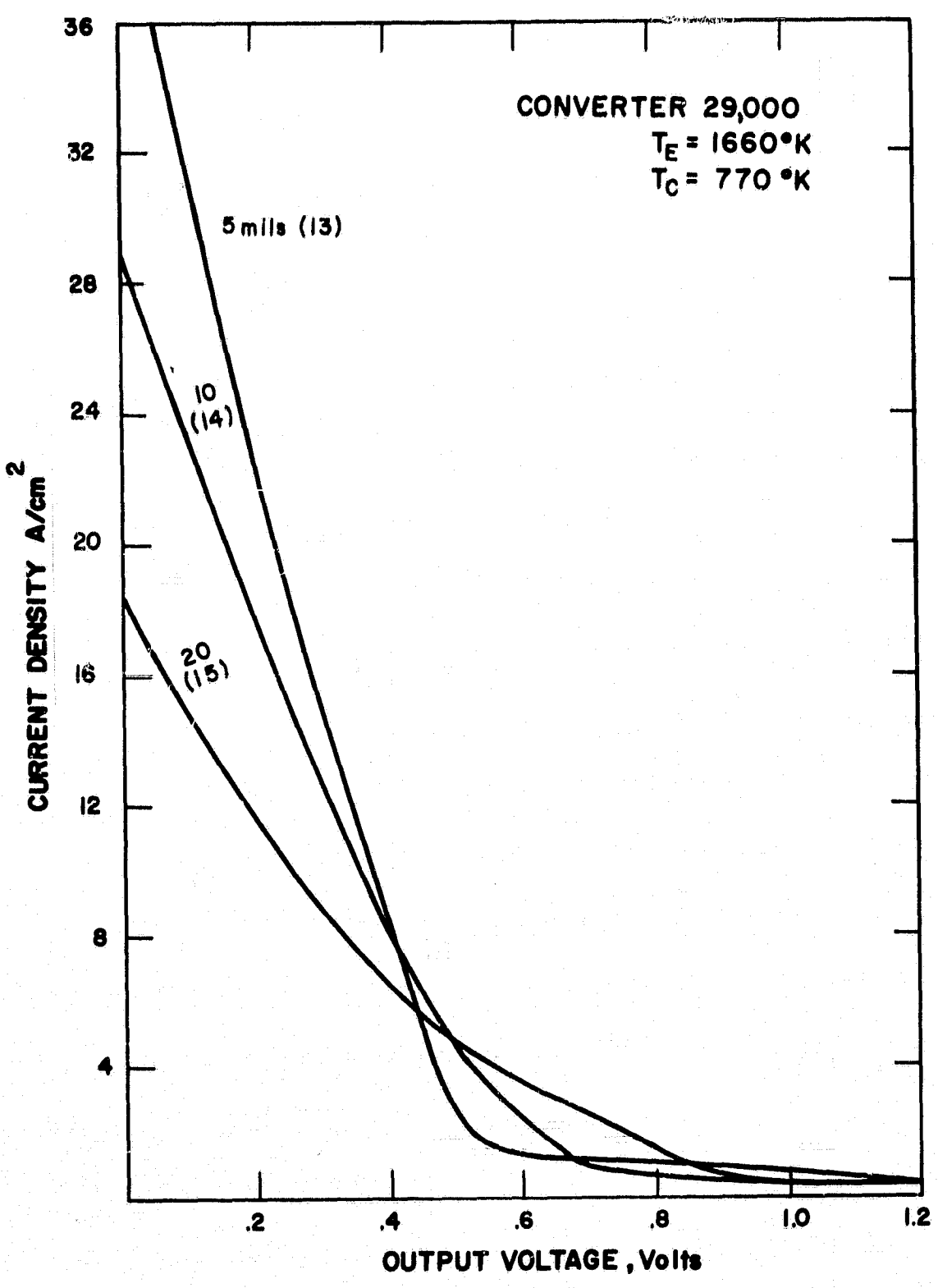


Figure III-5. Comparison of Cesium Optimized Envelopes at T_E = 1660° K for Several Spacings. (The number in the parenthesis indicates the run number.)

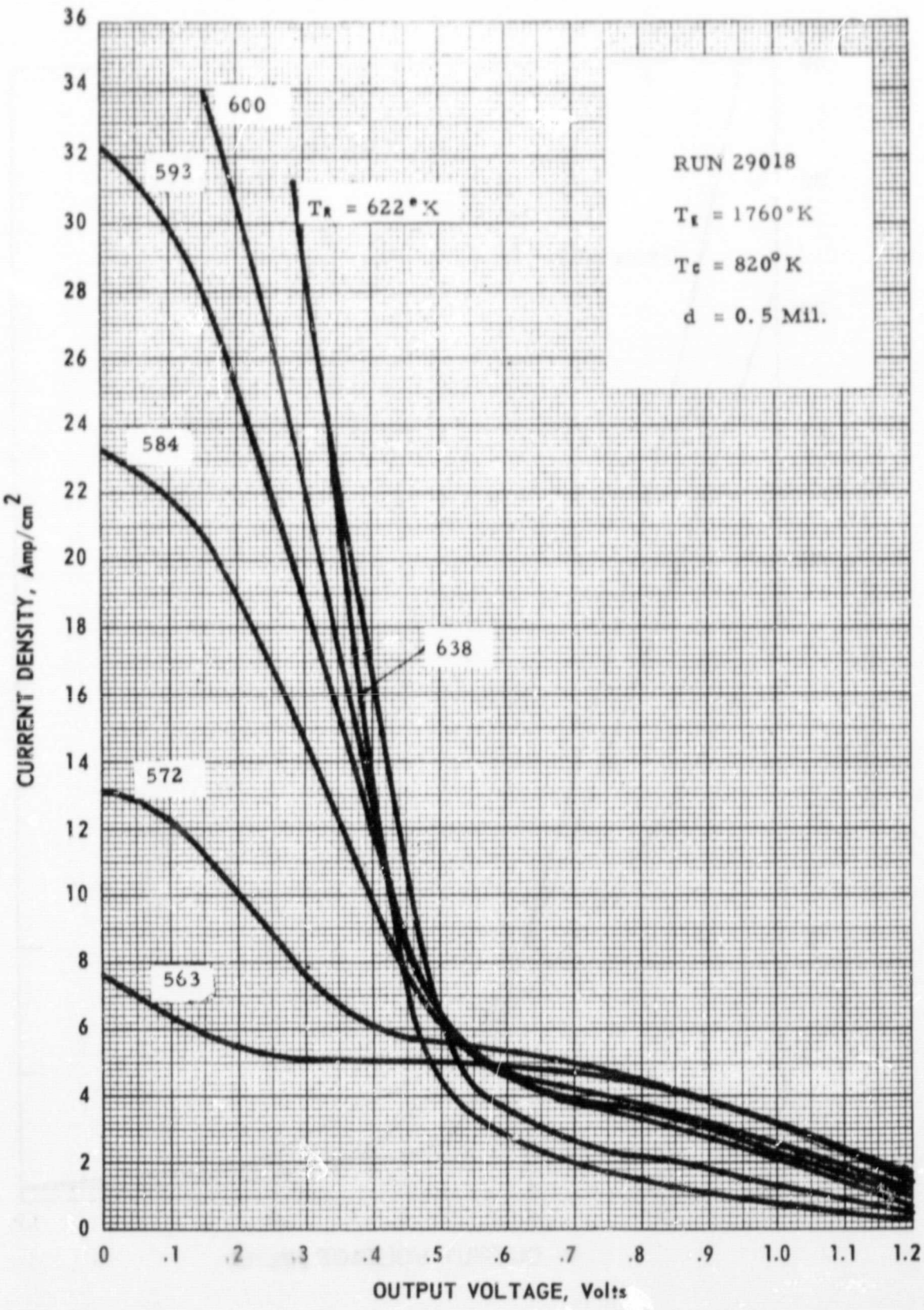


Figure III-6. Cesium-Temperature Family at T_E = 1760°K and Interelectrode Spacing of 0.5 mil.

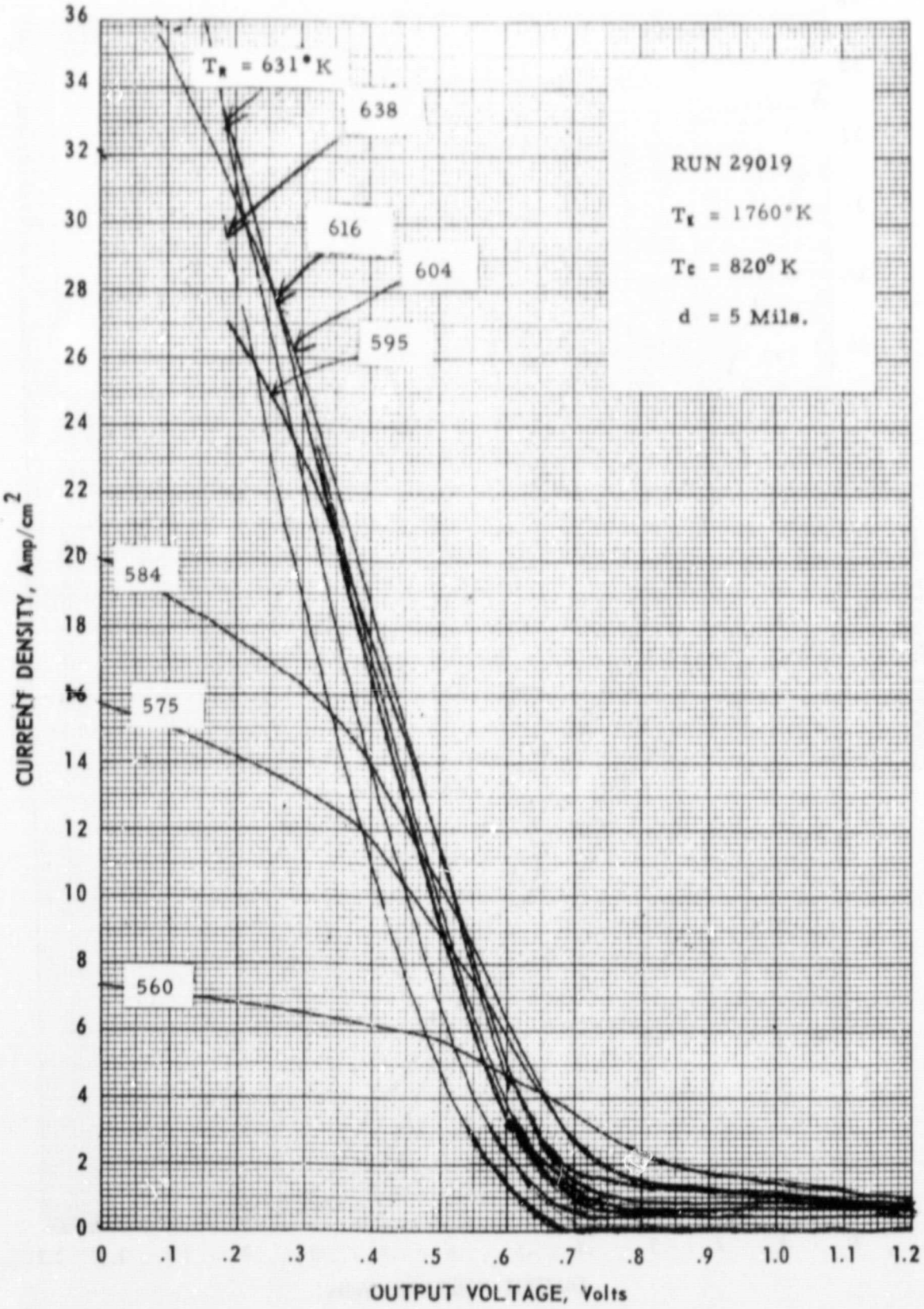


Figure III-7. Cesium-Temperature Family at T_E = 1760°K and d = 5 mils.

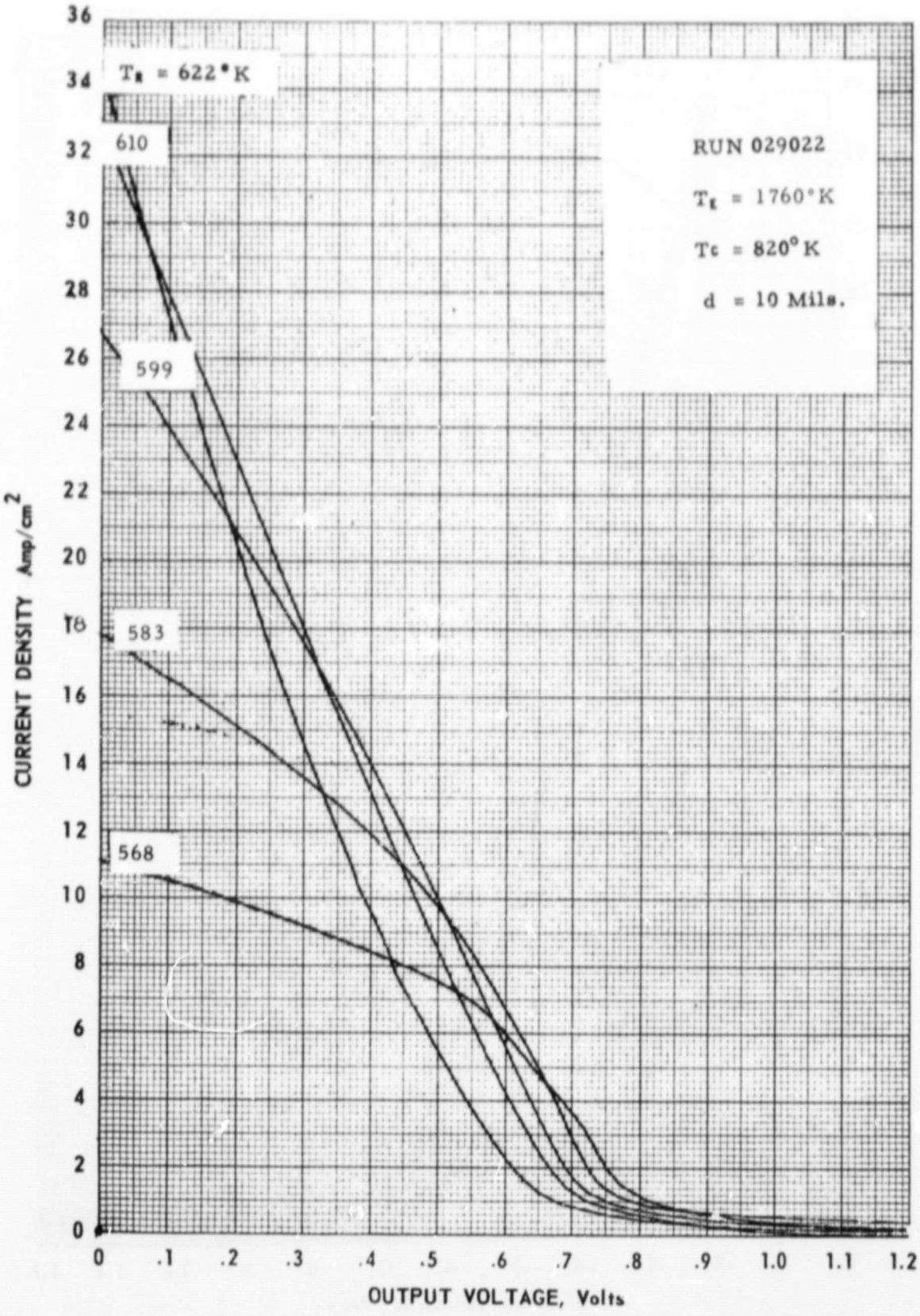


Figure III-8. Cesium-Temperature Family at T_E = 1760°K and d = 10 mils.

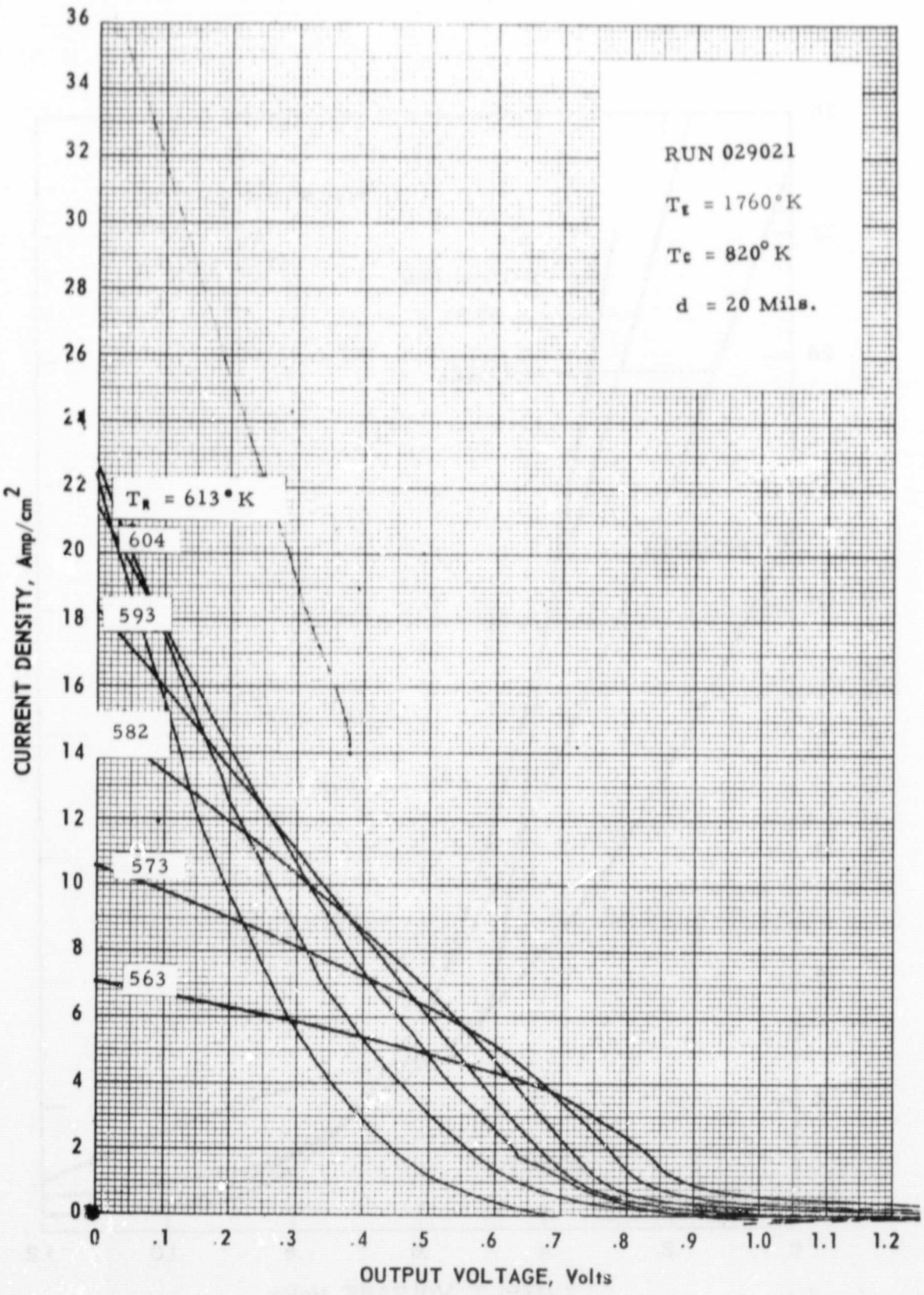


Figure III-9. Cesium-Temperature Family at T_E = 1760°K and d = 20 mils.

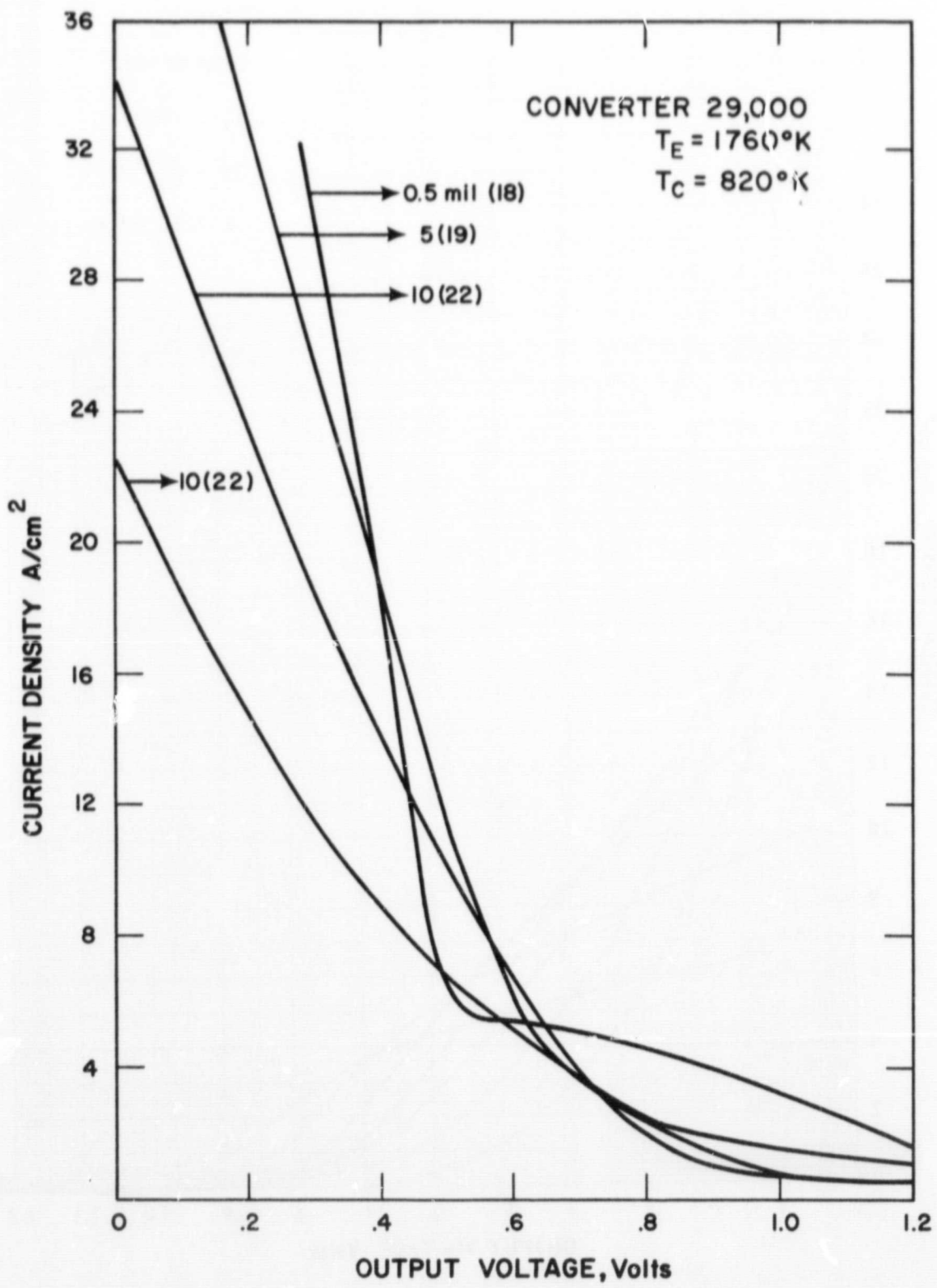


Figure III-10. Comparison of Cesium Optimized Envelopes at T_E = 1760°K for Several Interelectrode Spacings.

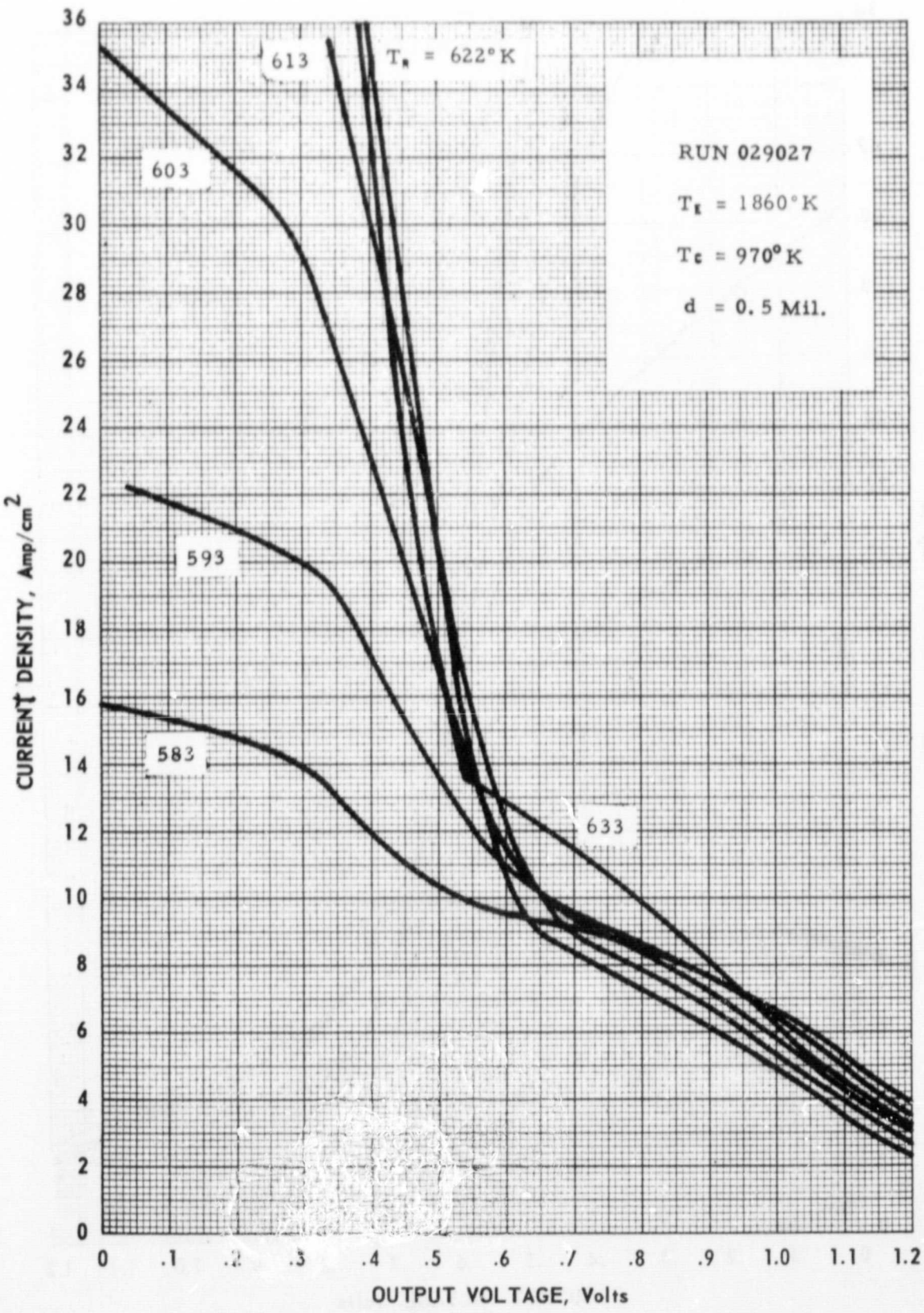


Figure III-11. Cesium-Temperature Family at T_E = 1860°K and d = 0.5 mil.

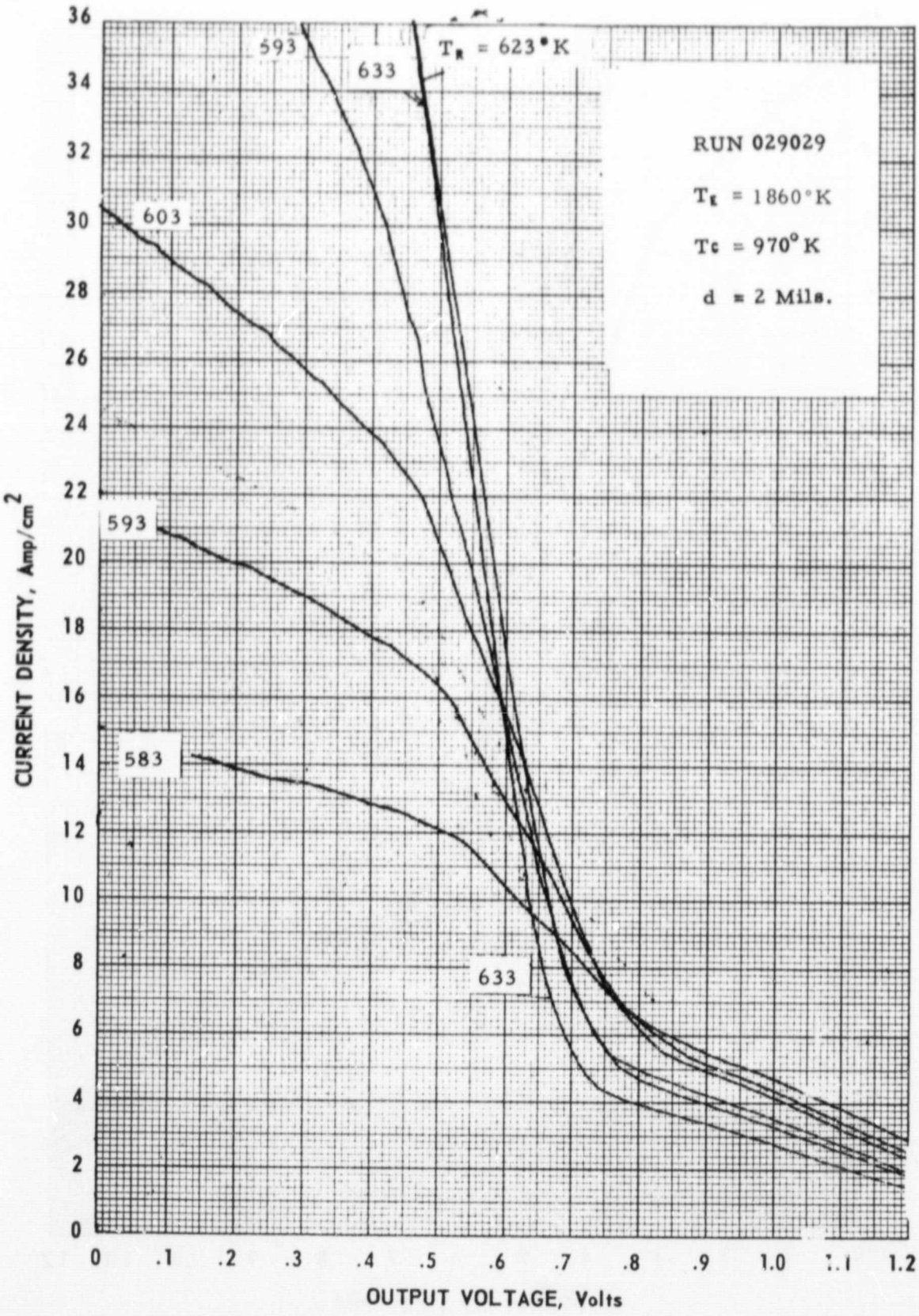


Figure III-12. Cesium-Temperature Family at T_E = 1860°K and d = 2 mils.

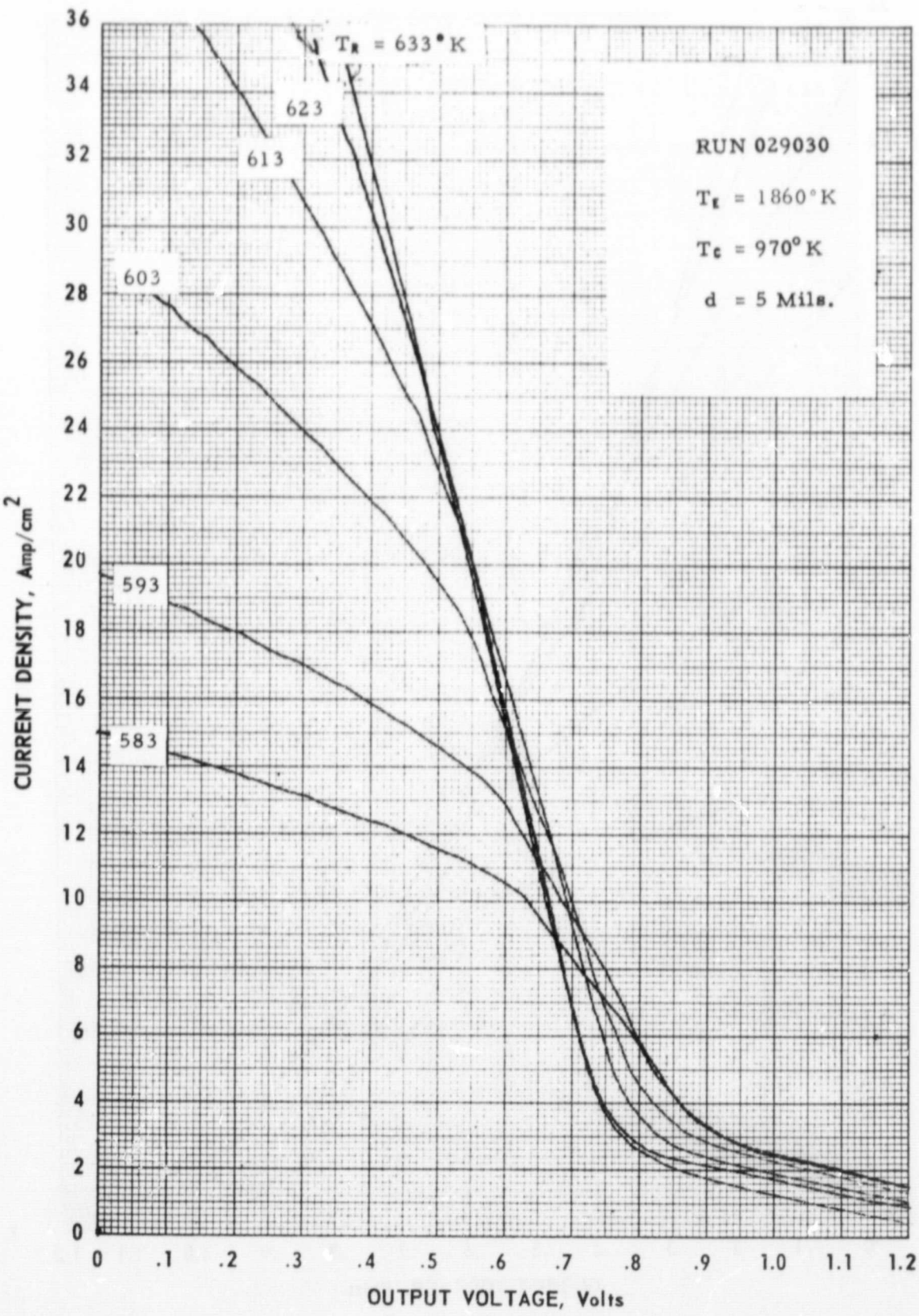


Figure III-13. Cesium Temperature Family at T_E = 1860°K and d = 5 mils.

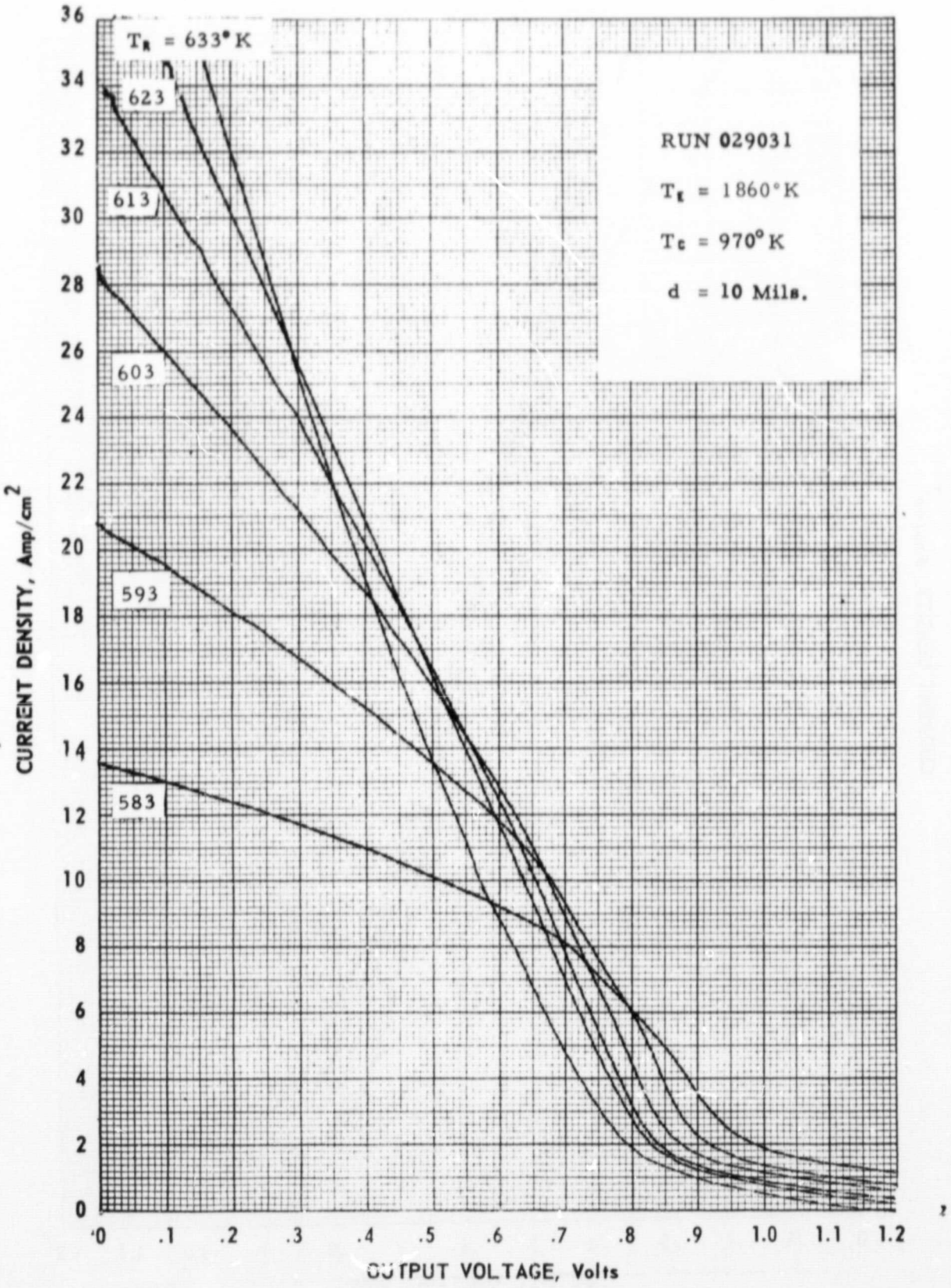


Figure III-14. Cesium Temperature Family at T_E = 1360°K and d = 10 mils.

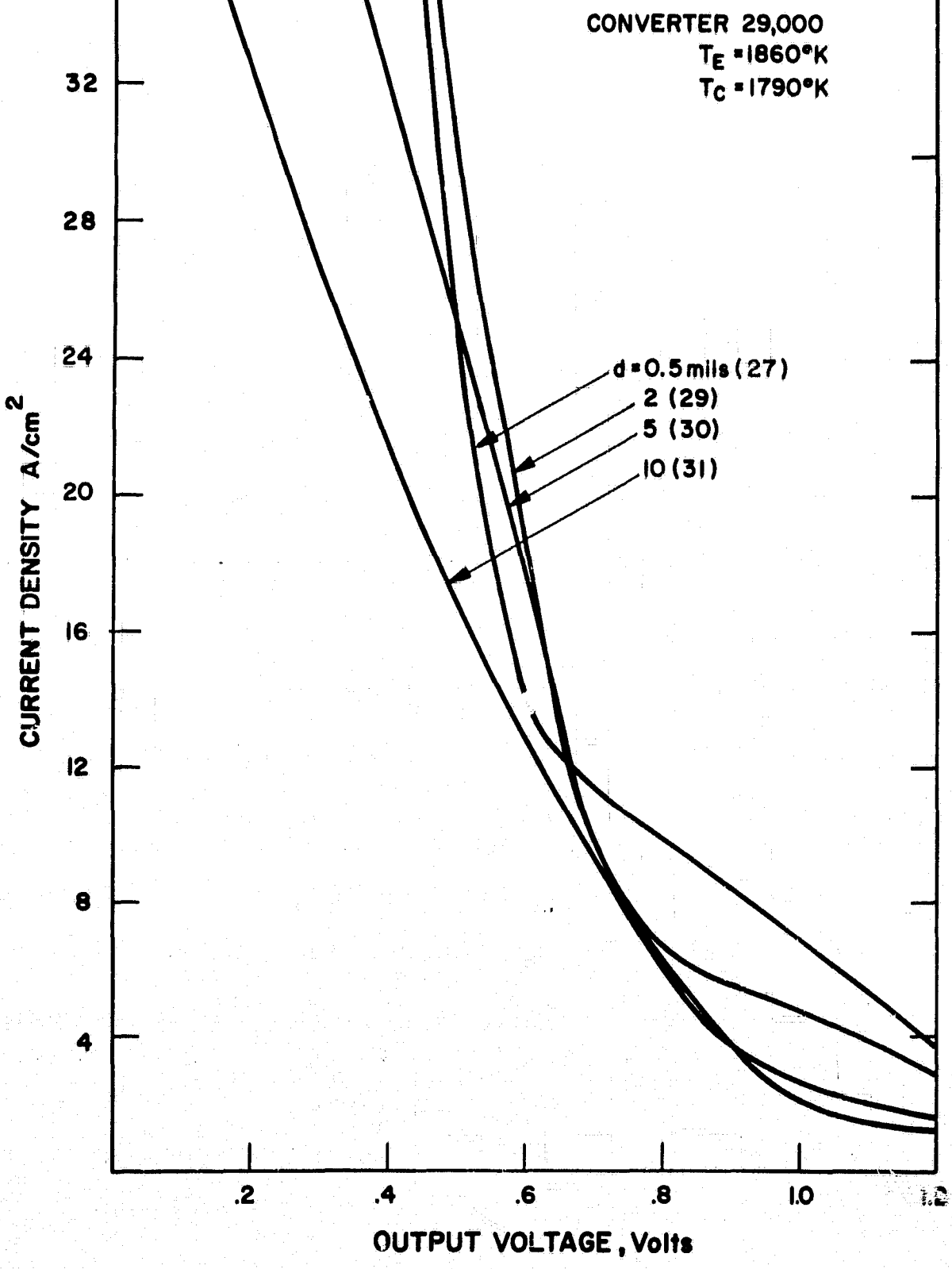


Figure III-15. Comparison of Cesium-Temperature Optimized Envelopes at T_E = 1860°K for Several Spacings.

The data from this converter can be compared with the data obtained previously[1] from a similar emitter and a molybdenum collector. Figure III-16 shows cesium-temperature envelopes for the two converters. These envelopes correspond to an emitter temperature of 1760°K and interelectrode spacings of 0.5, 5, 10, and 20 mils.

It can be seen from Figure III-16 that the curves from the two converters at equal spacings have the same slope. This indicates that the emitters of the two converters are similar, i.e., that the preparation of the emitters by means of electroetching and heat treatment is reproducible. There is no significant difference in the output voltage between envelopes of the same spacing. Therefore, the collector surfaces in these converters appear to have approximately the same work function characteristics. In the performance data obtained, optimum collector temperature for rhenium was about 100°K lower than that for molybdenum.

4. Work Function Data

The emitter work function was determined from the measured saturation current under ion-rich conditions. Data were obtained at emitter temperatures of 1560, 1660, 1760 and 1860°K for the cesium reservoir temperature range of 400 to 520°K. Typical original data are shown in Figure III-17. The computed work functions are plotted versus T_E/T_R in Figures III-18, III-19, III-20 and III-21, for T_E = 1560, 1660, 1760 and 1860°K, respectively. The scatter of the data is unusually low, especially at higher emitter temperature. The data from Figures III-18 through III-21 are superimposed in Figure III-22,

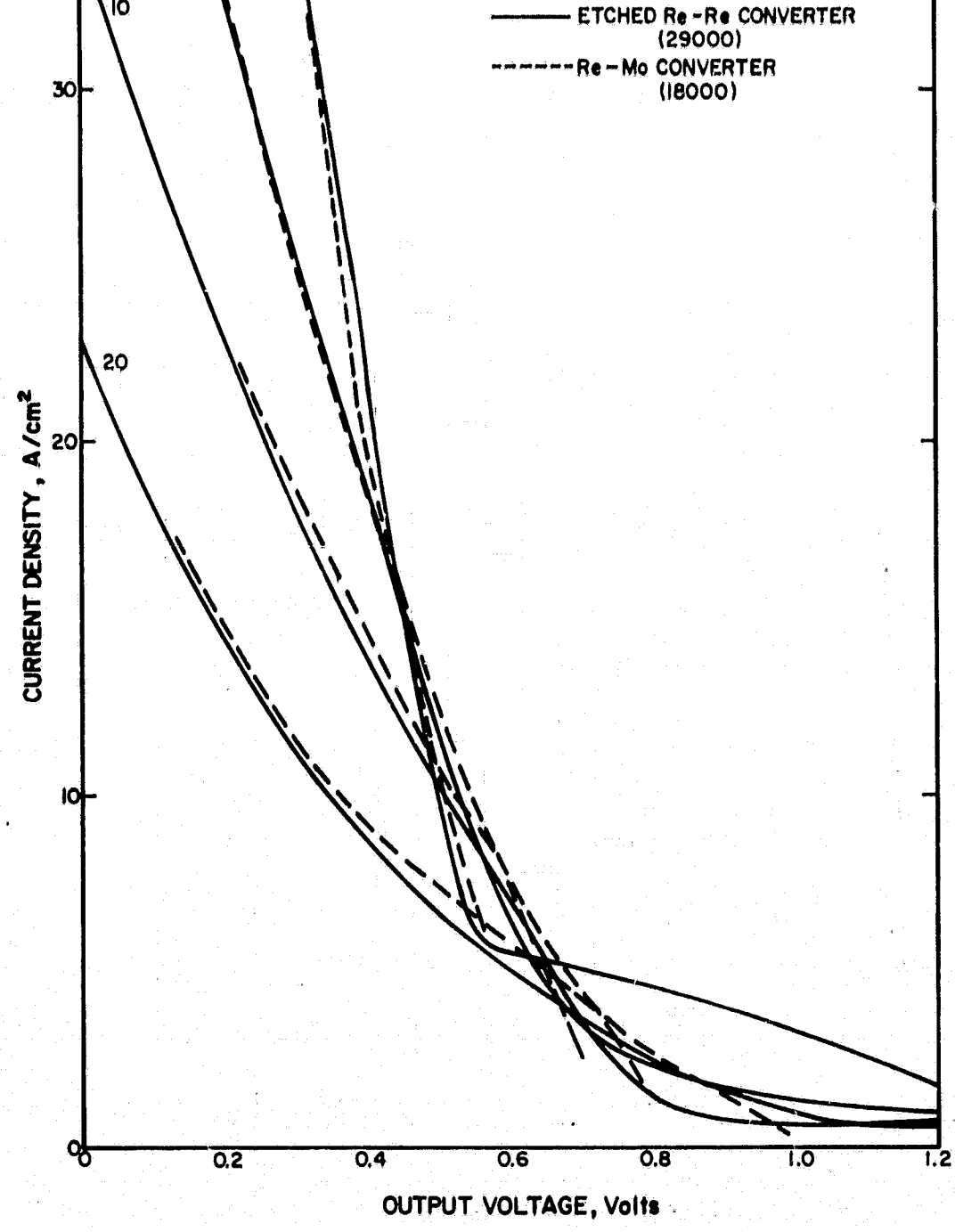


Figure III-16. Comparison of Cesium-Temperature Optimized Envelopes from the Present Rhenium-Rhenium Converter with those from a Rhenium-Molybdenum Converter.

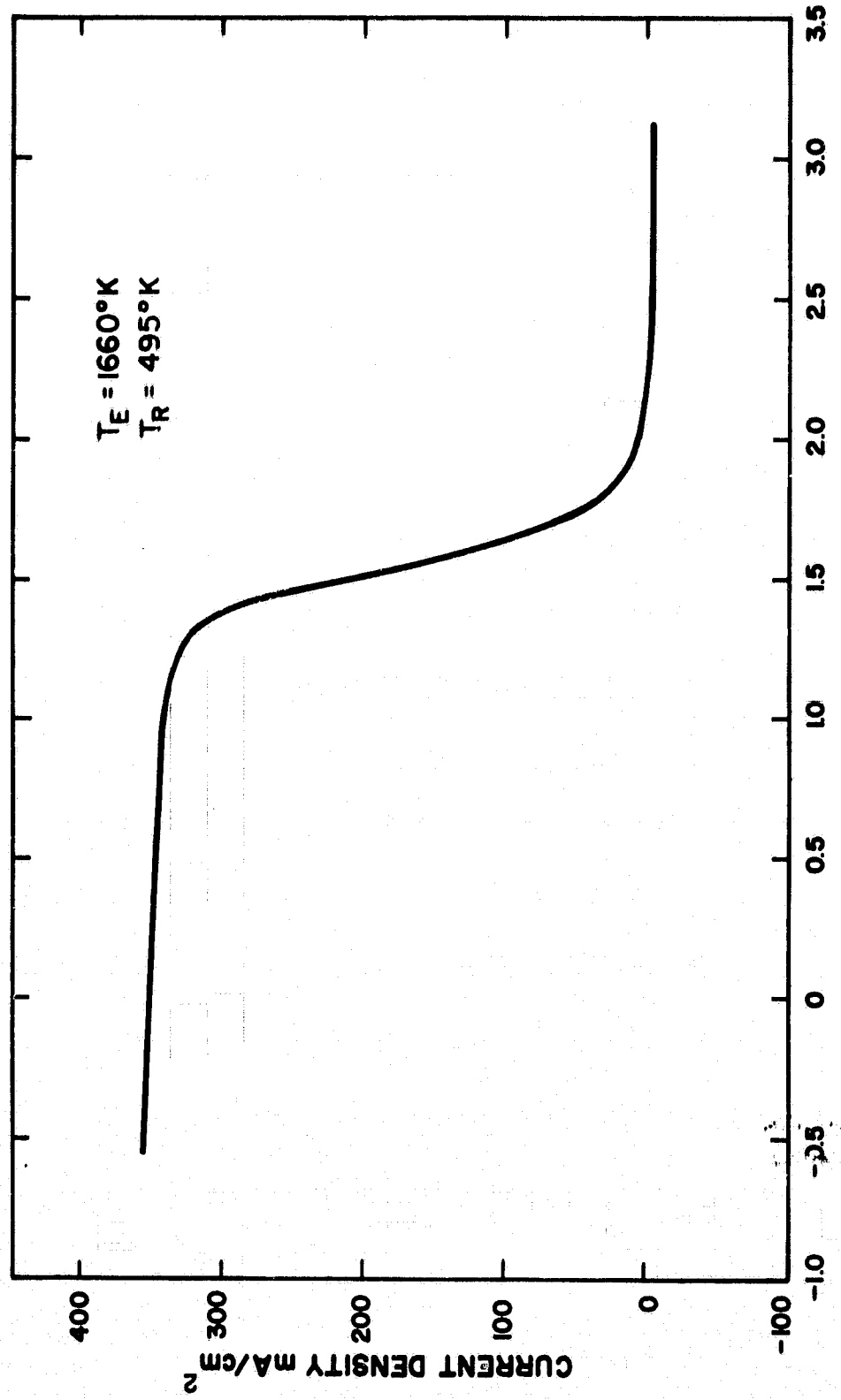


Figure III-17. Typical Original Data for Emitter Work Function Measurements.

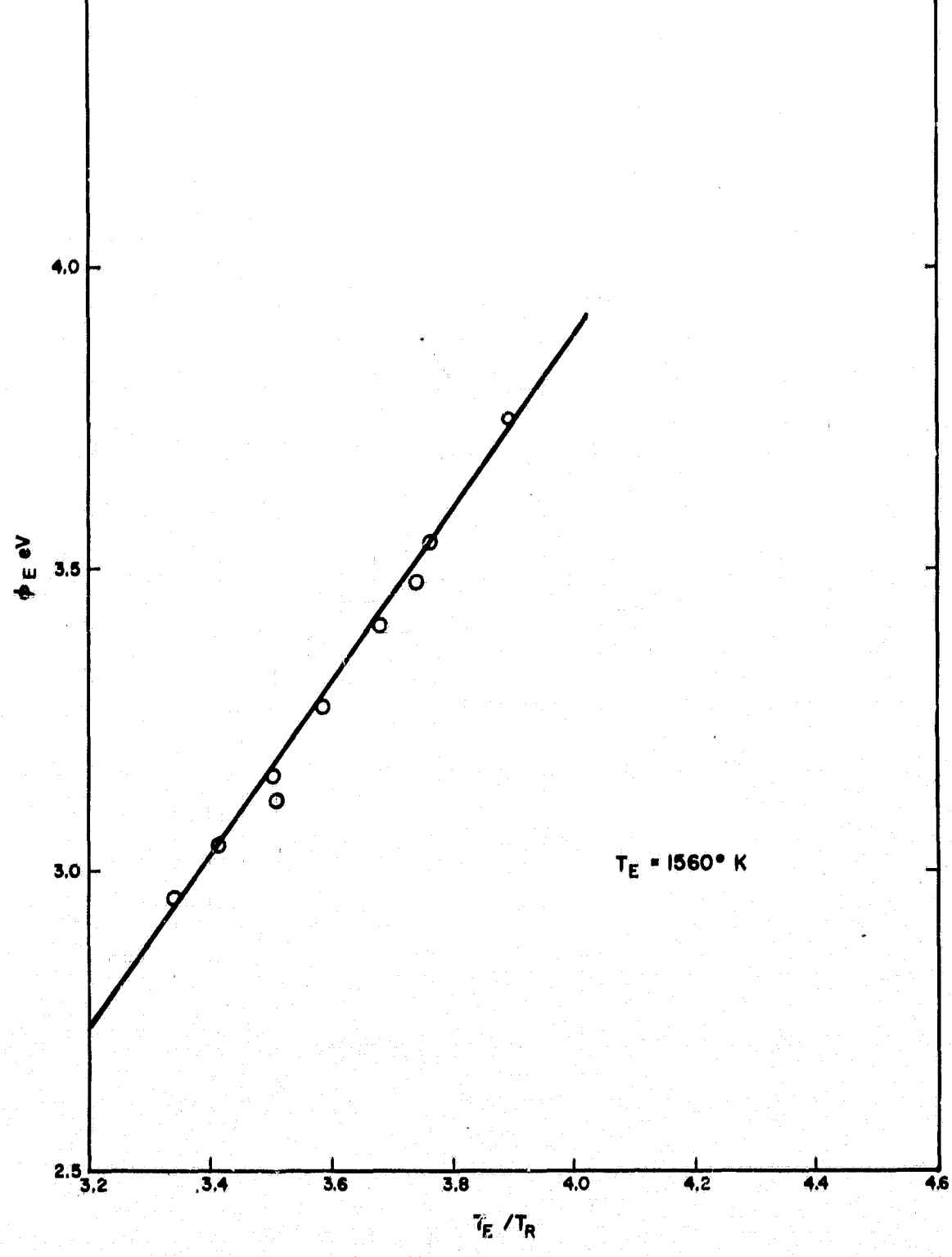


Figure III-18. Emitter Work Function Data at T_E = 1560°K.

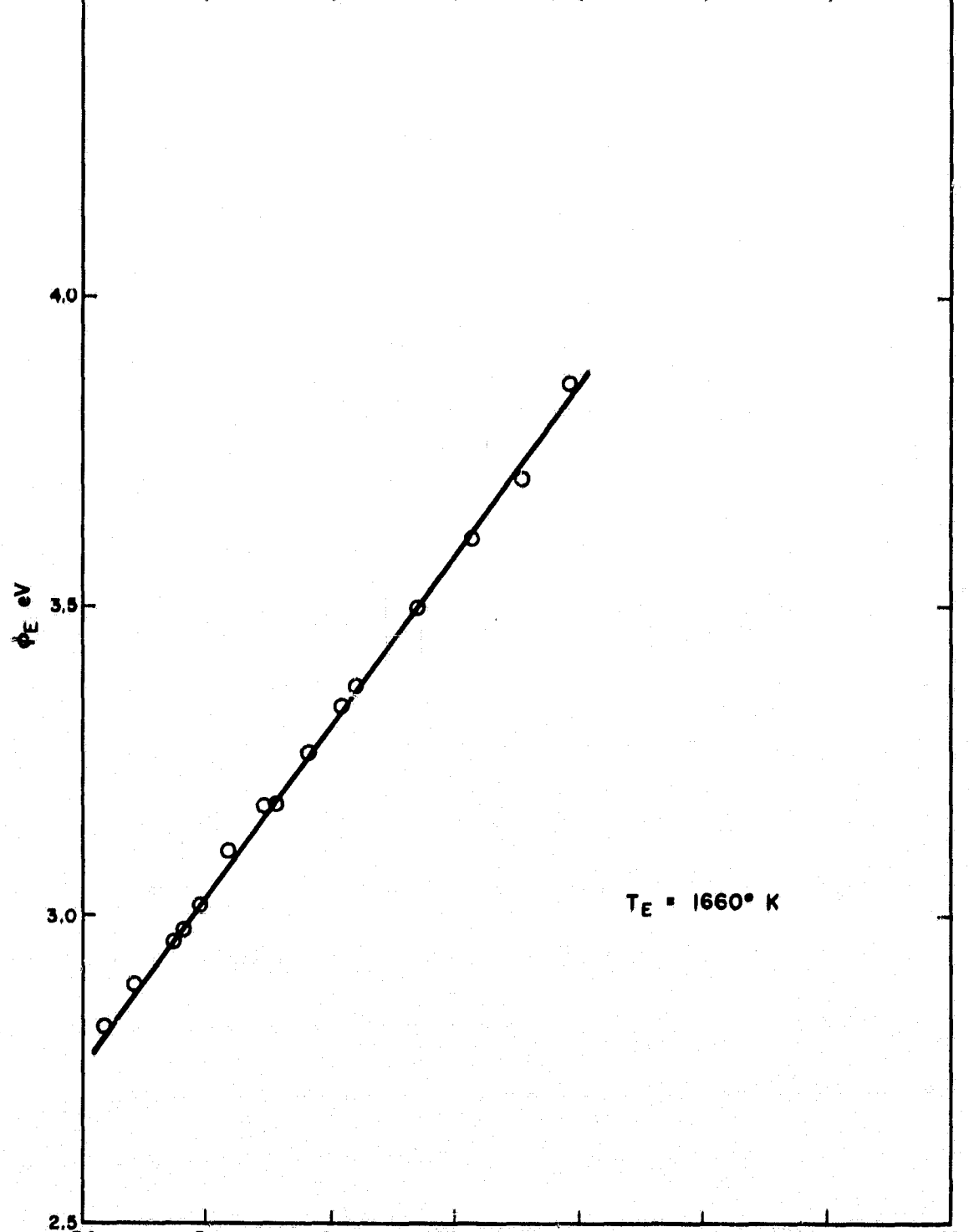


Figure III-19. Emitter Work Function Data at T_E = 1660°K.

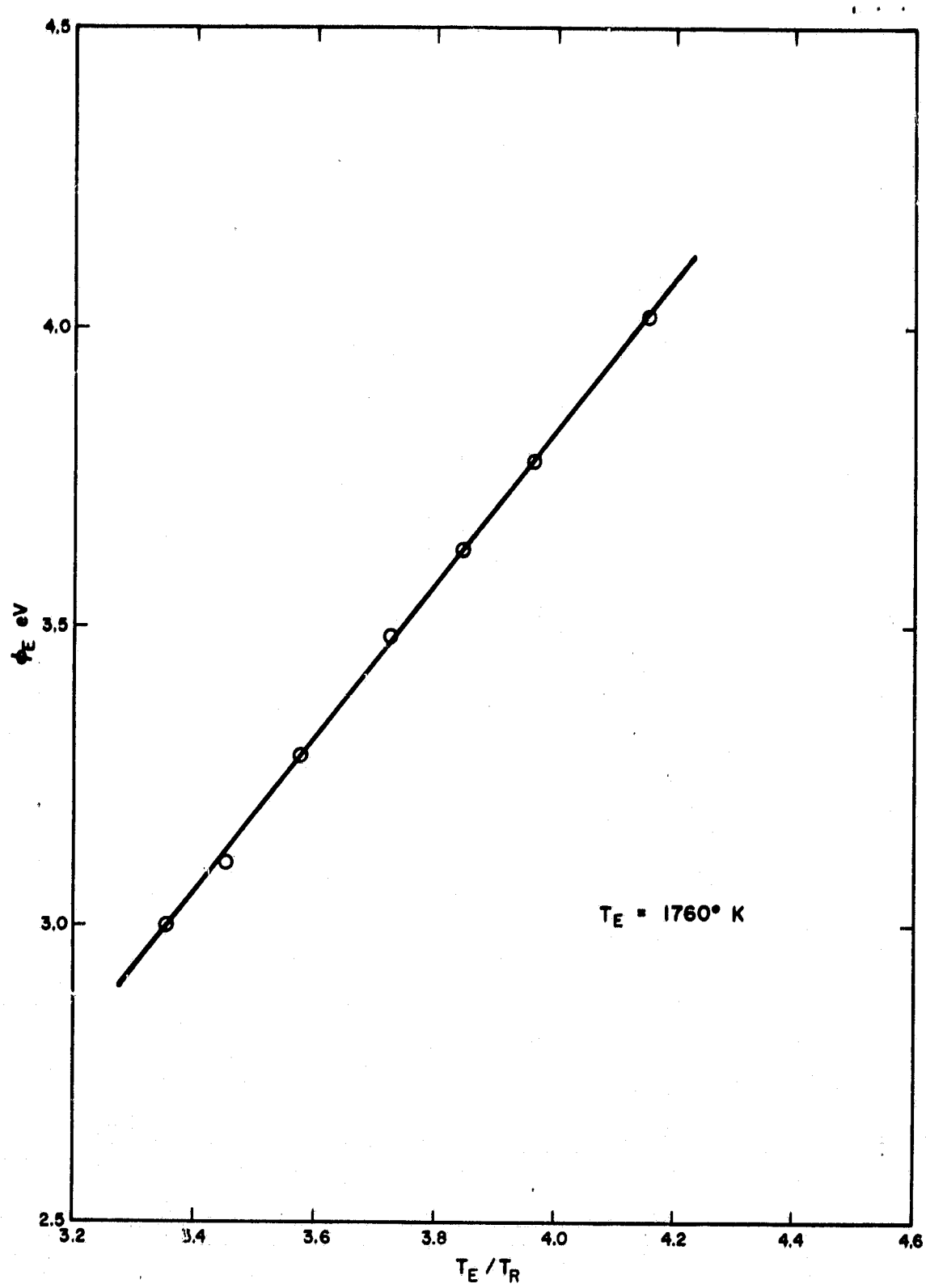


Figure III-20. Emitter Work Function Data at T_E = 1760°K.

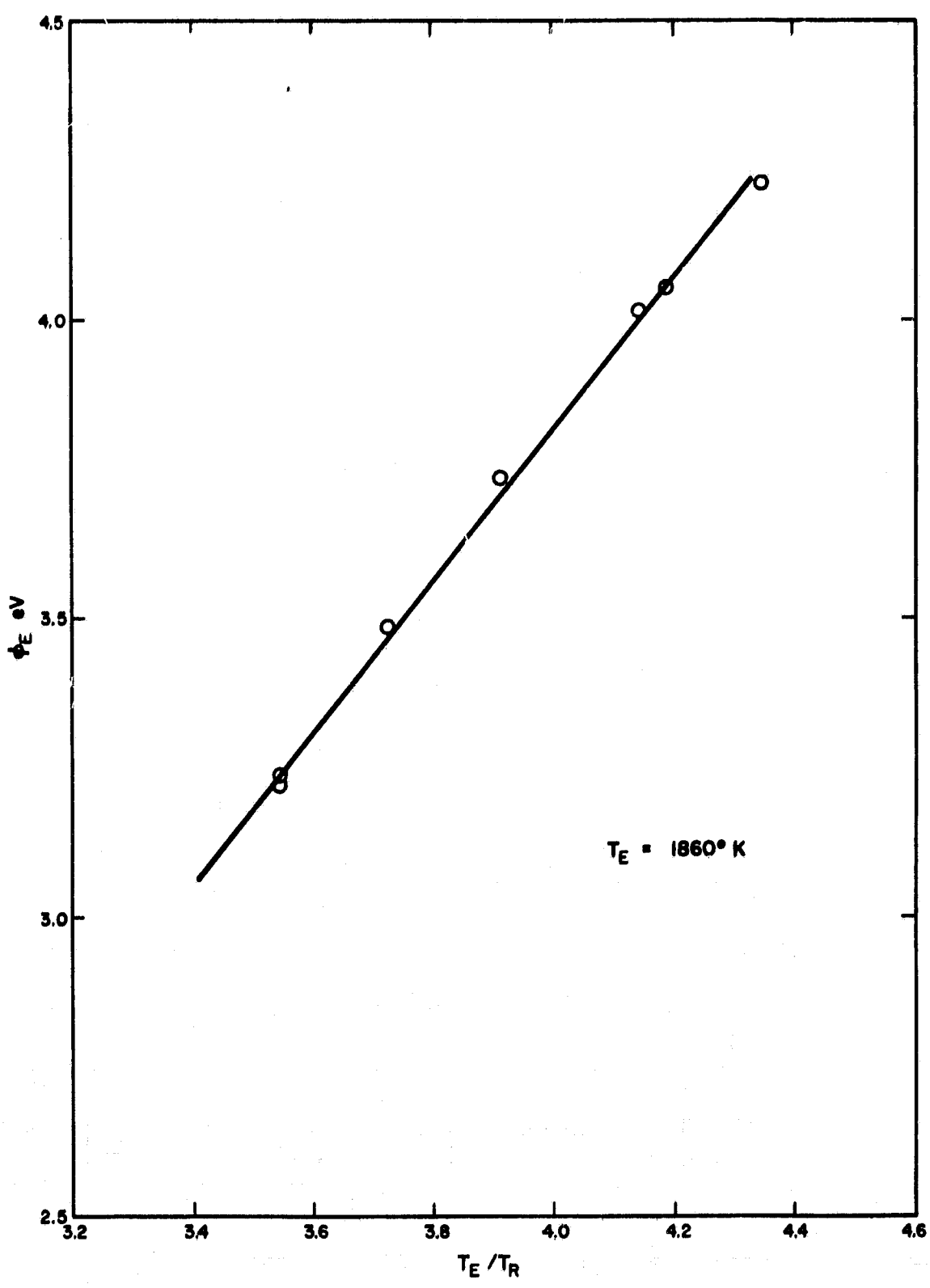


Figure III-21. Emitter Work Function Data at T_E = 1860°K.

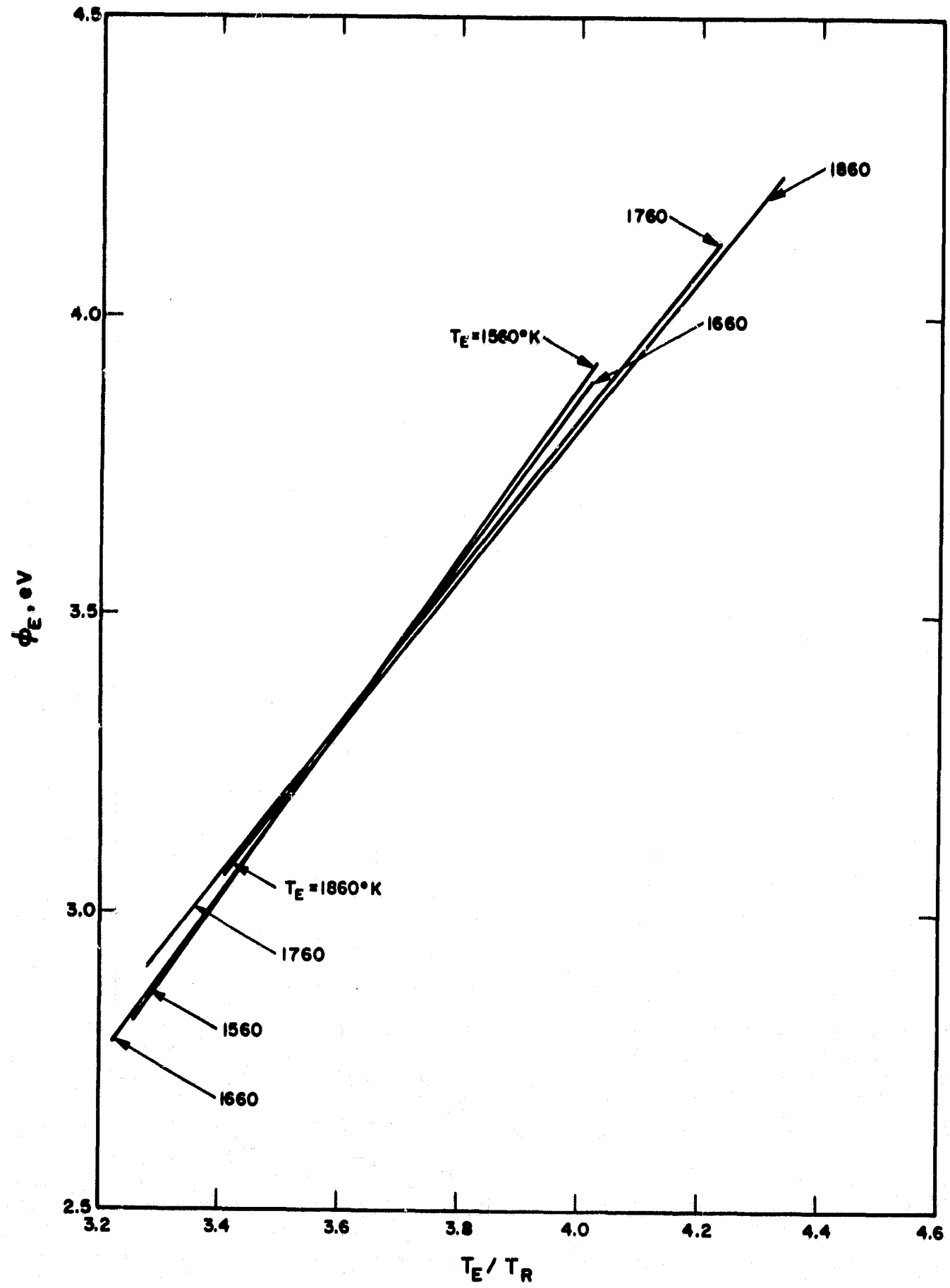


Figure III-22. Comparison of Emitter Work Function Data at Various Emitter Temperatures.

where it is seen that the work function has a small dependence on T_ℓ. In other words, the work function does not depend only on T_E/T_R.

A new correlation similar to the form given by Langmuir (The Collected Works of Irving Langmuir, Pergamon Press, Volume 3, page 390) was tried. φ_E was plotted versus kT_E lnP, where P is the pressure of cesium. This correlation is shown in Figure III-23 for the emitter temperatures of 1560, 1660, 1760 and 1860°K. Next φ_E was plotted versus kT_E ln (P/C) (Figure III-24), where $C = 3.6 \times 10^7$. The constant C is chosen in an attempt to obtain a universal relation between φ_E, T_E and P. The scatter in the data for this correlation is reduced, compared with the T_E/T_R correlation. The maximum scatter in the T_E/T_R correlation is about 0.10 eV, whereas in the kT_E lnP correlation it is about 0.05 eV (Figures IV-22 and IV-24).

5. Variable-Spacing Data

Families of volt-ampere characteristics were generated by varying the interelectrode spacing while all the other parameters were held constant. The cesium pressures and the emitter temperatures in these families were selected in such a way as to yield the volt-ampere characteristics at several values of cesium pressure for a given Pd and ion richness.

Figure III-25 summarizes the operating conditions of the variable-spacing data presented in Figures III-26 and III-32. Three variable-spacing families were obtained at the cesium pressures of 0.1. 0.4, and 0.8 torr (Figures III-26 to III-28). The emitter temperature in each case was chosen to maintain ion-rich conditions.

Two variable-spacing families were obtained under approximately neutral conditions at cesium pressures of 0.4 and 0.8 torr (Figures III-29 and III-30). Data were obtained under electron-rich conditions for cesium pressures of 1.6 and 3.2 torr (Figures III-31 and III-32). The interelectrode spacings in these data are 1.25, 2.5, 5, 10, 20, and 40, so that when they are coupled with cesium pressures of 0.1, 0.4, 0.8, . . . , they yield Pd values of . . . , 1, 2, 4, 8, ... From these families (Figures III-26 to III-32), many J-V curves are available for various combinations of P, Pd, d, and β, so that the effect of each parameter can be studied as the others are kept constant.

B. TUNGSTEN EMITTER

1. Introduction

In 1965, some preliminary results were reported from a converter using a specially prepared (110) single-crystal tungsten emitter.[3] The only two cesium families of volt-ampere characteristics obtained from this converter showed a significant improvement in performance over polycrystalline tungsten and rhenium. In this program an emitter was prepared using the same technique in order to investigate its performance and obtain parametric data.

2. Emitter Preparation

A single crystal of tungsten was obtained from the Linde Division of Union Carbide Corporation. This contained less than 10 ppm of any impurity and less than 30 ppm of total impurities.

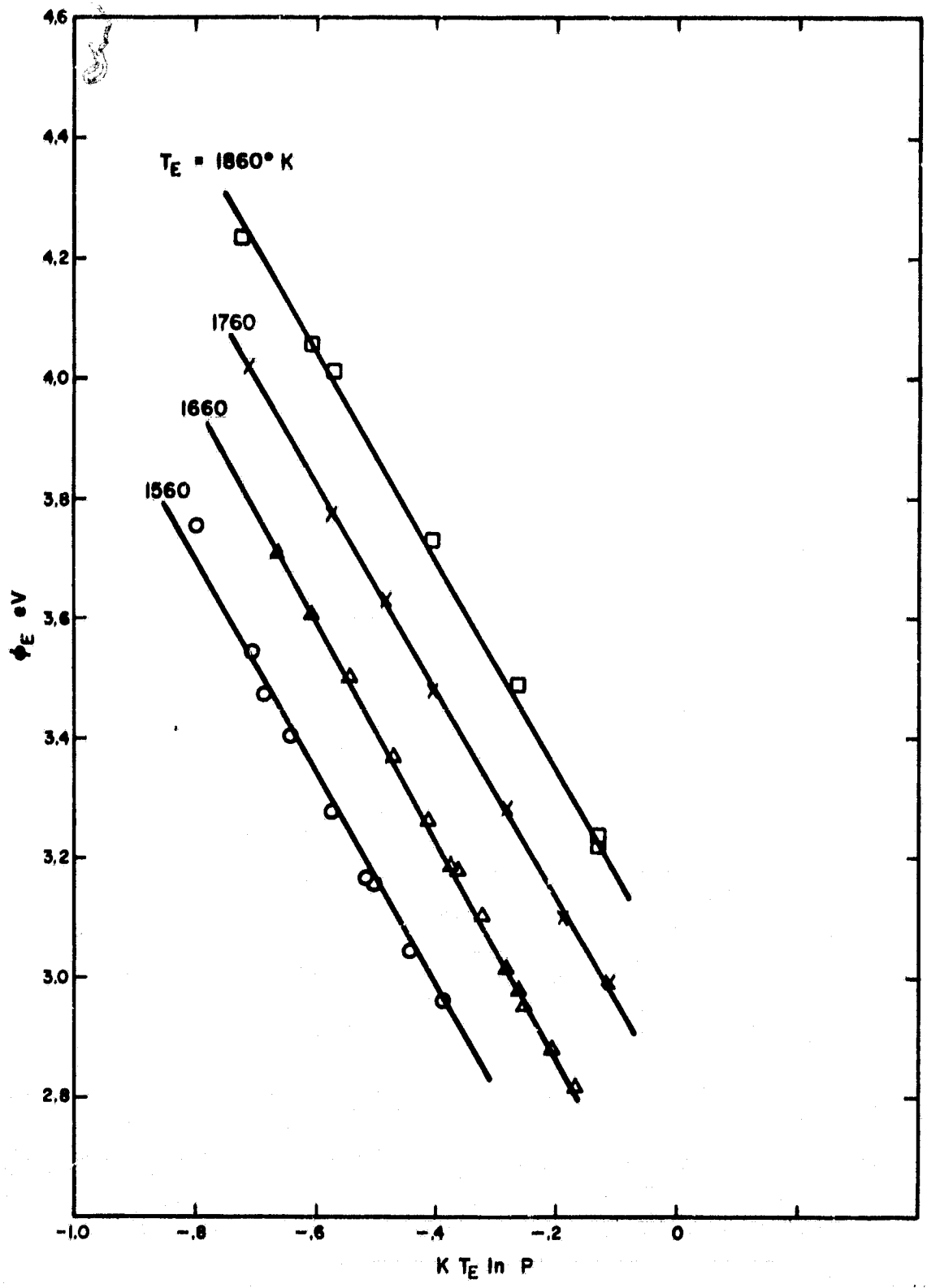


Figure III-23. An Alternate Plot of Emitter Work Function Data for Various Emitter Temperatures.

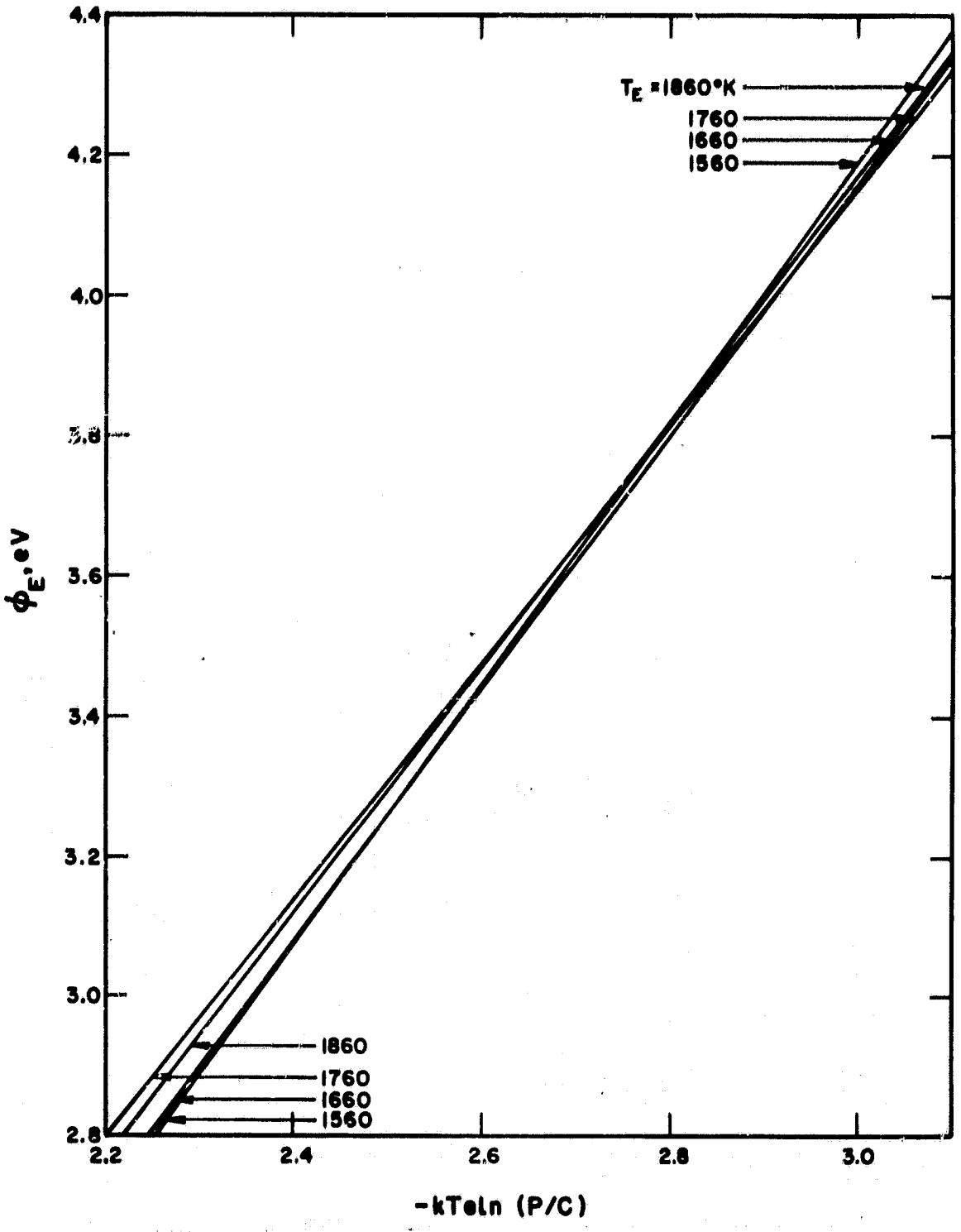


Figure III-24. An alternate Plot of Emitter Work Function Data for Various Emitter Temperatures.

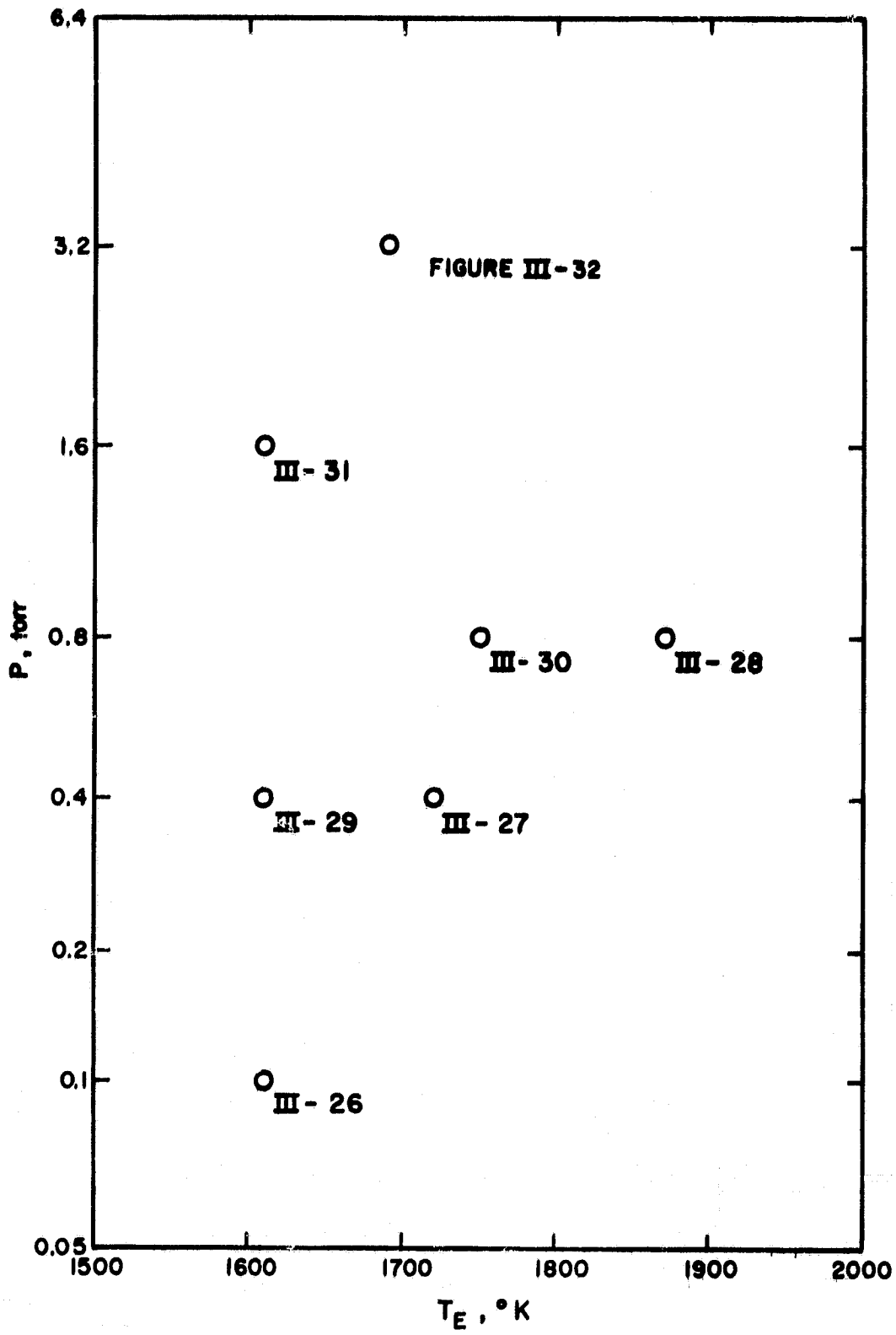


FIGURE III-32

Figure III-25. A Summary of the Operating Conditions under which Variable-Spacing Families were Obtained.

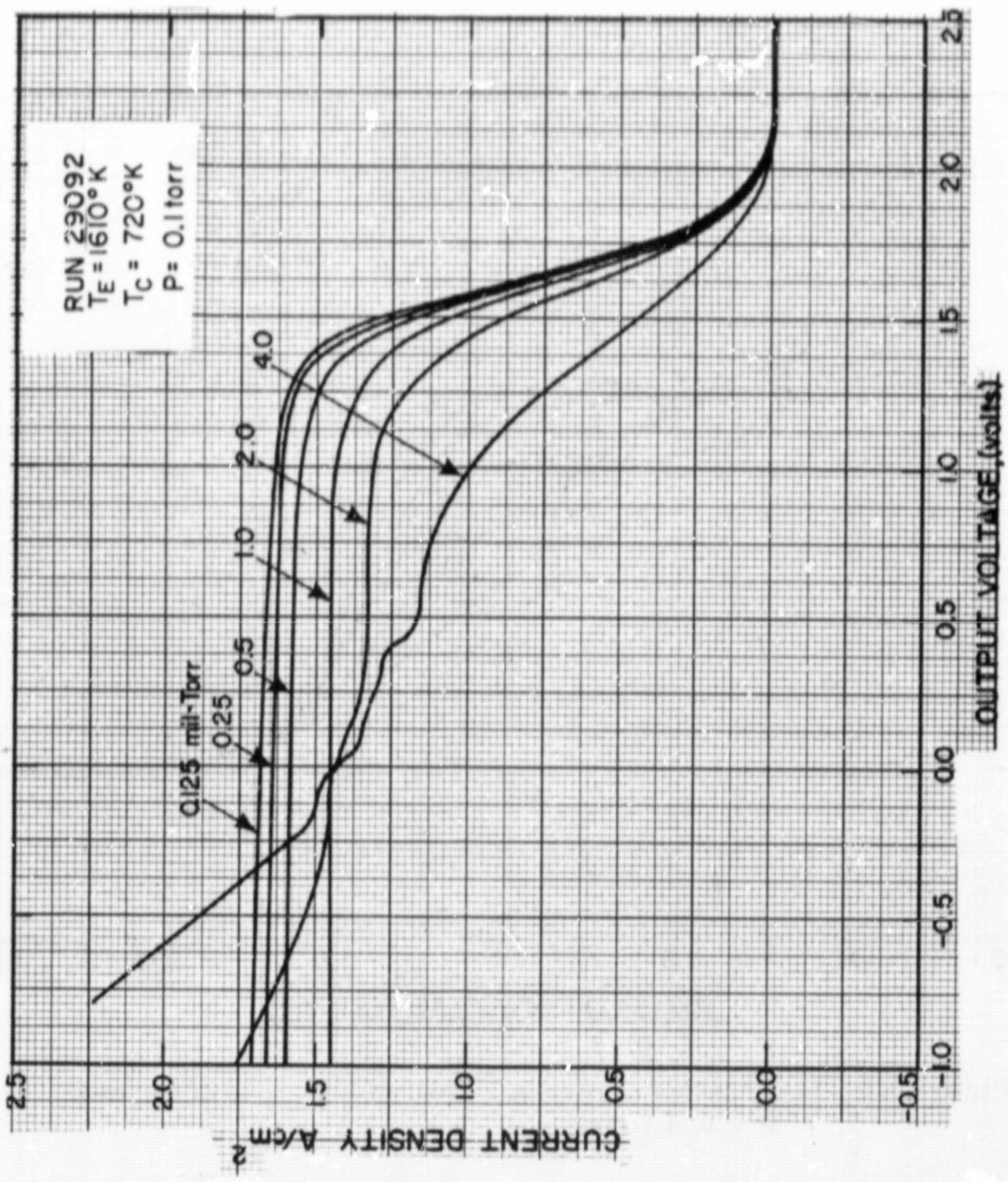


Figure III-26. Variable-Spacing Family at T_t = 1610°K and P = 0.1 torr.

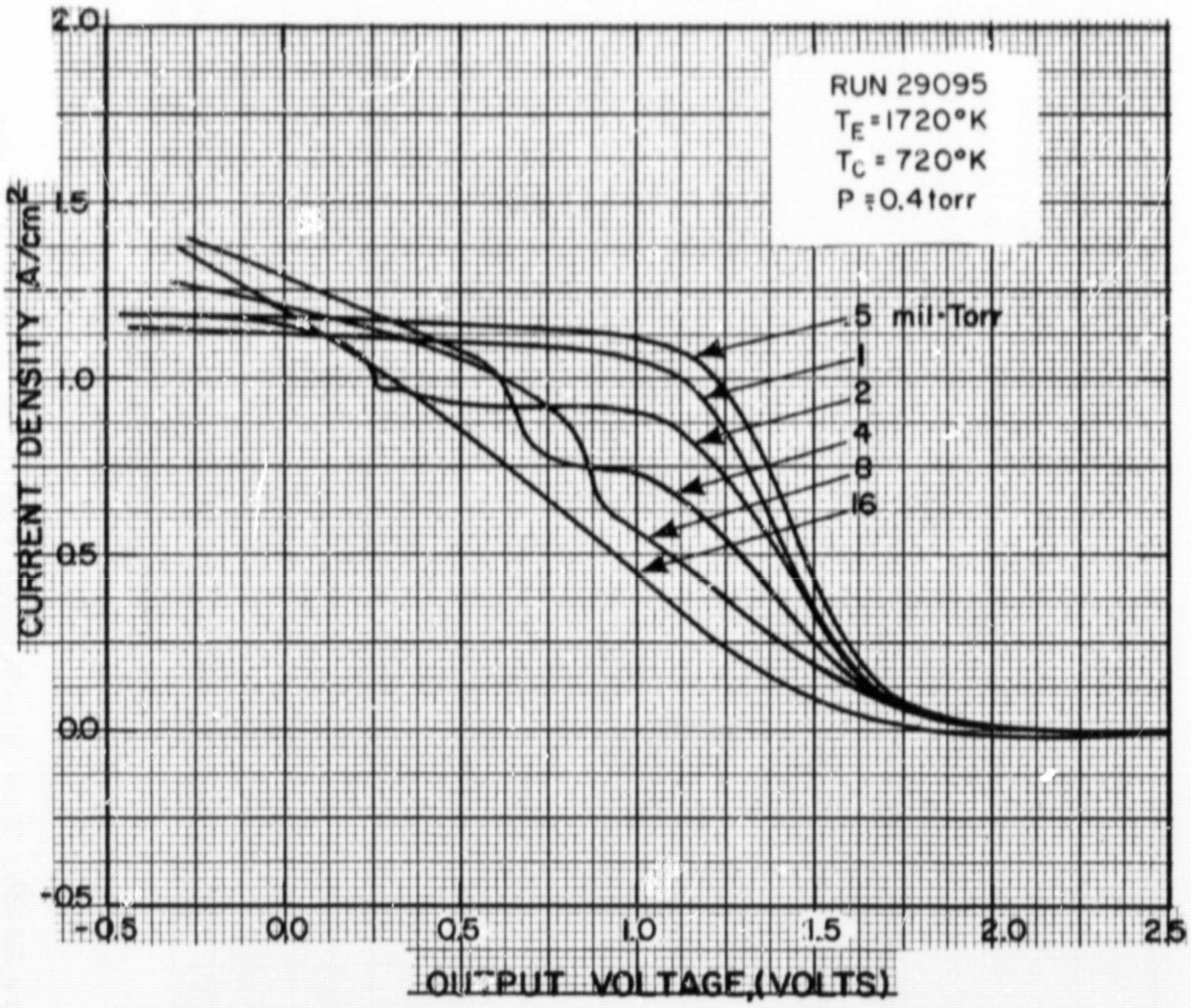


Figure III-27. Variable-Spacing Family at T_E = 1720°K and P = 0.4 torr.

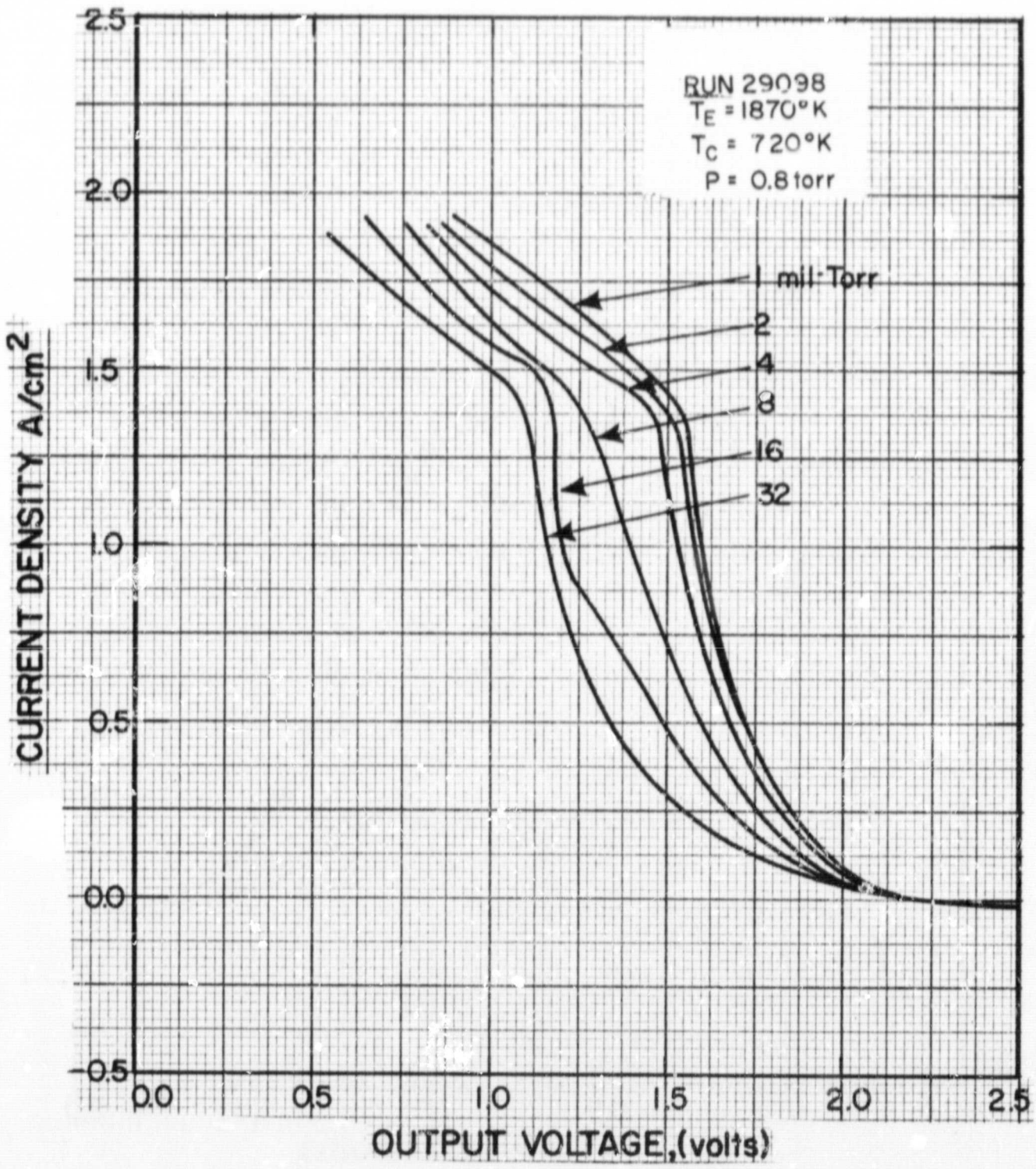


Figure III-28. Variable-Spacing Family at T_E = 1870°K and P = 0.8 torr.

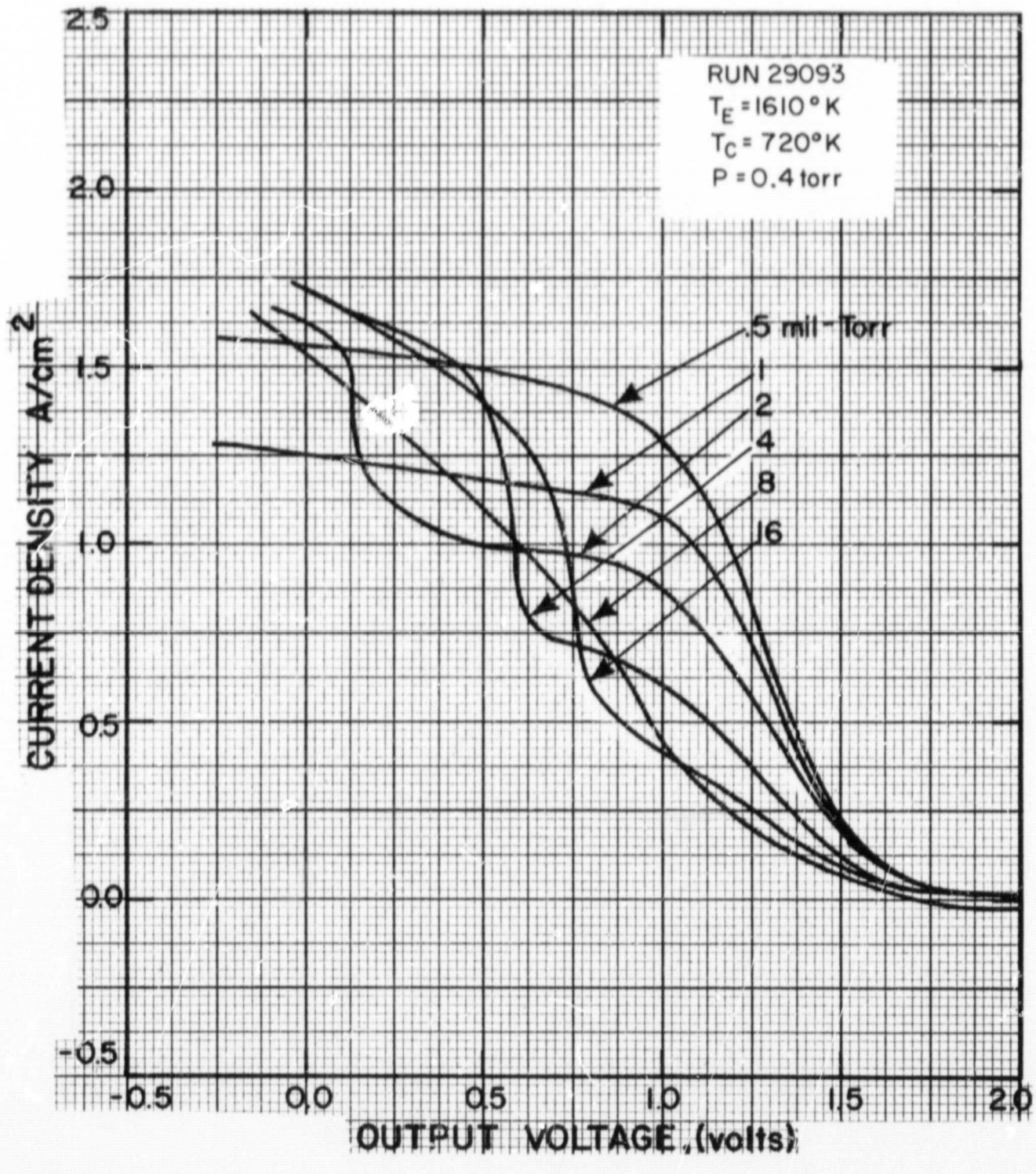


Figure III-29. Variable-Spacing Family at T_E = 1610°K and P = 0.4 torr.

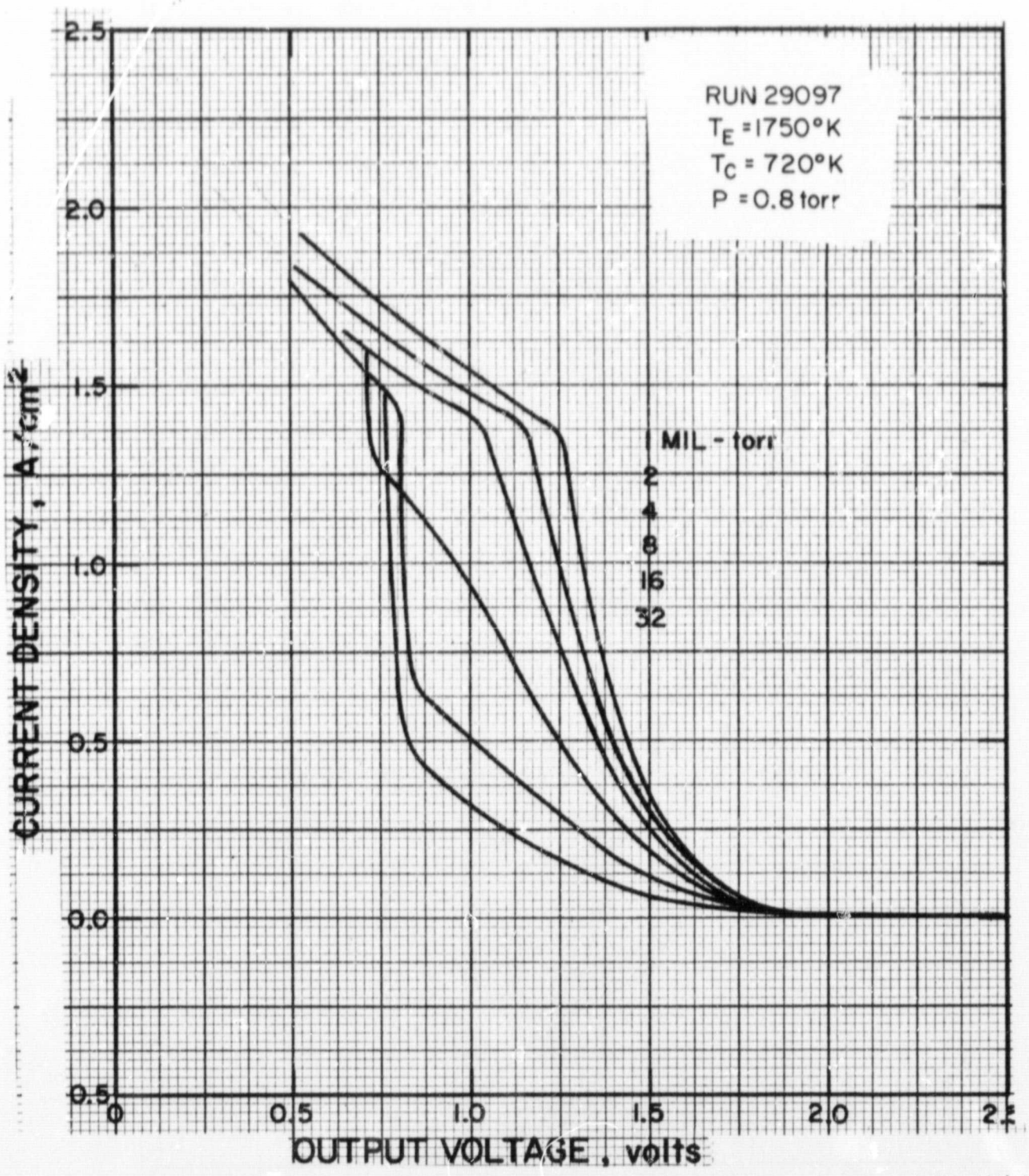


Figure III-30. Variable-Spacing Family at T_E = 1750°K and P = 0.8 torr.

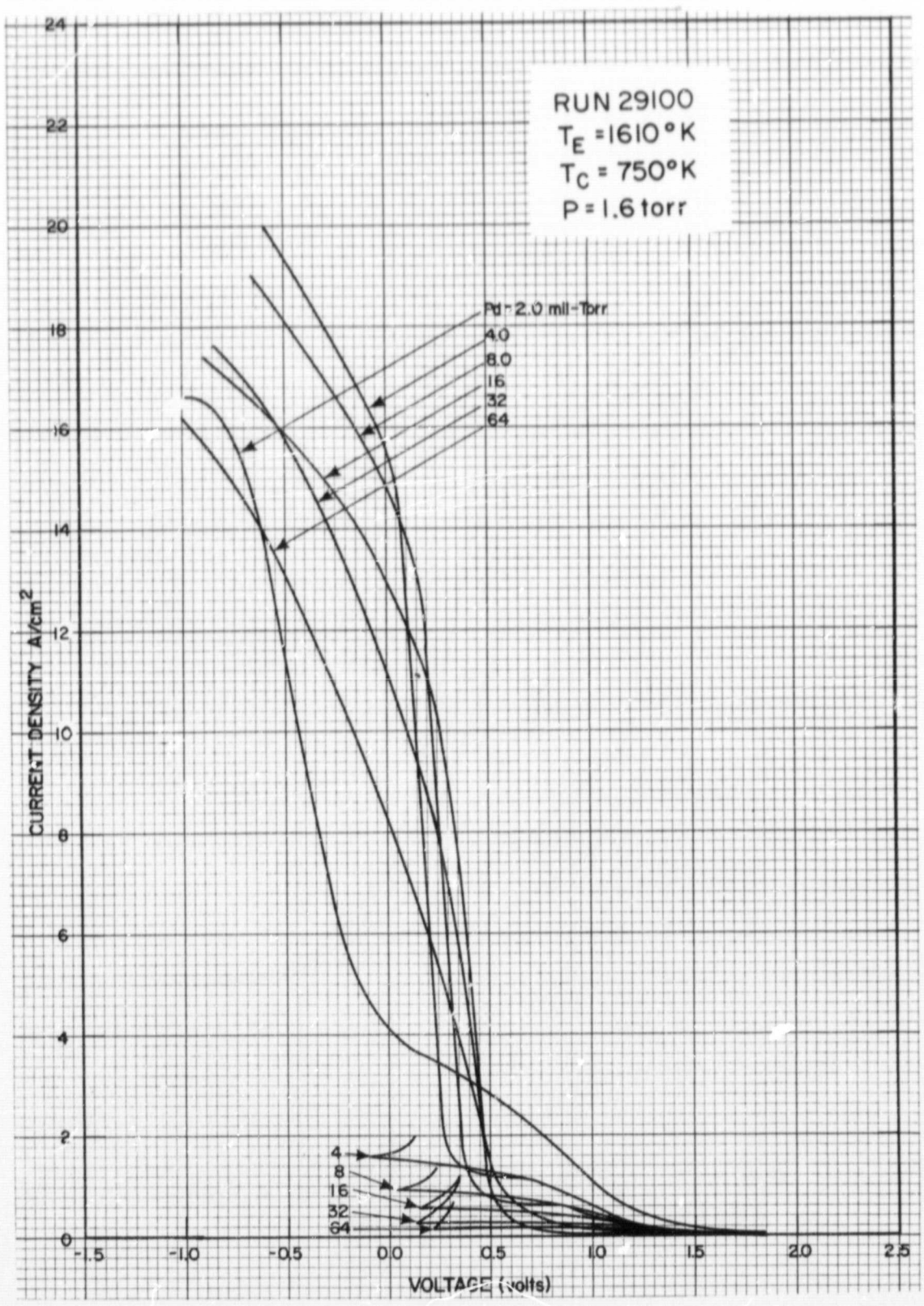


Figure III-31. Variable-Spacing Family at T_E = 1610°K and P = 1.6 torr. (Reduced in size.)

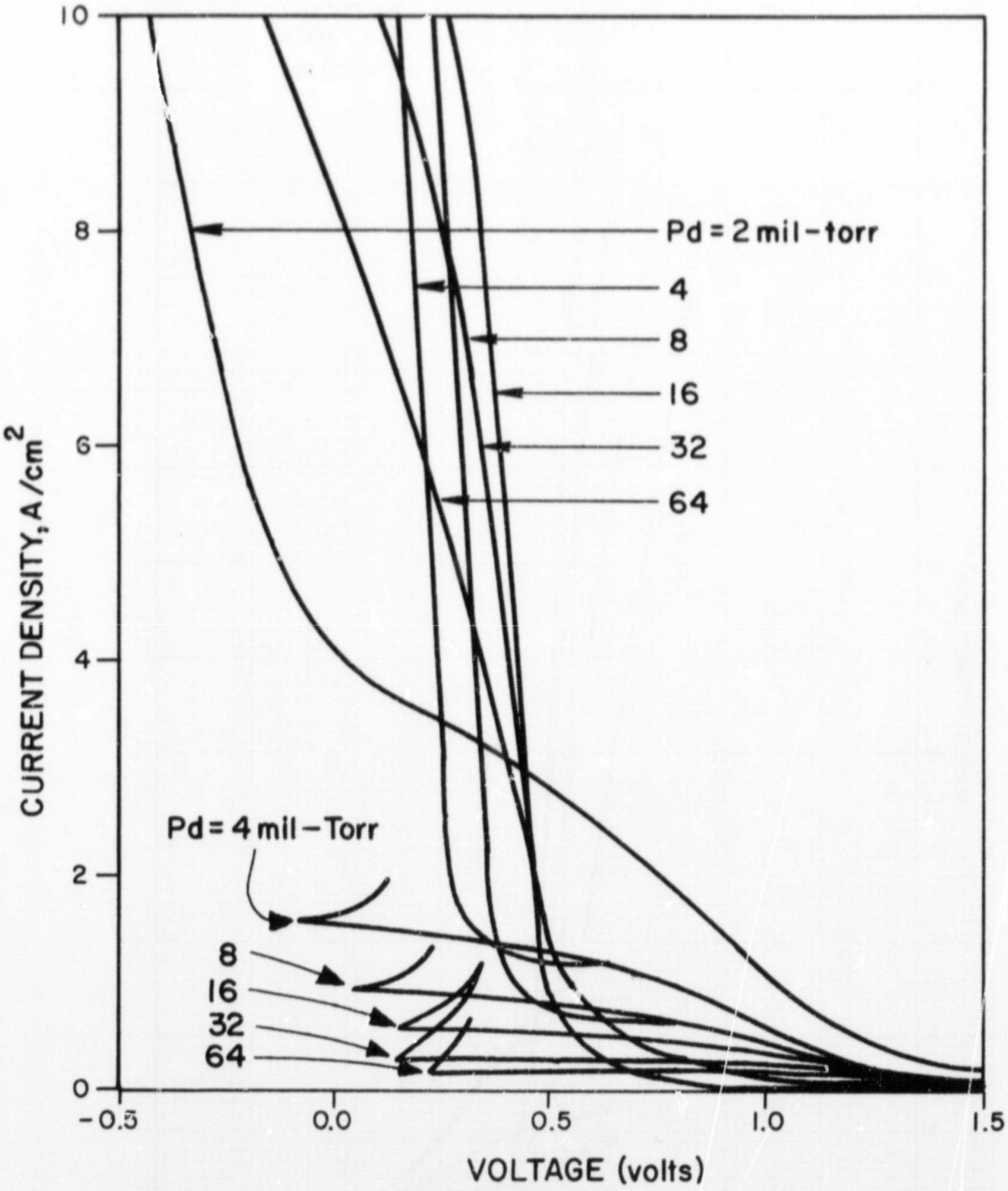


Figure III-31a. Variable-Spacing Family at T_E = 1610°K and P = 1.6 torr. (Not reduced.)

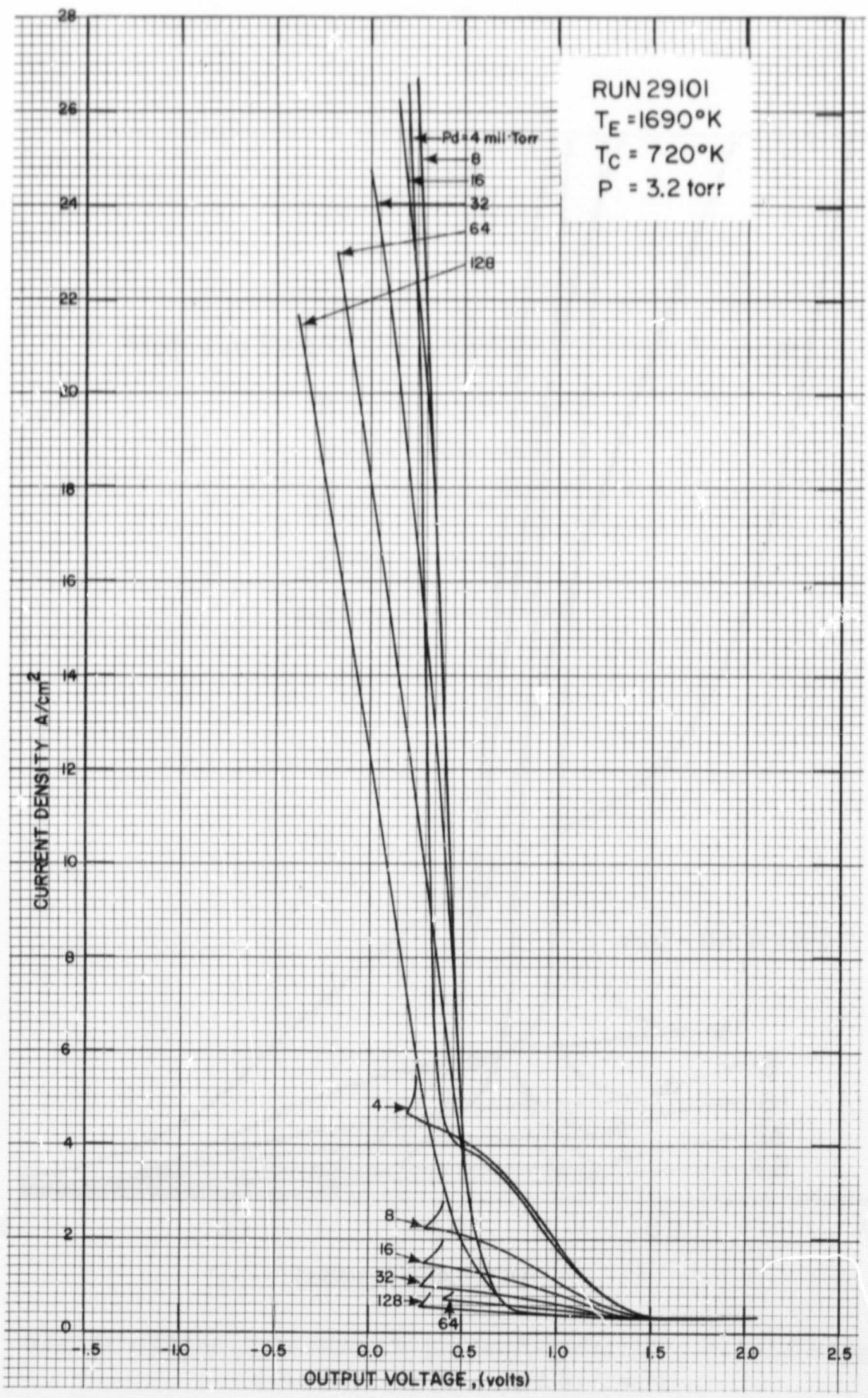


Figure III-32. Variable-Spacing Family at T_E = 1690°K and P = 3.2 torr. (Reduced in size.)

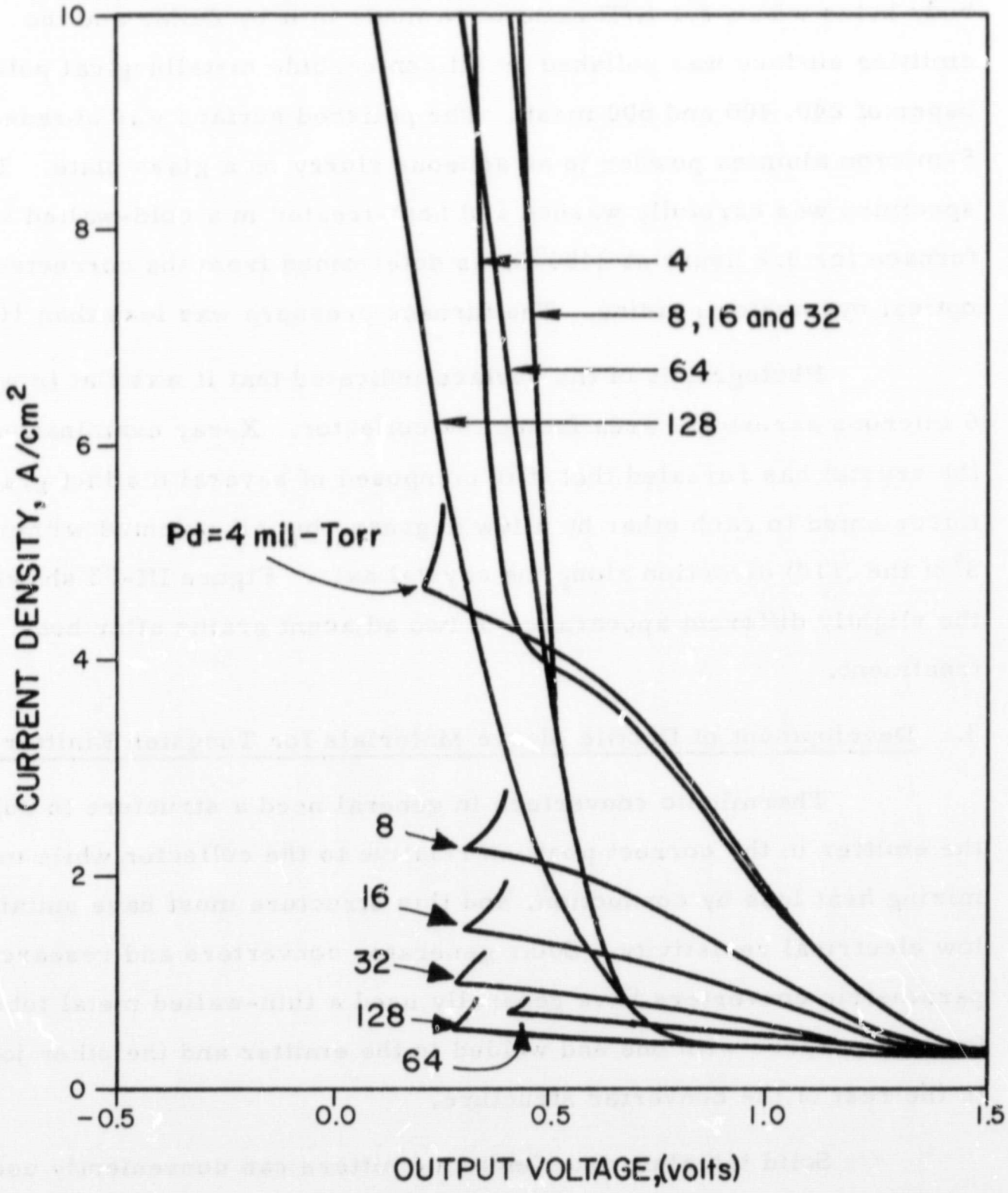


Figure III-32a. Variable-Spacing Family at T_E = 1690°K and P = 3.2 torr. (Not reduced.)

A slice was cut from the crystal by electrical-discharge machining (EDM), and ground to the correct thickness for the emitter. Black-body holes with a 5:1 L/D ratio were made in it by EDM, and the emitting surface was polished on silicon carbide metallurgical polishing paper of 240, 400 and 600 mesh. The polished surface was abraded with 5-micron alumina powder in an aqueous slurry on a glass plate. The specimen was carefully washed and heat-treated in a cold-walled vacuum furnace for 3.2 hours at 2450°C, as determined from the corrected optical pyrometer reading. The furnace pressure was less than 10^{-6} torr.

Photographs of the surface indicated that it was flat to within 6 microns across the area facing the collector. X-ray examination of the crystal has revealed that it is composed of several distinct grains misoriented to each other by a few degrees, but all oriented within 3° of the (110) direction along the crystal axis. Figure III-33 shows the slightly different appearance of two adjacent grains after heat treatment.

3. Development of Ductile Sleeve Materials for Tungsten Emitters

Thermionic converters in general need a structure to support the emitter in the correct position relative to the collector while minimizing heat loss by conduction, and this structure must have suitably low electrical resistivity. Solar generator converters and research parametric converters have generally used a thin-walled metal tube for this purpose with one end welded to the emitter and the other joined to the rest of the converter structure.

Solid tantalum and rhenium emitters can conveniently use thin-walled "sleeves" of the same element. A rhenium emitter can

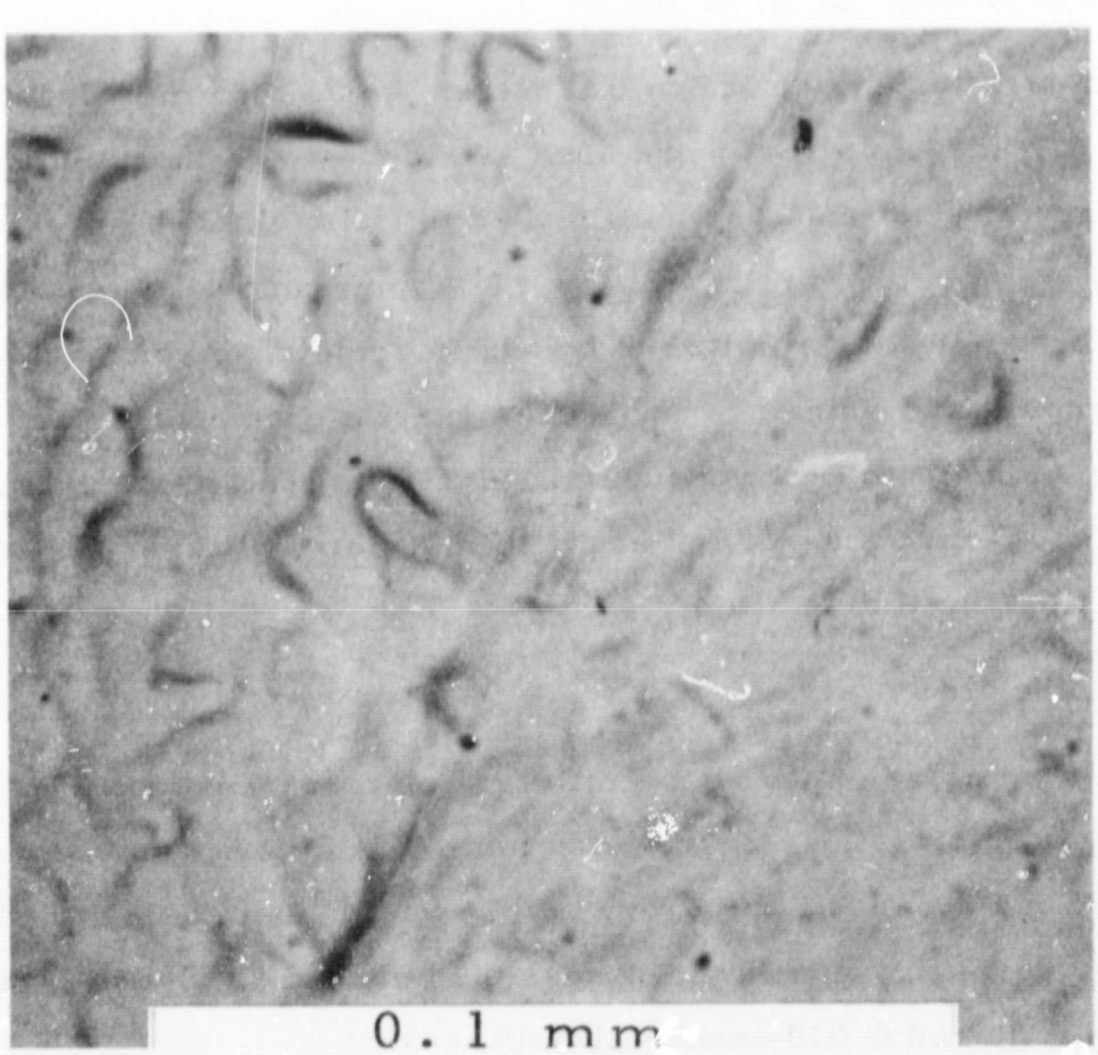


Figure III-33. Typical View of Grain Boundary Area of Emitter W-23.

also be hot-pressed to a tantalum substrate which is welded to a tantalum sleeve. Tungsten emitters pose a more difficult problem, for the hot end of the sleeve will recrystalize, so that a tungsten sleeve, if it could be fabricated, would be very brittle. The problem is aggravated by the great sensitivity of tungsten to contamination by interstitial elements, C, H, O and N.

In earlier work at Thermo Electron, tantalum, molybdenum, and TZM molybdenum alloys were used as sleeves with tungsten emitters. None of these was satisfactory; all tended to fail by brittle cracking where they were welded to the emitter. Rhenium cannot be used for sleeves because of the formation of brittle intermetallic compounds in welds between it and tungsten, but it does exert a pronounced ductilizing effect when alloyed with molybdenum or tungsten. The present work was carried out to devise sleeves for use with tungsten emitters, taking advantage of this ductilizing effect.

a. Materials

Three alloys made by two different methods were examined. Vapor-deposited tungsten - 26 wt% rhenium (W 26 Re) was obtained in tube form from San Fernando Laboratory. This was deposited on an 0.75-inch-diameter mandrel to a greater thickness than needed, and then ground down to the required 0.010-inch wall thickness.

Molybdenum - 50 wt% rhenium (Mo 50 Re) binary alloy and 30 wt% molybdenum - 30 wt% rhenium - 40 wt% tungsten (MoWRe) ternary alloy were obtained from Cleveland Refractory Metals, Inc., in the form of 0.020-in. sheet, rolled from powder metallurgy material. Sheets of these two materials were rolled into tube shapes of 0.75-in. diameter and

electron-beam welded to produce a longitudinal seam on each tube. At this point the tubes were helium leak-tight, except for an obvious weld defect on a section of the ternary alloy tube. Tubes were ground to 0.010-inch wall thickness.

b. Testing

Half-inch-long pieces were cut from the wrought and the vapor-deposited tubes, and were electron-beam welded to cylindrical tungsten slugs placed inside one end of each piece to simulate emitters. Each assembly was helium leak-tight. The assemblies were then subjected to seven rapid thermal cycles to 1880° C in vacuum, using rf induction heating. After this all assemblies were still leak-tight.

One W26Re assembly was subjected to manual destructive testing. The vapor-deposited sleeve was immediately cracked longitudinally. The sleeve material was clearly very brittle. The cracks were made to propagate along the sleeve to the weld, where they stopped. In contrast to the other materials examined, the weld zone was not more brittle than the sleeve material.

The MoRe and ternary wrought alloy assemblies were not mechanically tested after cycling. They were subjected to 200 hours of heating at 1880° C by electron-bombardment of the tungsten slugs, while the other ends of the sleeves stood on a molybdenum slab. This simulated the temperature gradients during operation. After this soaking, one sample of each material was tested destructively. The ternary MoWRe alloy specimen proved significantly stronger and more ductile than the W26Re above.

It distorted severely before any cracking occurred. The crack propagated readily around the weld zone under stress, but did not proceed ahead of the applied stress. The binary MoRe alloy sleeve proved even more difficult to rupture than the ternary; application of extreme force produced failure in the weld area. The sleeve itself was found to be more ductile than the ternary alloy sleeve. The weld zone where the binary alloy had fused to the tungsten presumably contained ternary alloys of various compositions.

The remaining sample assemblies of each wrought alloy were further soaked at 1800°C, the binary MoRe for a total of 781 hours, and the ternary MoWRe for a total of 300 hours. After this the grain structure in the weld zone of each specimen was fully recrystallized and showed considerable grain growth. The samples were again tested. Extensive force was needed to induce cracks in the binary alloy. The longitudinal cracks propagated through the hottest zone, near the weld, only with difficulty. When a crack reached the weld it travelled easily around the weld zone (see Figure III-34). The ternary alloy cracked more readily. It was clearly less ductile than the binary alloy, although cracks propagated less easily around the weld zone than in the binary specimen. Long soaking of W26Re sleeves indicated that they were at least as brittle after 220 hours and 550 hours at 1800°C as after welding.

It is concluded from these tests that the most suitable of the alloys tested (in the forms tested) for use as a sleeve to support a tungsten emitter is the binary Mo 50 wt% Re alloy. Such sleeves are now being used satisfactorily with tungsten emitters in converters.



Mo-Re Binary Alloy Sleeve
After 7 Cycles and 781 hrs.
At 1800 C

1 in.

Figure III-34. Mo-Re Binary Alloy Sleeve after 780 Hours at 1800 C and 7 cycles to Room Temperature.

They are brazed to the molybdenum emitter support flange, which operates below 1000° C. Such a sleeve was used successfully to incorporate a single-crystal tungsten emitter into the variable-spacing converter.

4. Variable-Spacing Converter

The basic design of the converter is similar to the rhenium-rhenium converter described in section A of this chapter. The collector and guard surfaces in this case are composed of two sheets of 20-mil tungsten which are brazed onto a molybdenum substrate.

5. Experimental Results

The emitter work function was measured under both ion-rich and electron-rich conditions. Typical data for the ion-rich condition are shown in Figure III-35, and for the electron-rich condition in Figure III-36. In Figure III-37 the reduced data are plotted as a function of T_E / T_R and show that the two measurements are in good agreement.

Families of volt-ampere characteristics were generated by varying the cesium reservoir temperature while the other parameters were held constant. Figures III-38 through III-43 show families of volt-ampere characteristics at T_E = 1560°K, for the interelectrode spacing range of 0.5 to 40 mils. The optimum collector temperature was 870°K. Each family defines an envelope representing the optimized performance with respect to cesium reservoir and collector temperatures. All the cesium optimized envelopes at T_E = 1560°K are shown in Figure III-44. These envelopes determine the optimized performance with respect to interelectrode spacing, cesium reservoir temperature and collector temperature. The cesium-temperature

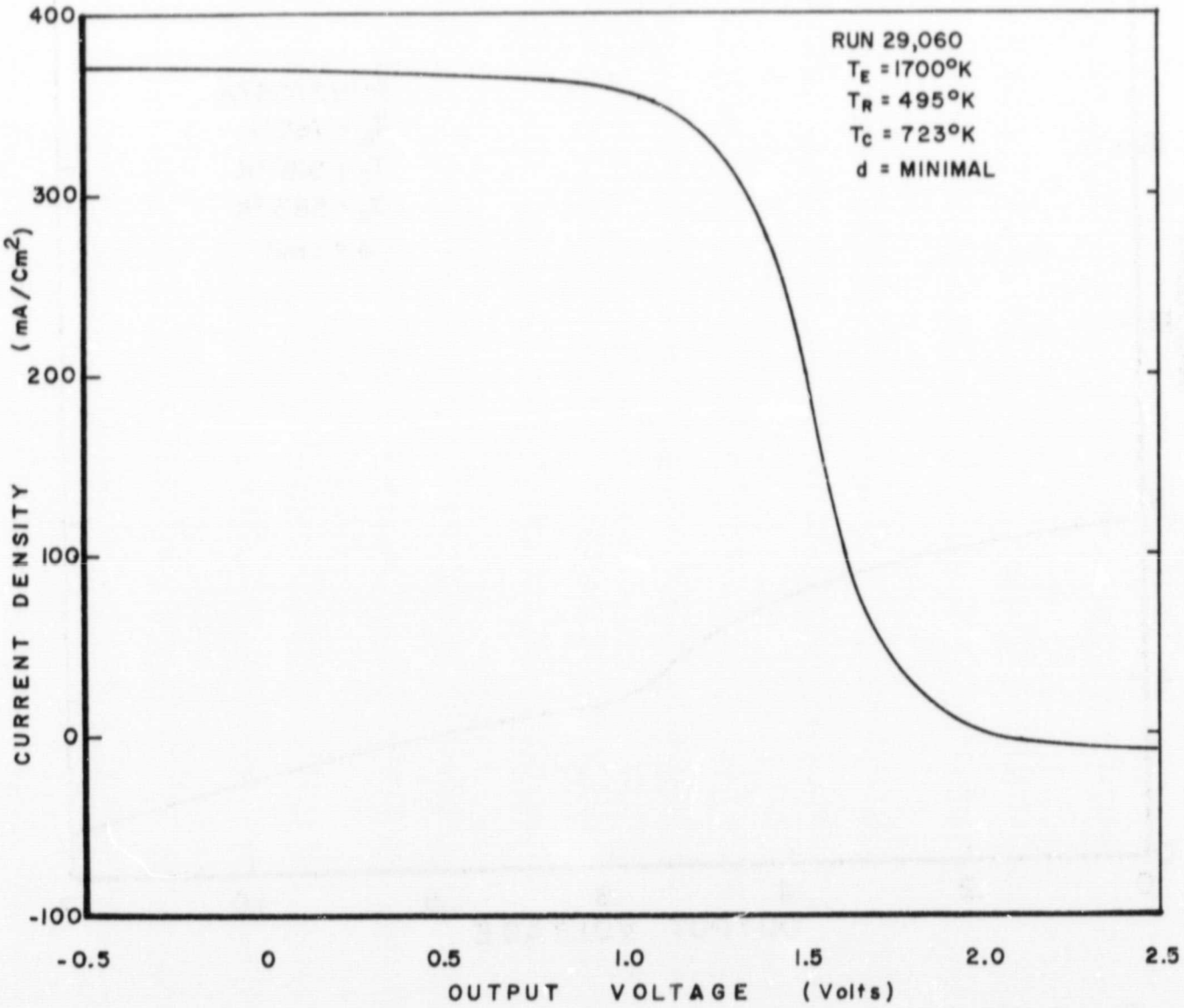


Figure III-35. Typical Data for Emitter Work Function Measurements under Ion Rich Conditions.

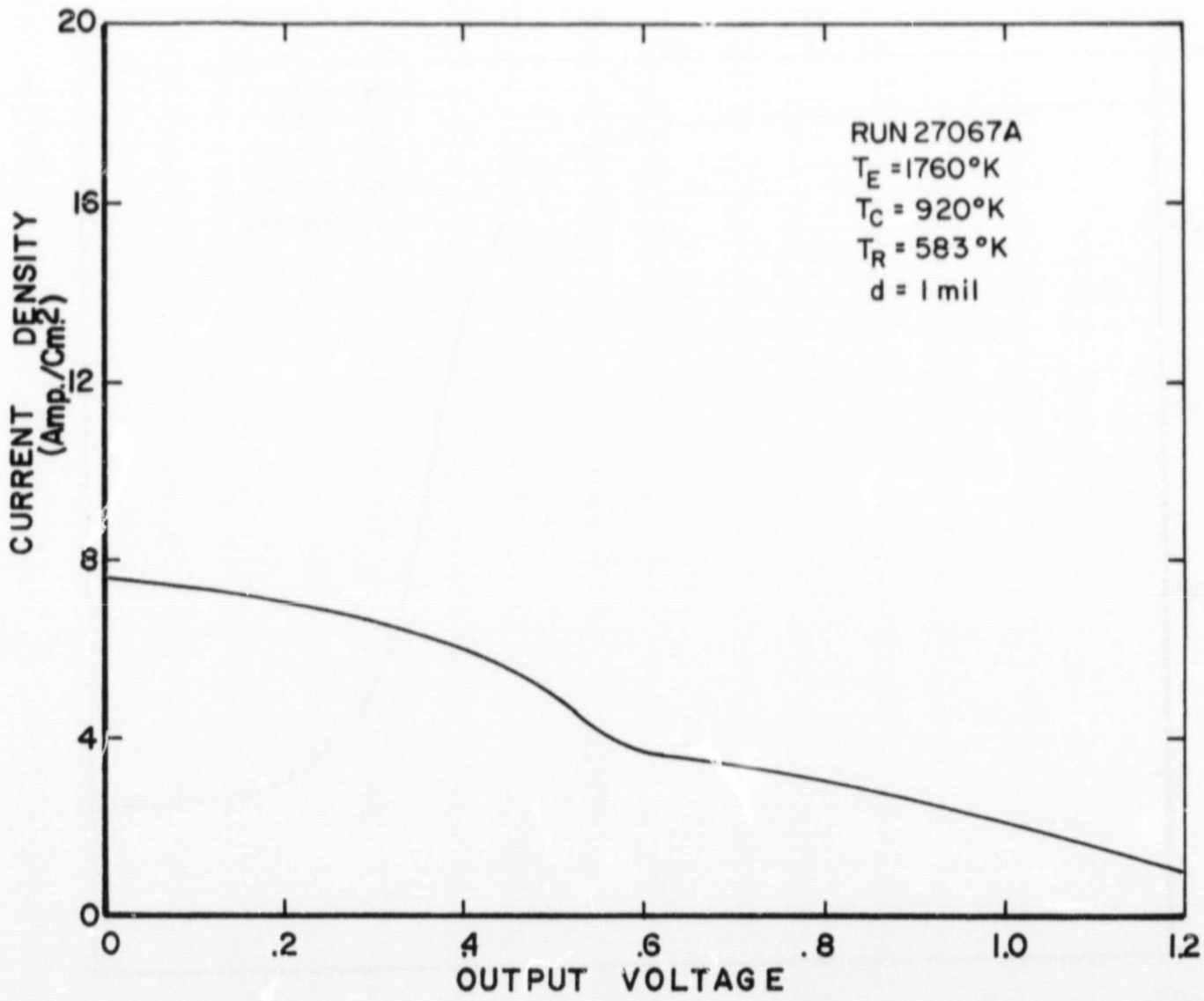


Figure III-36. Typical Data for Emitter Work Function Measurements under Electron Rich Conditions.

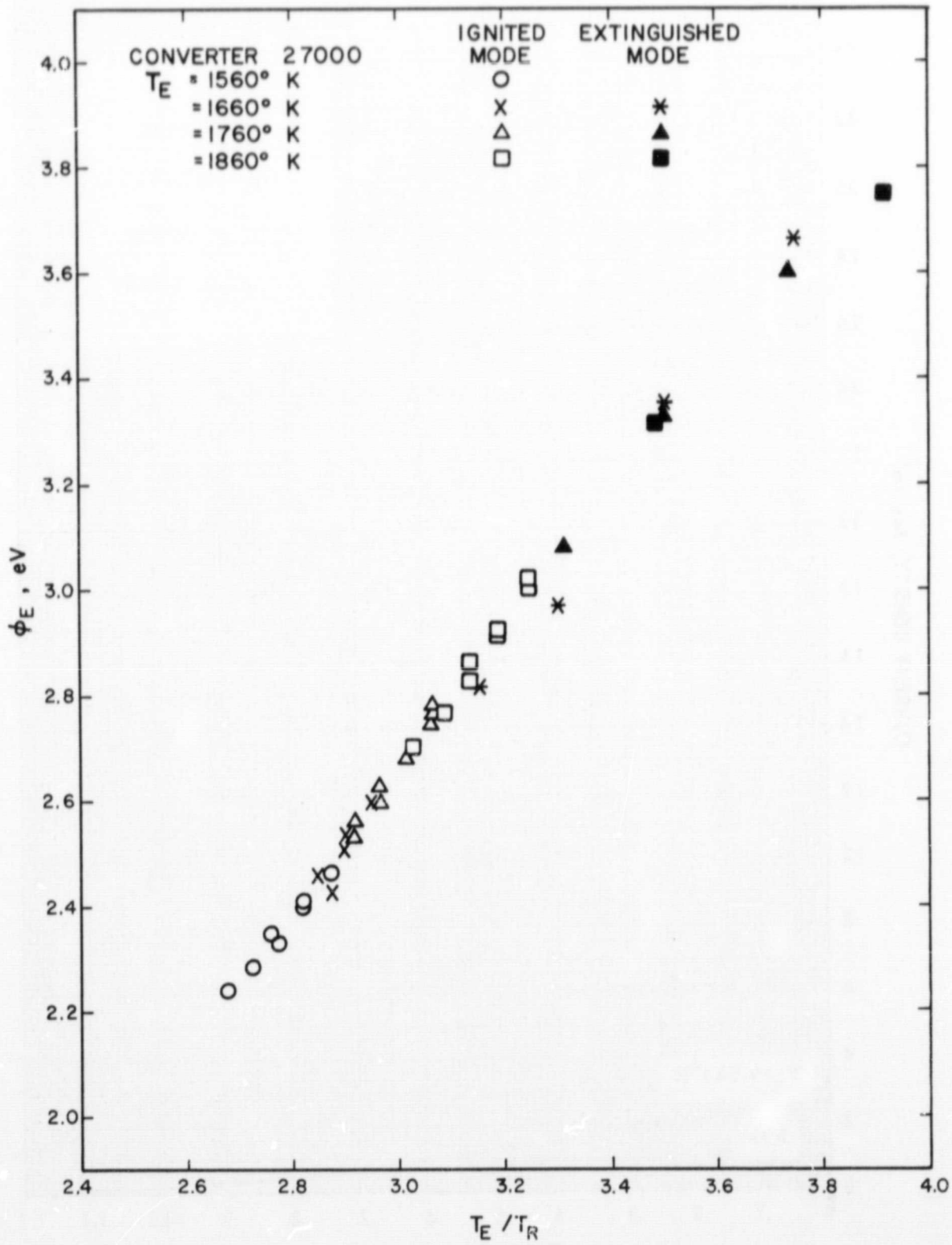


Figure III-37. Summary of Emitter Work Function Data.

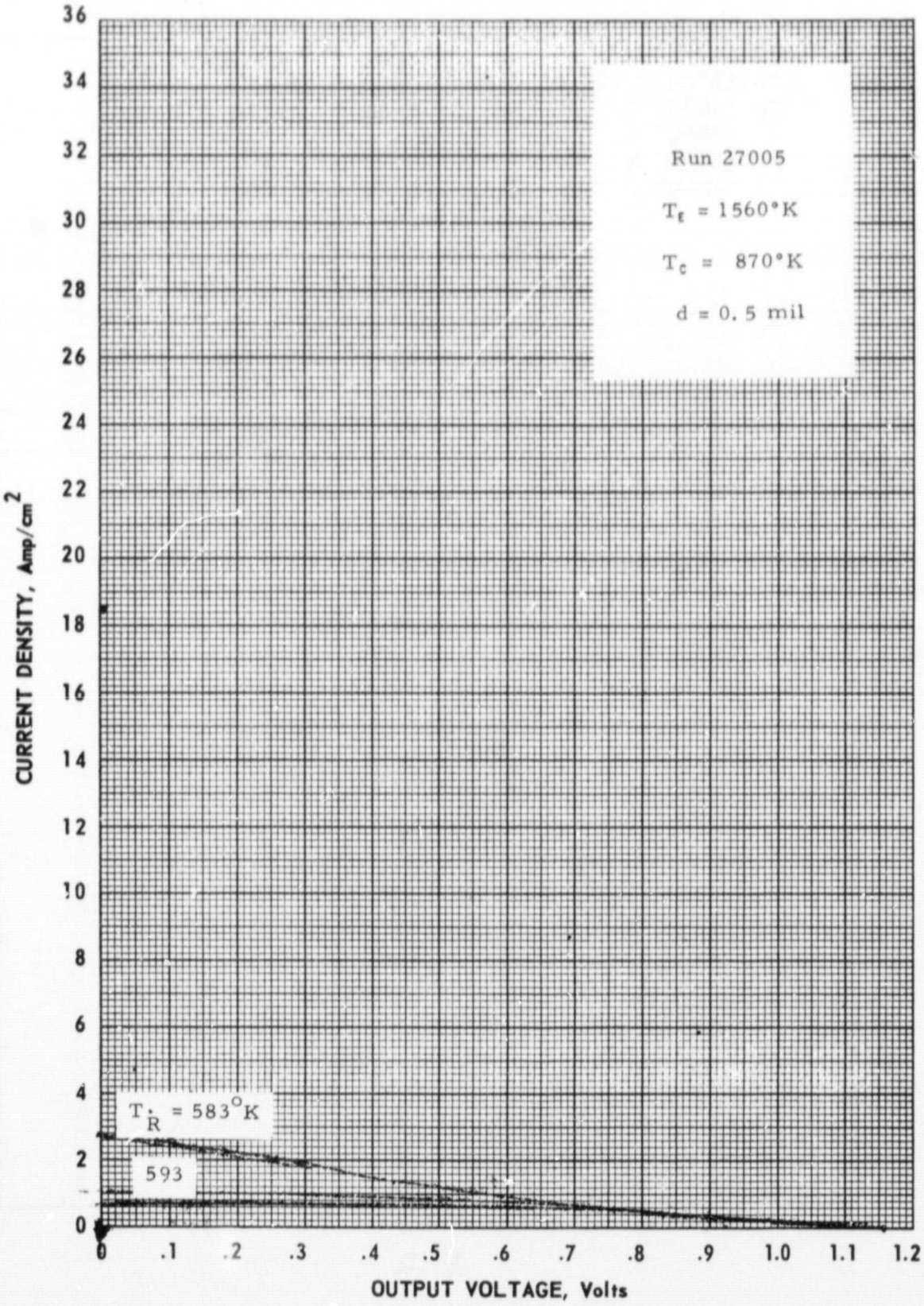


Figure III-38. Cesium-Temperature Family at T_E = 1560°K and d = 0.5 mil.

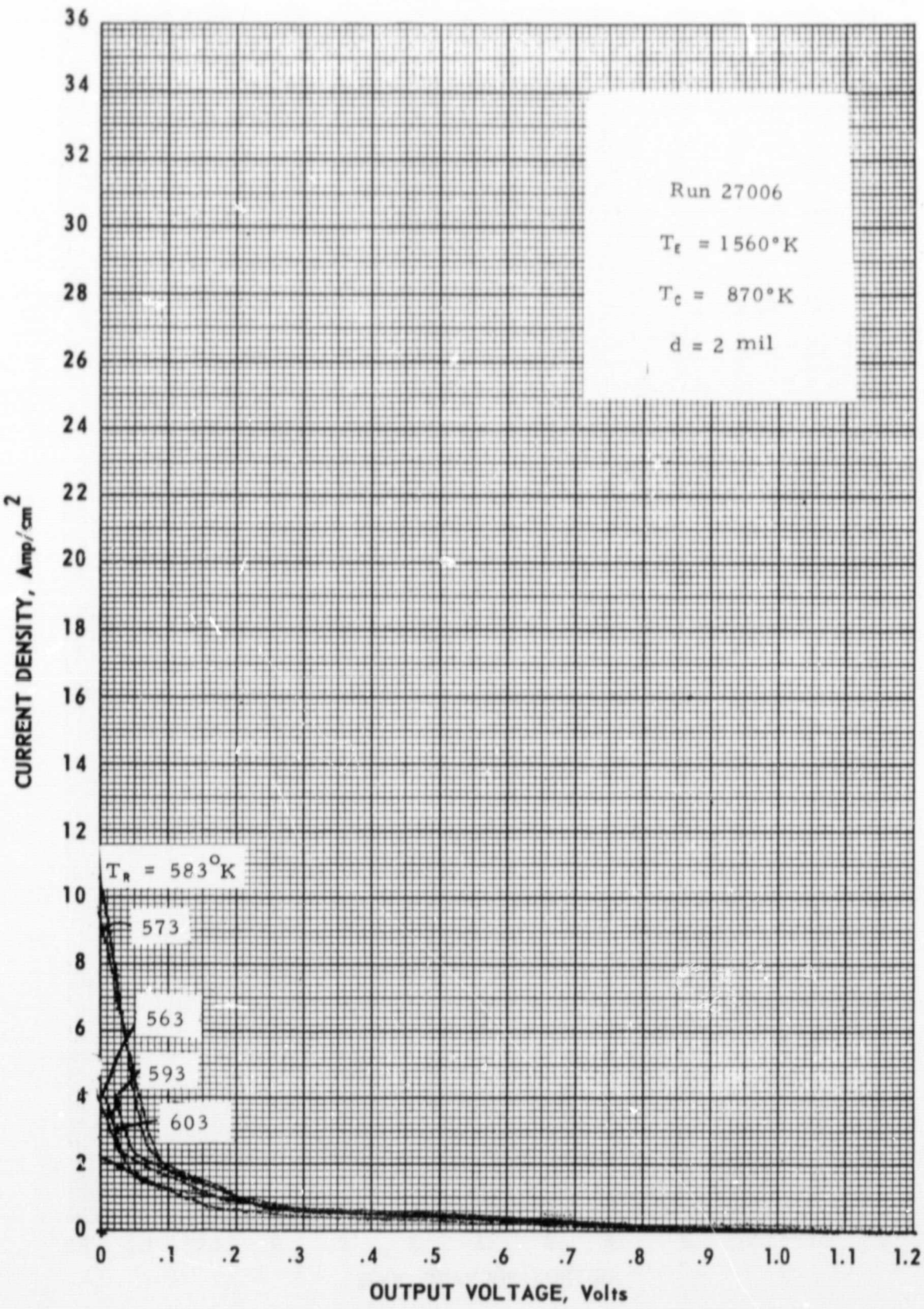


Figure III-39. Cesium-Temperature Family at T_E = 1560°K and d = 2 mils.

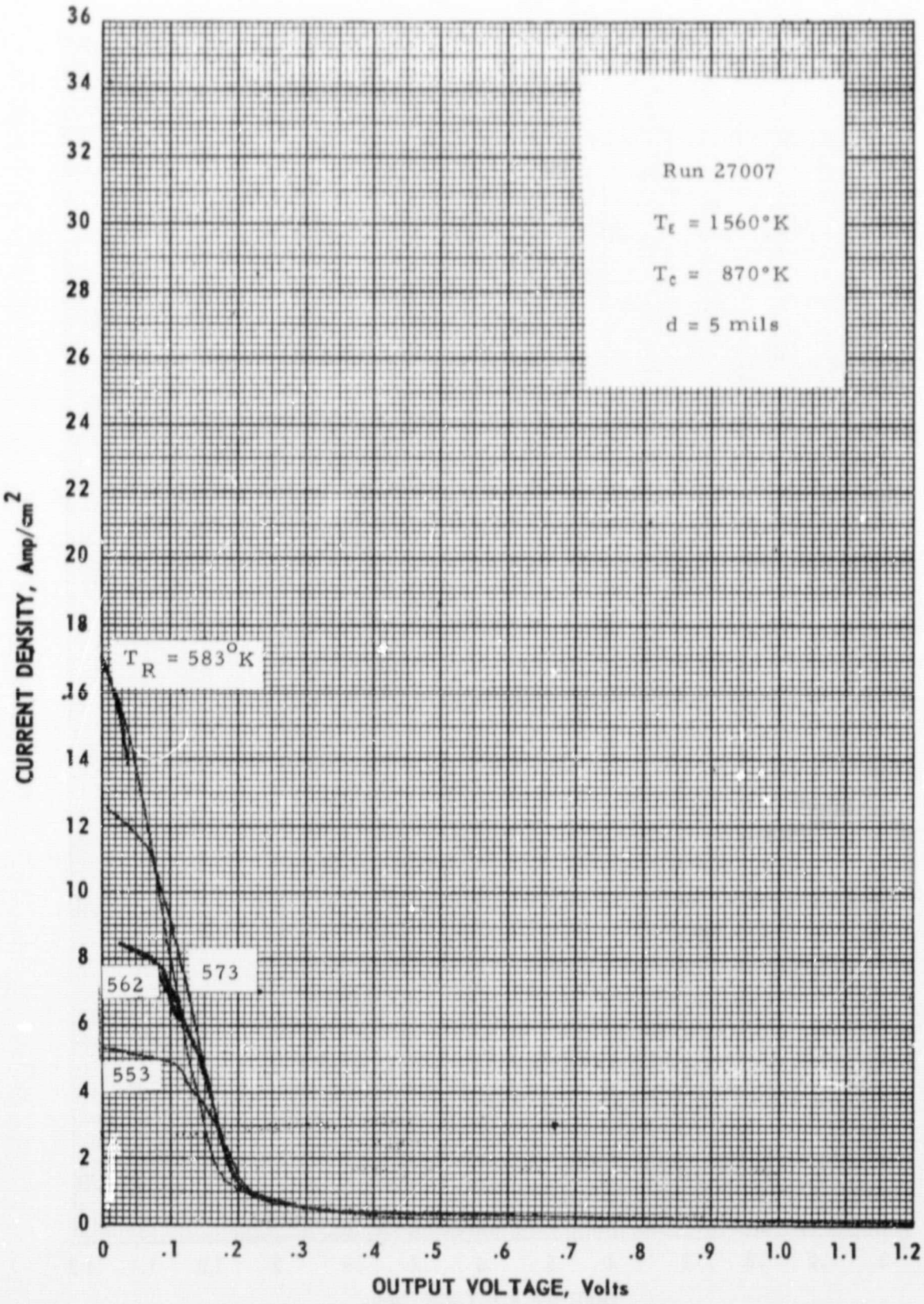


Figure III-40. Cesium-Temperature Family at T_E = 1560°K and d = 5 mils.

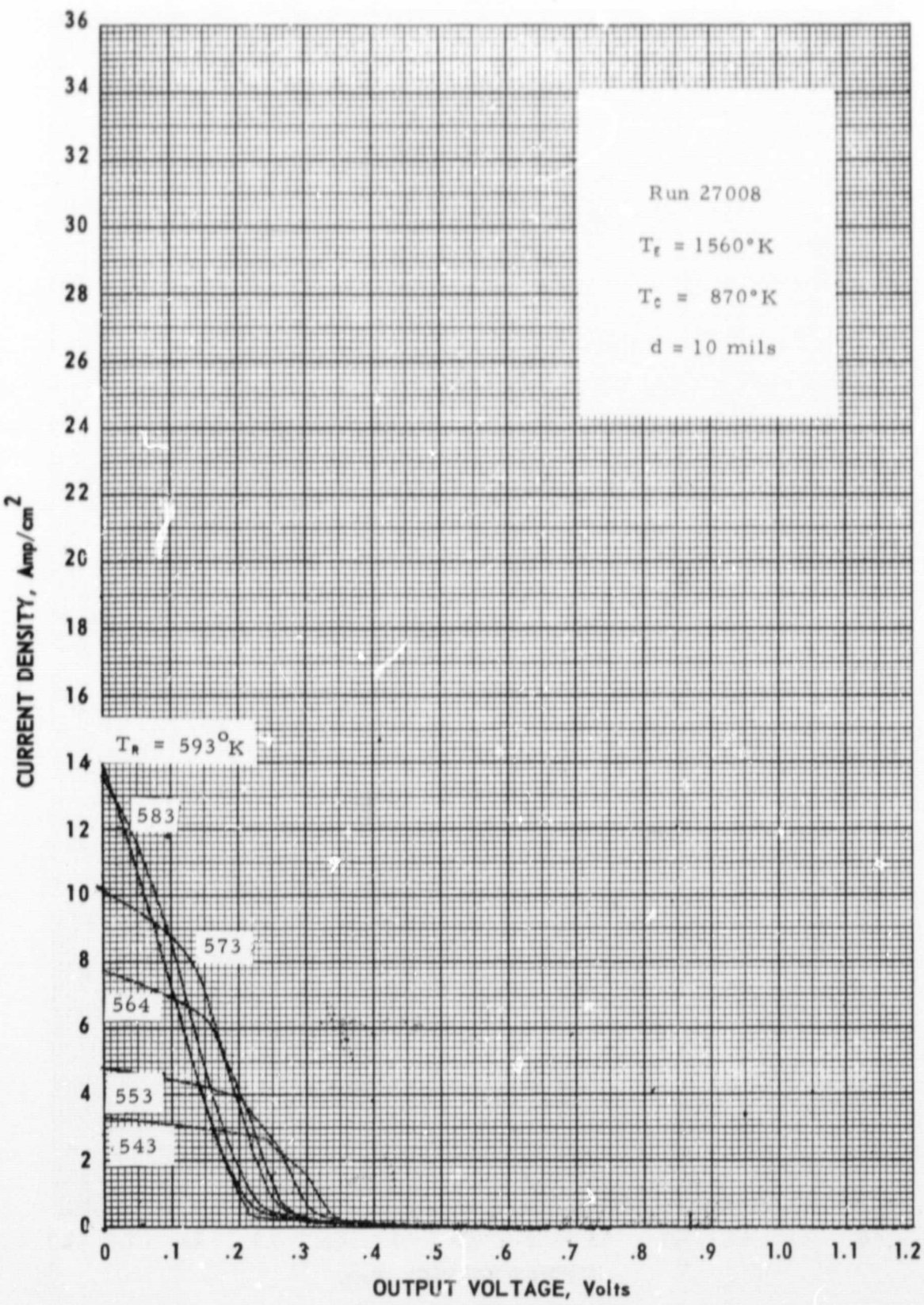


Figure III-41. Cesium-Temperature Family at T_E = 1560°K and d = 10 mils.

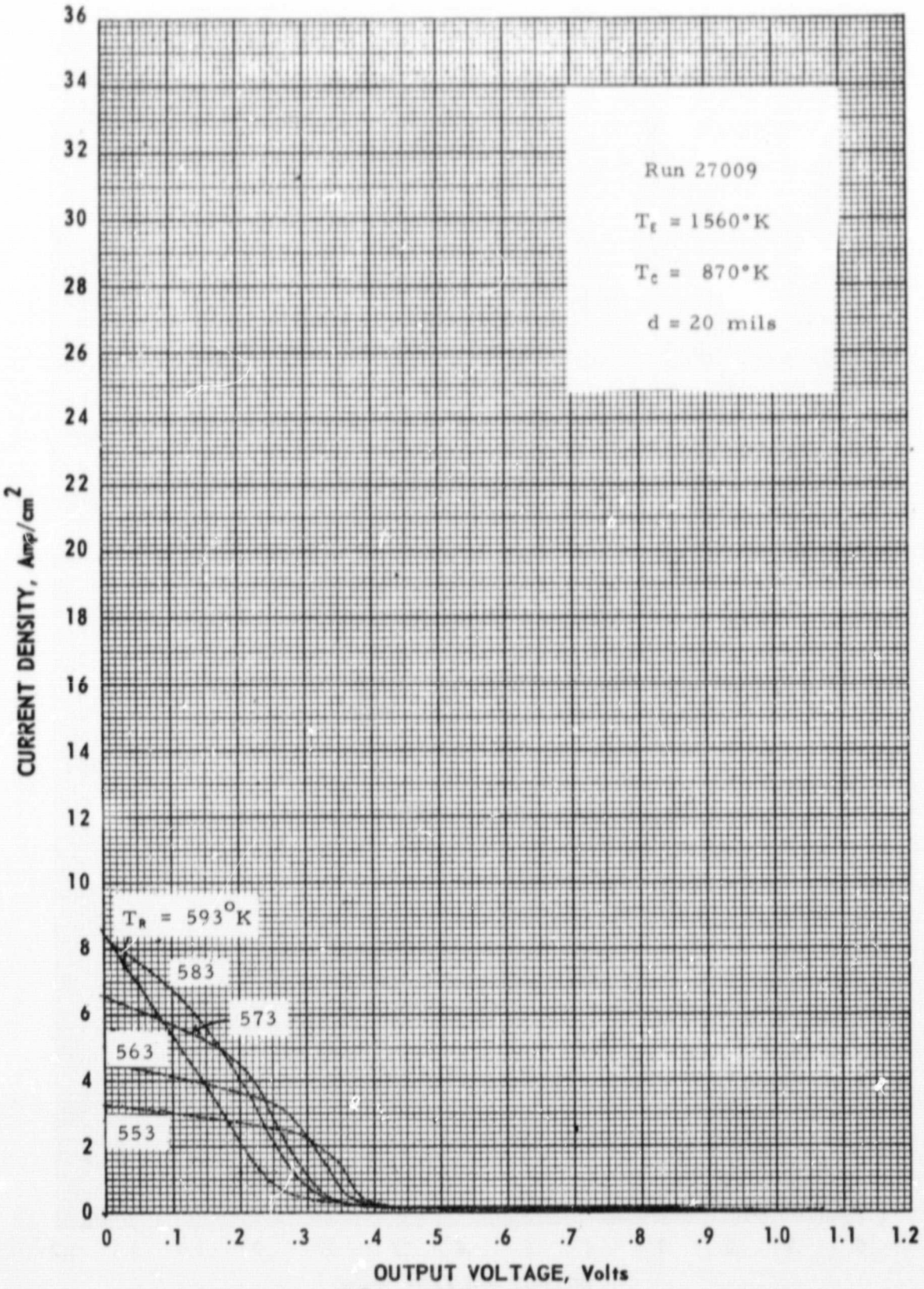


Figure III-42. Cesium-Temperature Family at T_E = 1560°K and d = 20 mils.

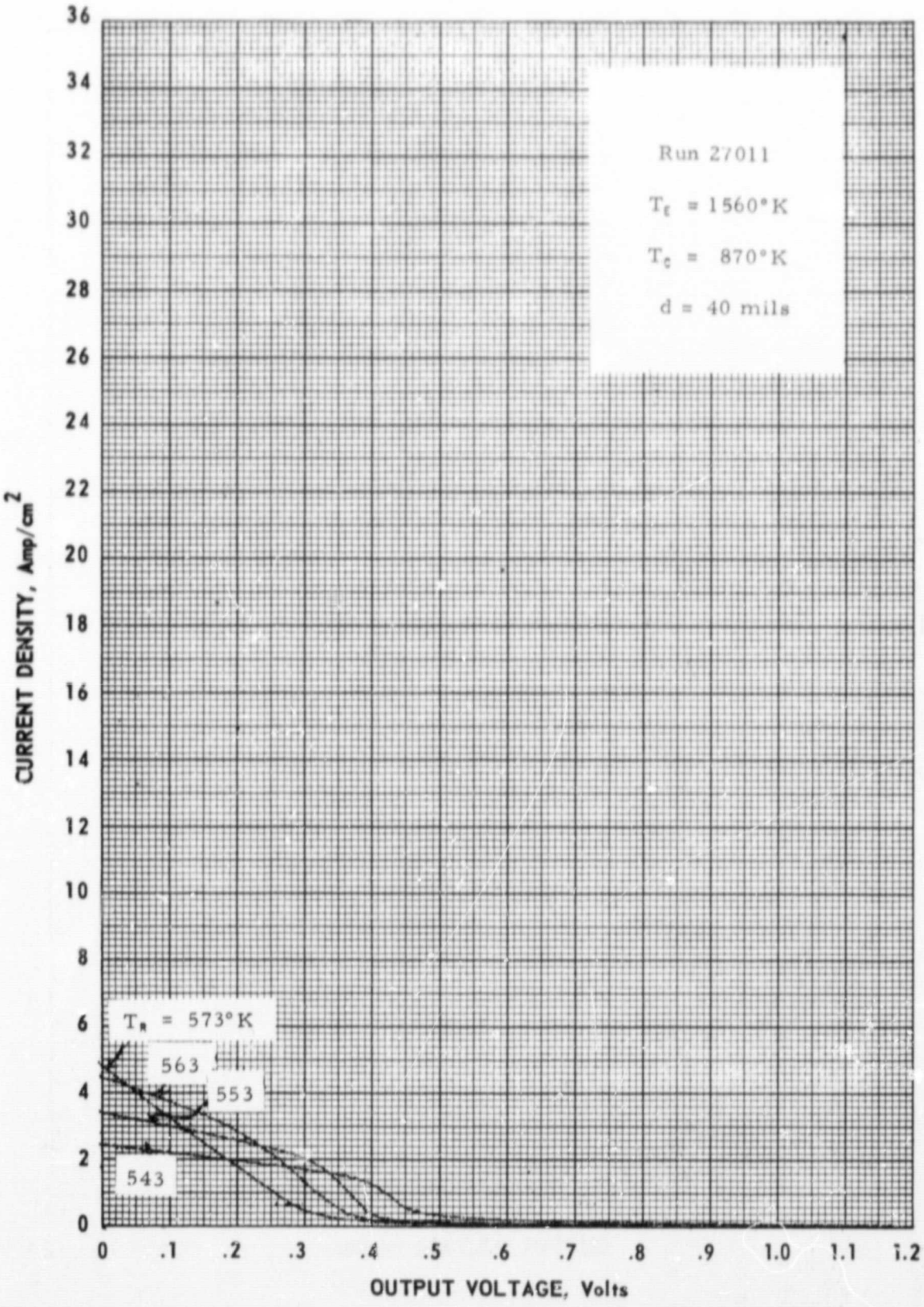


Figure III-43. Cesium-Temperature Family at T_E = 1560°K and d = 40 mils.

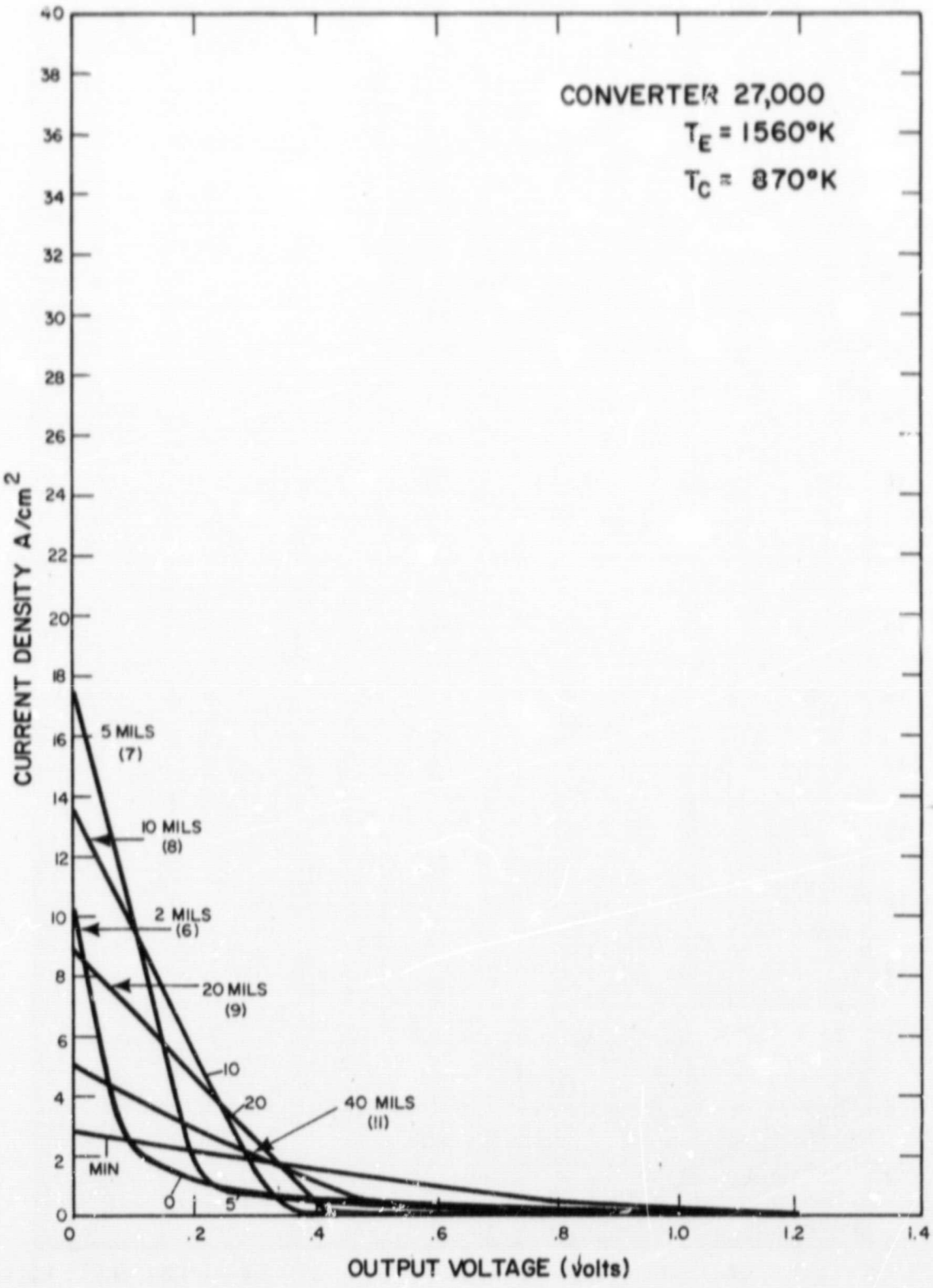


Figure III-44. Comparison of Cesium Optimized Envelopes at T_E = 1560°K for Several Spacings.

families at 1660° K are presented in Figures III-45 through III-48. The summary of cesium-temperature envelopes at various spacings is shown in Figure III-49. Similar data at emitter temperatures of 1760° K and 1860° K are shown in Figures III-50 through III-62.

The performance of this converter is considerably lower than that of a previous converter[3] using a similar emitter and a molybdenum collector. Figure III-63 shows a cesium family from the W-Mo converter at the emitter temperature of 1860° K and the interelectrode spacing of 5 mils. The corresponding family from the present converter is found in Figure III-60. The cesium pressure for a given current is considerably higher in the present converter, indicating a poor emitter surface.

The cesium envelope of the W-Mo converter at 5 mils is compared with the envelopes of the W-W converter at several spacings in Figure III-64. The slope of the 5-mil envelope of the W-Mo converter is approximately equal to the slope of the 2-mil W-W envelope. This implies that the emitter used in the W-Mo converter is far superior to that used in the W-W converter. Since the emitters of the two converters were prepared by the same technique, the discrepancy is not understood at this time. The larger shift in voltage between the 2-mil W-W envelope and the 5-mil W-Mo envelope indicates that the difference in performance is not solely due to the difference in the emitters but is also due to the collector materials used. Experimental data from a third emitter is needed before a definite conclusion can be made.

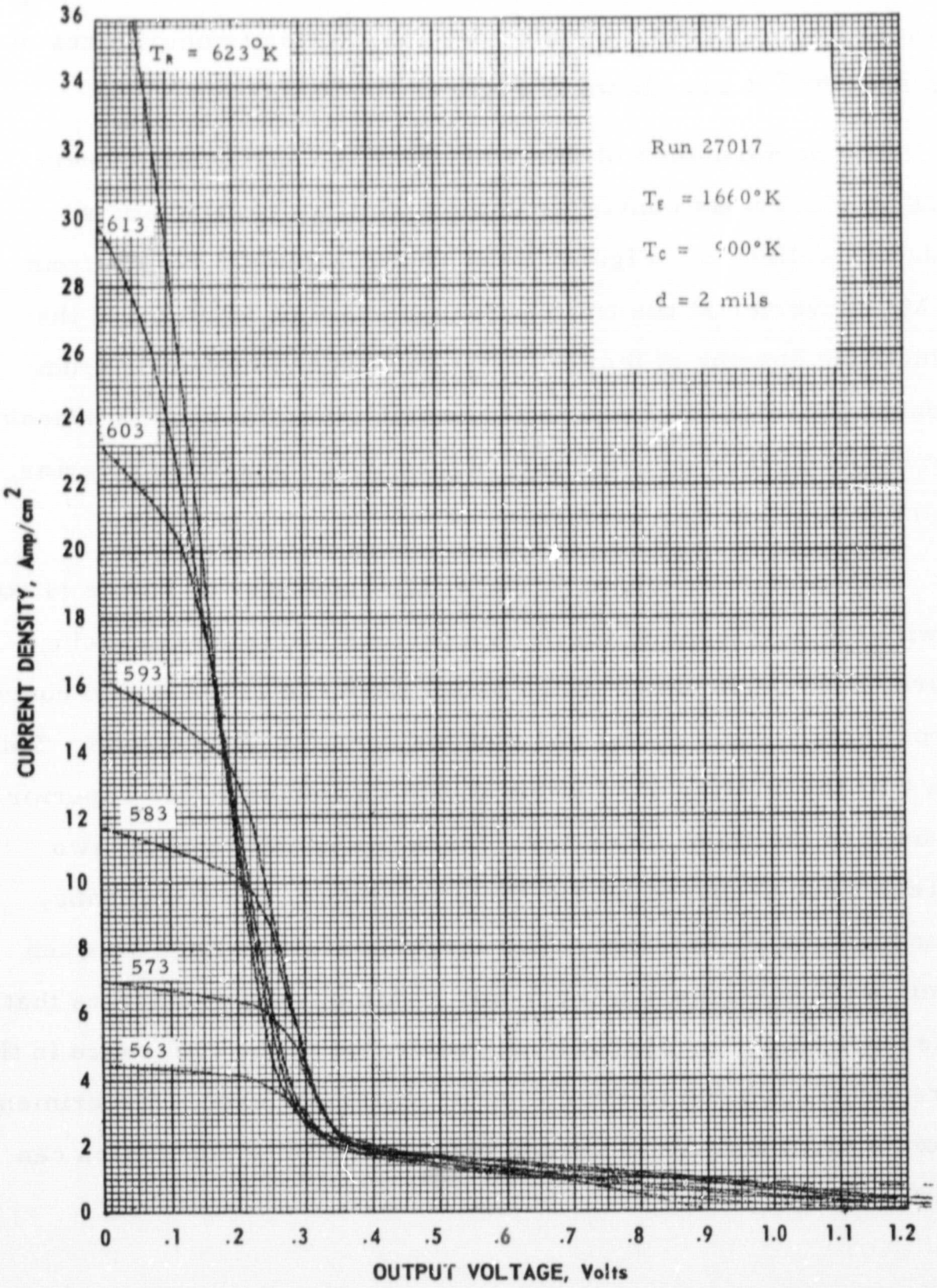


Figure III-45. Cesium-Temperature Family at T_E = 1660°K and d = 2 mils.

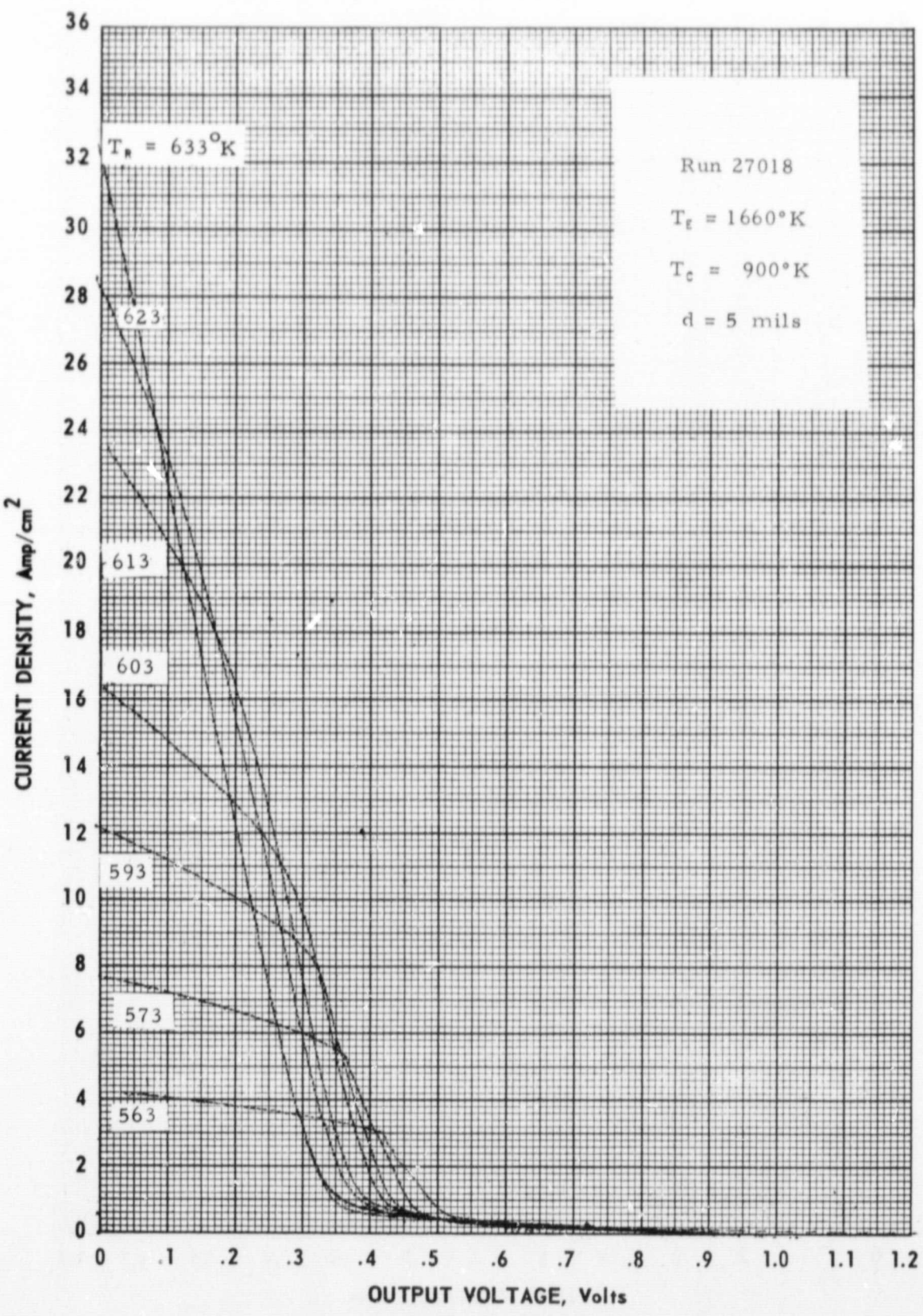


Figure III-46. Cesium-Temperature Family at T_E = 1660°K and d = 5 mils.

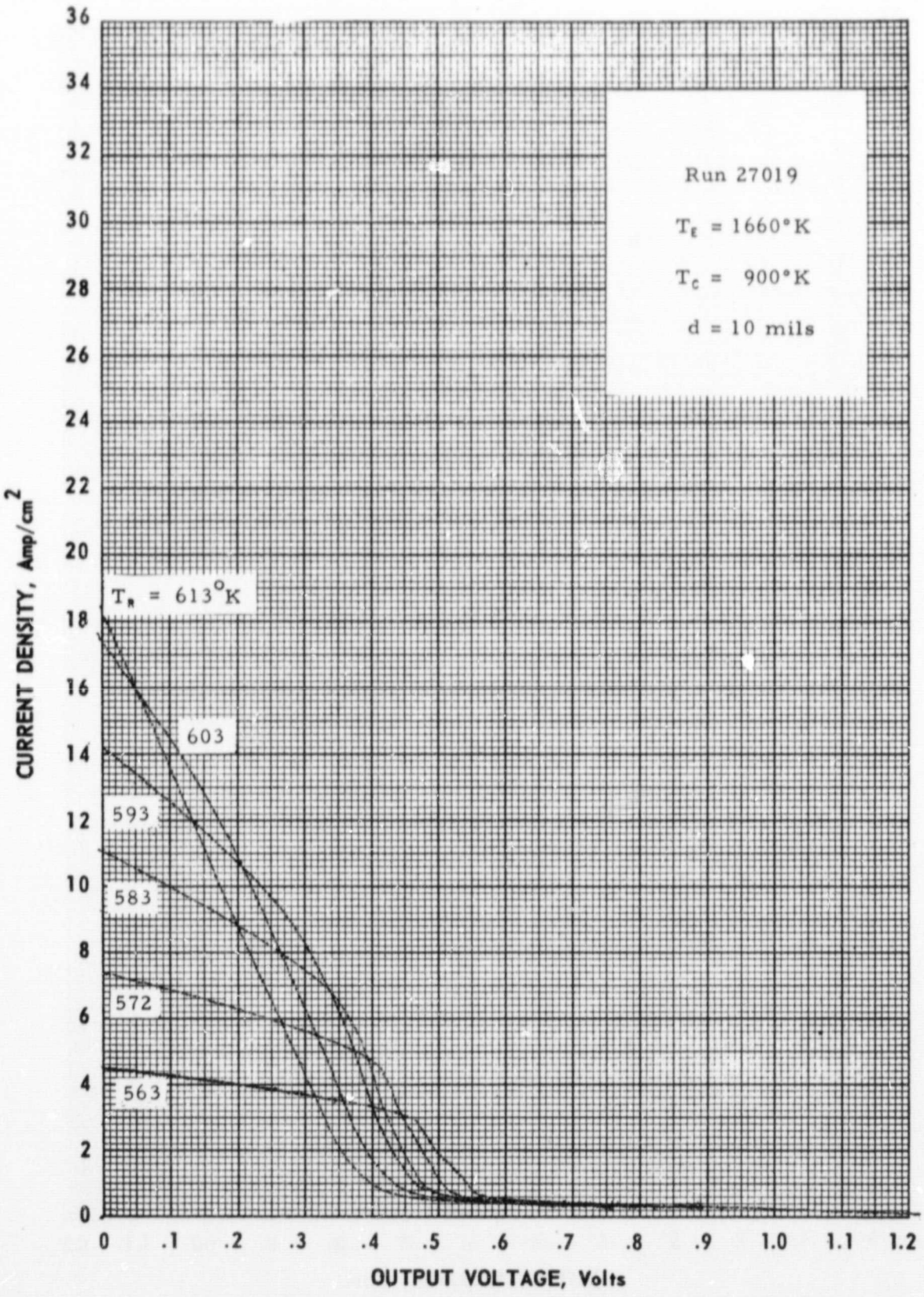


Figure III-47. Cesium-Temperature Family at T_E = 1660°K and d = 10 mils.

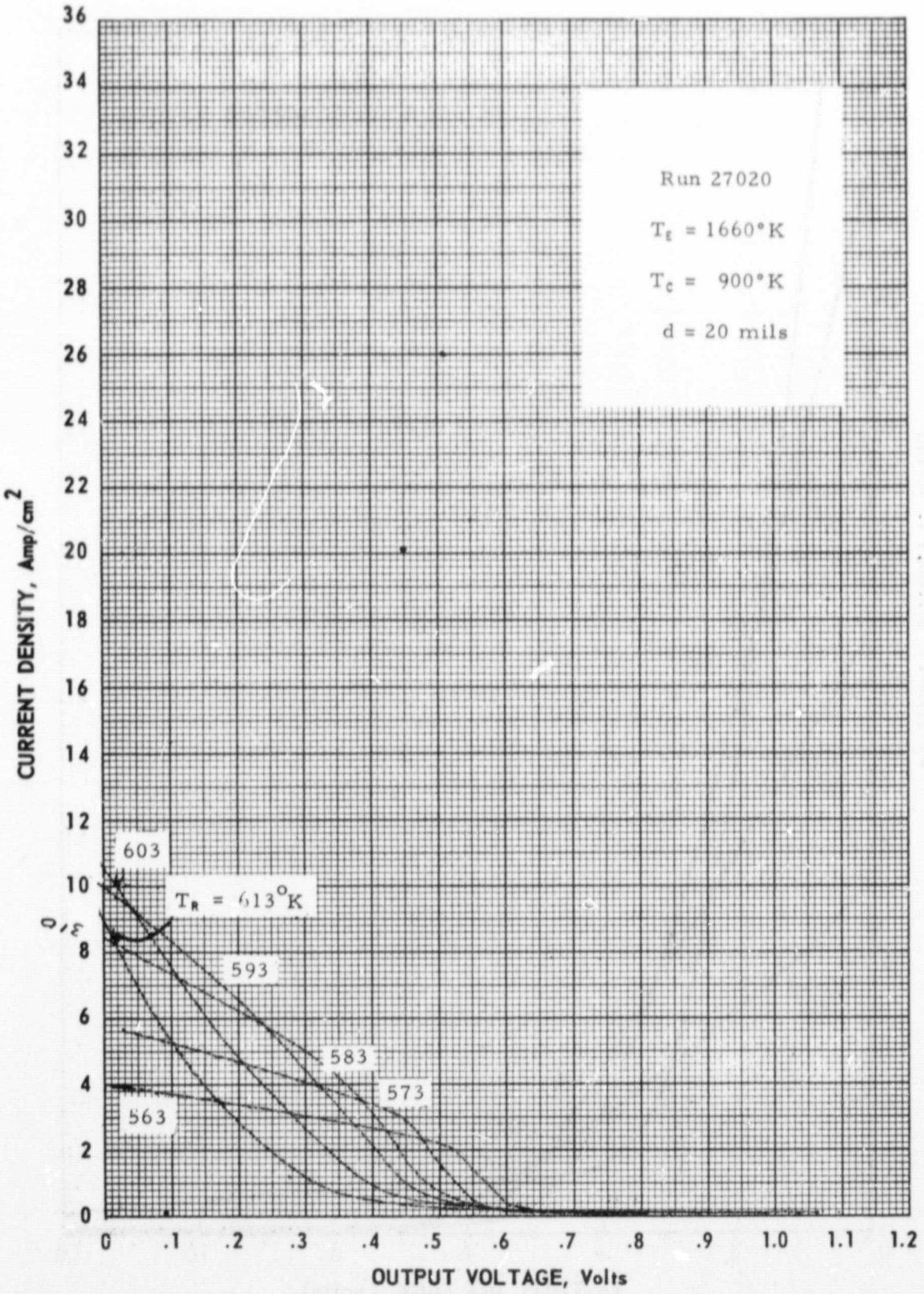


Figure III-48. Cesium-Temperature Family at T_E = 1660°K and d = 20 mils.

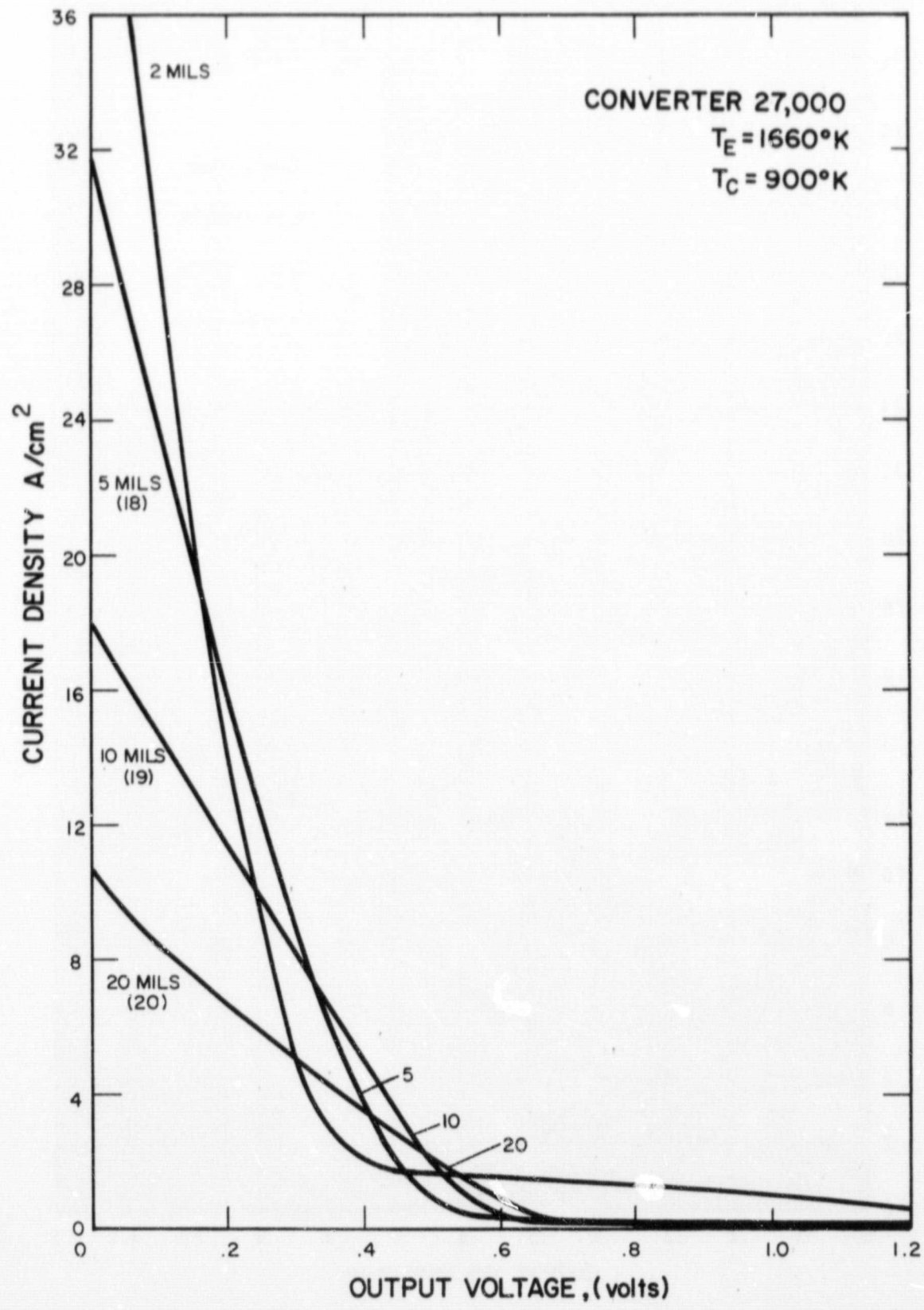


Figure III-49. Comparison of Cesium-Temperature Optimized Envelope at T_E = 1660°K for Several Spacings.

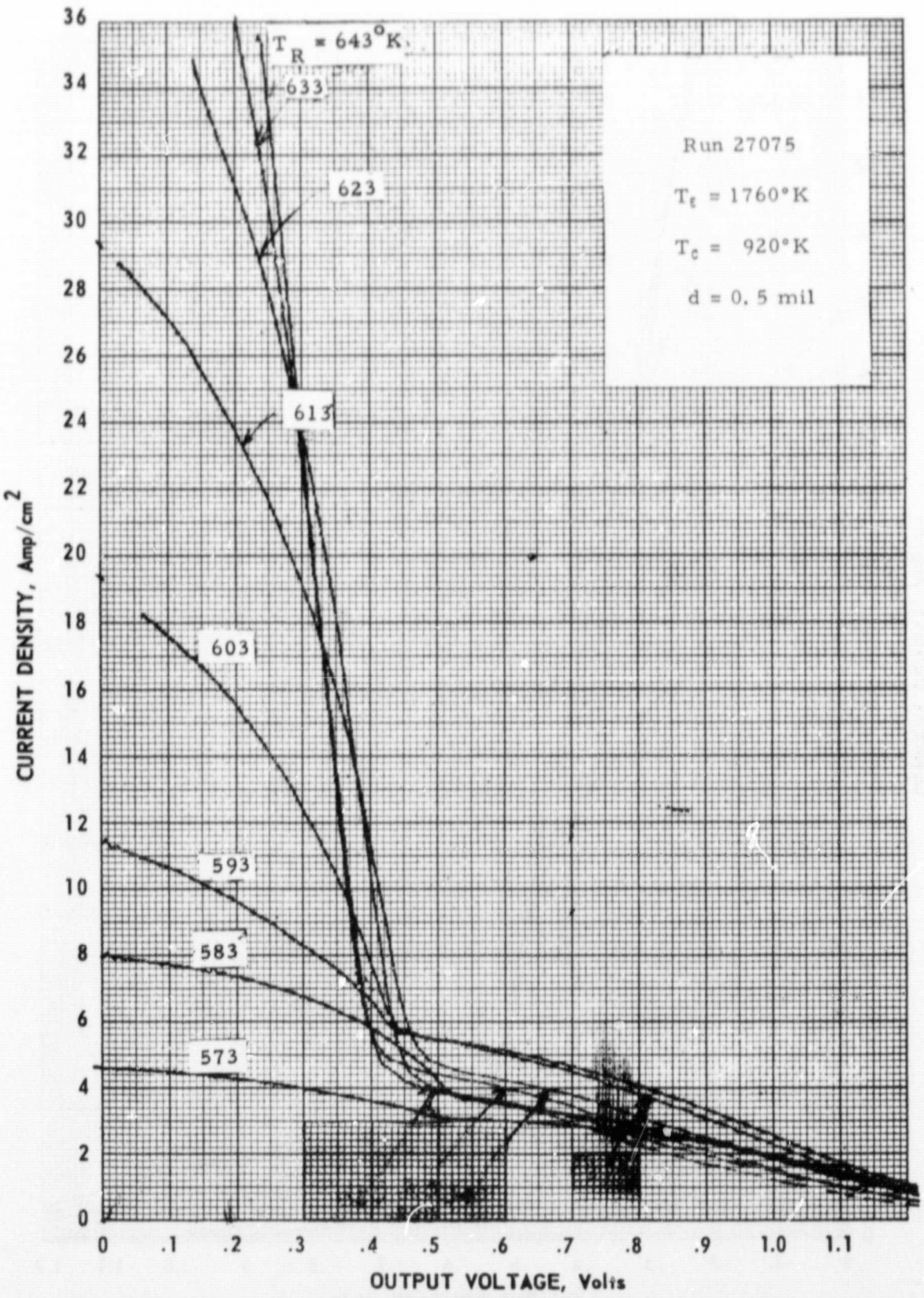


Figure III-50. Cesium-Temperature Family at T_E = 1760°K and d = 0.5 mil.

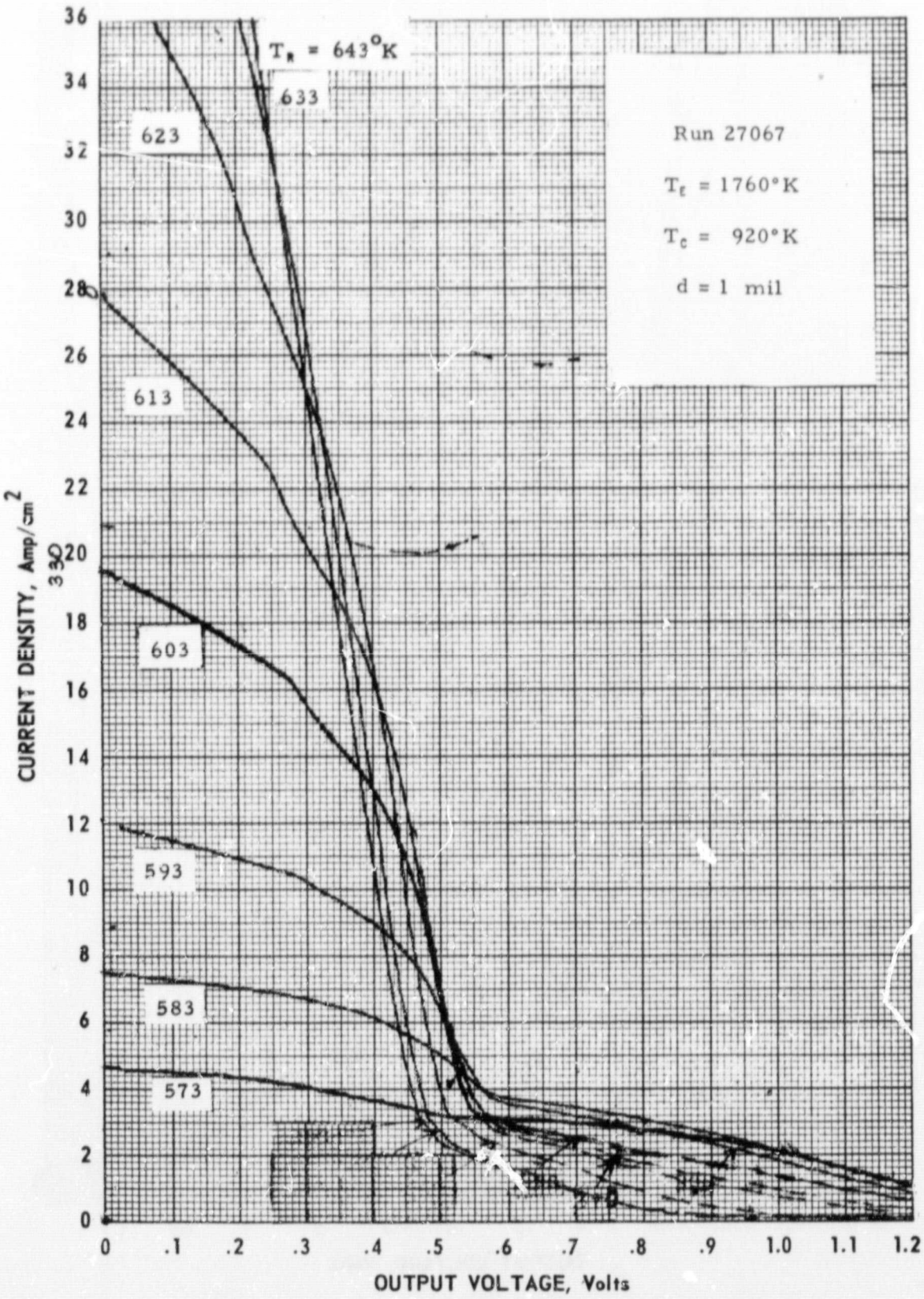


Figure III-51. Cesium-Temperature Family at T_E = 1760°K and d = 1 mil.

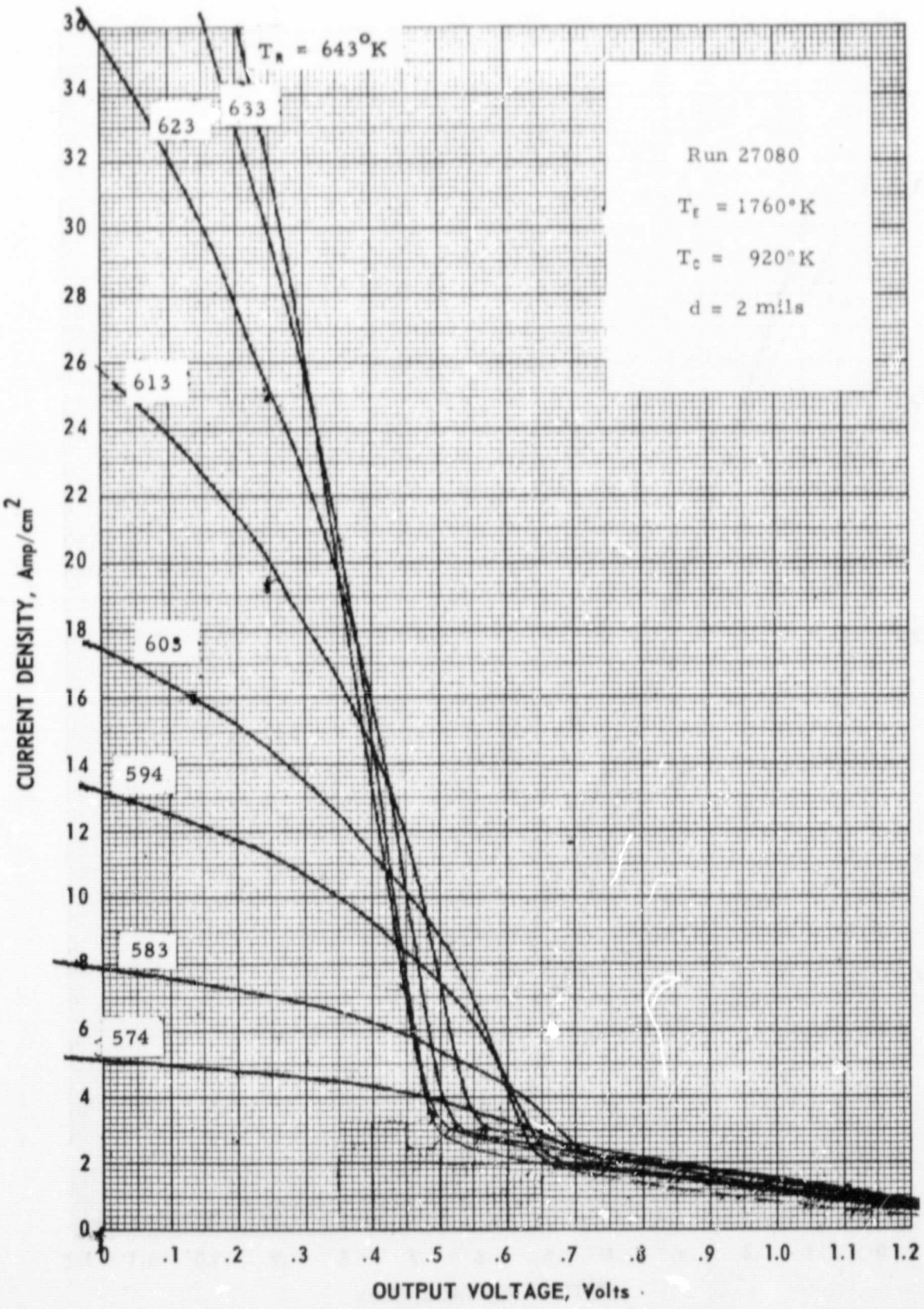


Figure III-52. Cesium-Temperature Family at T_E = 1760°K and d = 2 mils.

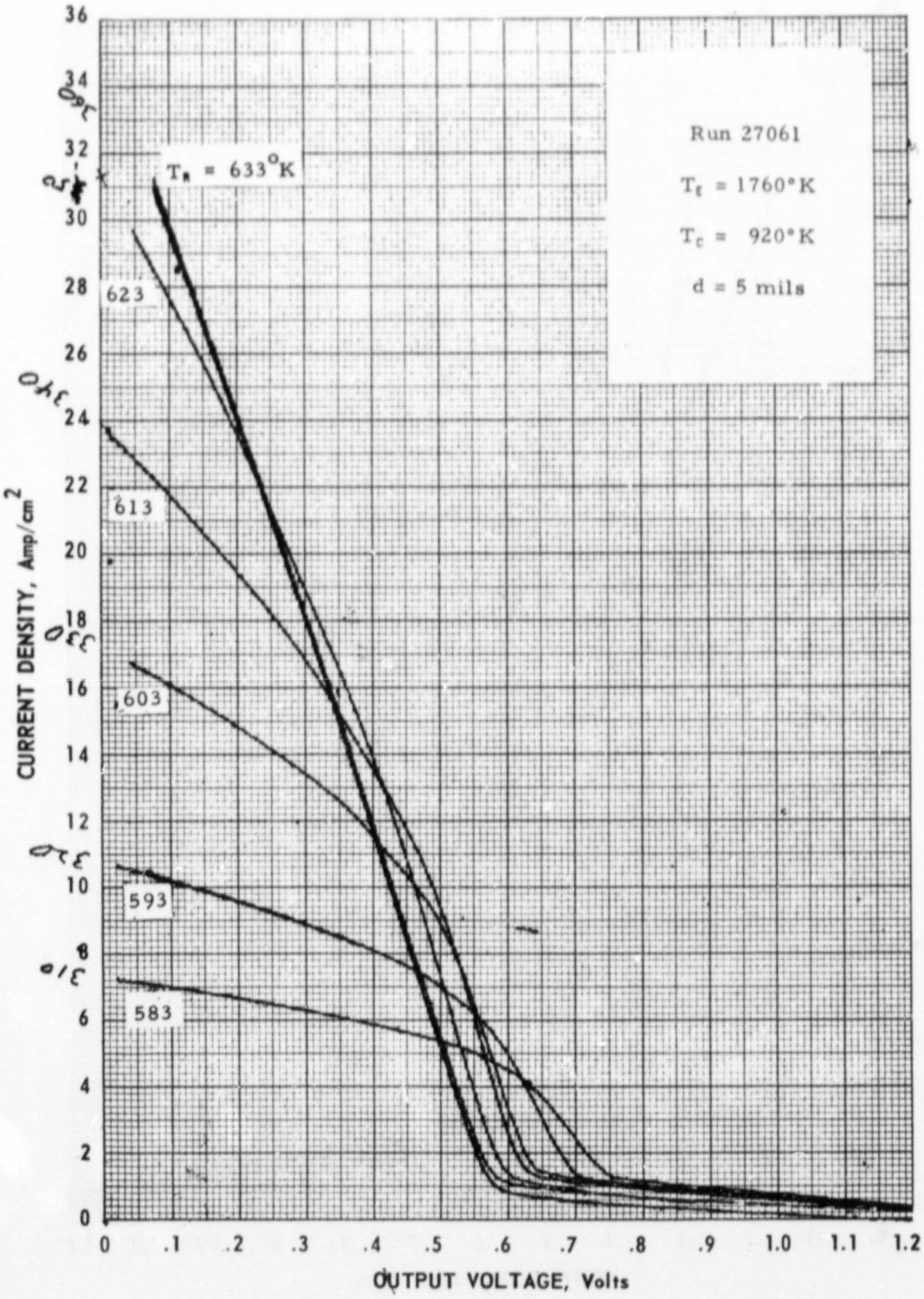


Figure III-53. Cesium-Temperature Family at T_E = 1760°K and d = 5 mils.

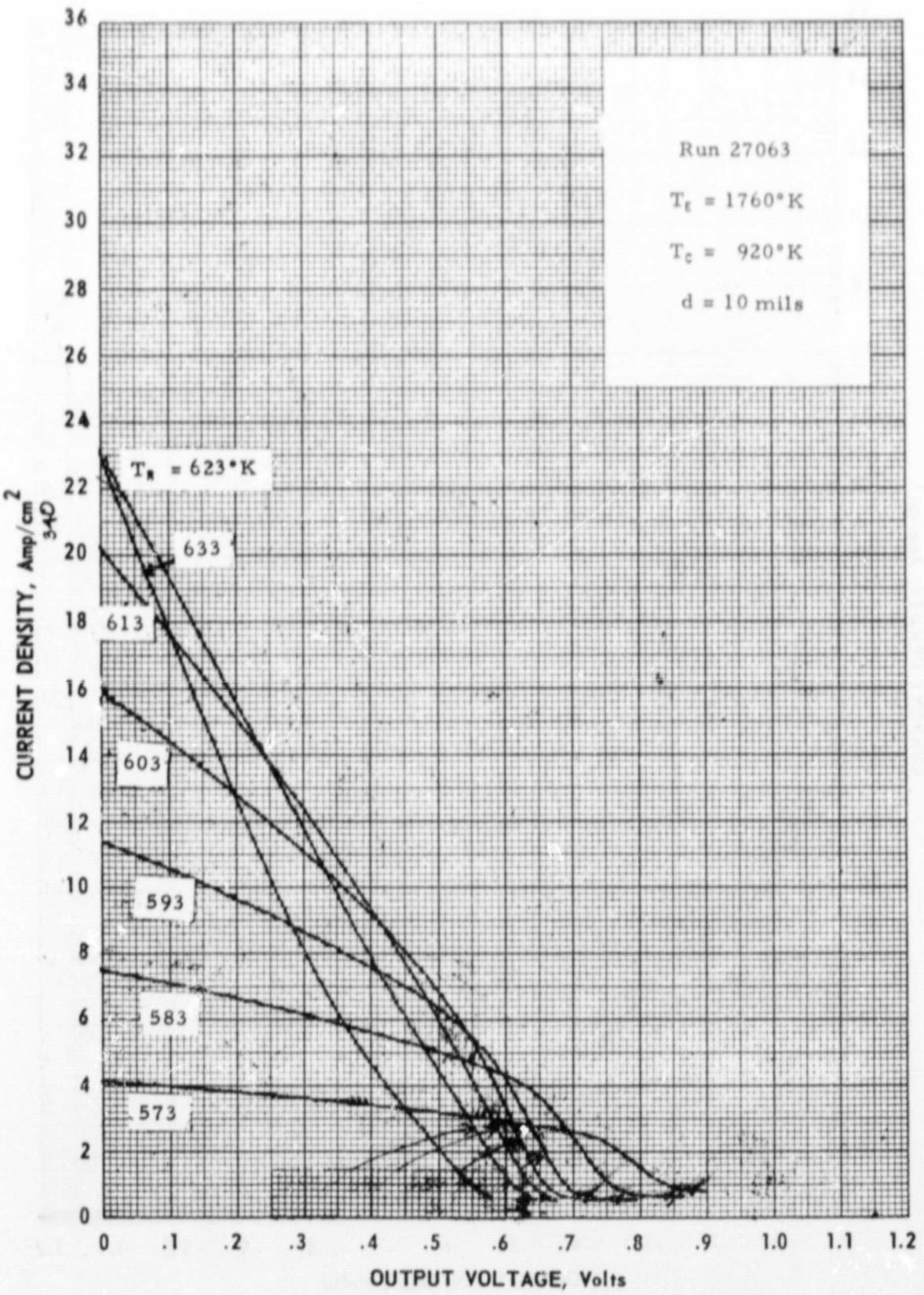


Figure III-54. Cesium-Temperature Family at T_E = 1760°K and d = 10 mils.

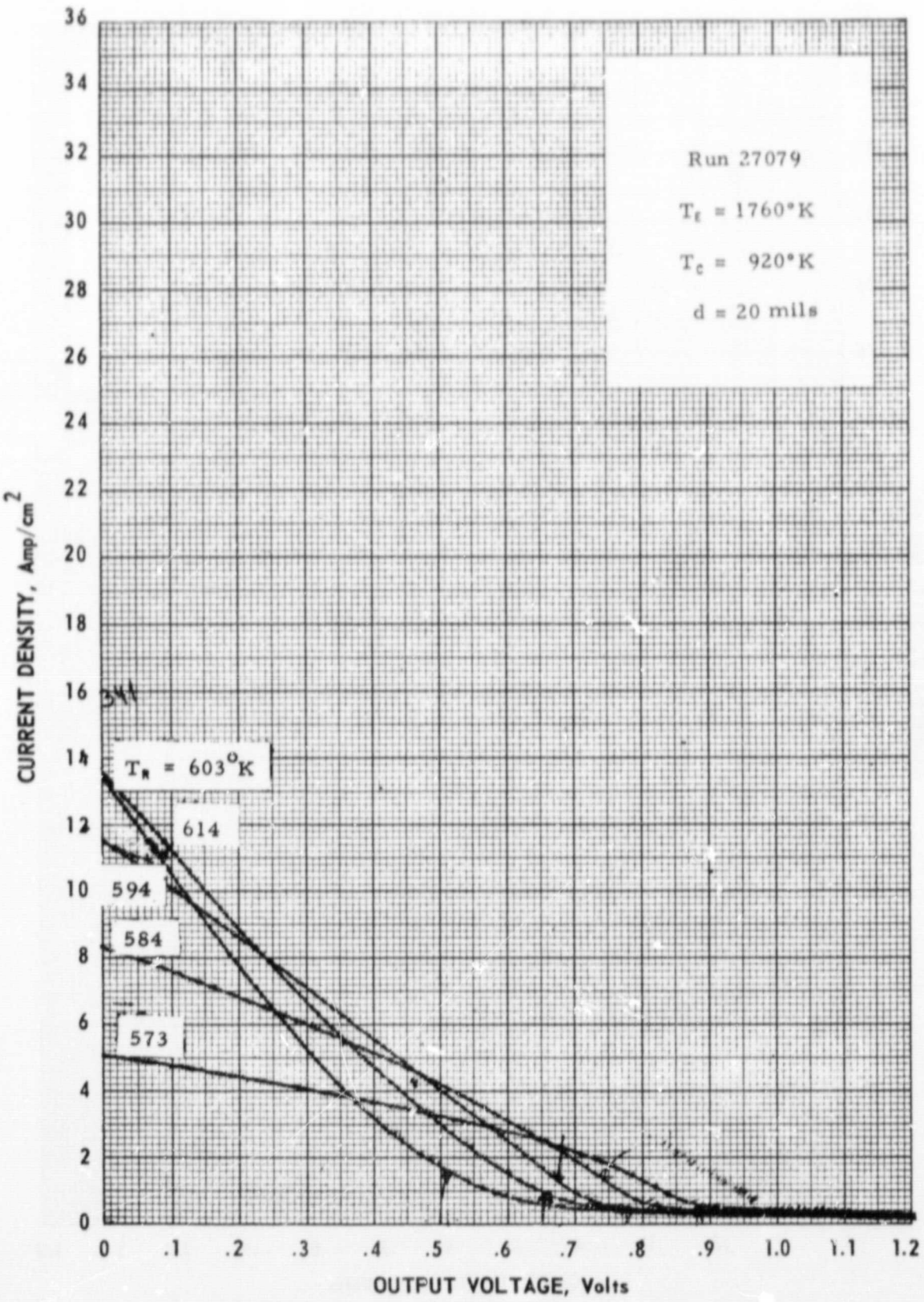


Figure III-55. Cesium-Temperature Family at T_E = 1760°K and d = 20 mils.

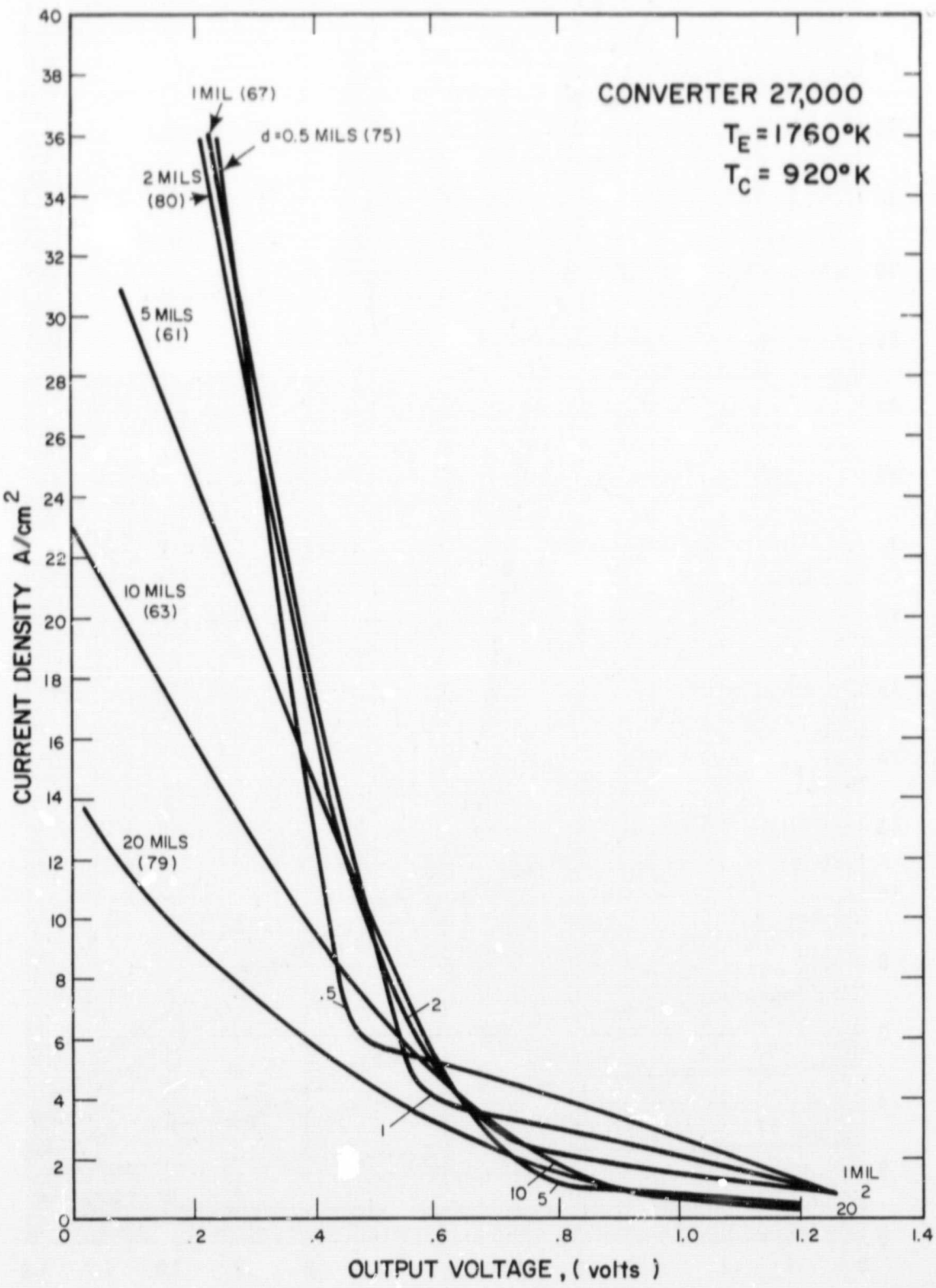


Figure III-56. Comparison of Cesium-Temperature Optimized Envelopes at T_E = 1760°K for Several Spacings.

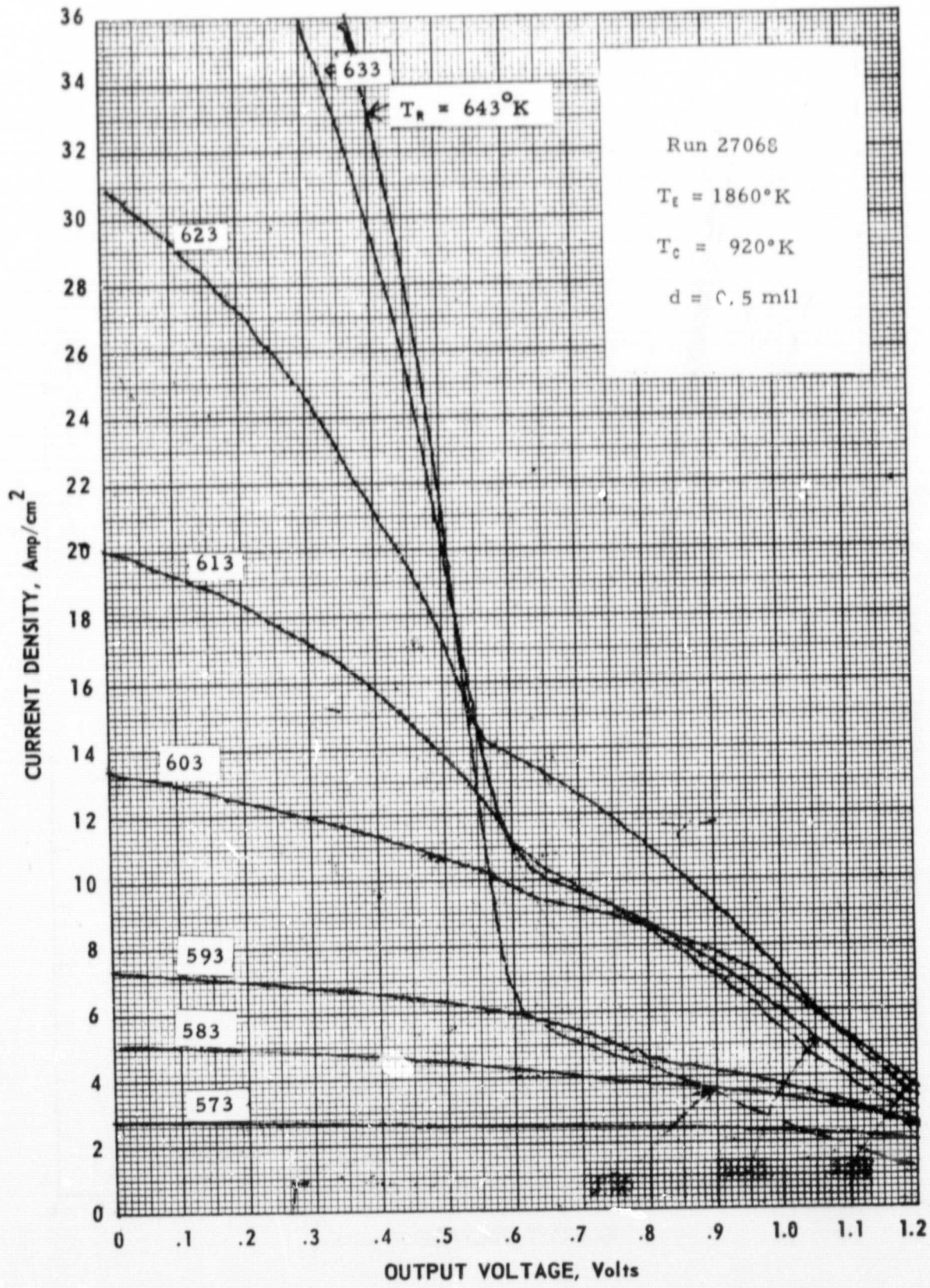


Figure III-57. Cesium-Temperature Family at T_E = 1860°K and d = 0.5 mil.

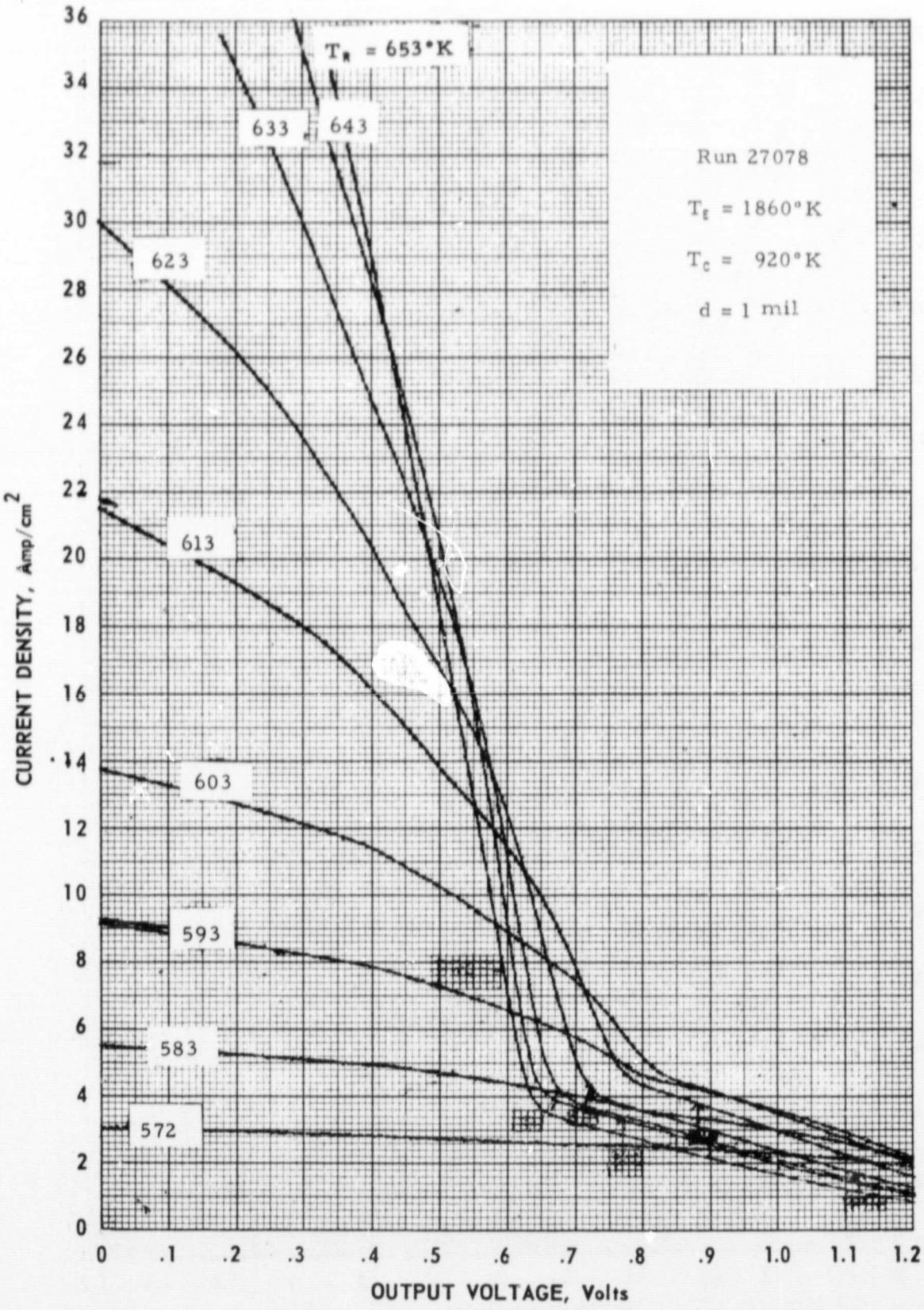


Figure III-58. Cesium-Temperature Family at T_E = 1860°K and d = 1 mil.

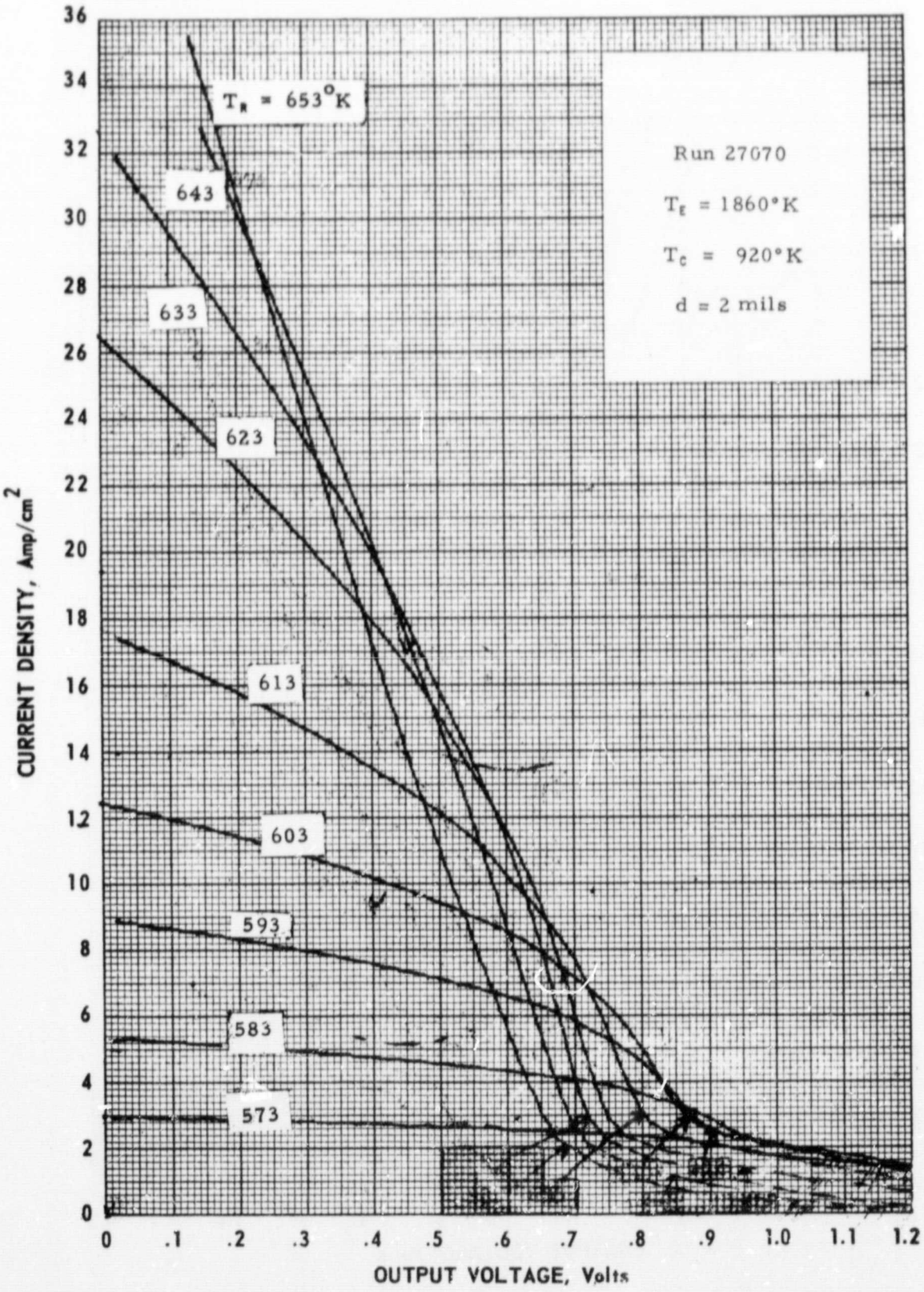


Figure III-59. Cesium-Temperature Family at T_E = 1860°K and d = 2 mils.

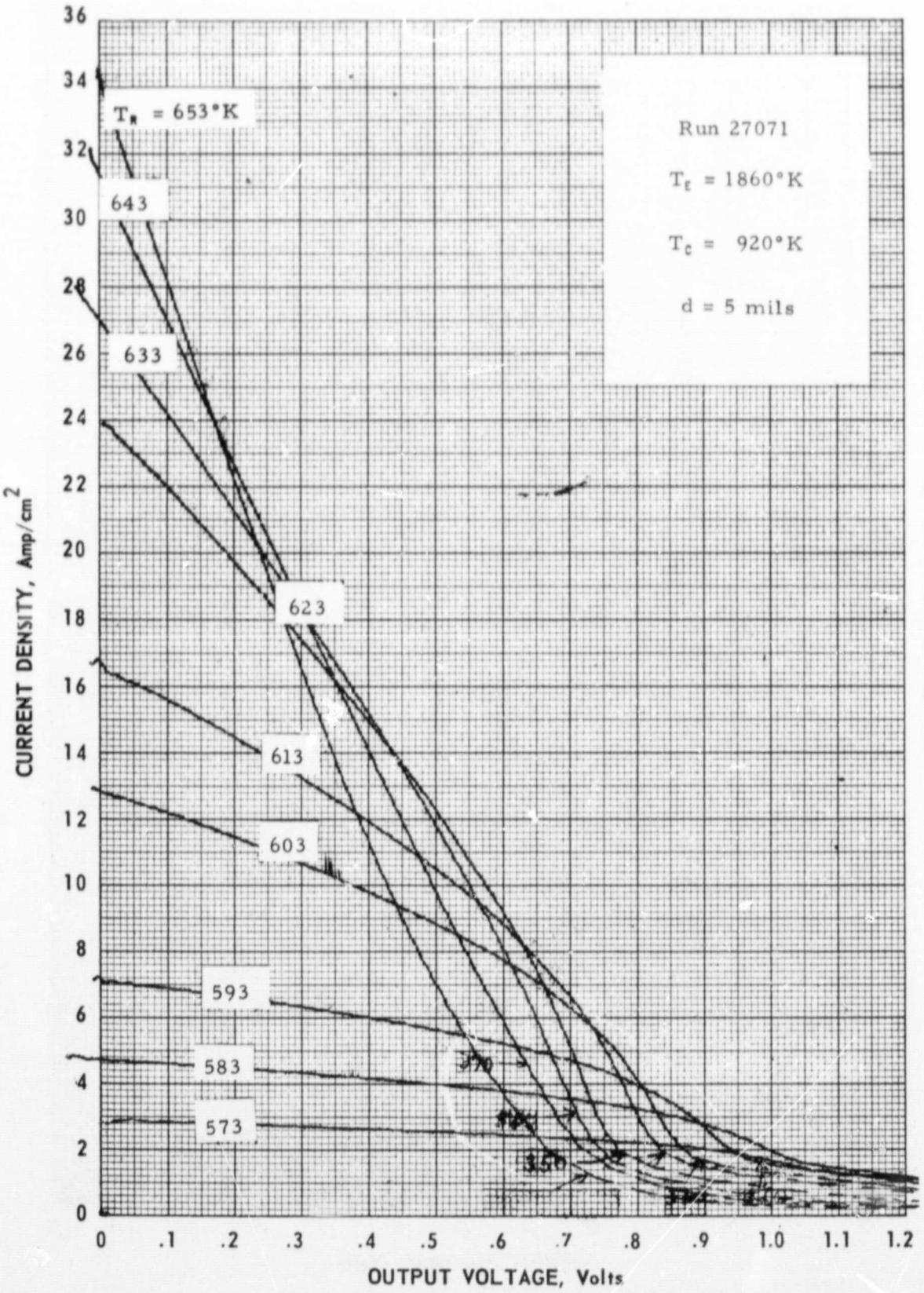


Figure III-60. Cesium-Temperature Family at T_E = 1860°K and d = 5 mils.

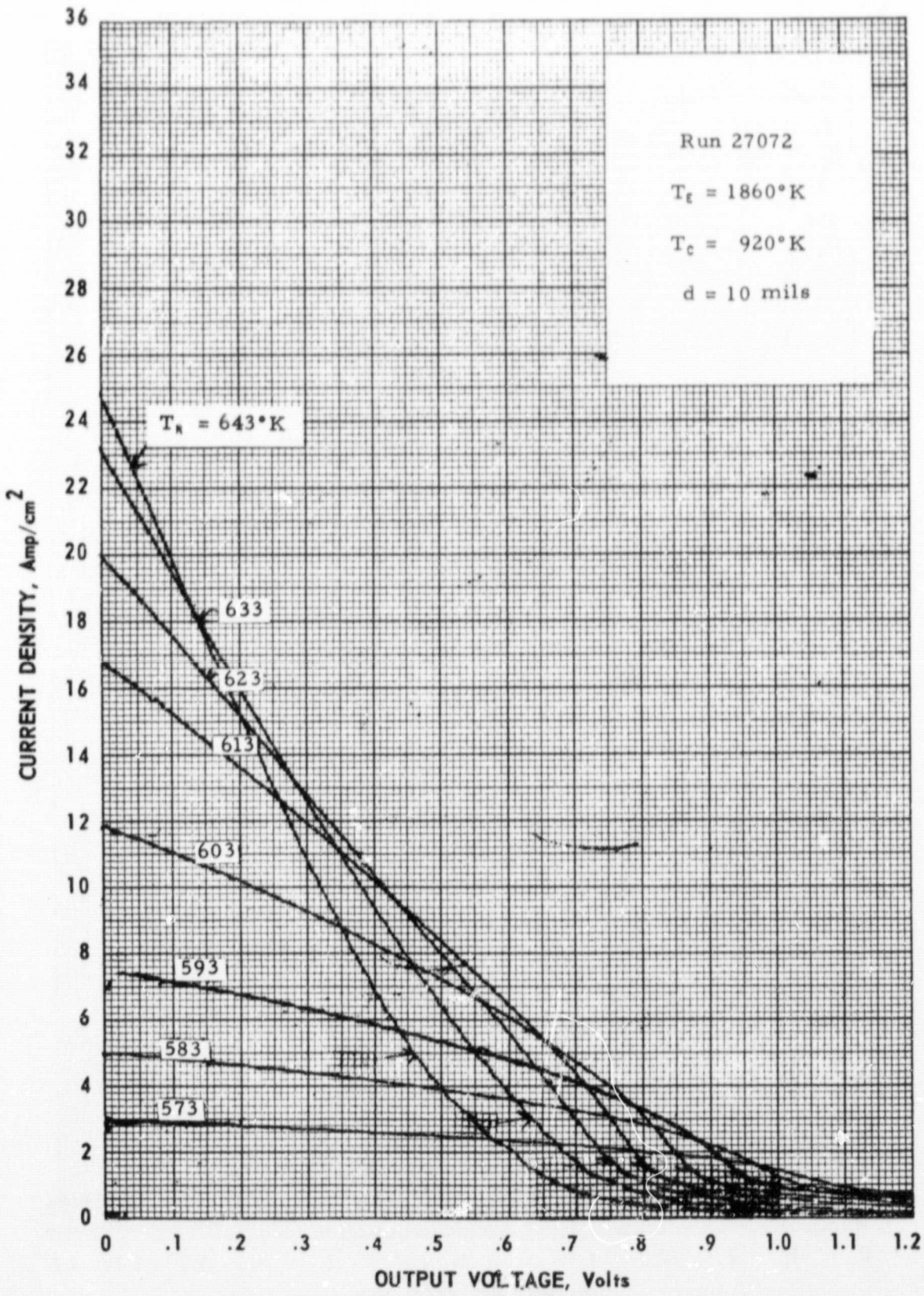


Figure III-61. Cesium-Temperature Family at T_E = 1860°K and d = 10 mils.

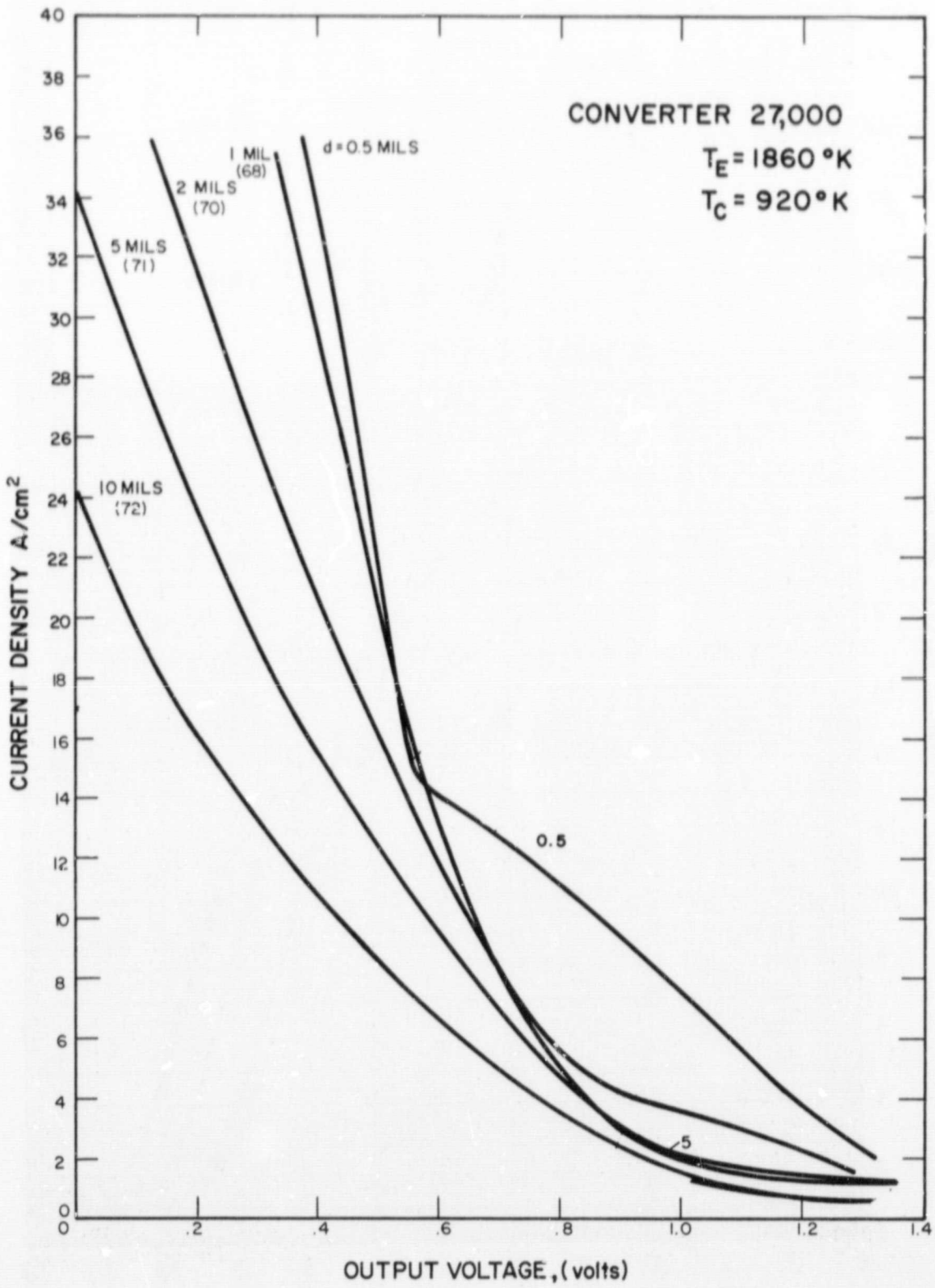


Figure III-62. Comparison of Cesium-Temperature Optimized Envelopes at T_E = 1860°K for Several Spacings.

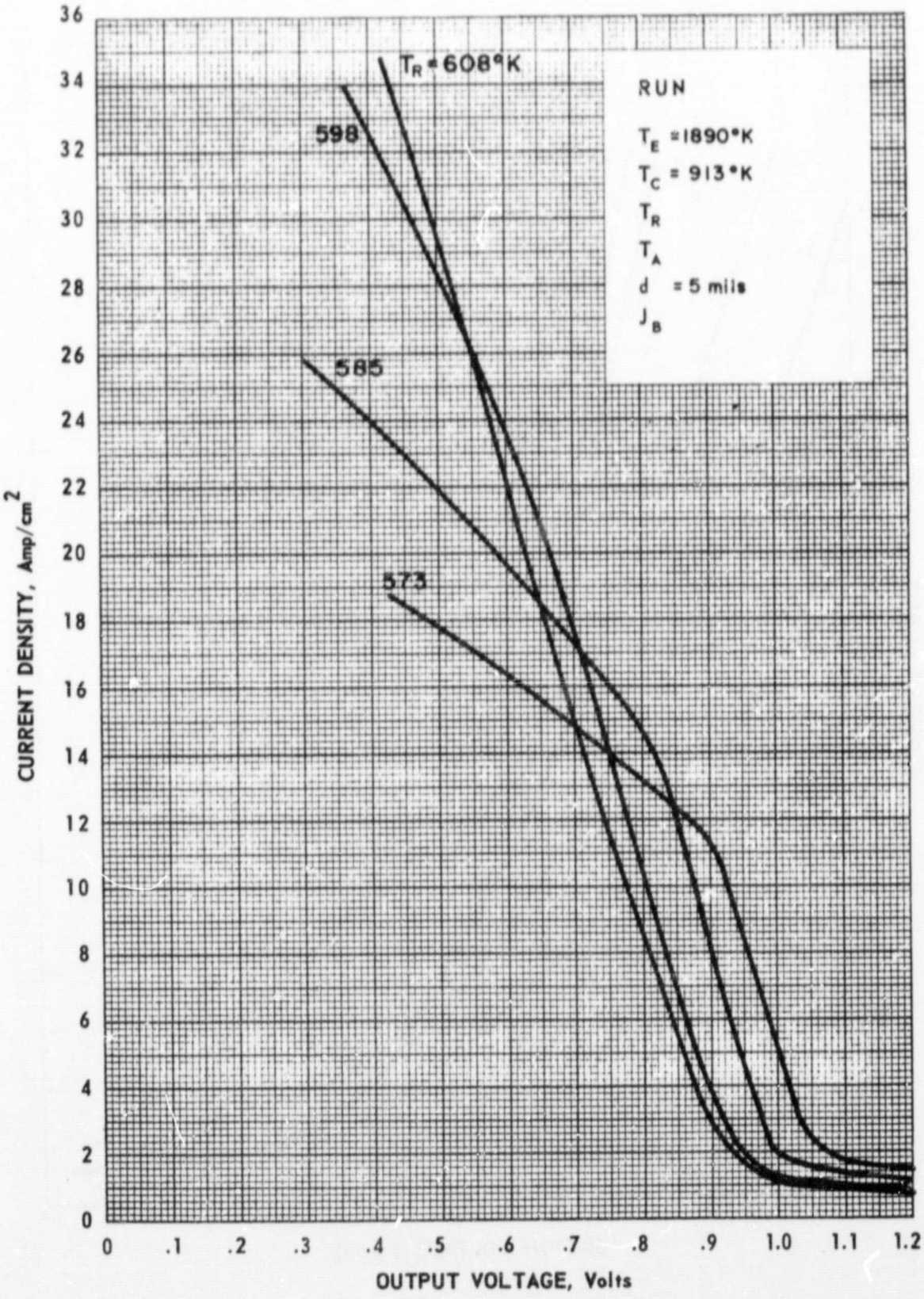


Figure III-63. Performance Data from a W-Mo Converter.

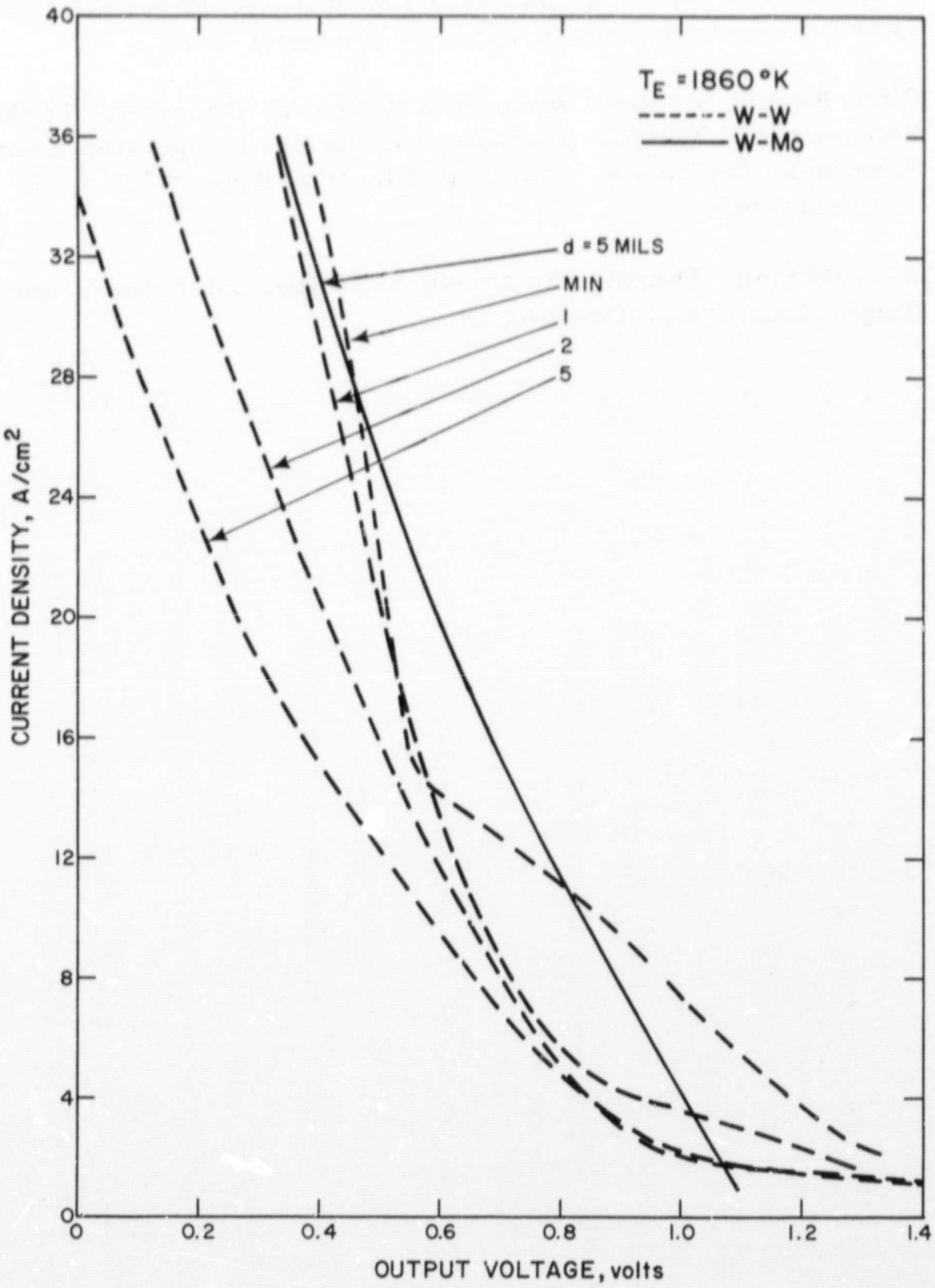


Figure III-64. Performance Comparison of W-Mo and W-W Converter.

REFERENCES FOR CHAPTER III

1. Final Report, Thermionic Research Program, Contract 951262, prepared for the Jet Propulsion Laboratory, Pasadena, California. Thermo Electron Report TE 12-67, August 1966.

2. Final Report for the Thermionic Research Program, Task IV, Contract No. 950661, prepared for the Jet Propulsion Laboratory, Pasadena, California. Thermo Electron Report TE 7-66, 2 August 1965.

3. M. Koskinen, Thermionic Conversion Specialist Conference, San Diego, California, October 1965.

CHAPTER IV

ELECTRONEGATIVE ADDITIVES FORMED IN SITU

F. Rufeh, D. Lieb, F. Fraim

A. OXIDES FORMED ON THE COLLECTOR AND GUARD SURFACES

1. Introduction

The characteristics of cesium-vapor thermionic converters have been well documented for a wide range of temperatures and interelectrode spacings and a variety of emitter and collector materials. These data define the performance limits to be expected from a simple cesium-only converter. One of the most promising techniques to improve converter performance is the use of electronegative additives.

The experiments of Langmuir and Villars[1] in 1931 showed the pronounced effects of small amounts of oxygen on the work functions of both cesiated and uncesiated tungsten. Recent experiments[2, 3] with thermionic converters have shown that approximately a monolayer of oxygen on the emitter surface improves the converter performance. Studies by Engelmaier and Stickney[4] have shown that, for a tungsten emitter in the temperature range from 1900°K to 2000° K, the oxygen pressure required for a monolayer coverage ranges from 10^{-8} to 10^{-6} torr. At lower temperatures even lower partial pressures are effective.

There are several techniques for providing oxygen on the emitter. In these experiments oxygen was provided by metal oxides formed on the collector and guard surfaces.

2. Experimental Apparatus

The converter used for these experiments is a variable-parameter research converter using a guarded molybdenum collector and a rhenium emitter. The test vehicle is described in Reference 5 and is shown schematically in Figure IV-1. The cesium reservoir is connected to a gas injection system by a nickel tubing. Any cesium that passes through this tubulation is condensed by the baffles and flows back to the reservoir.

The converter was first tested with cesium only, and the results of these tests provided reference data. All the cesium, about 2.5 g, was condensed on the collector and guard surfaces. Approximately 60 mg of oxygen was admitted to the diode and allowed to react with cesium. When the unreacted cesium was distilled back into its reservoir, the cesium reservoir could be operated in the normal manner. Since the collector was serving as a reservoir for the additive, the temperature of the collector and the oxygen pressure could not be varied independently.

3. Experimental Results

To study the effect of additive temperature on the emission characteristics, a volt-ampere family was obtained by varying the collector temperature while holding constant the emitter temperature T_e, the cesium reservoir temperature T_R and the interelectrode spacing d. A large increase in saturation current was observed on increasing the collector temperature from 573 to 773°K (Figure IV-2). The increase in saturation current expressed in terms of emitter work function is shown by the data points in Figure IV-3. The solid line

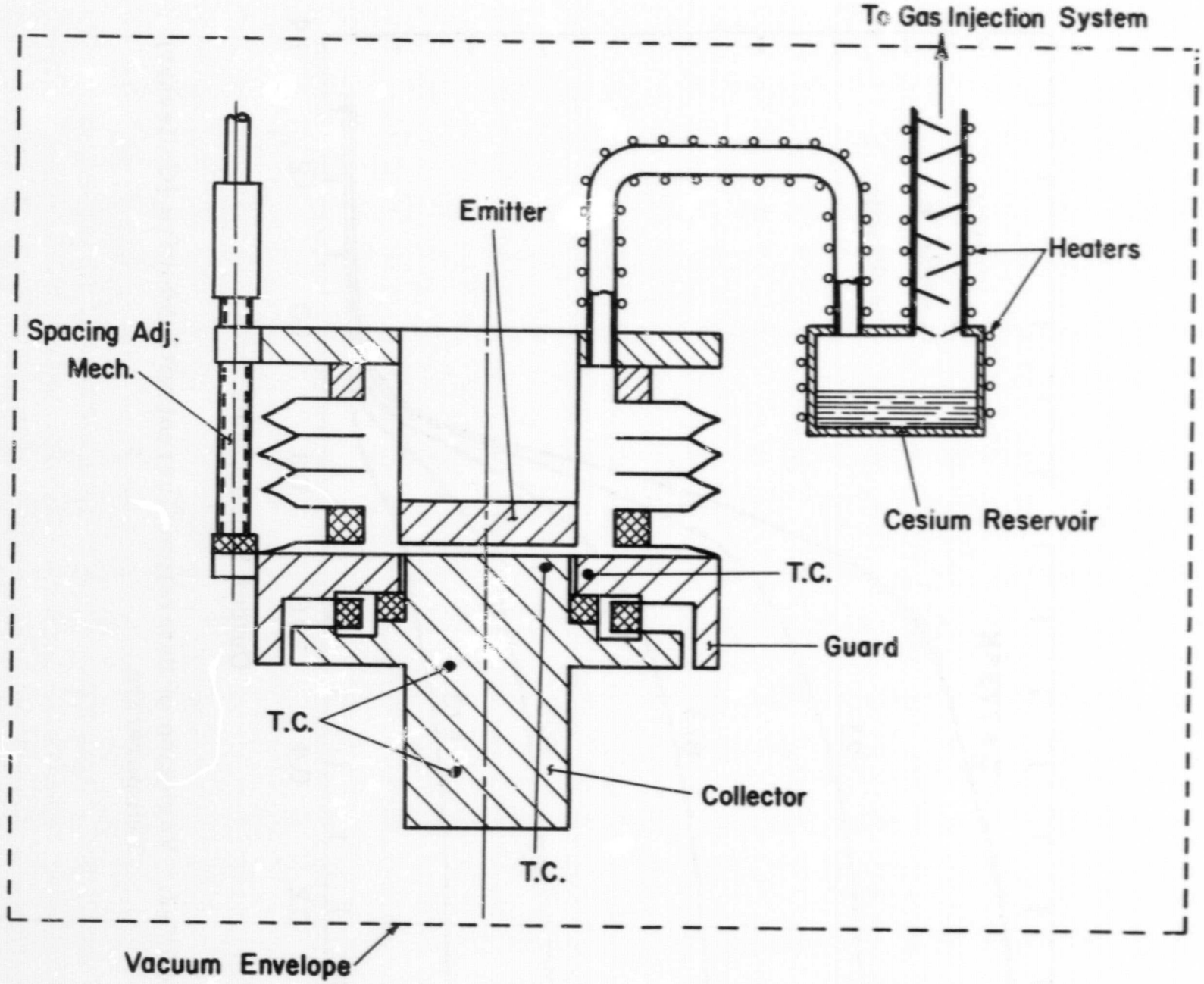


Figure IV-1. Schematic of the Test Diode.

THERMO ELECTRON ENGINEERING CORPORATION
TE-66-R-10-85

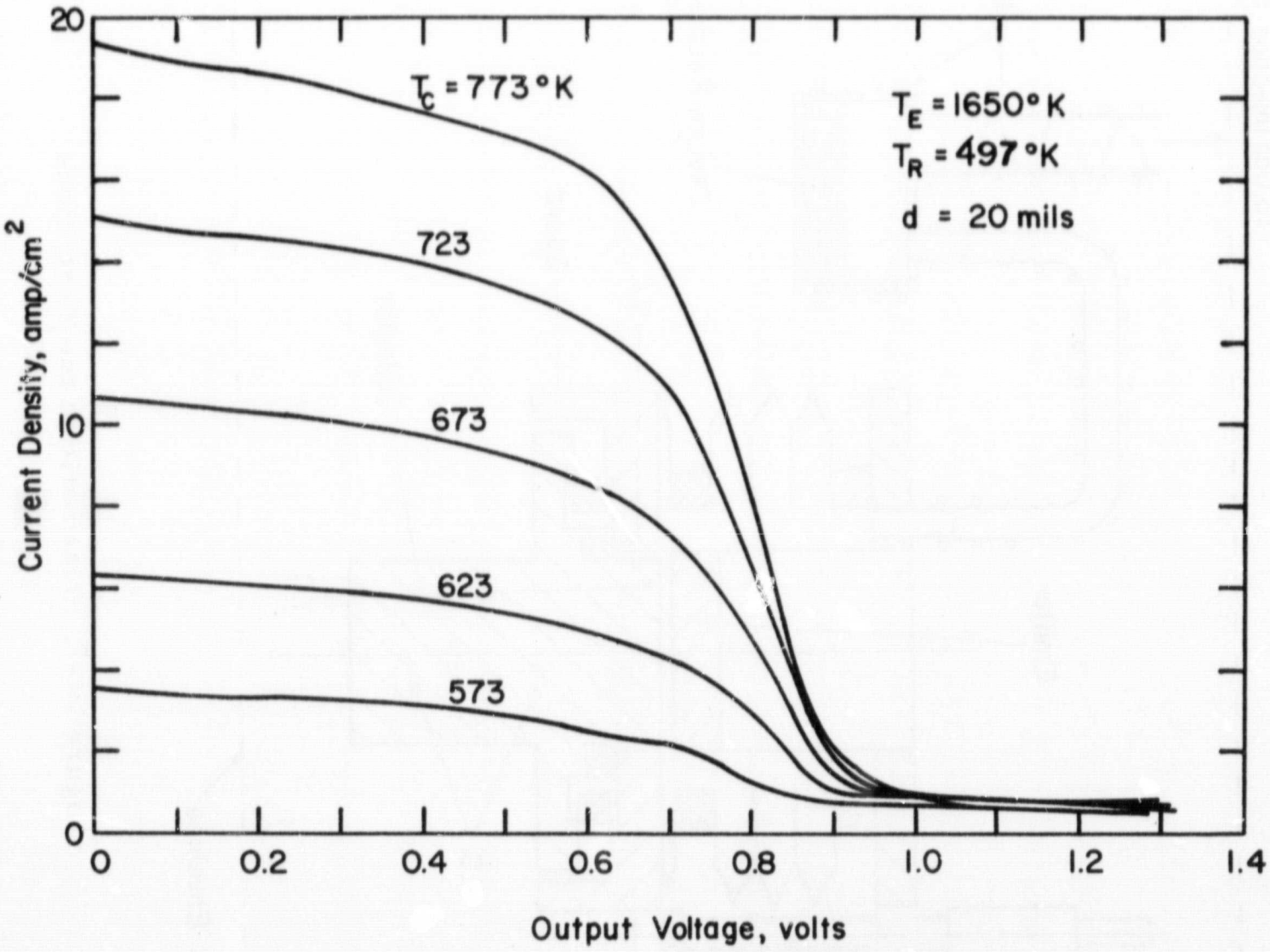


Figure IV-2. Variation of Saturation Current with Additive (Collector) Temperature.

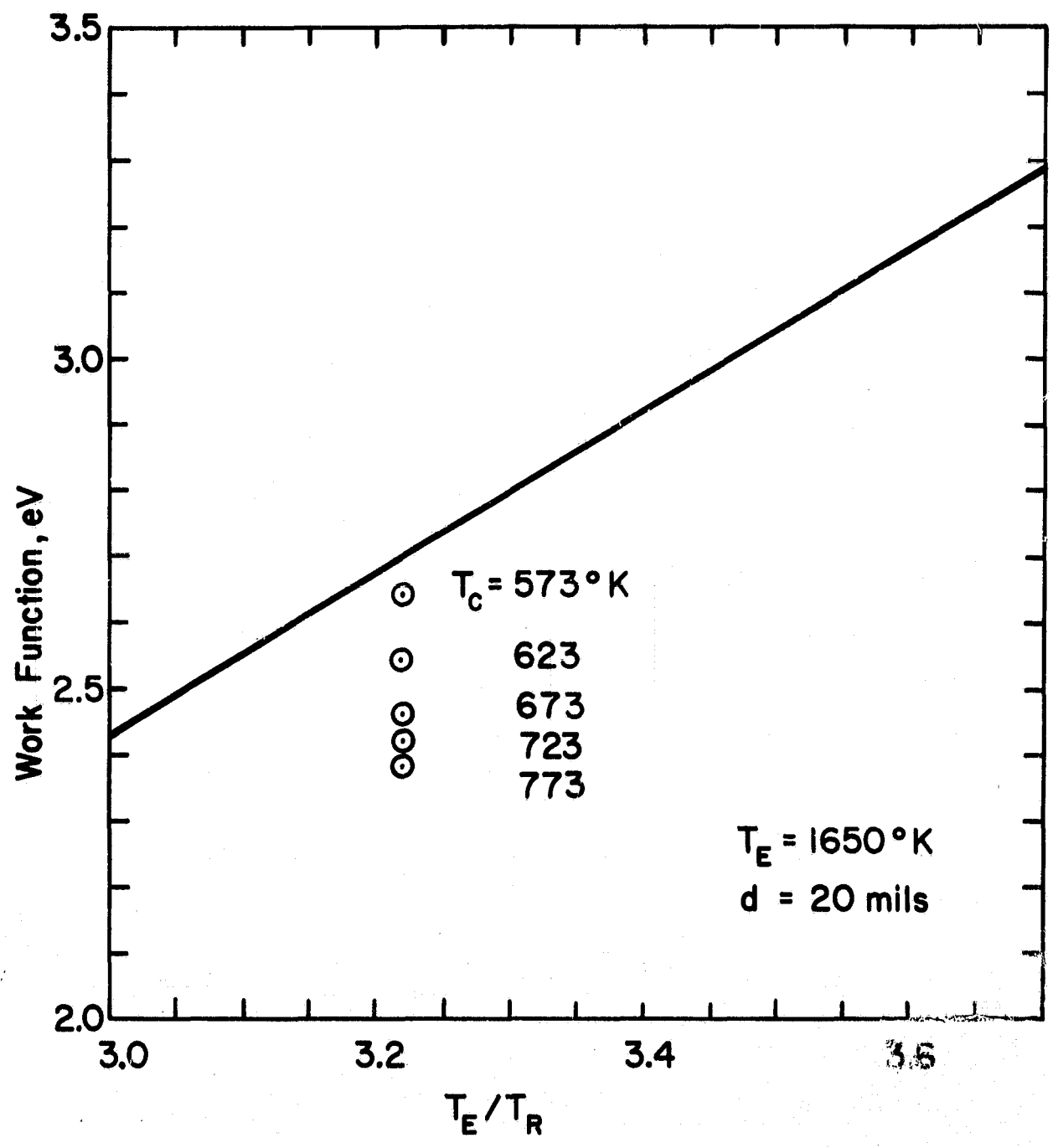


Figure IV-3. Variation of Emitter Work Function with Additive Temperature.

shows the work function plot for this emitter in the absence of oxygen. The emitter work function decreased by about 0.3 eV as the additive reservoir (collector) temperature was increased to 773° K. This change in work function corresponds to an increase of about 60° K in cesium temperature. These data were recorded at about 50-hour intervals for both increasing and decreasing collector temperatures and showed good reproducibility.

Collector-temperature and cesium-temperature families were obtained to evaluate the performance of the converter in the presence of additives and compare it with the cesium-only performance. The data cover the emitter temperature range of 1650° to 1850° K and the interelectrode spacing range of 5 to 20 mils. The collector temperature (and therefore the additive reservoir temperature) was kept at 720° K for most of these runs. A typical cesium family with oxygen is shown in Figure IV-4. It is interesting to observe a distinct difference between this family and the usual cesium family without oxygen. Unlike the cesium-only data, the J-V curves in Figure IV-4 do not cross each other, and the envelope of this family is also a member of the family, i.e., $T_R = 538°$ K. The output of the converter is quite insensitive to the cesium temperature. For example, in Figure IV-4 the output power at 0.5 volt stays constant, even if the cesium temperature is increased from 520° to 540° K. In the absence of the additive, this temperature variation changes the output by a factor of two. The performance of the converter is also relatively insensitive to the temperature of the cesium oxide reservoir when it is kept in the vicinity of its optimum value. Figure IV-2 shows that changing the additive temperature from 723° to 773° K changes the

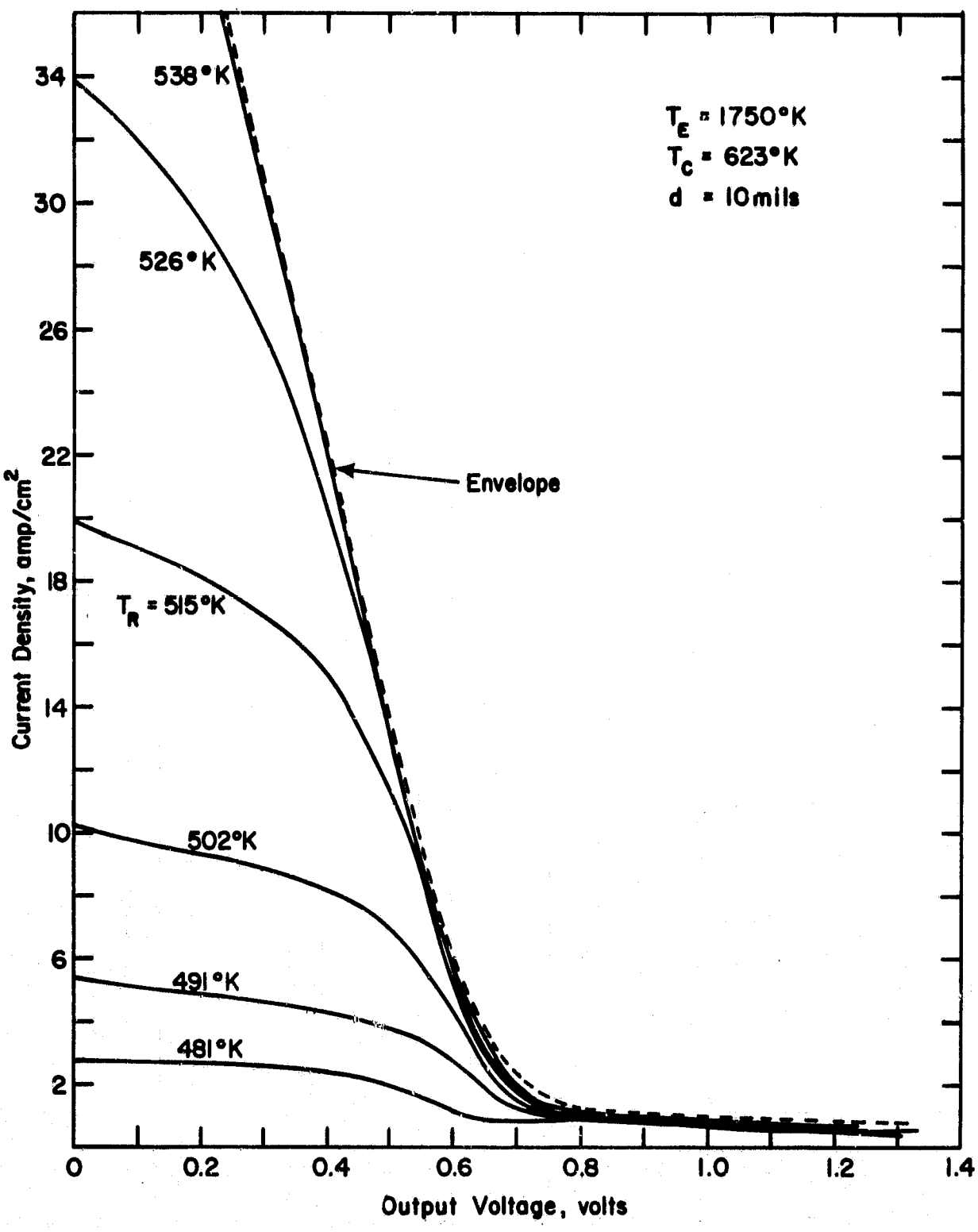


Figure IV-4. Typical Cesium Family in Presence of Additive.

current at 0.5 volt from 13 to 17 amperes, while a 50° change in cesium reservoir temperature would change the current by more than an order of magnitude.

The major effect of the addition of oxygen is observed by comparing the power output of the converter with and without cesium oxide (Figure IV-5). A substantial improvement in power is evident. Similar improvement in performance is shown at an emitter temperature of 1650° K in Figure IV-6. A summary for the other emitter temperatures is shown in Figure IV-7.

The effect of oxygen on performance can also be expressed in terms of interelectrode spacing. By making a comparison between the cesium envelope at 20 mils with oxygen and the cesium envelope at 5 mils without oxygen (Figure IV-8), it is clear that the use of oxygen allows an increase by a factor of 4 in the interelectrode spacing for the same power output. Oxygen addition reduces the required cesium pressure, which results in minimization of electron-cesium scattering.

To examine the stability of the oxygen effect, the converter was operated at a static point on the J-V curves for about 300 hours, at an emitter temperature of 1750° K, a cesium reservoir temperature of 515° K, and a collector temperature of 723° K. The static point was the output voltage of 0.6 volt. The performance was stable with a random variation of about 15%. To investigate performance stability under all operating conditions, the static data were interrupted periodically during the course of the 300 hours to record cesium temperature families for various emitter temperatures and interelectrode spacings. The data were reproducible with small variations (Figure IV-9).

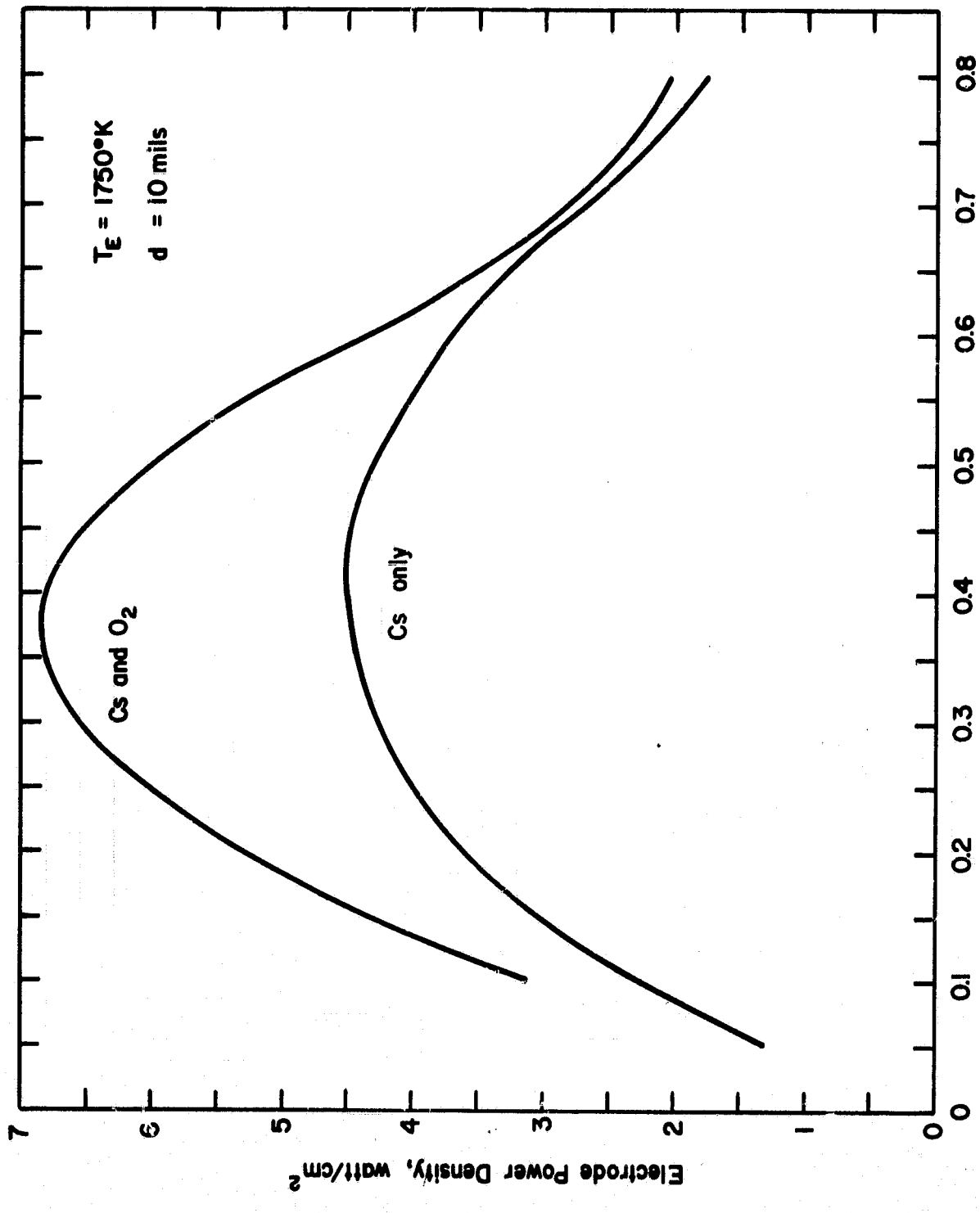


Figure IV-5. Comparison of Power Density With and Without Additive.

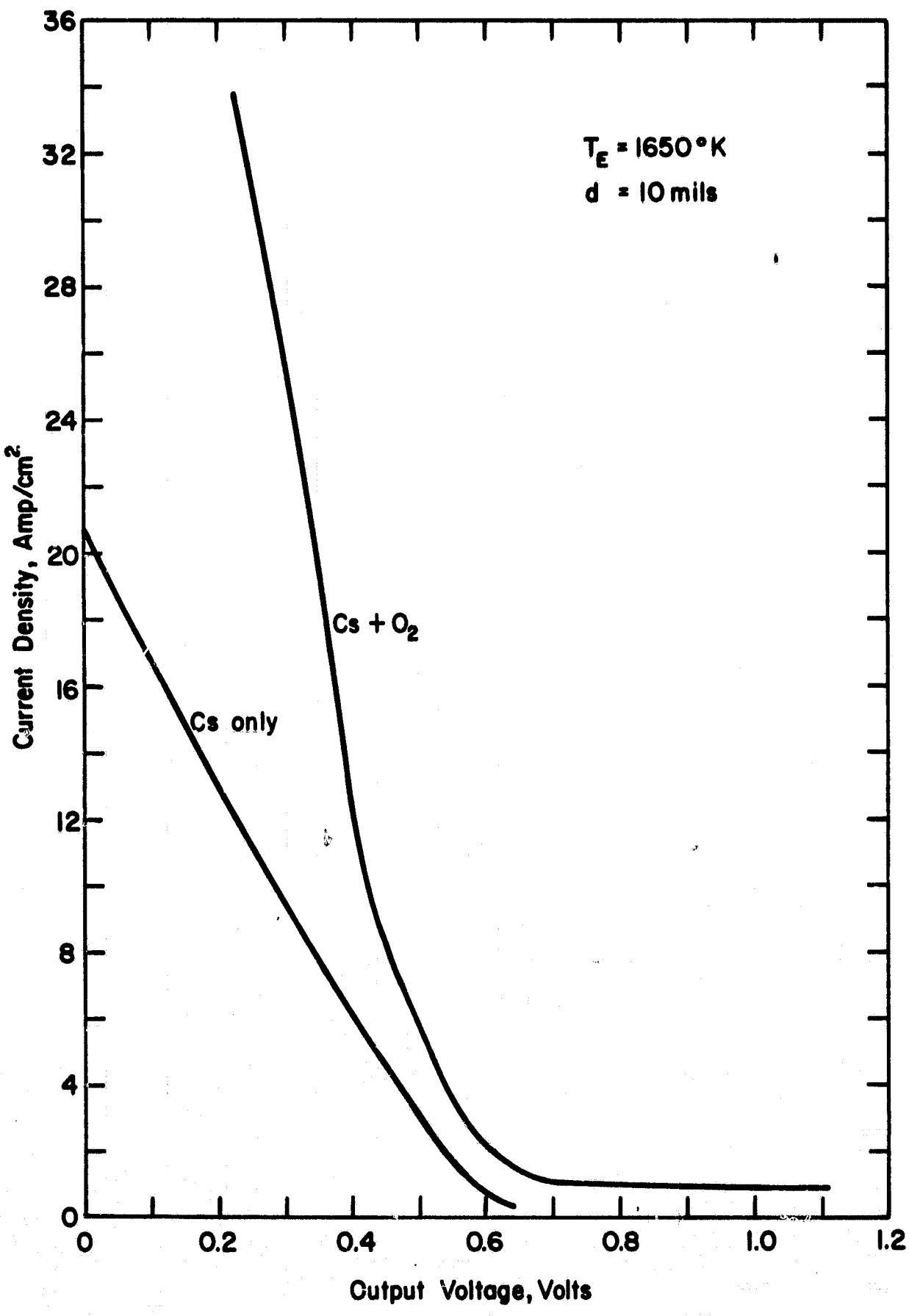


Figure IV-6. Comparison of Cesium Temperature Envelopes With and Without Additive.

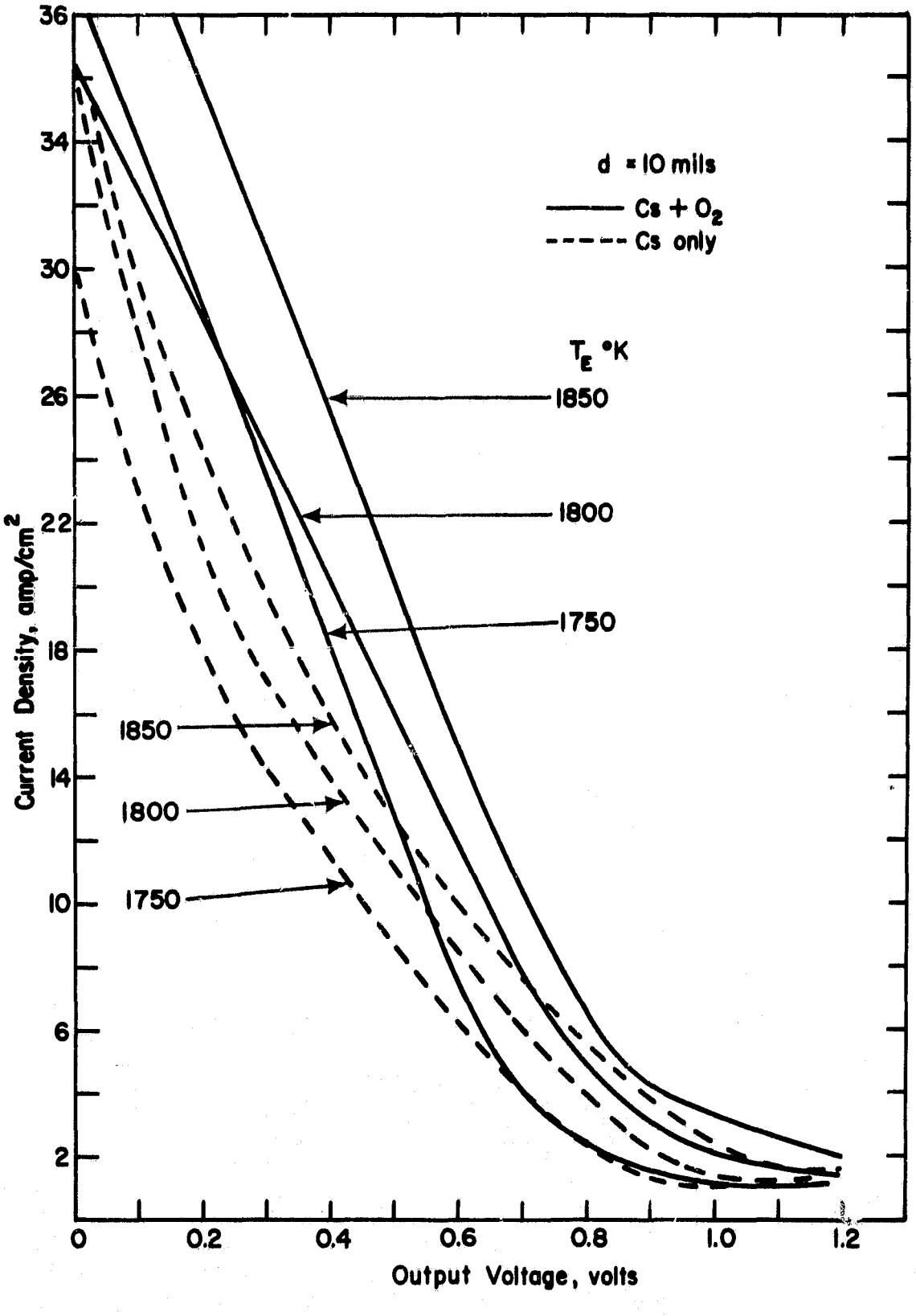


Figure IV-7. Comparison of Cesium Temperature Envelopes With and Without Additive.

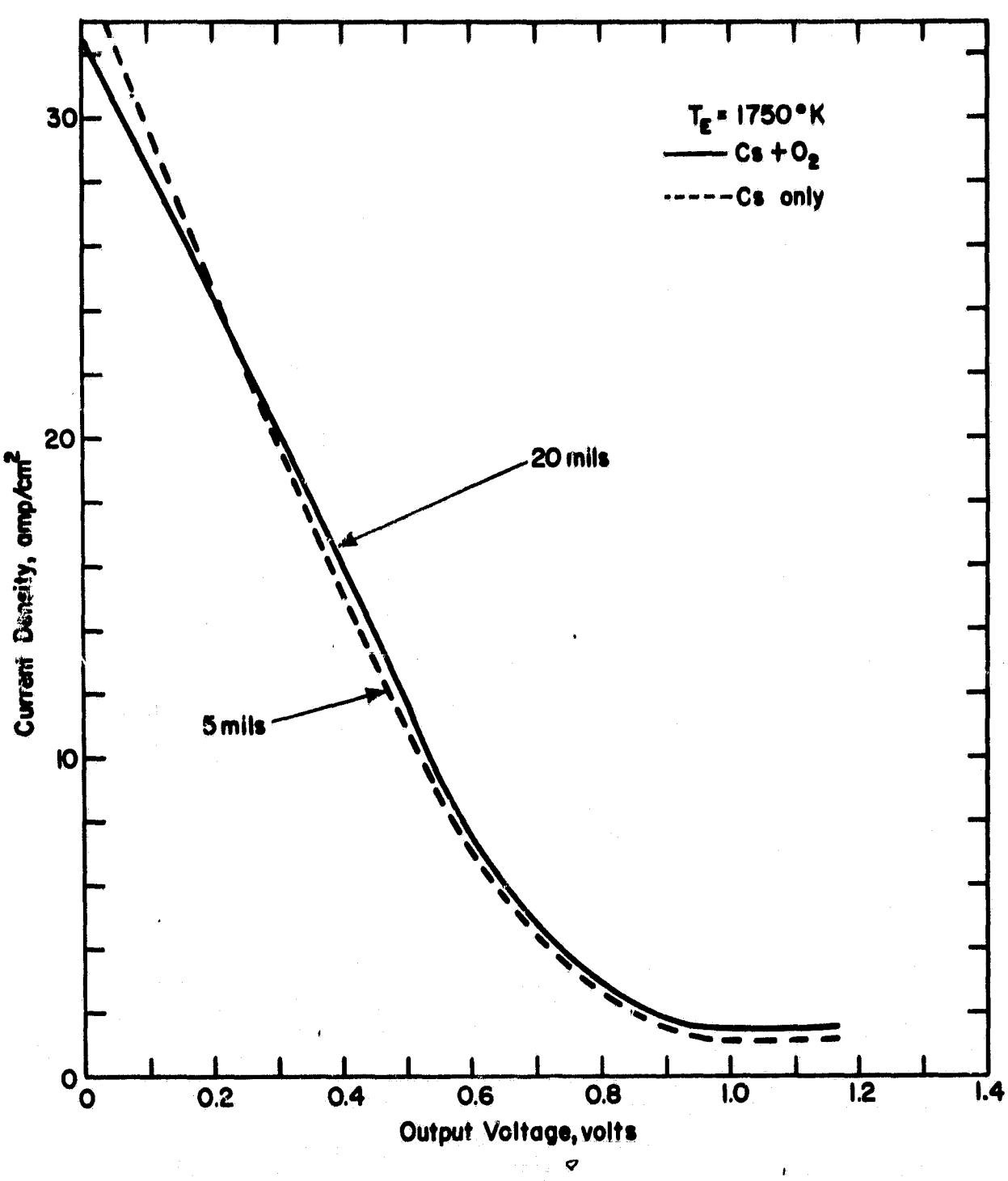


Figure IV-8. Comparison of Cesium Family Envelopes With and Without Additive.

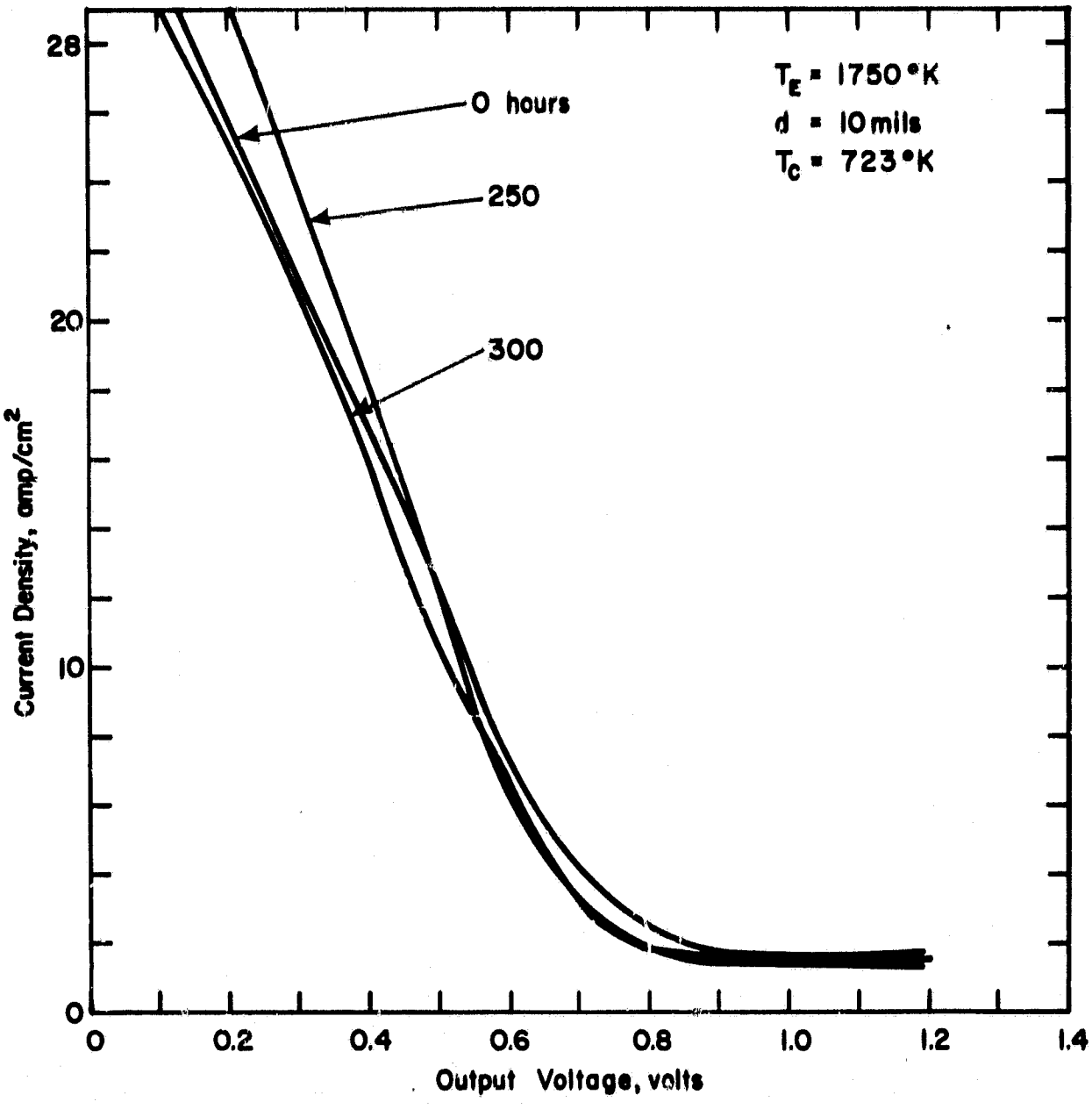


Figure IV-9. Comparison of Envelopes of Cesium Families at Various Time Intervals.

The emitter work function was also determined periodically from the J-V curves during this time. The data obtained at the various time intervals are shown in Figure IV-10. The times corresponding to the data points are not shown, as no trend was apparent and the scatter was random.

To examine the electrode circuits at the end of the 300 hours, the diode was disassembled. The emitter was clean and shiny (with no evidence of chemical attack) and its visual characteristics were the same as at construction time. A photograph of the emitter surface is shown in Figure IV-11. The two patches on the surfaces are grinding marks made during the fabrication. Before construction of the diode, they appeared shinier than the rest of the emitter, as they did after the disassembly. In examining before and after photomicrographs of the emitter surface (Figure IV-12), no evidence of possible etching due to oxygen (which would appear as hexagonal pitting) was found. The collector surface was covered with a thin black coating and the guard with a brown coating, as shown in Figure IV-13. When the deposit was cleaned with a moist swab, the surface appeared not to be corroded, although there was a discoloration.

This experiment has shown that oxygen can be used to produce a significant improvement in the performance of thermionic converters without causing any corrosion of the surfaces, an improvement which can be achieved for a wide range of operating conditions. The presence of this additive makes the performance of converters less sensitive to the cesium temperature. The improved output is stable and can be sustained for a long time.

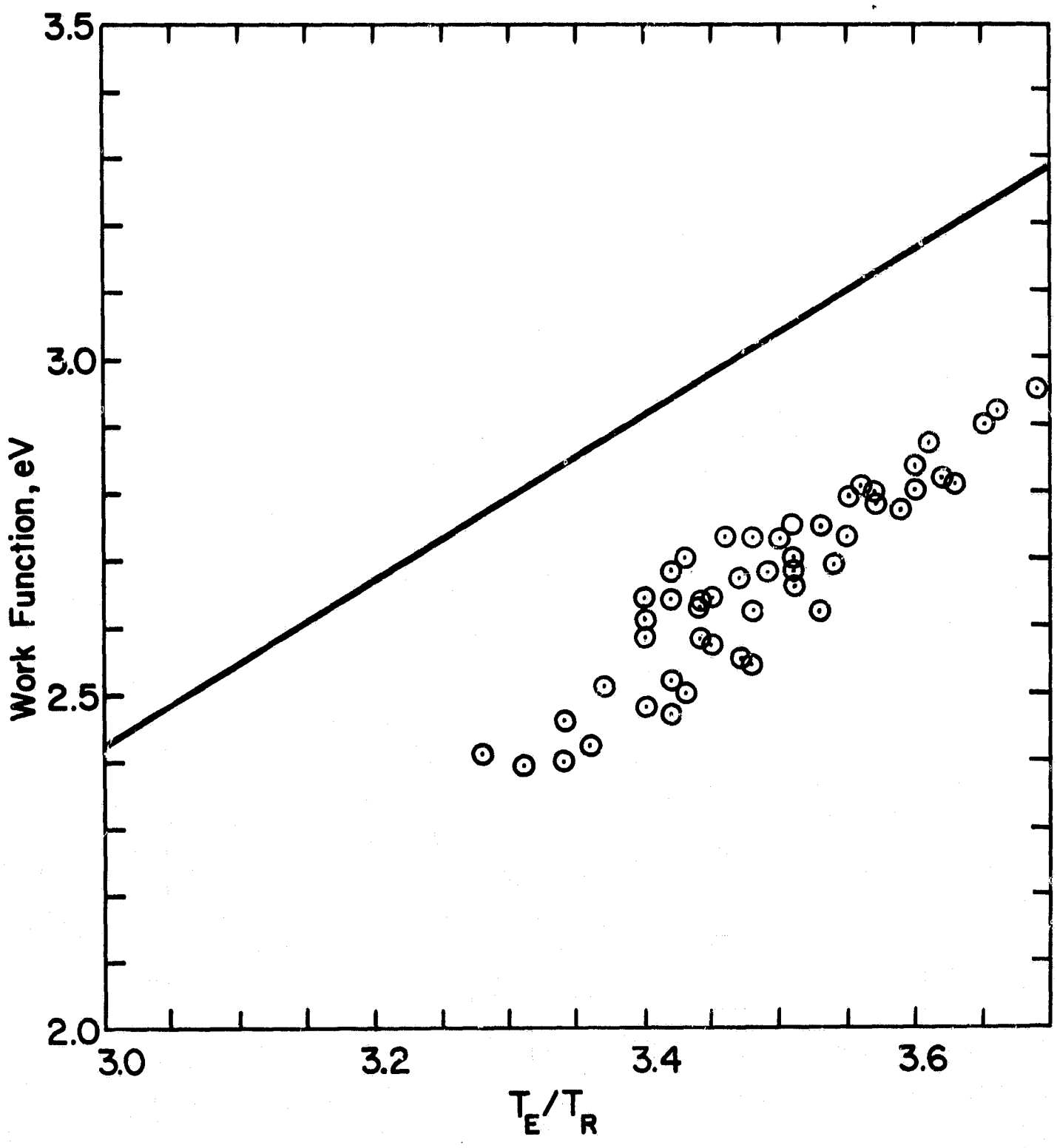


Figure IV-10. The Emitter Work Function During the Stability Test of the Diode.

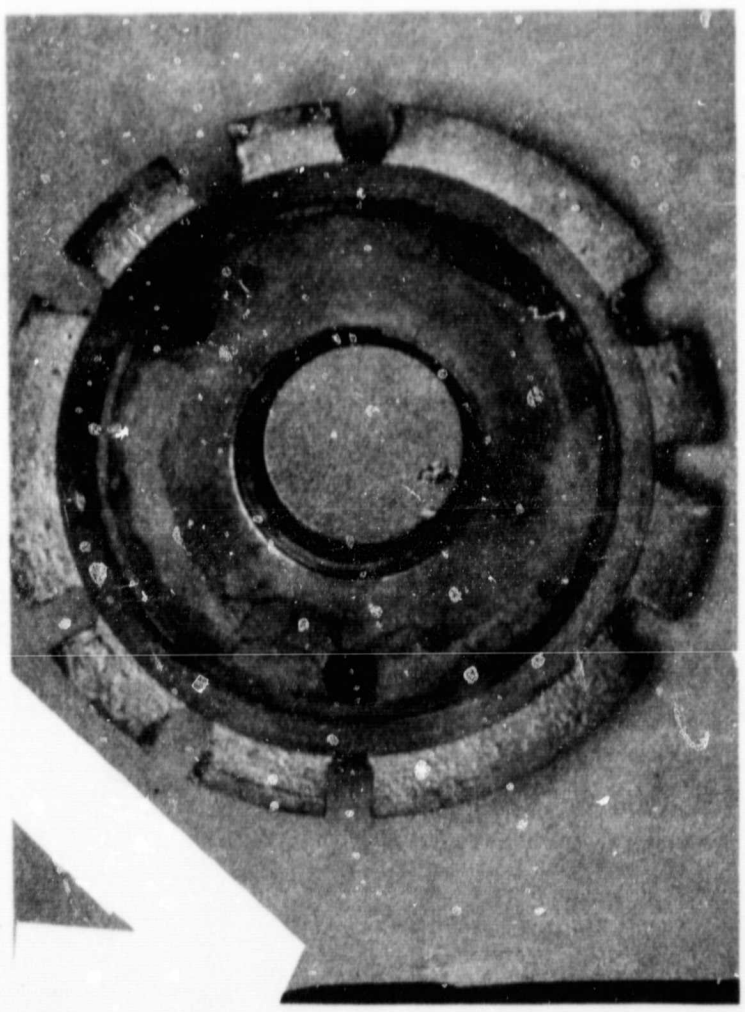
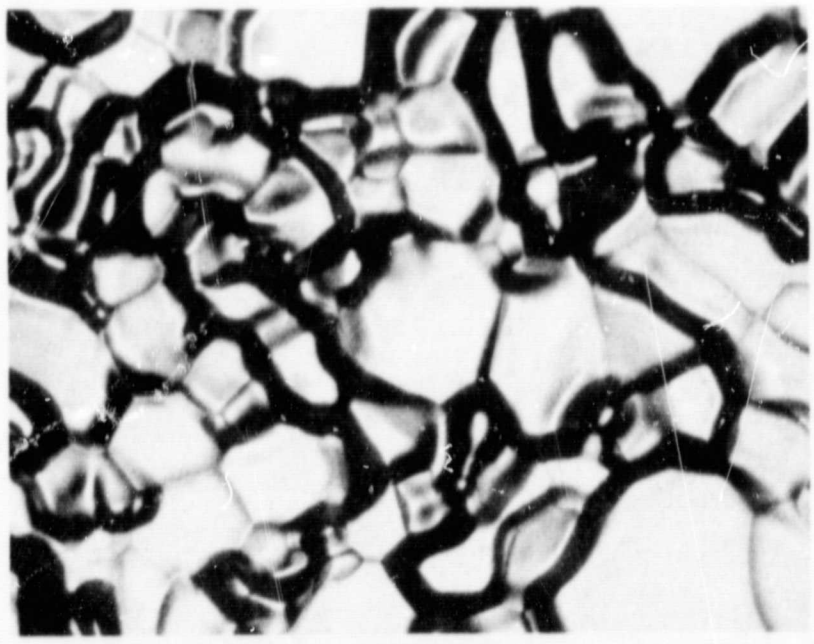
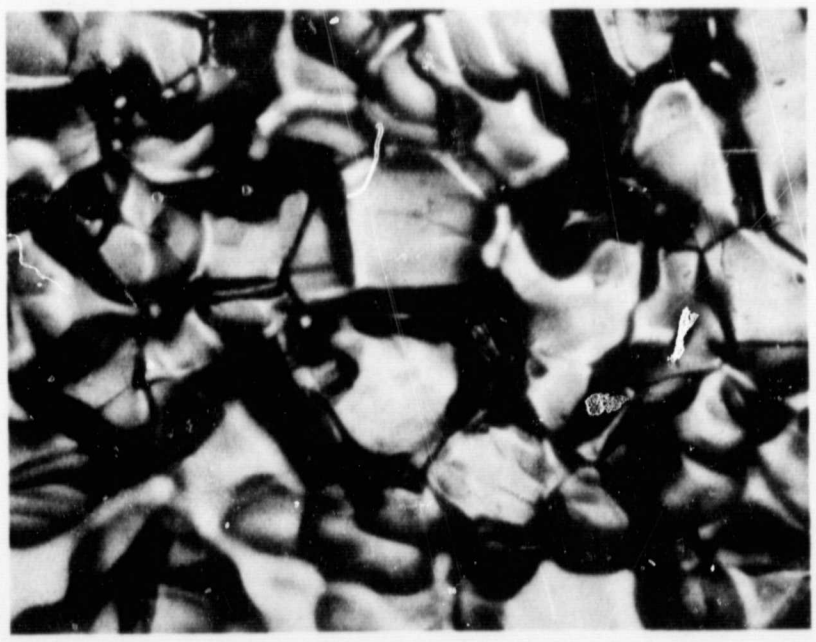


Figure IV-11. The Emitter Surface After the Disassembly of the Diode.



Before



After

Figure IV-12. Photomicrographs of the Emitter Surface Before Construction of the Diode and After the Disassembly.

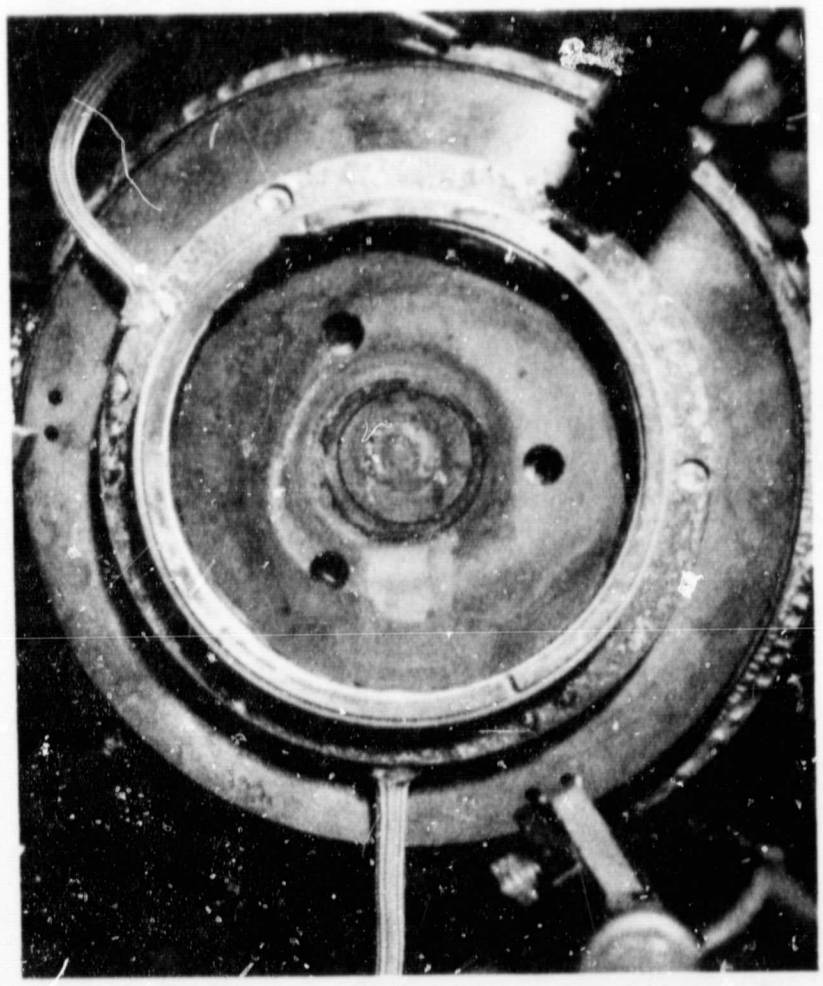


Figure IV-13. Photograph of the Collector Surface After Disassembly.

B. OXIDES FORMED IN THE ADDITIVE RESERVOIR

In the experiment described in section A, oxides were formed on the collector surface. Consequently, the temperature of the collector and the additive could not be varied independently. In order to determine the optimum collector and additive temperatures individually, it is desirable to place the additive in a separate reservoir.

If the additive is placed in a special reservoir, the question arises whether there will be any problems in the transport of the additive to the emitter surface. A fixed-spacing converter was designed and constructed to examine this question. This converter is equipped with a cesium reservoir which allows injection of gases into the internal volume of the diode (Figure IV-14). An additional reservoir is provided for use with the additive. Cesium oxide was formed in the additive reservoir by the following method: The additive reservoir was kept cold, and all the other components of the diode were heated. All of the cesium in the converter (about 2.5 grams) condensed in the additive reservoir. The volt-ampere characteristic of the diode was monitored to establish the completion of the distillation process. The diode was cooled, and a known quantity of oxygen was added to oxidize about one gram of the liquid cesium in the additive reservoir. Finally the converter was outgassed to eliminate any residual oxygen adsorbed on the surfaces.

To investigate the effect of the additive, families of volt-ampere characteristics were obtained by varying the additive reservoir temperature while keeping all the other parameters constant. Figure IV-15 shows a typical family at an emitter temperature of 1460°K and a cesium reservoir temperature of 433°K. A large increase in

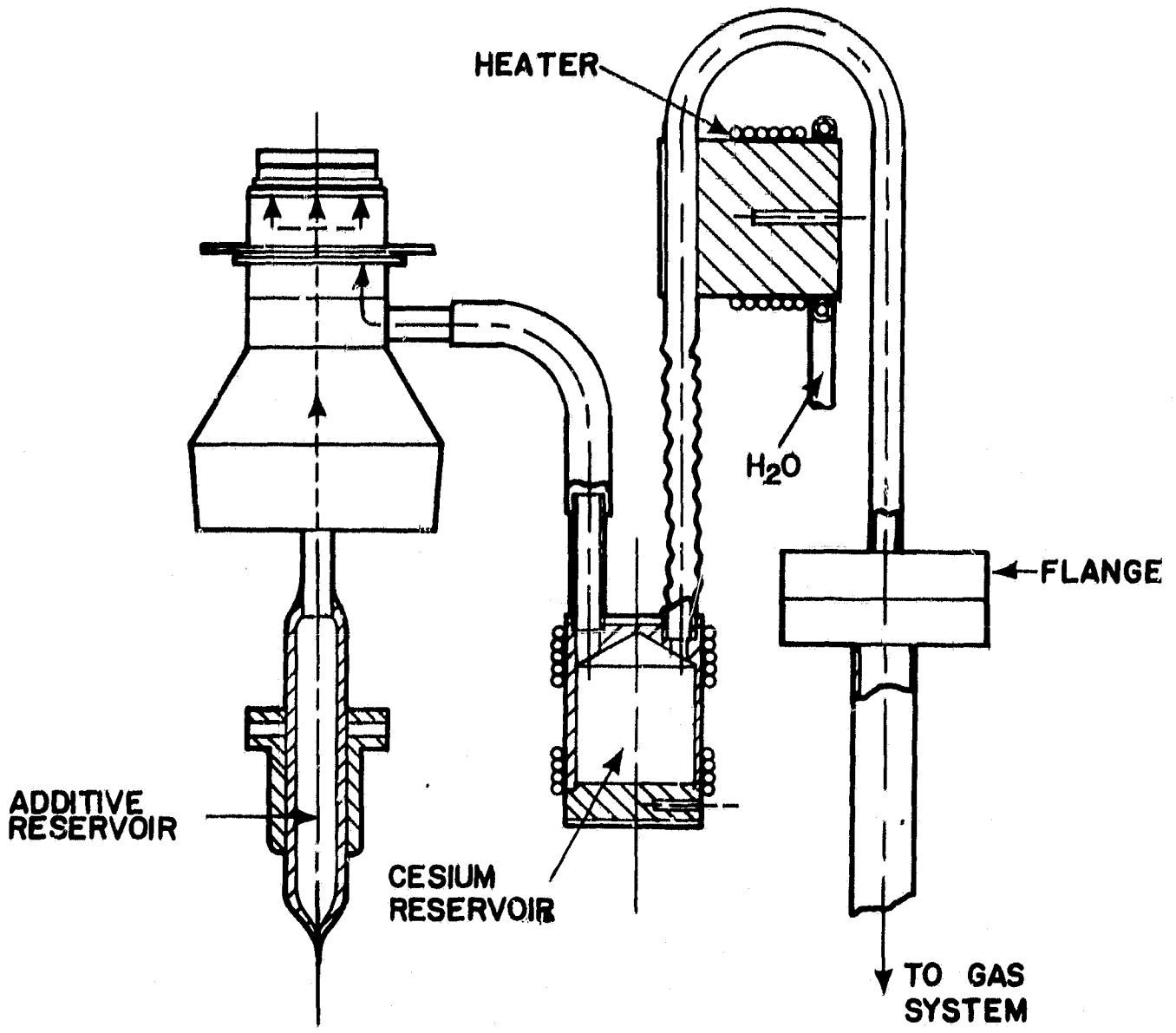


Figure IV-14. Schematic of the Fixed-Spacing Converter Used for Additive Experiments.

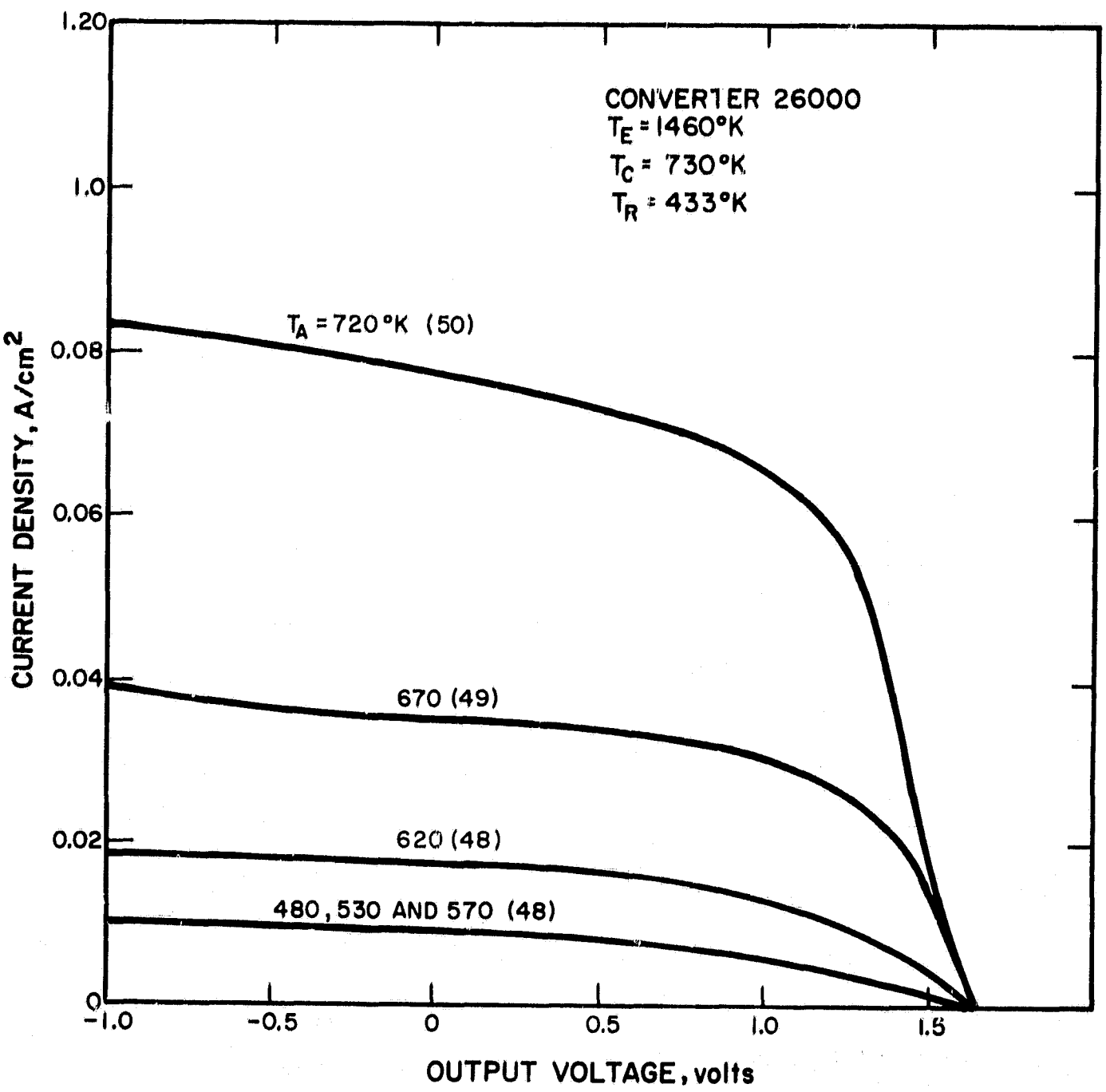


Figure IV-15. Dependence of Current Density on Additive Temperature at T_E = 1460°K and T_R = 433°K.

saturation current is evident when the additive temperature is increased from 570° to 720° K. Below 570° K, the saturation current was independent of the additive temperature. Similar families were obtained at cesium reservoir temperatures of 463, 488, 493, 503, and 523° K and at emitter temperatures of 1460 and 1560° K. Typical data is shown in Figures IV-16 through IV-18. Note that at low cesium pressures the dependence of electron current on additive temperature is strong, while at high cesium pressure this dependence is weak.

The stability of the additive effect was examined by operating the converter at fixed conditions for about 100 hours. The emitter temperature was maintained at 1560° K, the collector temperature at 820° K, and the cesium reservoir temperature at 493° K. The volt-ampere characteristic at an additive reservoir temperature of 670° K was recorded as a reference (the dashed curve in Figure IV-19). The additive temperature was raised to 770° K and was maintained at this level throughout the 100 hours of testing. The volt-ampere characteristics recorded at various time intervals are summarized in Figure IV-19. A slow improvement in performance was observed during this time period, and even after 100 hours equilibrium was not reached. The long time required to achieve equilibrium is due to the low rate of transport of the additive from its reservoir to the emitter surface.

This test was then terminated in order to examine the additive effect at higher cesium and emitter temperatures. Data were obtained at an emitter temperature of 1760° K, and a cesium temperature of 583° K. The volt-ampere characteristics were recorded for

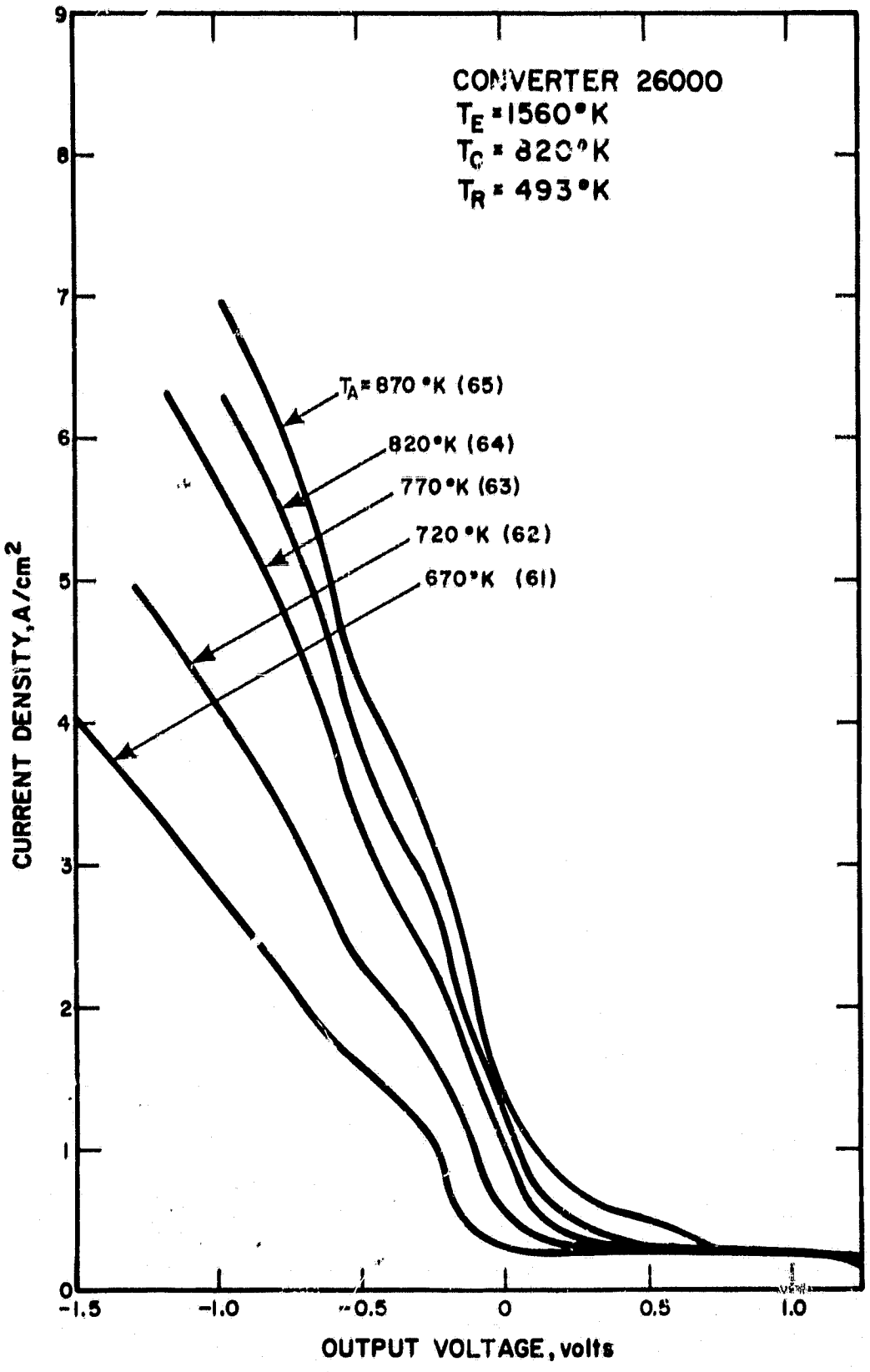


Figure IV-16. Dependence of Current Density on Additive Temperature at T_E = 1560°K and T_R = 493°K.

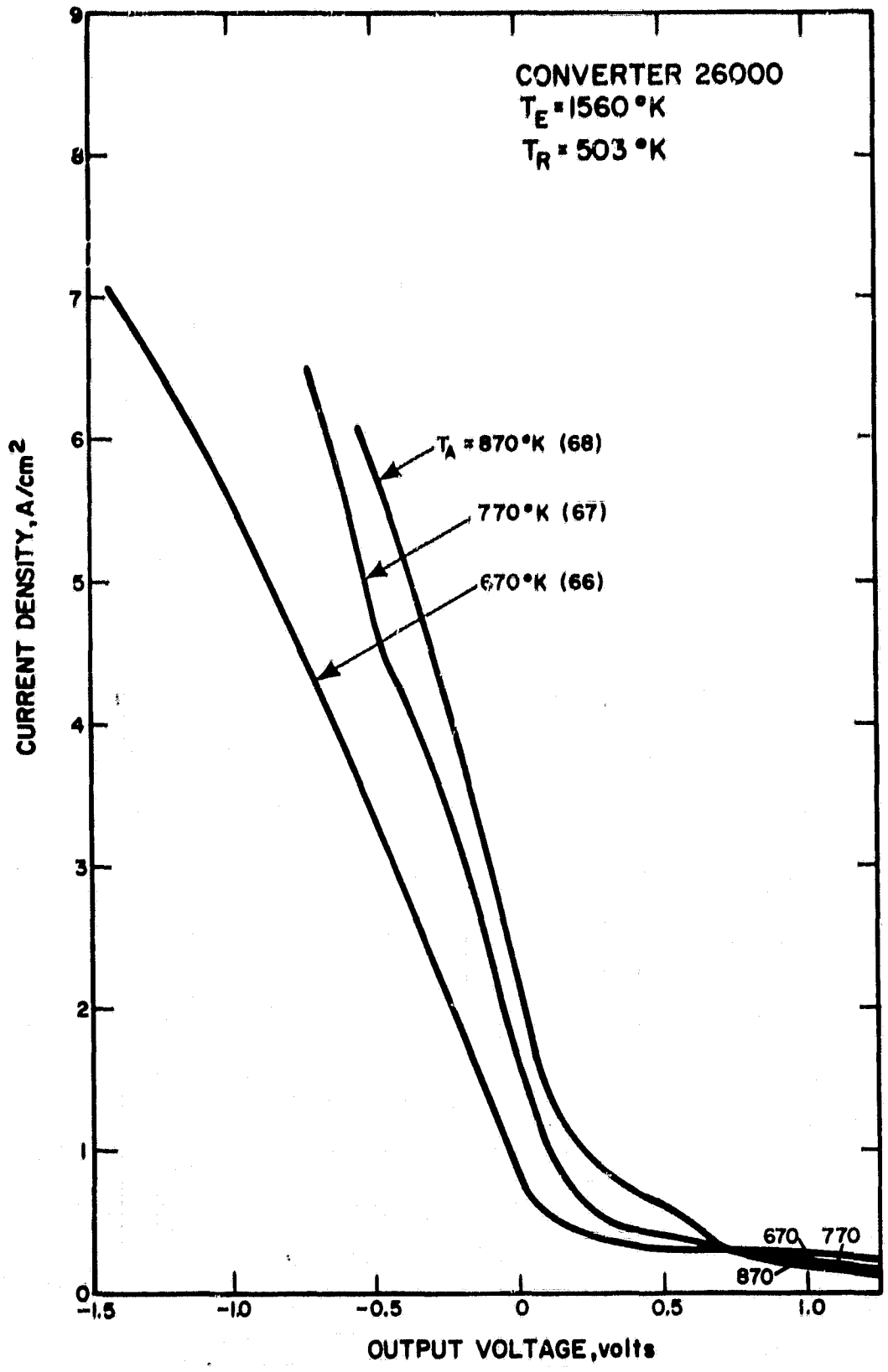


Figure IV-17. Dependence of Current Density on Additive Temperature at T_E = 1560°K and T_R = 503°K.

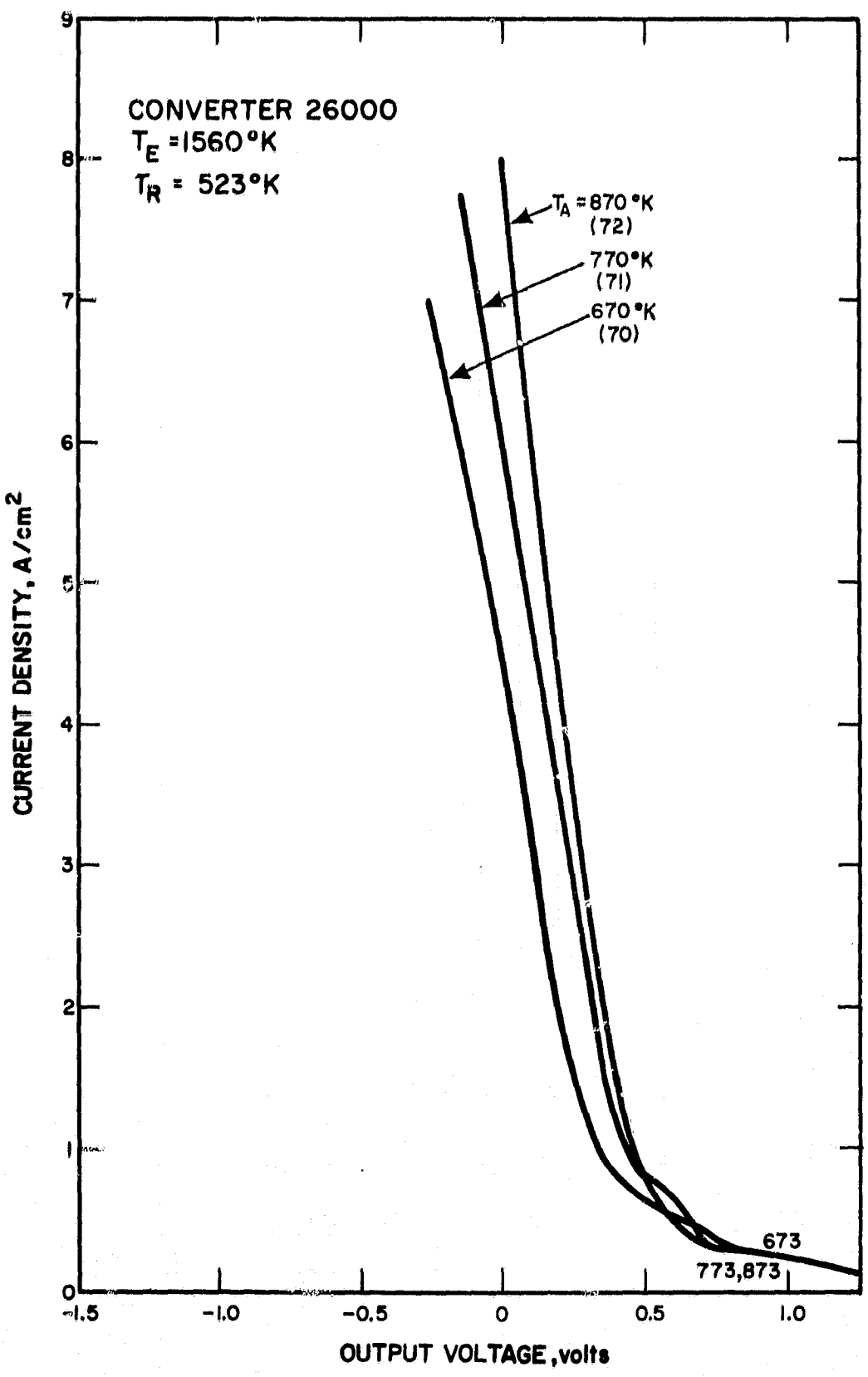


Figure IV-18. Dependence of Current Density on Additive Temperature at T_E = 1560°K and T_R = 523°K.

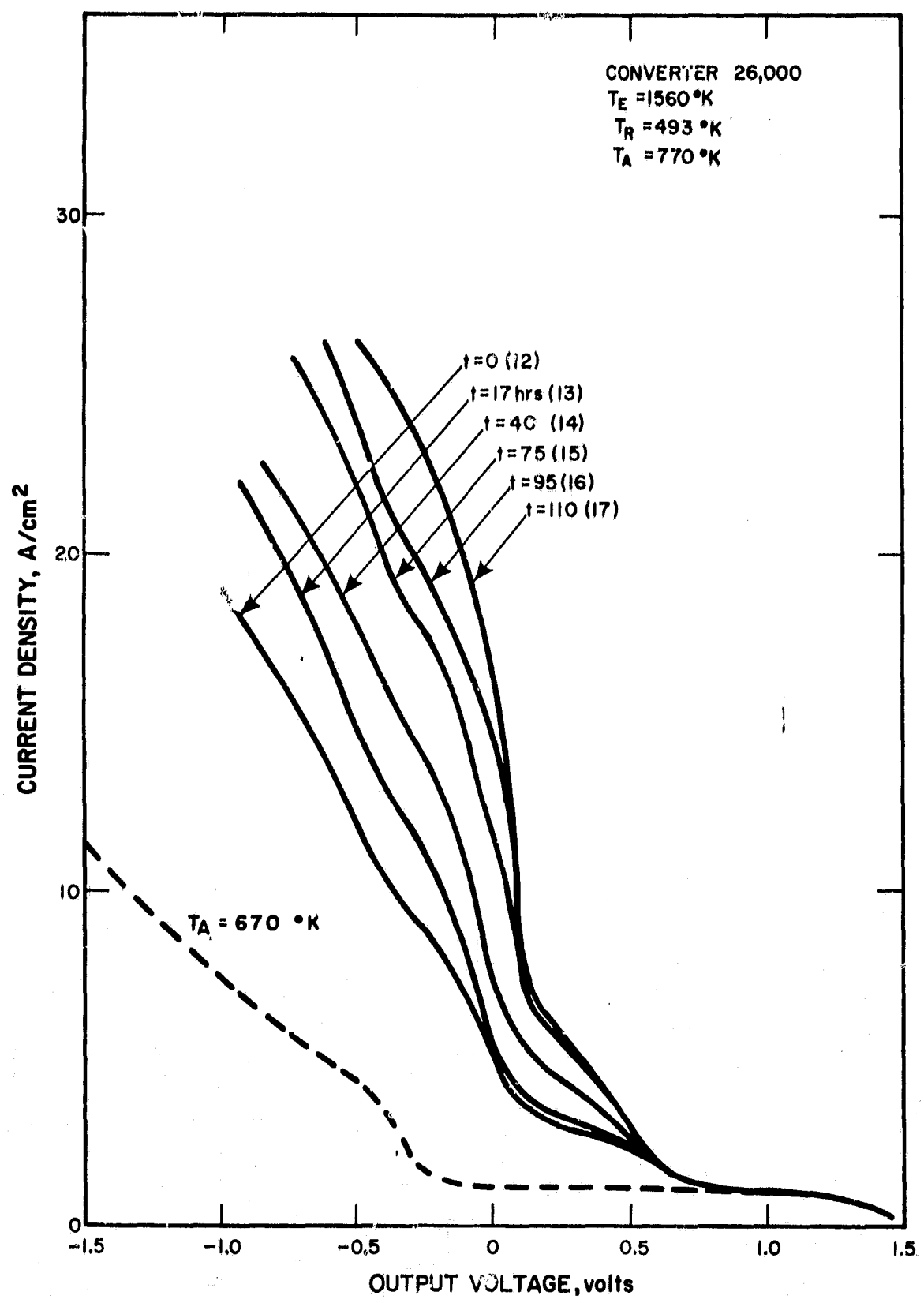


Figure IV-19. Variation of Current Density with Time After Increasing the Additive Temperature from 670 to 770°K.

additive temperatures in the range of 750 to 1000° K, and the results are shown in Figure IV-20. A significant additive effect is evident, although complete equilibrium has probably not been achieved. Each curve is taken at a time t_s after the indicated additive temperature is set.

The volt-ampere characteristics were recorded for various additive temperatures at an emitter temperature of 1960° K and a cesium temperature of 593° K (Figure IV-21). The additive effect under these conditions was much less than the effect observed at T_E = 1760° K and T_R = 583° K (Figure IV-20). There are two reasons for this difference:

1. A higher additive arrival rate is required to achieve a given coverage on the emitter surface at T_E = 1960° K than at T_E = 1760° K.

2. The additive transport is more impeded at a cesium temperature of 593° K than at a temperature of 583° K.

C. DISCUSSION

A particular technique was used in the experiments described in sections A and B to provide oxygen in thermionic converters. The results show that the technique used in these experiments for providing a continuous supply of oxygen to the emitter surface is quite promising. Although it is not clear which oxide (or oxides) is responsible for the reduction of emitter work function, the results of the two experiments were similar. In both experiments the additive effect appeared at an additive temperature of about 670° K, and the emission increased with increasing additive temperature.

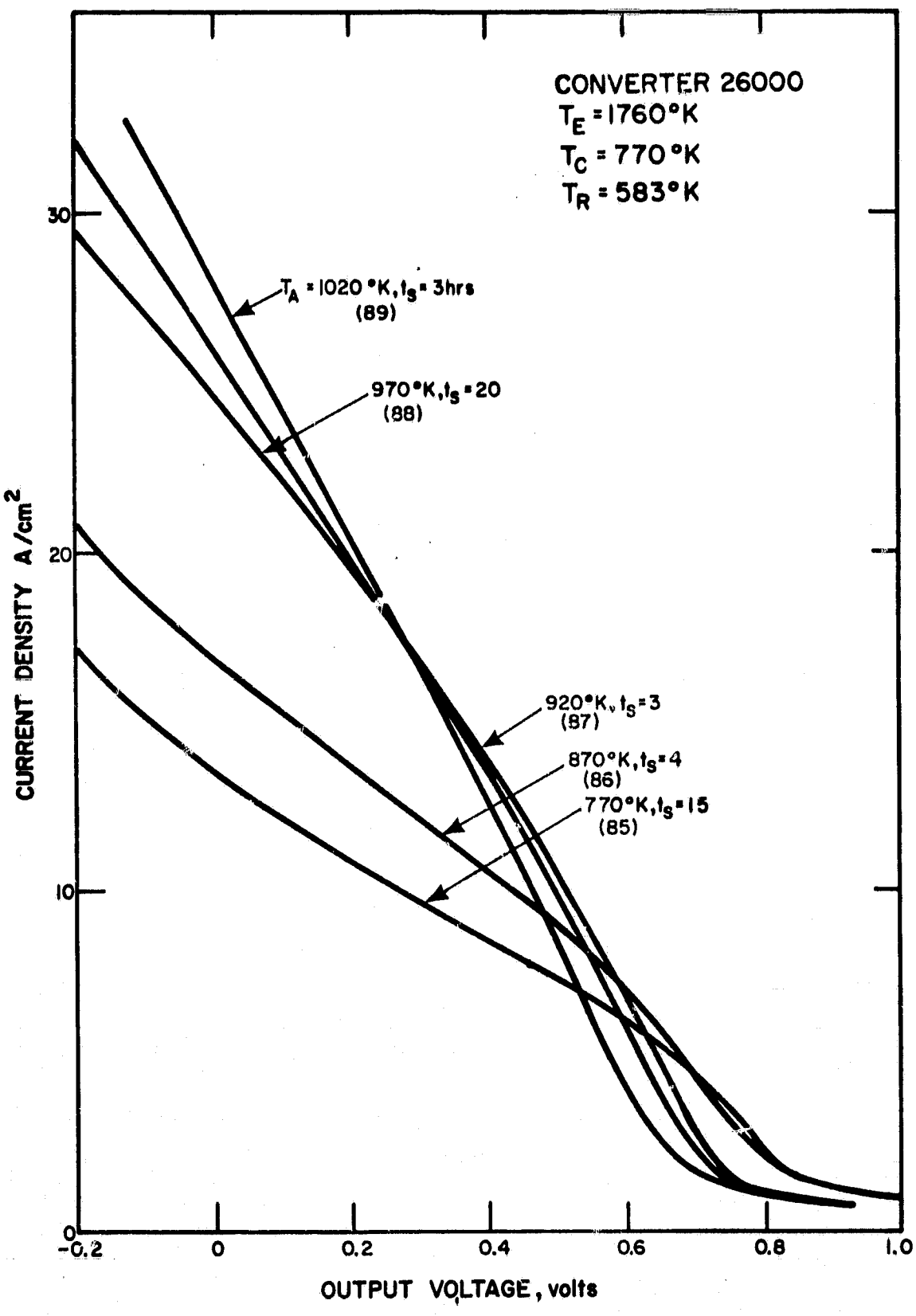


Figure IV-20. Dependence of Current Density on Additive Temperature at T_E = 1760°K and T_R = 583°K.

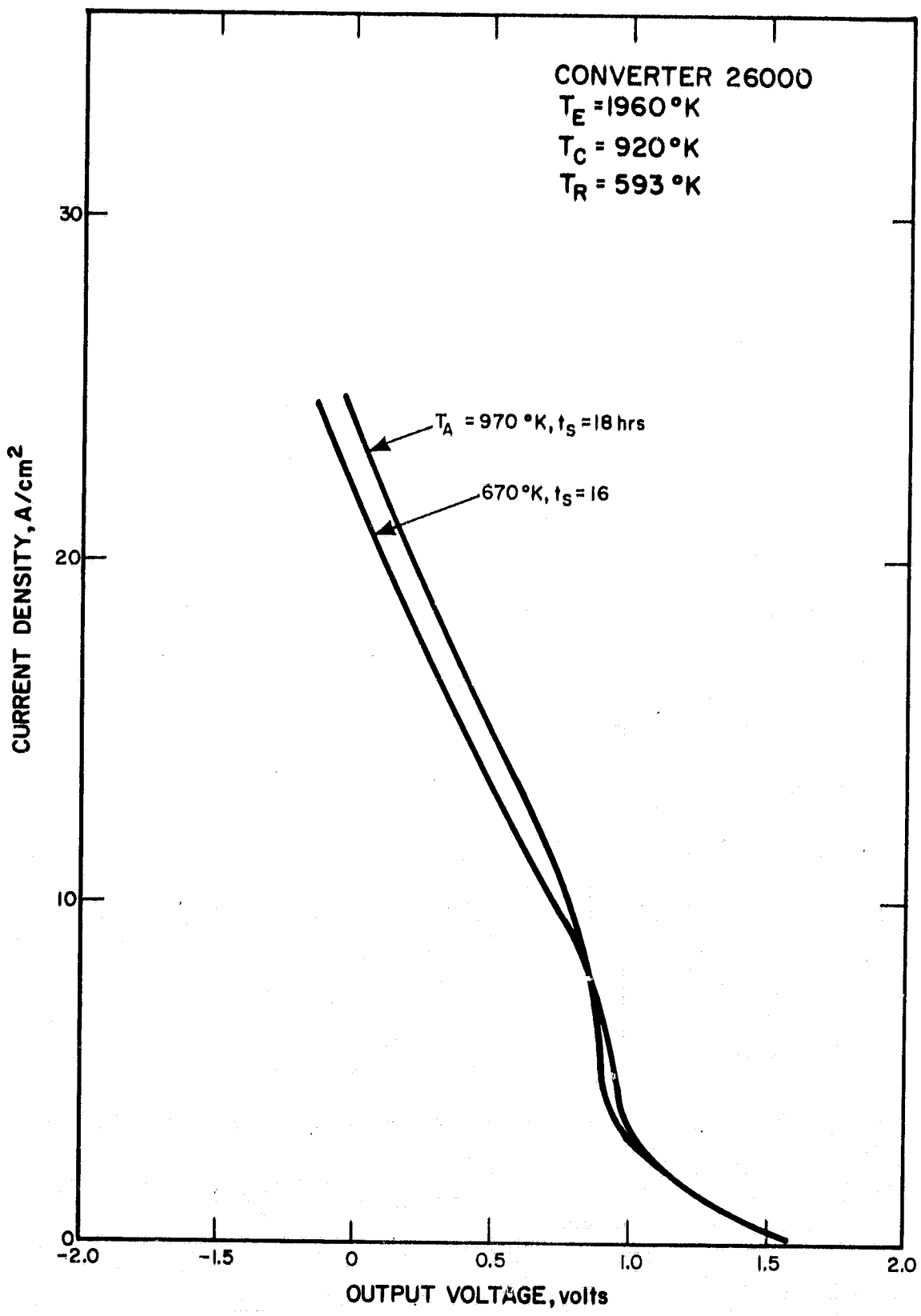


Figure IV-21. Dependence of Current Density on Additive Temperature at T_E = 1960°K and T_R = 593°K.

A major difference was observed between the results of the two experiments. In the first experiment, each time the additive temperature was varied, the additive effect was observed without any perceptible time lapse and equilibrium was reached almost instantaneously. In the second experiment a long time interval was required to establish equilibrium. This difference is probably related to the difference in the location of the additive in the two converters.

In the first experiment the additive was formed on the surface of the collector, and there were no difficulties in the transport of the additive from the collector surface to the emitter. In the second experiment the additive was formed in a reservoir which was relatively far from the emitter surface. In this case transport of the additive to the emitter surface was impeded by collision with cesium atoms. Depending on the pressure of cesium, a time interval of 1 to 100 hours was required to establish equilibrium each time the additive temperature was varied.

These results indicate that the source of oxygen must be placed as close as possible to the emitter surface. Since the operating temperature of the additive reservoir is quite close to the usual collector temperatures, the collector surface appears to be a suitable location for the source of oxygen.

D. CONVERTER PERFORMANCE WITH CESIUM OXIDE ONLY

The converter described in section B was used to investigate the possibility of operating a converter with cesium oxide only. All of the cesium in the converter was condensed in the cesium reservoir by keeping it cold while heating the rest of the converter to 670° K. The

cesium reservoir was then pinched off, leaving only cesium oxide (in the additive reservoir). Families of volt-ampere characteristics were obtained at three emitter temperatures by varying the additive reservoir temperatures. The cesium-oxide-only data are shown in Figures IV-22, IV-23, and IV-24. The family obtained is quite similar to a cesium family from a cesium-only converter, and that family defines an envelope which represents the optimized performance with respect to cesium oxide. This data can be compared with cesium-only performance obtained at the same emitter temperatures before the introduction of oxygen into the converter (Figures IV-25, IV-26, and IV-27). A major difference between the two sets of data is that the additive temperatures are about 100° K higher than the cesium temperatures. Therefore the coldest member of the additive-only converter is 100° K hotter than the coldest member of the cesium converters. This feature is significant in most thermionic applications, where special cooling must be applied to keep the cesium reservoir cold. Figures IV-28, IV-29 and IV-30 show a comparison of the envelopes of the cesium-only and the additive-only families. The cesium-oxide envelopes have a higher slope than the cesium envelopes because the cesium pressures are lower and electron scattering is less. At T_E = 1860° K, the power output with cesium oxide is higher than with cesium. At an emitter temperature of 1660° K, however, the power output with cesium oxide is less than with cesium because the interelectrode spacing for cesium oxide is not optimum.

The converter was then operated continuously at an emitter temperature of 1760° K and a cesium oxide temperature of 623° K for 400 hours. Figure IV-31 shows stable performance within ±15%.

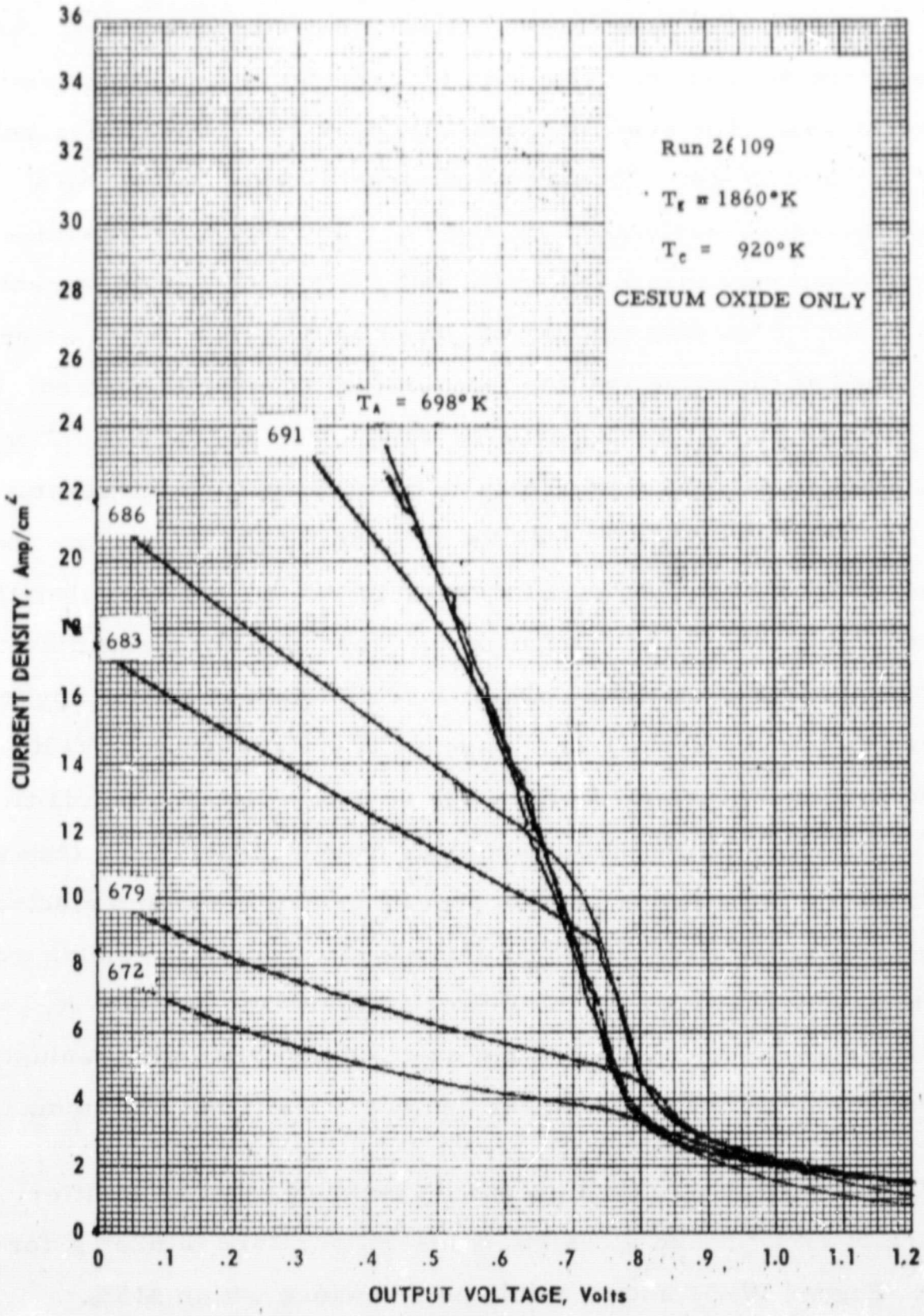


Figure IV-22. Family of Volt-Ampere Characteristics Obtained by Varying the Cesium Oxide Temperature at T_E = 1860°K

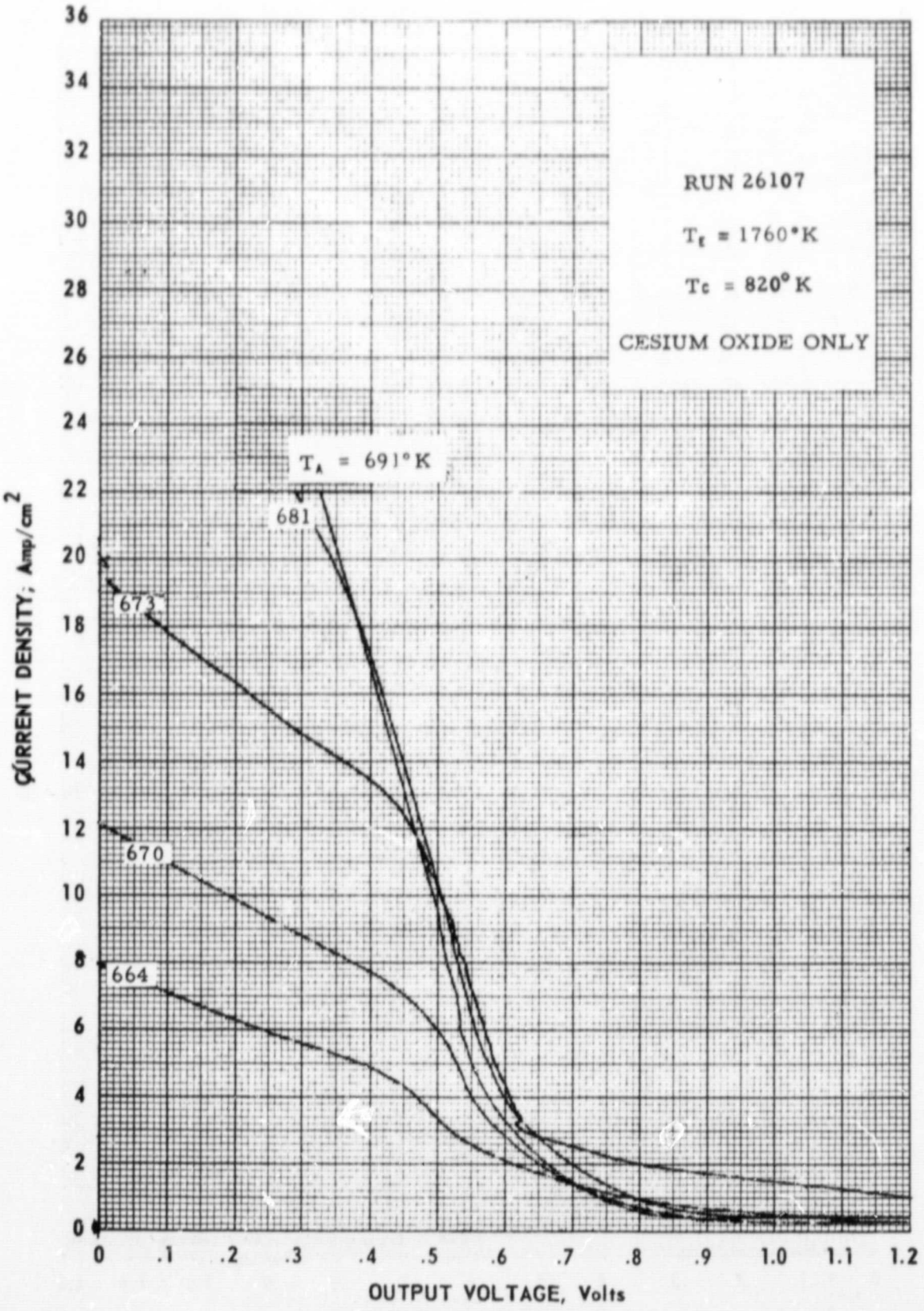


Figure IV-23. Family of Volt-Ampere Characteristics Obtained by Varying the Cesium Oxide Temperature at T_E = 1760°K

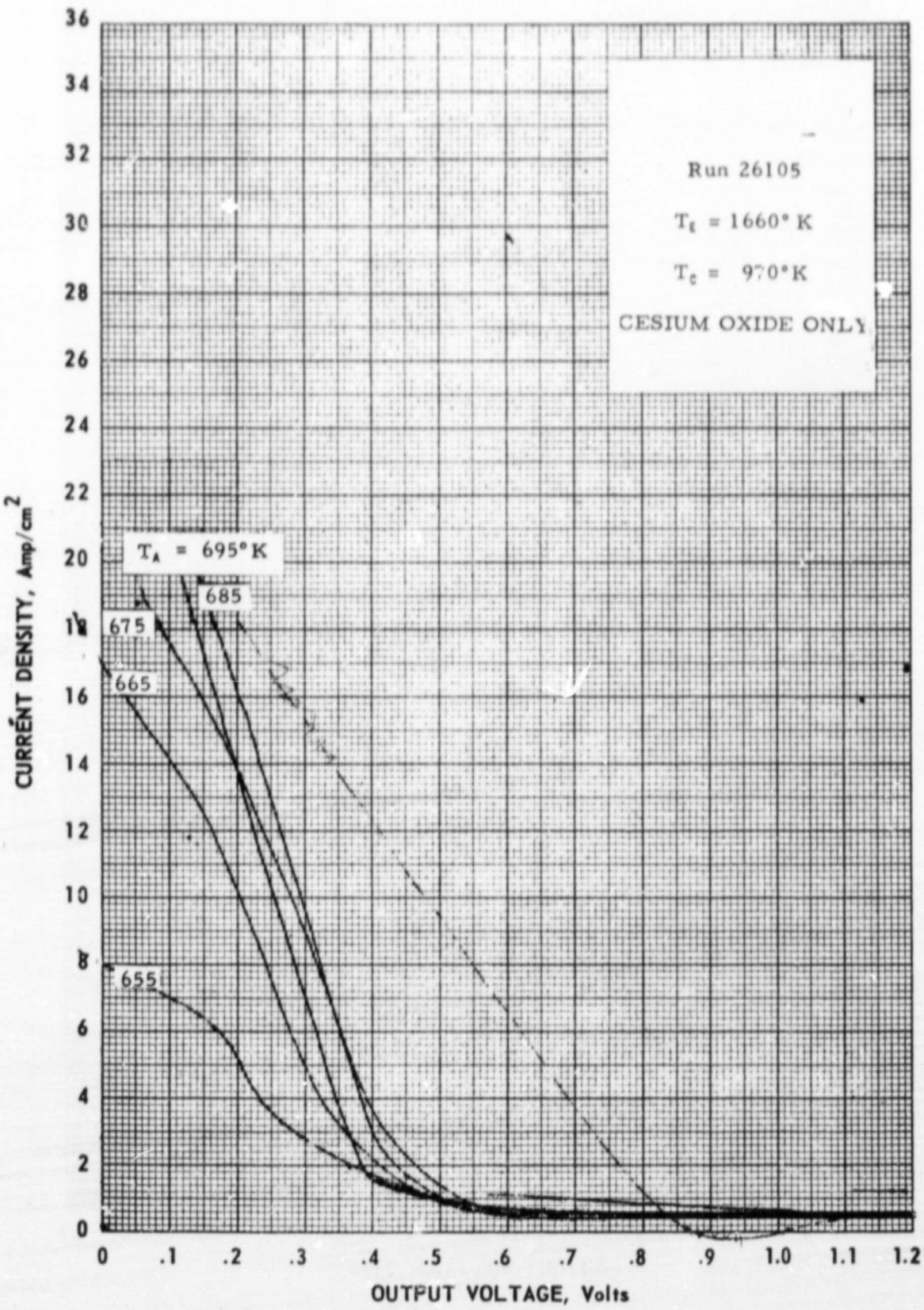


Figure IV-24. Family of Volt-Ampere Characteristics Obtained by Varying the Cesium Oxide Temperature at T_E = 1660°K.

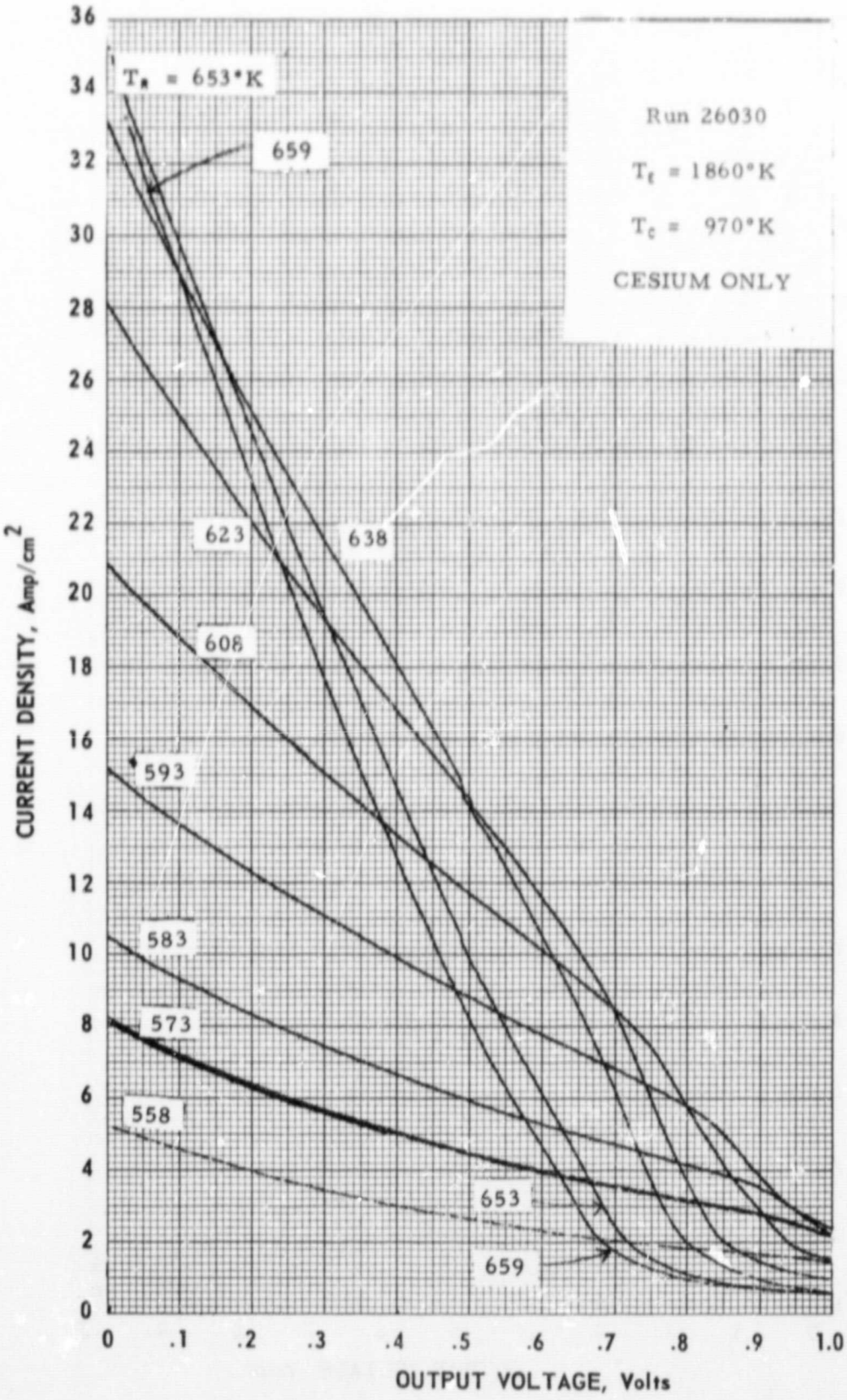


Figure IV-25. Family of Volt-Ampere Characteristics Obtained by Varying the Cesium Temperature at T_E = 1860°K.

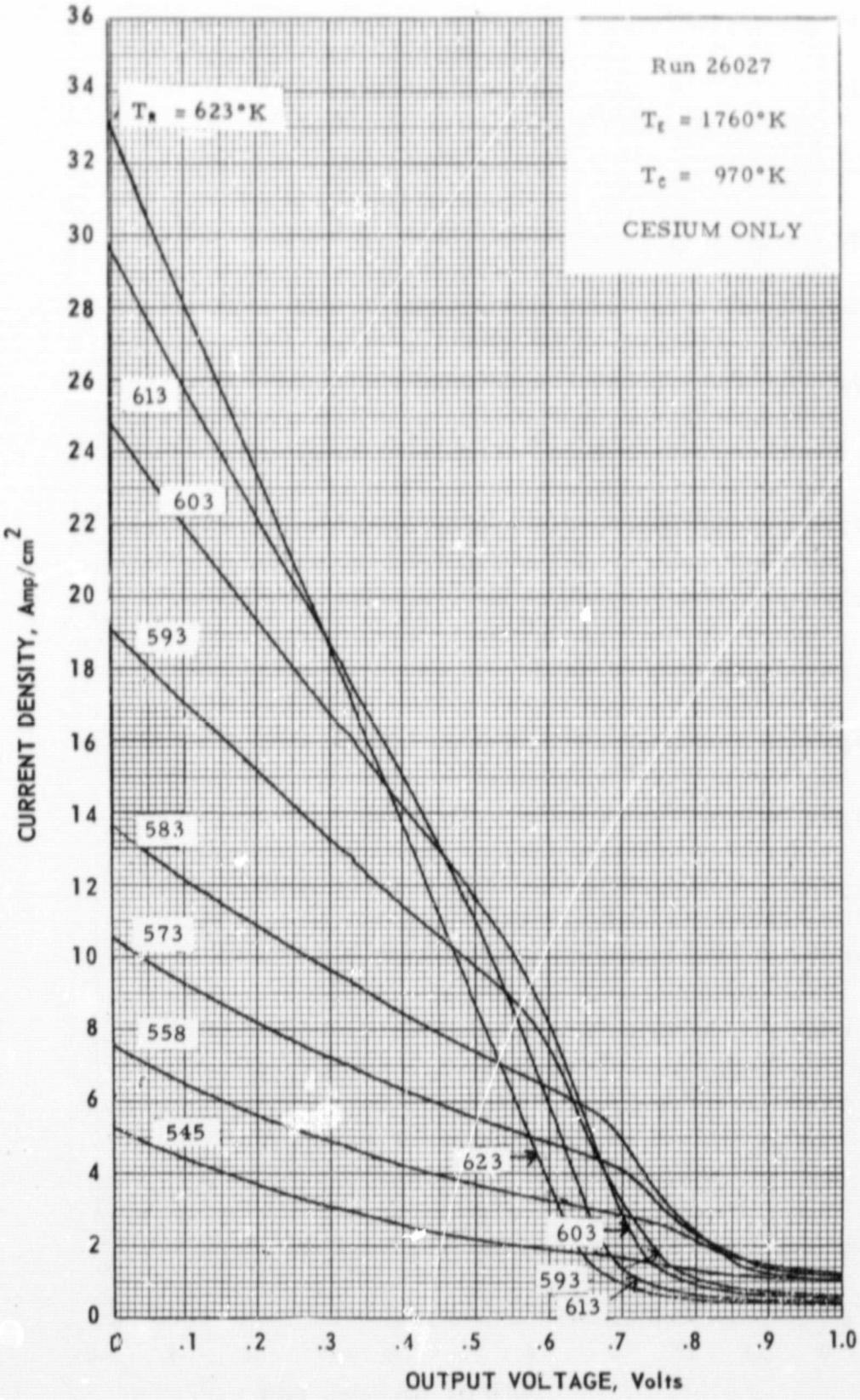


Figure IV-26. Family of Volt-Ampere Characteristics Obtained by Varying the Cesium Temperature at T_E = 1760°K.

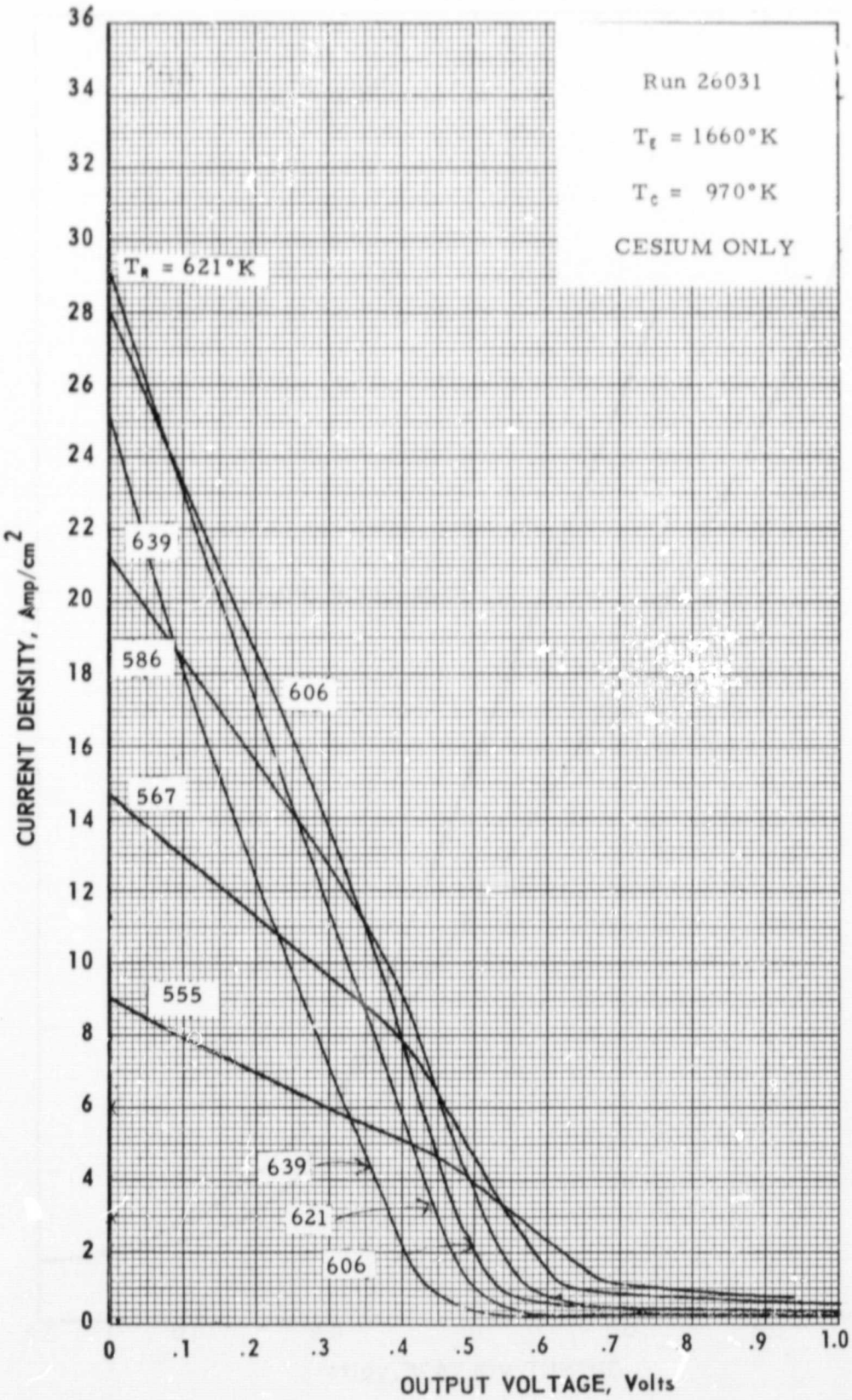


Figure IV-27. Family of Volt-Ampere Characteristics Obtained by Varying the Cesium Temperature at T_E = 1660°K.

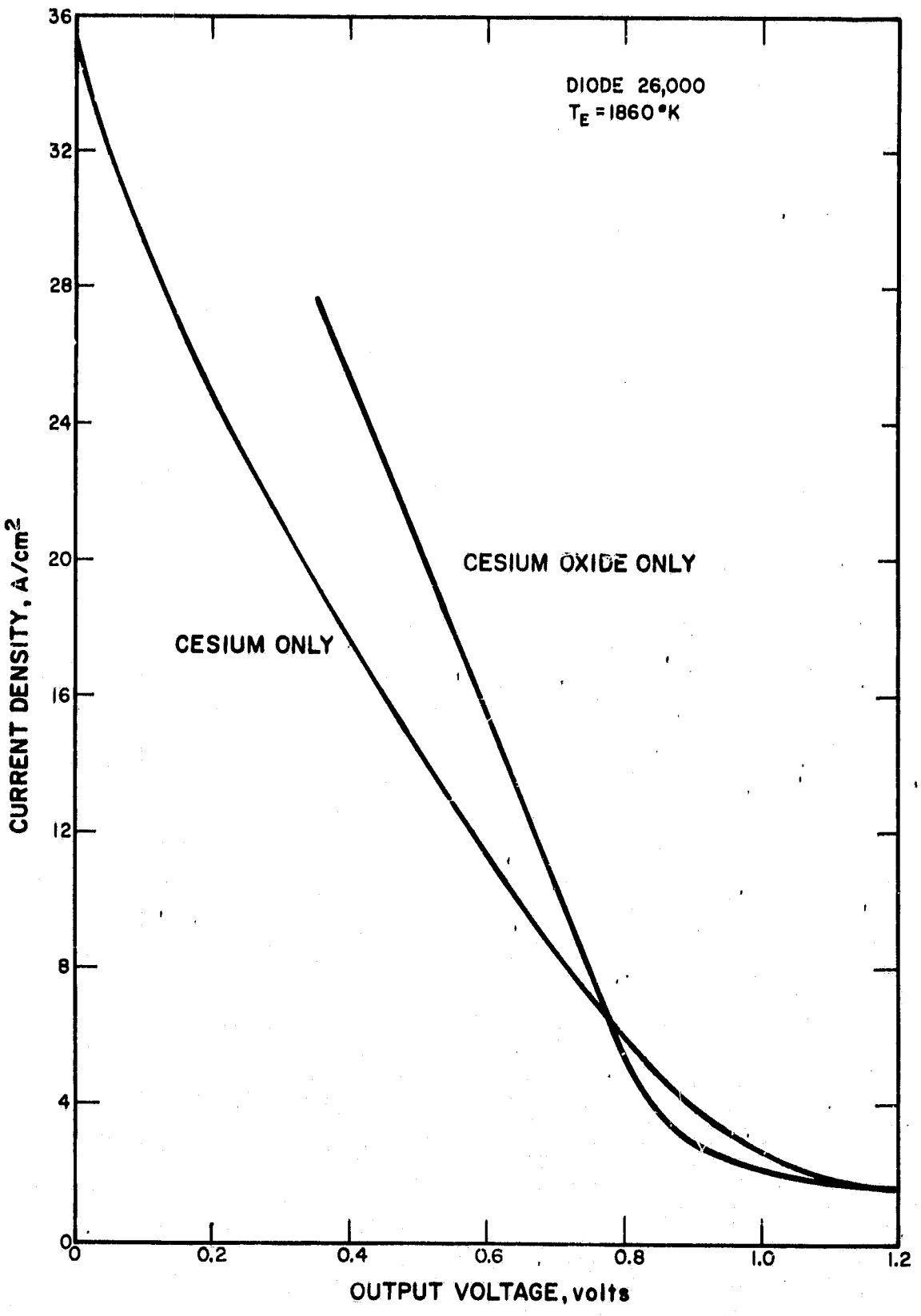


Figure IV-28. Performance Comparison of the Cesium-Oxide Converter with a Cesium Converter at T_E = 1860°K.

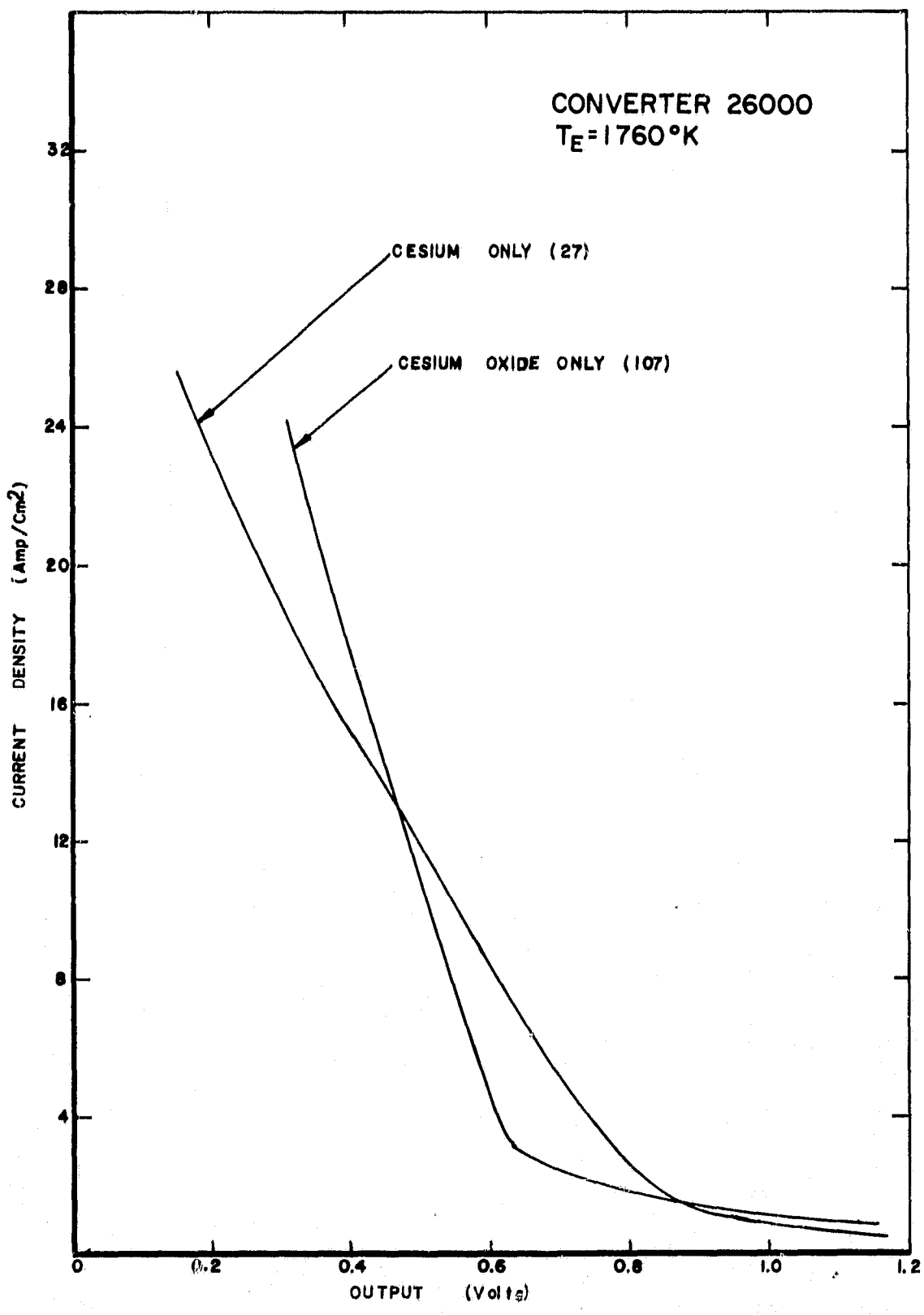


Figure IV-29. Performance Comparison of the Cesium-Oxide Converter with a Cesium Converter at T_E = 1760°K.

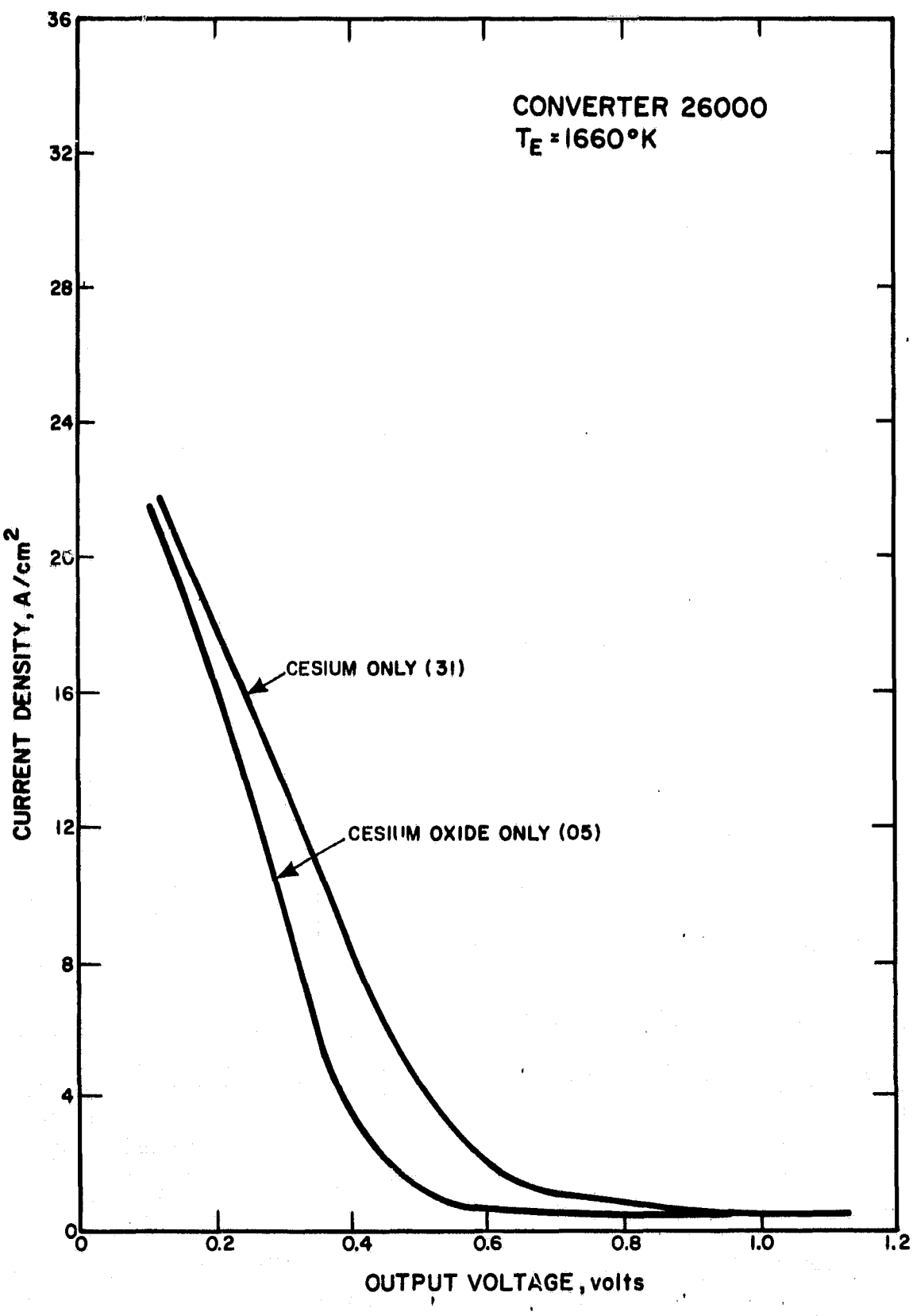


Figure IV-30. Performance Comparison of the Cesium-Oxide Converter with a Cesium Converter at T_E = 1660°K.

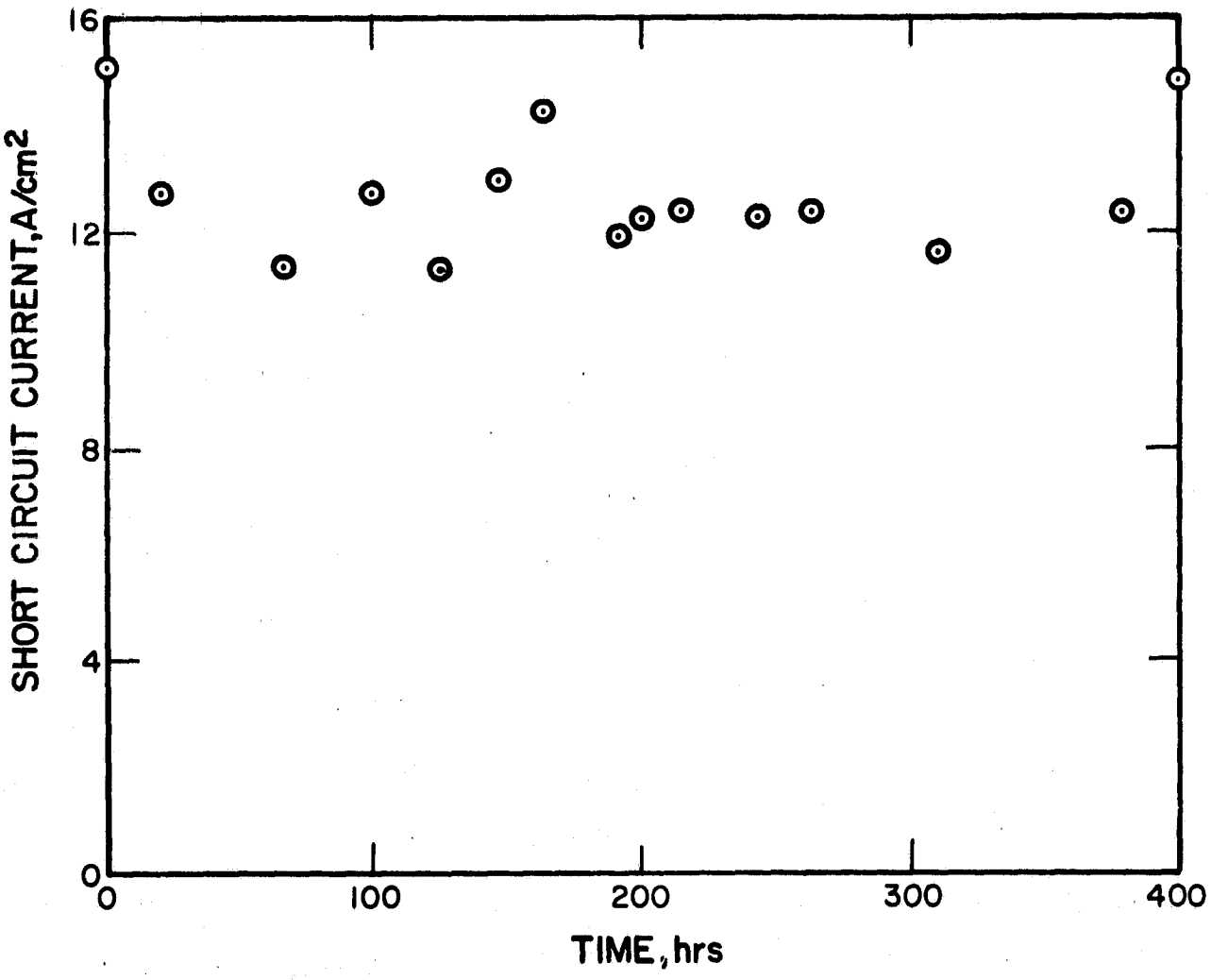


Figure IV-31. Results of a 400-Hour Life Test at an Emitter Temperature of 1760°K and a Cesium Oxide Temperature of 623°K.

This experiment shows the possibility of operating a thermionic converter with cesium oxide only in some particular applications. There are two potential advantages to this technique. First, the converter uses only one reservoir for cesium and oxygen. Second, the coldest member of the converter is at 670 to 720°K, while in the conventional cesium converters the coldest member is 570 to 620°K. As mentioned earlier, to remove cesium from this converter, it was heated to 670°K while the cesium reservoir was kept cold, and then the cesium reservoir was pinched off. As shown by the data in Figures IV-22 to IV-24, the operating temperature for the cesium-oxide reservoir is in the range of 670 to 720°K. Probably if the cesium distillation had been carried out at a higher temperature, the operating temperature for the cesium oxide reservoir would also have been increased. The higher temperature range makes cesium oxide more attractive for most applications. A detailed mass spectrometric analysis of the cesium-oxygen system will be made in the continuation of this program.

E. OTHER EXPERIENCES WITH CESIUM-OXYGEN SYSTEMS

After a variable-spacing converter is constructed it is used almost continuously either to produce parametric data for theoretical analysis or to aid in design calculations for hardware converters. After a time the converter fails, usually due to the development of a leak. The occurrence of such a leak has been regarded as an end to the useful life of the converter, and data accumulation has been terminated.

During this year's work, testing was continued on a tungsten-tungsten converter after a leak developed, in order to accumulate additional data on additive performance. The leak in this converter

apparently caused formation of metal oxides on the collector and guard surfaces. These metal oxides acted as additives, and a definite reduction of the emitter work function was observed when the additive temperature was raised to about 900°K (Figure IV-32). The dependence of emitter work function on collector temperature was reproducible and stable during the several hundred hours of testing, and resulted in a substantial increase in output curent. Data were obtained before and after formation of the oxides in the emitter temperature range of 1660 to 1860°K for an interelectrode spacing range of 1 to 20 mils.

Typical cesium-only data for the emitter temperature of 1900°K are shown in Figures IV-33 to IV-35, and additive data for the same conditions are shown in Figures IV-36 to IV-38. The optimized cesium envelopes with and without additive are compared in Figure IV-39. At an interelectrode spacing of 10 mils, for example, the power output with additives is better than the cesium-only data by a factor of four. Additional data are given in the Appendix.

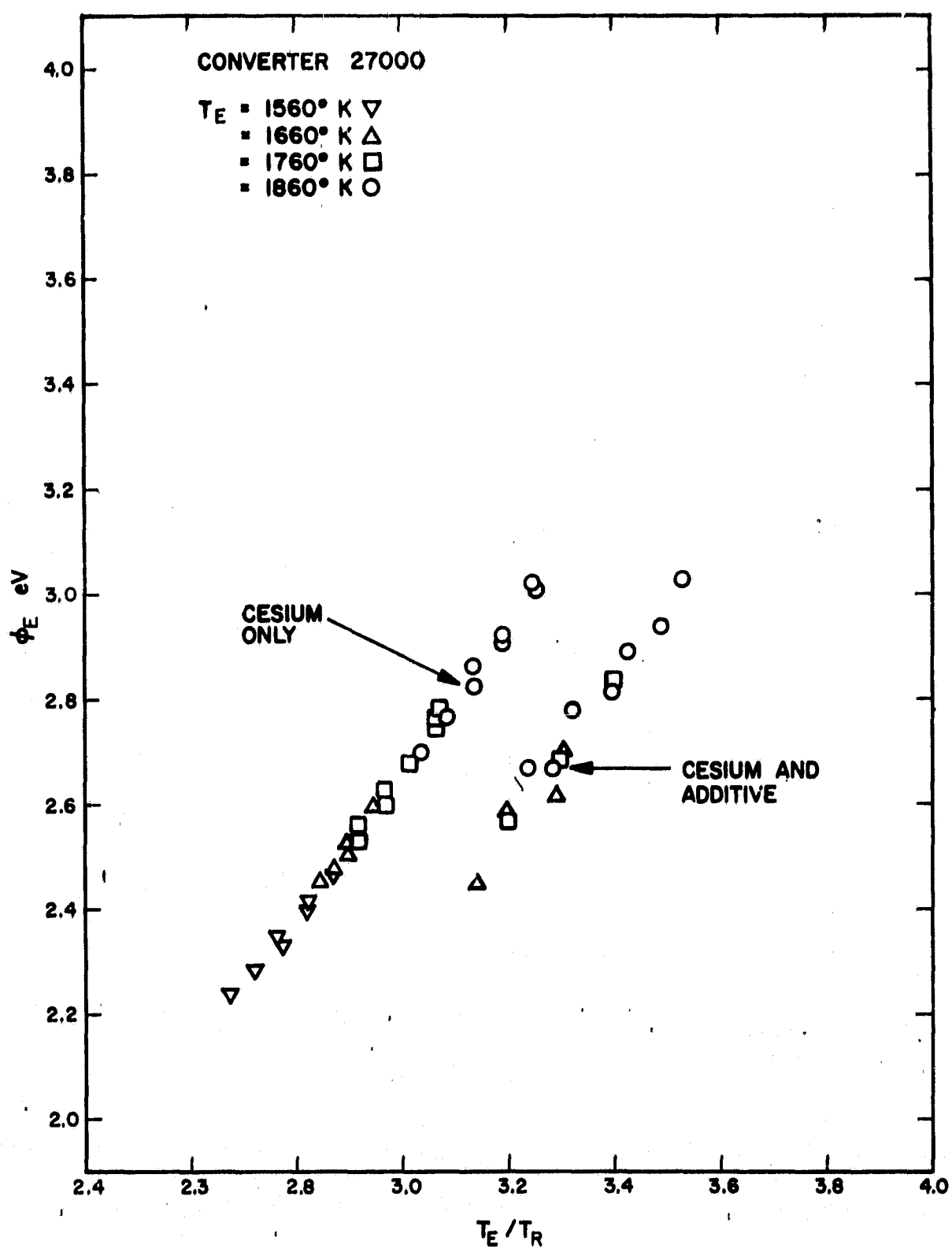


Figure IV-32. Emitter Work Function Depression by Additives.

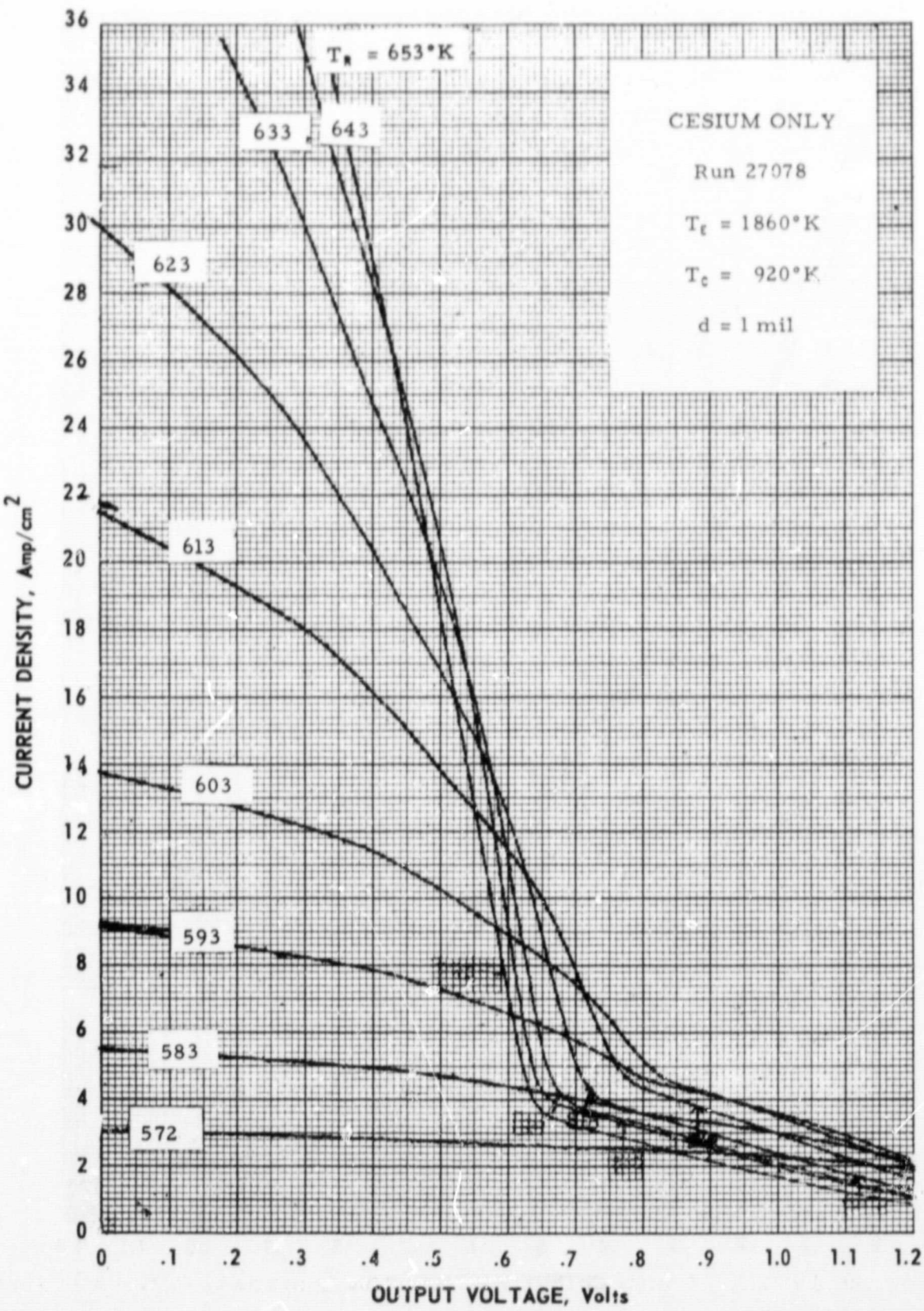


Figure IV-33. Converter Performance with Cesium Only at T_E = 1860°K and d = 1 mil.

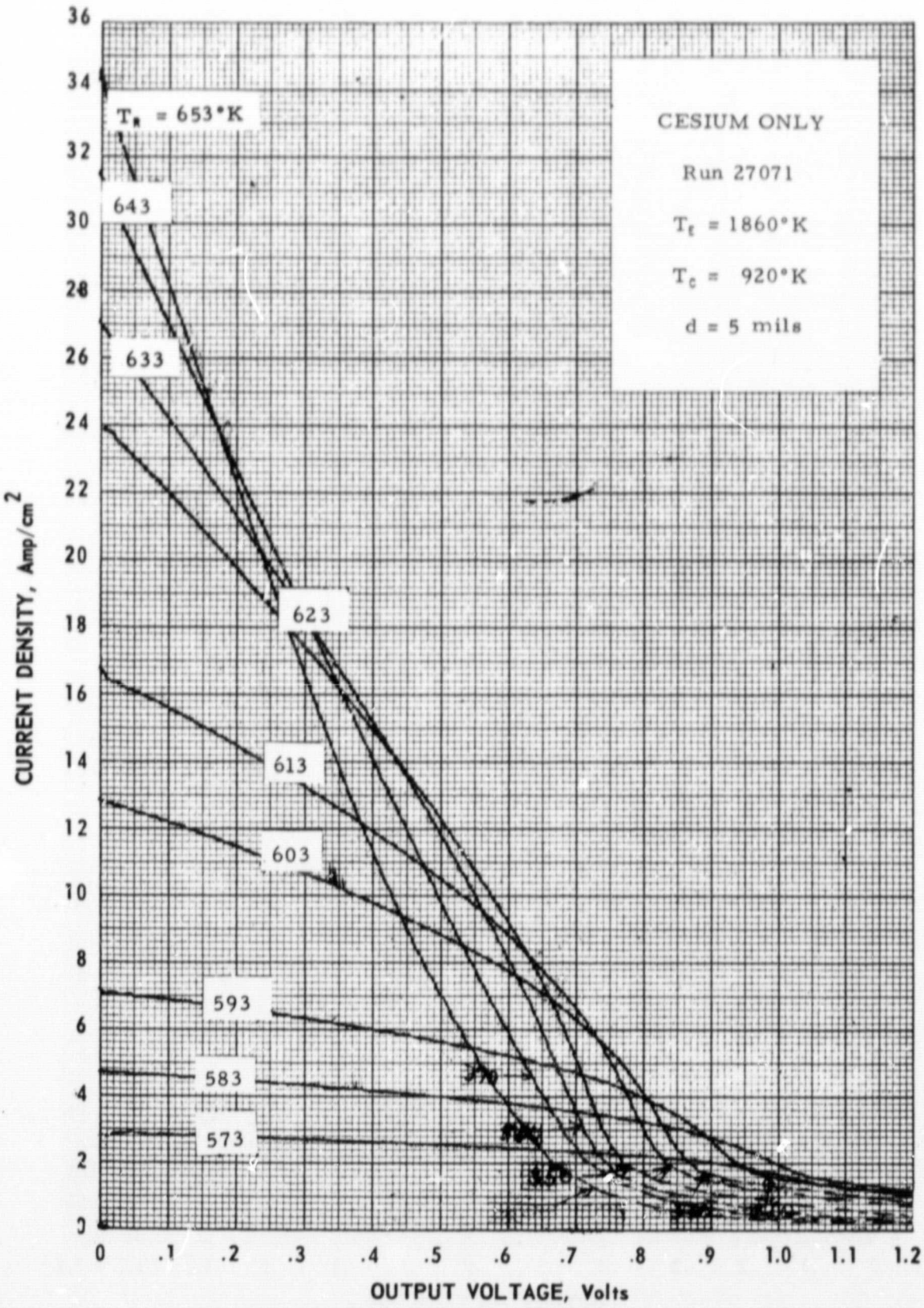


Figure IV-34. Converter Performance with Cesium Only at T_E = 1860°K and d = 5 mils.

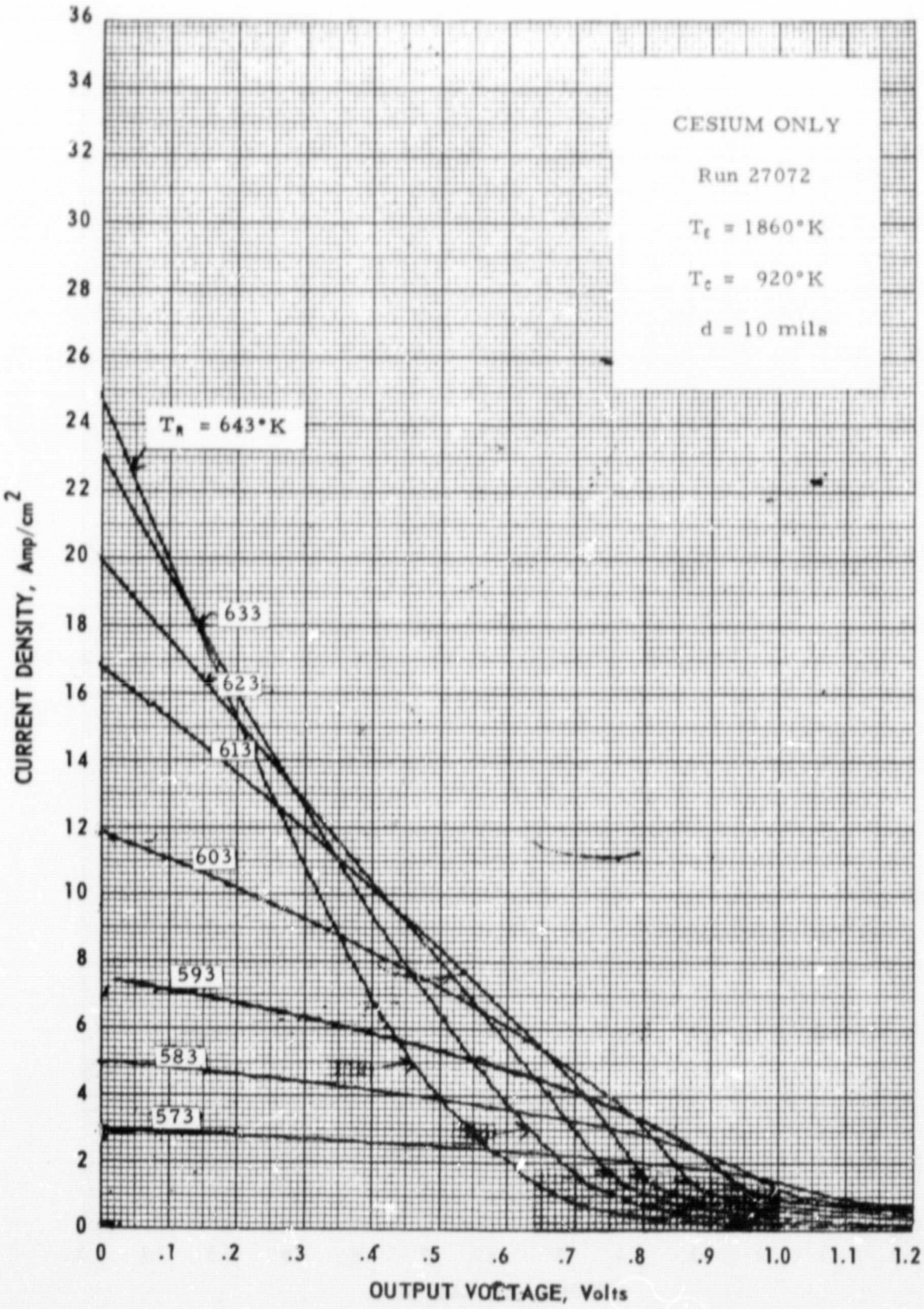


Figure IV-35. Converter Performance with Cesium Only at T_E = 1860°K and d = 10 mils.

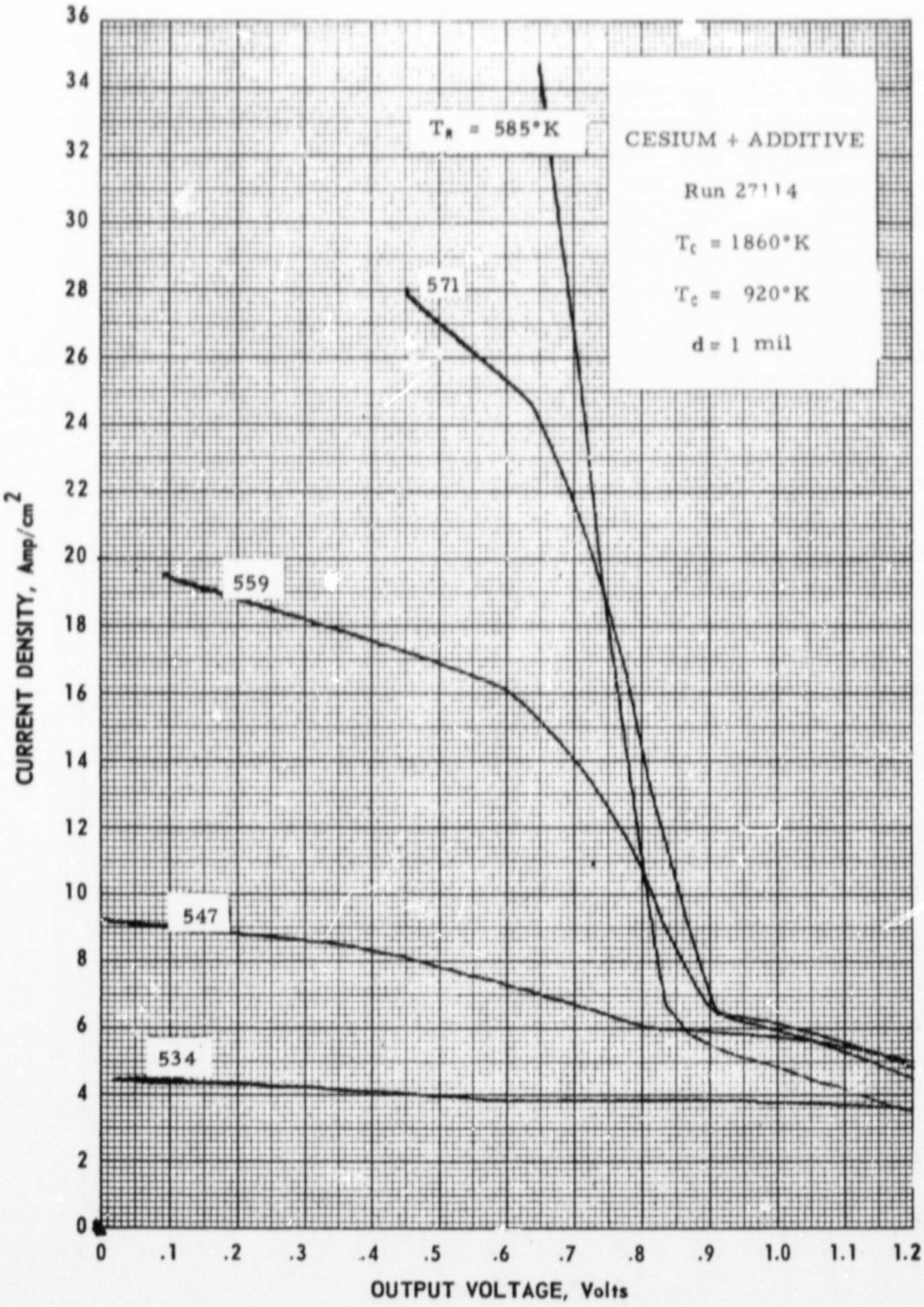


Figure 1v-- Converter Performance with Cesium plus Additive at T_E 1860°K and d = 1 mil.

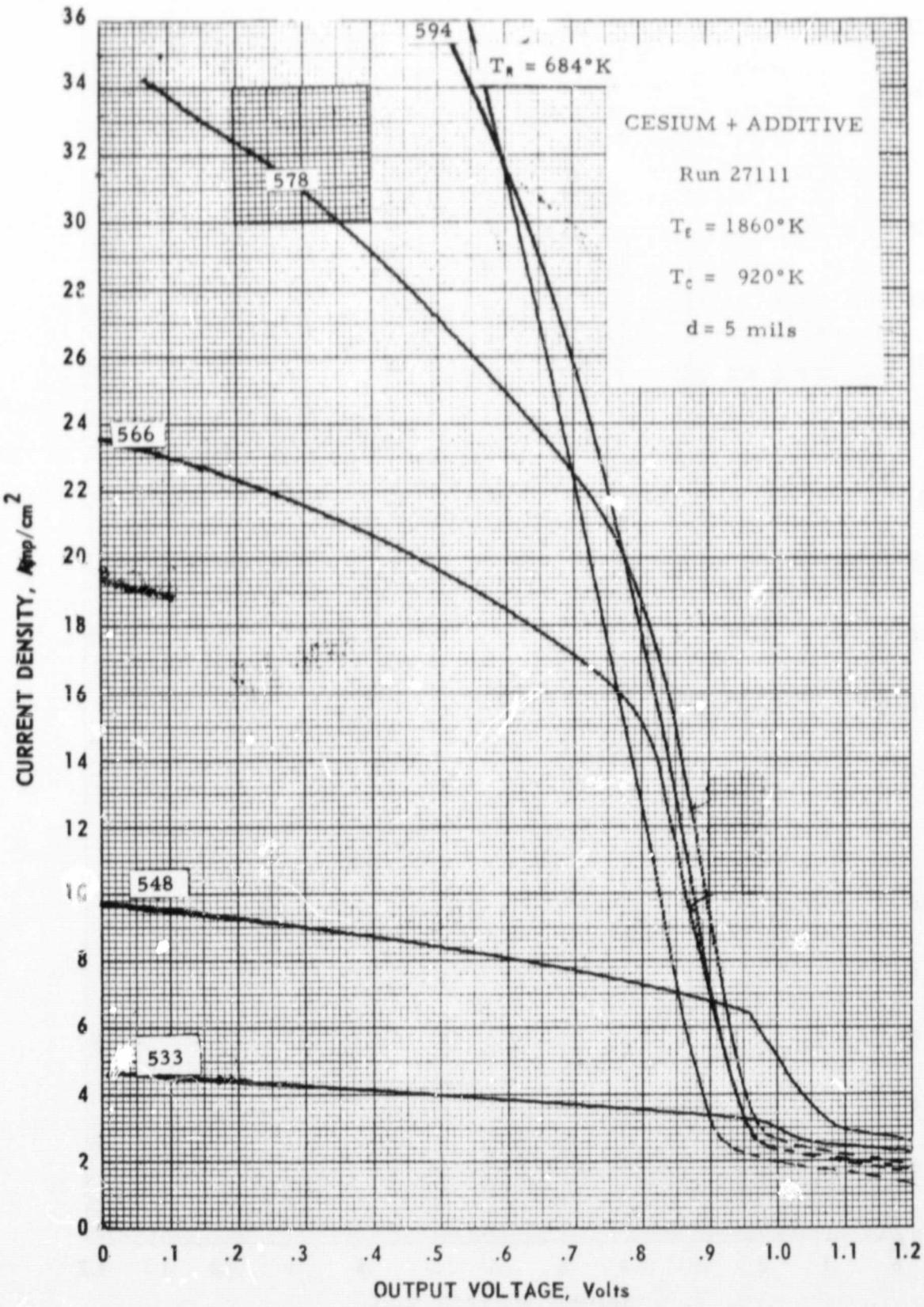


Figure IV-37. Converter Performance with Cesium plus Additive at T_E = 1860°K and d = 5 mils.

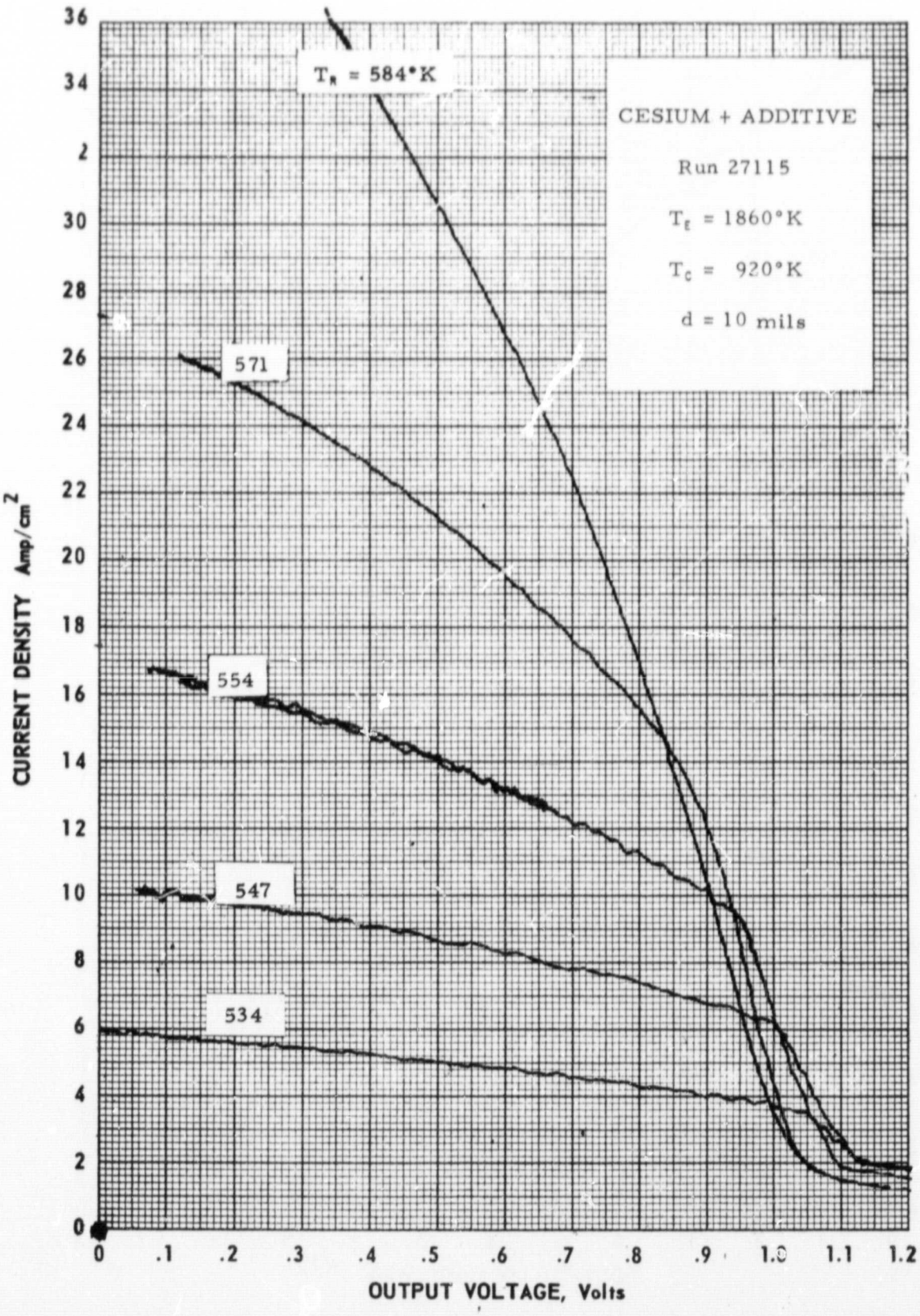


Figure IV-38. Converter Performance with Cesium plus Additive at T_E = 1860°K and d = 10 mils.

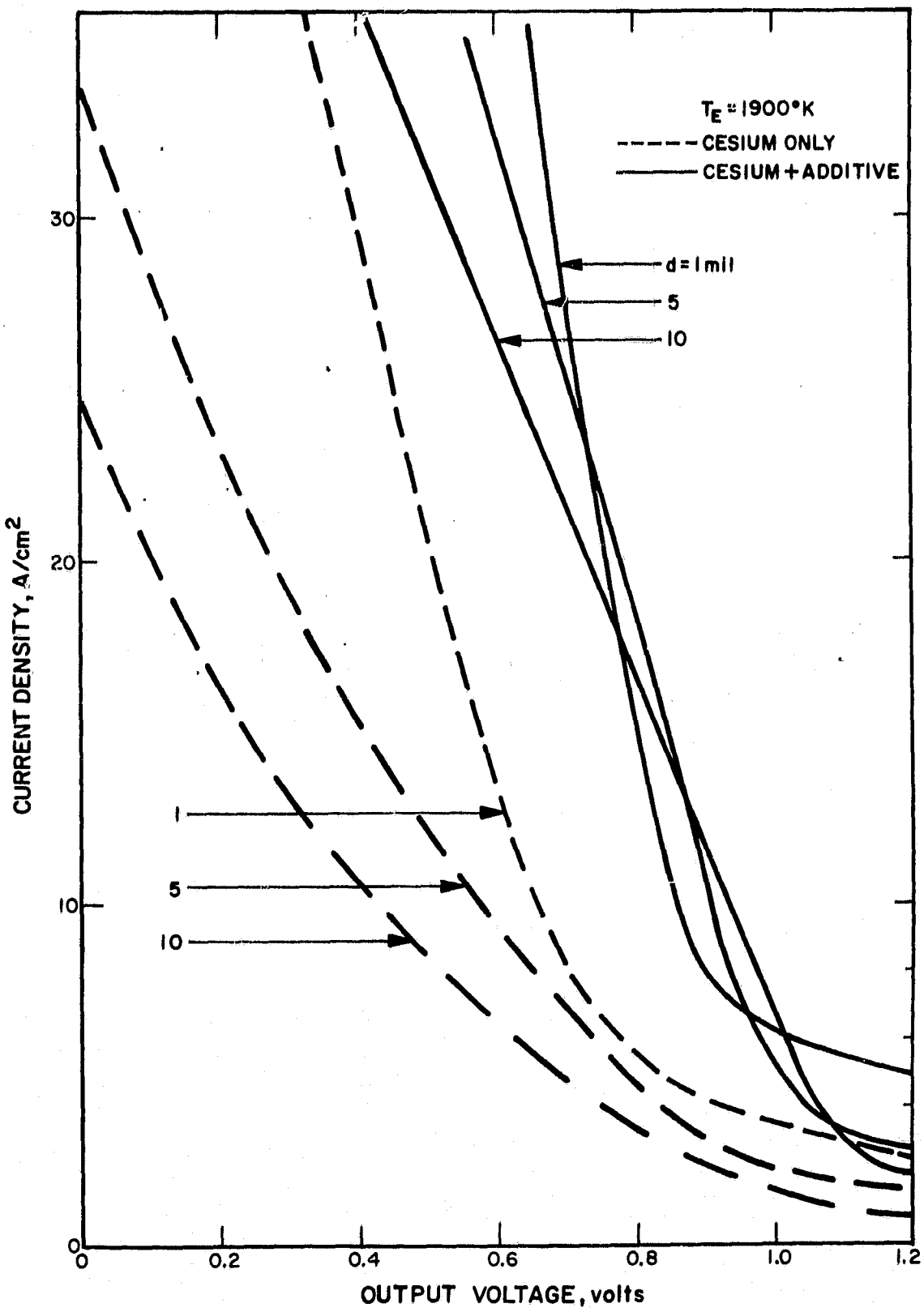


Figure IV-39. Comparison of Performance With and Without Additives at T_E = 1860°K for Several Interelectrode Spacings.

REFERENCES FOR CHAPTER IV

1. I. Langmuir and D. S. Villars, "Oxygen Films on Tungsten - Part I, A Study of Stability by Means of Electron Emission in Presence of Cesium Vapor," J. Am. Chem. Soc. 53, 486 (1931).

2. V. C. Wilson, "Operation and Analysis of a Plane Parallel Cesium Thermionic Converter with an Oxygen Treated Tantalum Emitter," Thermionic Conversion Specialist Conference, Gatlinburg, Tennessee, 1963.

3. J. D. Levine et al., "Oxygen as a Controllable, Reversible and Beneficial Additive in the Cesium Converter," Thermionic Conversion Specialist Conference, San Diego, California, October 1965.

4. W. Engelmaier and R. Stickney, "Thermionic and Adsorption Characteristics of a Single-Crystal Tungsten Filament Exposed to Oxygen," Proc. Phys. El. Conf., M.I.T., 1966.

5. S. S. Kitrilakis, F. Rufeh, D. Lieb and L. van Someren, "Final Report, Thermionic Research Program," prepared for the Jet Propulsion Laboratory under Contract No. 951262, Thermo Electron Report TE 12-67, 1966.

CHAPTER V

MOLYBDENUM TRIOXIDE AS AN OXYGEN SOURCE

F. Fraim, F. Holly and L. van Someren

A. INTRODUCTION

Past work with electronegative additives has shown the strong effects that oxygen has on thermionic diode performance. It has been the intent of previous experiments to provide oxygen gas to the emitter directly by either introducing gaseous oxygen into the converter or by decomposing an oxygen compound in the converter. It was the intent of the present experiments to volatilize a stable metal oxide from a separate reservoir and to decompose the metal oxide vapor at the emitter, thereby releasing oxygen. With oxygen produced only at the emitter, other parts of the converter would have less probability of being corroded. Furthermore, the vapor pressure of the metal oxide necessary to yield oxygen at the pressures required is usually greater than the oxygen pressure, and this should facilitate its transport through the cesium.

The effects of cesium oxides have been discussed in Chapter IV. Here, we consider MoO_3. This oxide is somewhat more convenient for study because its chemistry appears to be less complex and many publications on its chemistry and thermodynamic properties were available. Also, it appears that MoO_3 is a promising source of oxygen since the expected reservoir temperature (850-950° K) is near the usual collector temperatures. Therefore, several diode experiments with MoO_3 were prepared while experiments involving differential thermal analysis (DTA) and mass spectrometry were designed to provide the appropriate understanding of the oxides of cesium as they would exist in a converter.

The present chapter covers the work done this year with MoO_3. This work includes: (1) a thermochemical analysis of MoO_3 as an oxygen additive, and its compatibility with various diode materials; (2) differential thermal analysis of MoO_3 and mixtures of MoO_3 with various materials; (2a) compatibility tests; and (3) four thermionic diode experiments to determine the effects of MoO_3 and to check the results of the analysis.

B. ANALYSIS OF MoO_3 AS AN OXYGEN SOURCE

This section describes the results of a literature search on the behavior of MoO_3 and its more fundamental properties, and then describes the most likely reactions that should occur in a thermionic converter to supply oxygen to the emitter. The results from the literature are then used to calculate the expected oxygen pressures. The literature search led to a series of contradictory results which indicated that not only does MoO_3 have to be considered but also Mo_3O_9. The latter is the predominant gaseous species under some conditions. Much of the confusion in the literature appears to be due to the presence of this compound, as we shall see in the following description of the compound.

1. Description of MoO_3

Molybdenum trioxide is a stable, white or slightly yellow crystalline powder. Its melting point is 1068°K. This oxide has considerable vapor pressure; it begins to sublime around 970°K. The oxide in the solid state is a nonconductor of electricity. It dissolves slightly (1-2 g/l) in water, and the resulting solution is slightly acidic, pH $\simeq$ 4.0 - 4.5. Even small traces of ammonia, alkali, or alkaline buffers increase the solubility of MoO_3 to a considerable degree. From such solutions polymolybdates crystallize.

Molybdenum trioxide forms two hydrates: $MoO_3 \cdot H_2O$ and $MoO_3 \cdot 2H_2O$. The monohydrate exists in two allotropic modifications and is stable over a wide range of conditions.[1]

Molybdenum trioxide is reduced by hydrogen, by a number of metals including molybdenum, and by various other compounds such as phosphine, arsine, and ammonia.

Molybdenum trioxide is peculiar in several ways, and confusion has grown out of the loose way in which the term " molybdic acid" is applied to both MoO_3 and $(NH_4)_6H_8Mo_7O_{28}$. The latter compound, ammonium paramolybdate, is available commercially as " molybdic acid 85%. " It is definitely a mixture of polymolybdates since it contains more MoO_3 than is permitted by the formula of the paramolybdate. Even the slight impurities in the distilled water used in working with molybdates may distort results so that an undetermined mixture of polymolybdates, MoO_3, and its hydrates, is obtained when molybdic oxide is prepared. These considerations suggest why discrepancies appear in the published values for the properties of molybdenum trioxide, even in its melting point, its vapor pressure, and its solubility in water.

2. Vapor Pressure of Solid and Liquid MoO_3

The vapor pressure of molybdenum trioxide as a function of temperature is not a well known property in spite of the number of workers who studied the phenomenon. One of the earliest measurements is due to Feiser,[2] who calculated the vapor pressures from the evaporation rate between 873°K and 1428°K assuming that the gaseous MoO_3 consists of the monomer. The vapor pressure of liquid MoO_3 has been recently studied by Selikman et al.,[10] and their data agree with those of Feiser. Two studies were reported recently[3, 4] in which the Knudsen effusion method was used. The enthalpy of sublimation reported differed by almost 9 Kcal/ mole of vapor, which figure is outside the range of experimental errors.

Berkowitz and co-workers[5] have determined the vapor species using mass spectroscopy. The trimer is the main gaseous species for

the temperature range 850°K to 1000°K. Smaller quantities of Mo_4O_2 and Mo_5O_{15} were also found. The partial pressure of the monomer at these temperatures is negligibly small.

The vapor pressure of solid MoO_3 was measured by Gulbransen et al[6] using the Knudsen effusion method with a vacuum microbalance. The trioxide was obtained by collecting the condensed volatile oxides after oxidation of pure molybdenum rod at temperatures of 1300°K - 1900°K. Before each measurement the cell and the sample were flooded with oxygen at the temperature of the measurement. The vapor pressures were calculated from the measured rates of evaporation. For the molecular weight of the vapor, the calculated values of Horbe et al.[4] were used. The Clausius-Clapeyron equation was determined by the method of least squares from the vapor pressure-temperature data.

$$\log P \text{ (torr)} = - \frac{16,480}{T} + 16.50 \pm 0.04$$

where P is the vapor pressure of solid $(MoO_3)_{\overline{n}}$ and $\overline{n}$ is the average molecular association number ($\overline{n}$ = 3.3 at 900°K) $\Delta H_{s \rightarrow g}$ = 75.4 ± 1 kcal/mole. The corresponding equation for the vaporization of the liquid oxide is

$$\log P \text{ (torr)} = - \frac{7,692}{T} + 8.257$$

From the standard free energies of formation of gaseous and condensed MoO_3, the partial pressure of the monomer can be calculated if the vapor behaves ideally. The following table contains the partial pressure of the monomer and the total pressure of molybdenum trioxide (which consists of the pressure mainly due to trimer but contains

the pressures due to tetramer, pentamer and some dimer besides the monomer) as a function of the absolute temperature.

Vapor Pressure of Molybdenum Trioxide

Solid MoO_3	700°K	800°K	900°K	1,000°K	1,068°K
P_T (torr)	9.1×10^{-8}	7.9×10^{-5}	1.5×10^{-2}	1.0	11.7
P_{MoO_3} (torr)	1.8×10^{-17}	1.5×10^{-13}	1.7×10^{-10}	4.7×10^{-8}	1.2×10^{-6}

Liquid MoO_3	1,100°K	1,200°K	1,300°K	1,400°K	1,430°K
P_T (torr)	18.4	70.3	219	579	760
P_{MoO_3} (torr)	3.7×10^{-6}	9.0×10^{-5}	1.3×10^{-3}	1.3×10^{-2}	--

3. Thermodynamic Data Concerning the Molybdenum Oxygen System

The most stable oxide of molybdenum is the dioxide, which is a lead grey crystalline powder. It differs from the trioxide in many respects. The MoO_2 is a good conductor of electricity and is nonvolatile. The standard free energy of formation of solid MoO_2 was determined by means of e. m. f. measurements across solid electrolytic chains.[7] However, better values were obtained by Galvanic cell measurements involving the solid electrolyte $Zr_{0.85}Ca_{0.15}O_{1.85}$ between 1023°K and 1373°K.[8] Comparison with mass spectroscopic data extends the upper limit of validity to 1800°K:

$$Mo_{(s)} + O_{2(g)} \rightleftarrows MoO_{2(s)}$$

$$\Delta F^\circ_1 = -137,500 + 40.0\,T \qquad [cal/mole]$$

The standard free energy of formation of solid MoO_3 is given by

$$Mo_{(s)} + \frac{3}{2} O_{2(g)} \rightleftarrows MoO_{3(s)}$$

$$\Delta F^\circ_s = -177,000 + 59.0\,T$$

$$300°K < T < 1068°K$$

and that of liquid MoO_3:

$$Mo_{(s)} + \frac{3}{2} O_{2(g)} \rightleftarrows MoO_{3(\ell)}$$

$$\Delta F^\circ_\ell = -160.2 + 43.3\,T$$

$$1068°K \leq T \leq 1400°K$$

The standard free energy of formation of the gaseous trimer, the major species in $(MoO_3)_{\overline{n}}$ vapor is given by:[9]

$$3Mo_{(s)} + \frac{9}{2} O_2 \rightleftarrows Mo_3O_{9(g)}$$

$$\Delta F^\circ_1 = -455,200 + 114.7\,T$$

The formation of gaseous monomer has the following standard free energy:

$$\Delta F^\circ_3 = -76,580 + 5.31\,T$$

which was calculated from vapor pressure data. Figure V-1 shows the different st ndard free energies of formation as a function of the absolute temperature. So, the following reaction:

$$3MoO_{3(g)} \rightleftarrows Mo_3O_{9(g)}$$

has the standard free energy of trimerization:

$$\Delta F^\circ_{4a} = -223,460 + 96.07\,T$$

which may be somewhat too negative. From mass spectroscopic data, the following equation is obtained:

$$\Delta F^\circ_{4b} = -222,800 + 88.6\,T$$

This is too negative because of the existence of tetramer and pentomer.

The evaporation of $MoO_{3(s)}$ below the melting point is accompanied by the following standard free energy change:[6]

$$3MoO_{3(s)} \rightleftarrows Mo_3O_{9(g)}$$

$$\Delta F^\circ_5 = 75,400 - 62.30\,T$$

The standard free energy of the sublimation of solid MoO_3 into gaseous monomer is given by

$$\Delta F^\circ = 100,400 - 53.7\,T$$

The standard free energy changes of the oxidation of molybdenum oxide into solid MoO_3, into gaseous MoO_3, and into $Mo_3O_{9(g)}$ can be

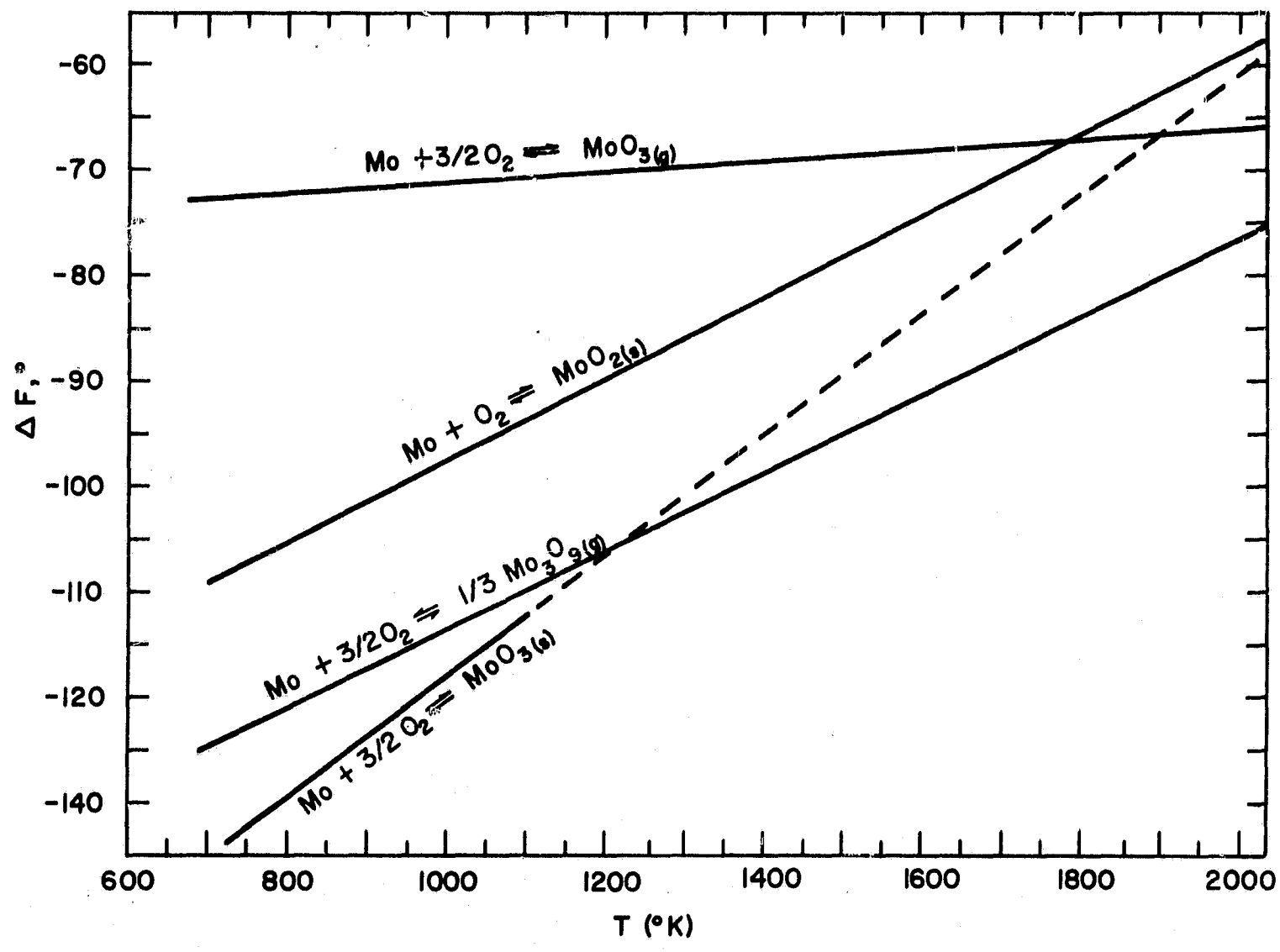


Figure V-1. Standard Free Energy of Formation of Molybdenum Oxides.

calculated from the respective standard free energies of formation (see Figure V-2):

$$MoO_{2(s)} + \frac{1}{2}O_{2(g)} \rightleftarrows MoO_{3(s)} \qquad \Delta F^\circ = -39,500 + 19.0\,T$$

$$MoO_{2(s)} + \frac{1}{2}O_{2(g)} \rightleftarrows MoO_{3(g)} \qquad \Delta F^\circ = +60,900 - 34.7\,T$$

$$MoO_{2(s)} + \frac{1}{2}O_{2(g)} \rightleftarrows \frac{1}{3}Mo_3O_{9(g)} \qquad \Delta F^\circ = -14,367 - 1.77\,T$$

All these equations tie together well. The heat term from the mass spectroscopy work looks like as good an agreement as could be expected.

4. Use of Molybdenum Trioxide in the Converter

If solid molybdenum trioxide is used as an additive, it could be placed in a reservoir of temperature T_R. The solid would vaporize and partially decompose at this temperature. The processes of interest at $T = T_R$ are:

$$MoO_{3(s)} \rightleftarrows Mo_3O_{9(g)} \qquad \Delta F^\circ_5$$

and

$$MoO_{3(s)} \rightleftarrows MoO_{2(s)} + \frac{1}{2}O_{2(g)} \qquad \Delta F^\circ_7 = \Delta F^\circ_1 - \Delta F^\circ_s$$

$$\Delta F^\circ_7 = 39,500 - 19.0\,T$$

The pressures of the trimer can be calculated from the standard free energy change of the process:

$$P_{Mo_3O_9} = \exp\left[-\Delta F^\circ_5 (T_R)/RT_R\right]$$

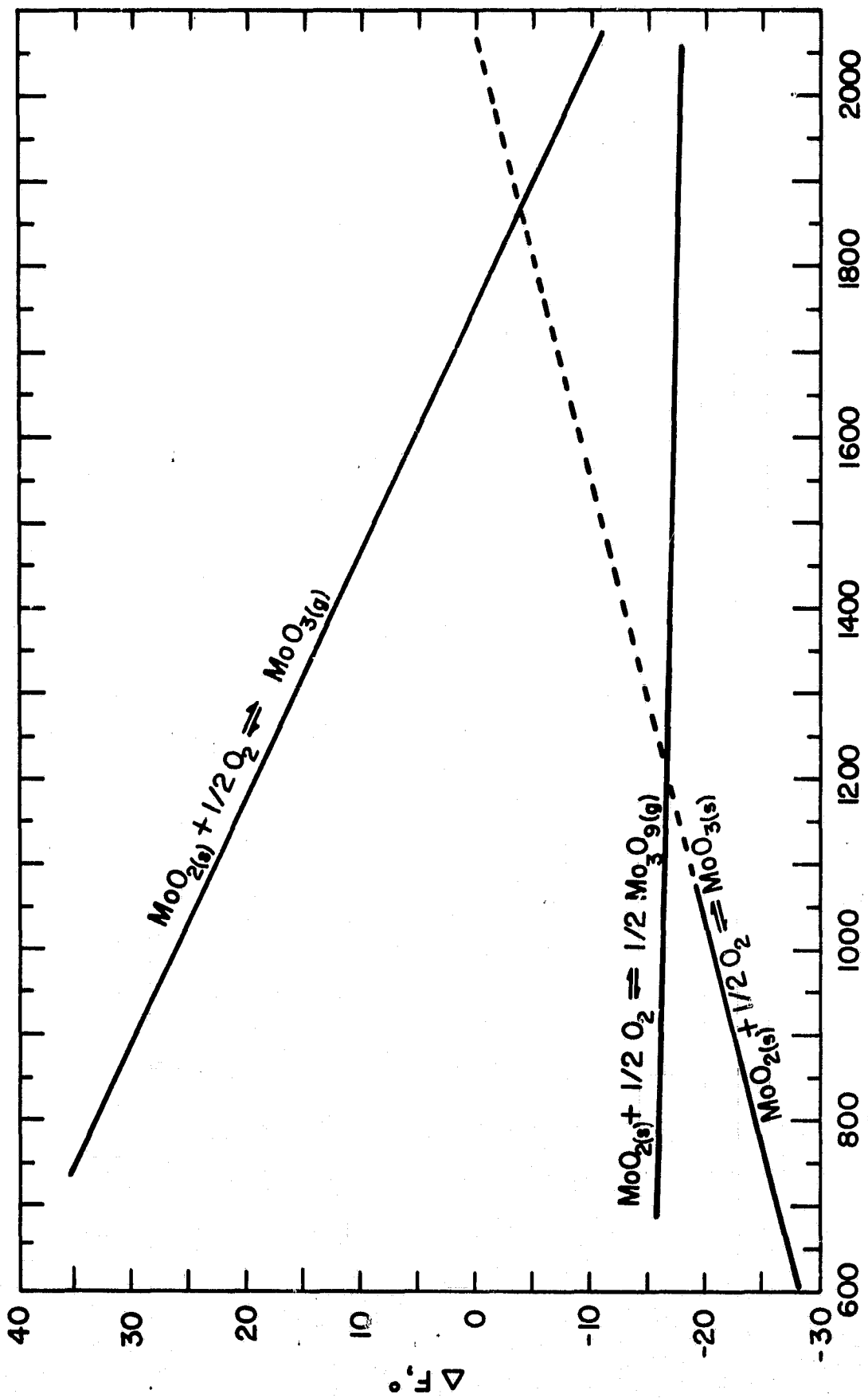


Figure V-2. Standard Free Energies of Oxidation of Molybdenum Dioxide.

Since in the temperature range $600°K \leq T \leq 1,000°K$ the vapor phase consists almost entirely of the trimer, its pressure is practically equivalent to the total pressure.

The pressure of oxygen can be calculated from the partial decomposition of molybdenum trioxide:

$$P_{O_2} = \exp\left[2\Delta F°_7 (T_R)/RT_R\right]$$

The following table contains the equilibrium pressures of the trimer and oxygen over solid MoO_3 at various reservoir temperatures. This dissociation pressure of oxygen is also shown in Figure V-3.

T_R	600°K	700°K	800°K	900°K	1,000°K
$P_{Mo_3O_9}$ (torr)	1.1×10^{-11}	9.0×10^{-8}	7.9×10^{-5}	1.5×10^{-2}	1.0
P_{O_2} (torr)	2.6×10^{-18}	3.3×10^{-14}	4.0×10^{-11}	1.0×10^{-8}	8.3×10^{-7}

So the vapor mixture would consist mainly of the trimer and would contain a small amount of oxygen. The temperature of the vapor at the emitter would become much higher, depolymerization would take place:

$$Mo_3O_{9(g)} \rightleftarrows 3MoO_{3(g)} \qquad -\Delta F°_4$$

The ratio of the two pressures is given by the relation:

$$\frac{P_{MoO_3}}{\left(P_{Mo_3O_9}\right)^{1/3}} = \exp\left[\frac{\Delta F°_4(T_E)}{3R\,T_E}\right]$$

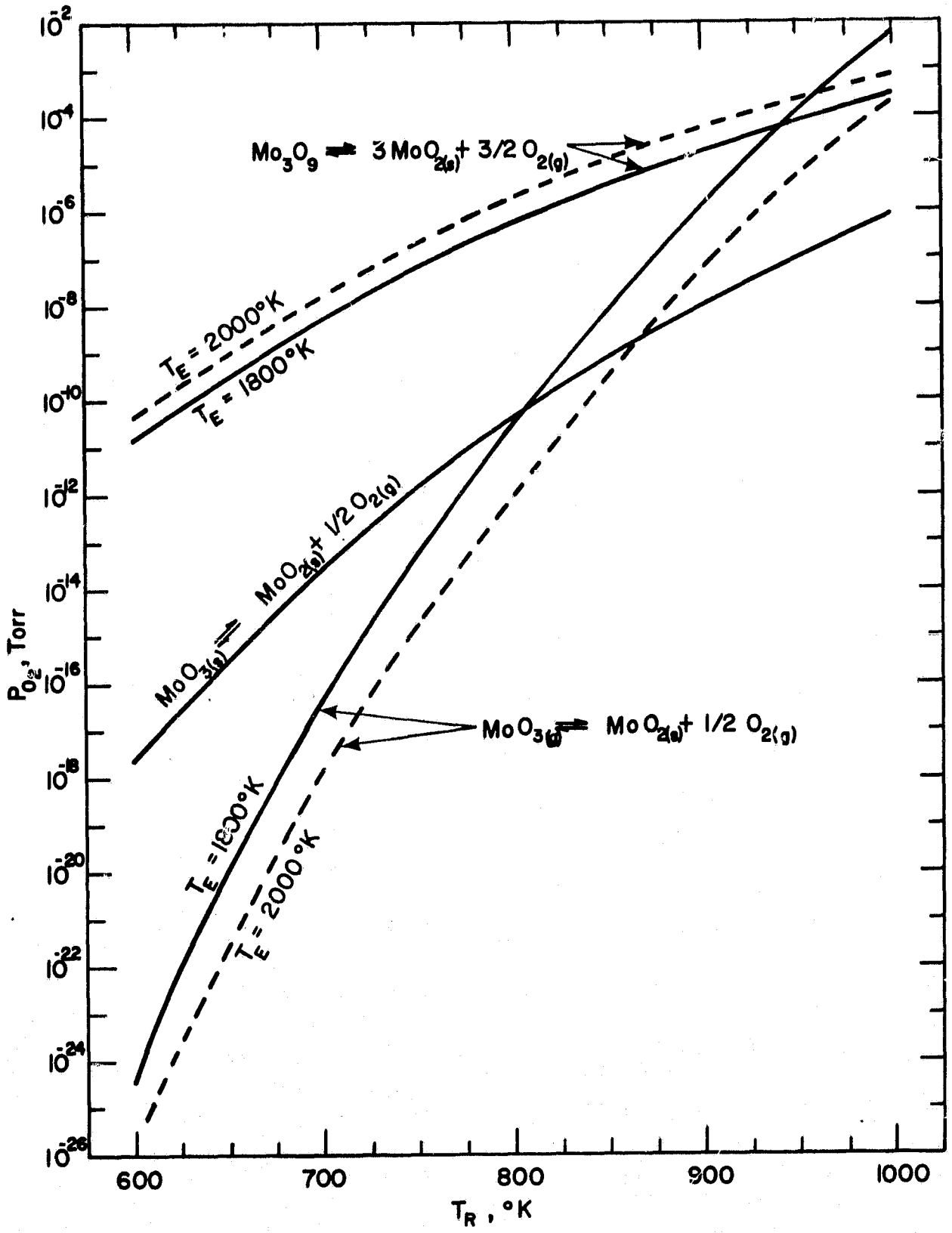


Figure V-3. Equilibrium Oxygen Pressure as a Function of Additive Reservoir Temperature.

It can be shown that at emitter temperatures as high as 1,800°K and 2,000°K, if the pressure of the trimer is below 1 torr, practically all the trimer will dissociate into monomers, so the pressure of the monomer is given by:

$$P_{MoO_3} = 3P_{Mo_3O_9}(T_R)$$

The monomer will decompose according to the following reaction:

$$MoO_{3(g)} \rightleftarrows MoO_{2(s)} + \frac{1}{2}O_{2(g)} \qquad -\Delta F^\circ_6$$

The equilibrium oxygen pressure is equal to:

$$P_{O_2} = P^2_{MoO_3} \exp\left[\frac{2\Delta F^\circ_6(T_E)}{R \cdot T_E}\right]$$

So. for the various reservoir temperatures the following oxygen pressures may be obtained at the emitter:

T_R	600°K	700°K	800°K	900°K	1000°K
P_{MoO_3}	3.3×10^{-11}	2.7×10^{-7}	2.4×10^{-4}	4.5×10^{-2}	1.0*
P_{O_2} (1800°K)	9.1×10^{-25}	6.1×10^{-7}	4.8×10^{-11}	1.7×10^{-6}	4.7×10^{-4}*
P_{O_2} (2000°K)	3.0×10^{-26}	2.0×10^{-18}	1.6×10^{-12}	5.6×10^{-8}	3.1×10^{-6}

*Calculated from the decomposition of Mo_3O_9.

Figure V-3 contains three types of dissociation curves. One, the dissociation curve of solid MoO_3, has already been discussed. The second type is based on the assumption that no conversion of trimer into monomer takes place at the emitter, and the trimer pressure at the emitter is equal to the vapor pressure of the solid molybdenum trioxide held at the additive reservoir temperature. The third type of dissociation curve is based upon the assumption that all the trimer had converted to monomer at the emitter, so the monomer pressure is given by the relation

$$P_{MoO_3} = 3 P_{Mo_3O_9}(T_R)$$

As can be seen from Figure V-3, the decomposition of the monomer at the emitter gives the lowest oxygen pressure, especially at the lower reservoir temperatures, so this reaction will determine the oxygen pressure of the emitter. Hence, the reservoir temperature should be almost 900°K to provide oxygen at sufficient pressure to the emitter.

C. REACTIONS OF MoO_3 WITH DIODE MATERIALS

Thermodynamic calculations have been carried out to investigate the compatibility of MoO_3 with materials present in a diode at typical operating temperatures. The calculations were carried out for molybdenum, nickel, tantalum, niobium, copper and tungsten. Reactions with both solid MoO_3 and gaseous Mo_3O_9, the major species in gas phase, were considered. Solid-solid interactions may occur with the reservoir wall or with other materials in the diode where MoO_3 may condense. Solid-gas interactions may occur with the diode materials on which the oxide vapor does not condense. It should be noted that in practice the latter type of reactions may be inhibited by an adsorbed monolayer of cesium on the metal surfaces.

The calculations are presented here, and the results are tabulated in Table V-1. For the solid MoO_3-metal reaction the criterion for possible reaction is the value of the free energy for the reaction. If ΔF is negative the reaction will occur. The standard free energy values, $\Delta F°$, can also be used in such a qualitative way. Gaseous Mo_3O_9 will not react with the respective metals if the calculated equilibrium pressure is greater than the actual MoO_3 pressure in the system. The maximum actual pressure that can exist in the system is the equilibrium vapor pressure of the condensed oxide determined by its temperature.

1. Reduction of Solid Molybdenum Trioxide by Molybdenum

Although the standard free energy of formation of molybdenum trioxide has a larger negative value than that of molybdenum dioxide, the free energy charge per oxygen atom is larger for the dioxide;

TABLE V-1

REACTION	700°K			1000°K		
	ΔF°(Kcal)	$P_{Mo_nO_{3n}}$ (Torr)	Conclusion	ΔF°(Kcal)	$P_{Mo_nO_{3n}}$ (Torr)	Conclusion
REDUCTION OF SOLID MOLYBDENUM TRIOXIDE						
$Mo_{(s)} + 2\ MoO_{3(s)} \rightleftarrows 3\ MoO_{2(s)}$	-48	8×10^{-8}	Reaction Occurs	-50	9×10^{-3}	Reaction Occurs
$2\ Cu_{(s)} + \frac{1}{3} MoO_{3(s)} \rightleftarrows Cu_2O_{(s)} + \frac{1}{3} Mo_{(s)}$	+18	8×10^{-8}	No Reaction	+17	9×10^{-3}	No Reaction
$Cu_{(s)} + \frac{1}{3} MoO_{3(s)} \rightleftarrows CuO_{(s)} + \frac{1}{3} Mo_{(s)}$	+24	8×10^{-8}	No Reaction	+24	9×10^{-3}	No Reaction
$Ni(\beta) + \frac{1}{3} MoO_{3(s)} \rightleftarrows NiO_{(s)} + \frac{1}{3} Mo_{(s)}$	+4.2	8×10^{-8}	No Reaction	+4.1	9×10^{-3}	No Reaction
$2\ Ta_{(s)} + \frac{5}{3} MoO_{3(s)} \rightleftarrows Ta_2O_{5(s)} + \frac{5}{3} Mo_{(s)}$	-184	8×10^{-8}	Reaction Occurs	-183	9×10^{-3}	Reaction Occurs
$W_{(s)} + MoO_{3(s)} \rightleftarrows WO_{3(s)} + Mo_{(s)}$	-21	8×10^{-8}	Reaction Occurs	-27	9×10^{-3}	Reaction Occurs
$2\ Nb_{(s)} + \frac{4}{3} MoO_{3(s)} \rightleftarrows Nb_2O_4 + \frac{4}{3} Mo_{(s)}$	-136	8×10^{-8}	Could Occur, Not preferred	-77	9×10^{-3}	Could Occur, Not Preferred
$2\ Nb_{(s)} + \frac{5}{3} MoO_{3(s)} \rightleftarrows Nb_2O_5 + \frac{5}{3} Mo_{(s)}$	-150	8×10^{-8}	Reaction Occurs	-150	9×10^{-3}	Reaction Occurs
$2\ Cu_{(s)} + MoO_{3(s)} \rightleftarrows Cu_2O_{(s)} + MoO_{2(s)}$	-16	8×10^{-8}	Reaction Occurs	+0.8	9×10^{-3}	Reaction Questionable
$Ni(\beta) + MoO_{3(s)} \rightleftarrows NiO_{(s)} + MoO_{2(s)}$	-6.0	8×10^{-8}	Reaction Occurs	12	9×10^{-3}	Reaction Occurs
REDUCTION OF GASEOUS MOLYBDENUM TRIOXIDE (TRIMER)						
$Mo_{(s)} + 2\ MoO_{3(g)} \rightleftarrows 3\ MoO_{2(s)}$	-118	4×10^{-16}	Reaction Occurs	-96	3×10^{-8}	Reaction Occurs
$2\ Cu_{(s)} + \frac{1}{3} Mo_3O_{9(g)} \rightleftarrows Cu_2O_{(s)} + MoO_{2(s)}$	-12.4	1.7×10^{-9}	Reaction Occurs	-7.1	1.8×10^{-2}	Reaction Occurs
$Cu_{(s)} + \frac{1}{3} Mo_3O_{9(g)} \rightleftarrows CuO_{(s)} + MoO_{2(s)}$	-6.7	4.0×10^{-4}	No Reaction	-5.4	$6.8 \times 10^{+2}$	No Reaction
$Ni(\beta) + \frac{1}{3} Mo_3O_{9(g)} \rightleftarrows NiO_{(s)} + MoO_{2(s)}$	-26.1	2.8×10^{-22}	Reaction Occurs	-18.9	2.9×10^{-10}	Reaction Occurs
$2\ Ta_{(s)} + \frac{5}{3} Mo_3O_{9(g)} \rightleftarrows Ta_2O_{5(s)} + 5\ MoO_{2(s)}$	-336	8.5×10^{-61}	Reaction Occurs	-303	1.4×10^{-37}	Reaction Occurs
$W_{(s)} + Mo_3O_{9(g)} \rightleftarrows WO_{3(s)} + 3\ MoO_{2(s)}$	-111	1.2×10^{-32}	Reaction Occurs	-92.5	4.7×10^{-18}	Reaction Occurs
$2\ Nb_{(s)} + \frac{4}{3} Mo_3O_{9(g)} \rightleftarrows Nb_2O_4 + 4\ MoO_{2(s)}$	-258	3.8×10^{-58}	Reaction Occurs	-230	1.4×10^{-35}	Could Occur, Not Preferred
$2\ Nb_{(s)} + \frac{5}{3} Mo_3O_{9(g)} \rightleftarrows Nb_2O_5 + 5\ MoO_{2(s)}$	-302	1.7×10^{-54}	Could Occur, Not Preferred	-269	3.9×10^{-33}	Could Occur, Not Preferred

therefore, the dissociation pressure of oxygen is greater above solid MoO_3 than above solid MoO_2. Hence the dioxide is the more stable oxide, and molybdenum trioxide can be reduced by metallic molybdenum, both forming the dioxide:

$$2MoO_{3(s)} + Mo_{(s)} \rightleftarrows 3MoO_{2(s)}$$

The standard free energy of this reaction can be obtained from the difference between the standard free energy of formation of $3MoO_{2(s)}$ and the standard free energy of formation of $2MoO_{3(s)}$:

$$\Delta F°(T) = -58,500 + 2.0\,T$$

$$300°K \leq T \leq 1068°K$$

$$\Delta F°(673°K) = -57.2 \text{ kcal}$$

Thus at 400°C the reaction should proceed to form molybdenum dioxide.

2. Reduction of Solid MoO_3 by Cu, Ni, Ta, W, and Nb

The standard free energy of the decomposition

$$MoO_{3(s)} \rightleftarrows Mo_{(s)} + \frac{3}{2}O_{2(g)}$$

is given by

$$\Delta F°_s(T) = 177,000 - 59.0\,T$$

$$300°K \leq T \leq 1068°K$$

$\Delta F°$ (700°K) = 135.7 kcal $\Delta F°$ (1000°K) = 118 kcal

If the oxidation of the metal can be described as

$$mM_{(s)} + \frac{n}{2}O_{2(g)} \rightleftarrows M_mO_{n(s)} \qquad \Delta F^\circ_x$$

where ΔF°_x is the standard free energy of the reaction, then the standard free energy of the reaction,

$$\frac{n}{3}MoO_{3(s)} + mM_{(s)} \rightleftarrows \frac{n}{3}Mo_{(s)} + M_mO_{n(s)} \qquad \Delta F^\circ_y$$

can be calculated from ΔF° and ΔF°_x according to

$$\Delta F^\circ_y = \frac{n}{3}\Delta F^\circ_s + \Delta F^\circ_x$$

Copper - Both cuprous and cupric oxide may form. For cuprous oxide, $m = 2$ and $n = 1$, and

$$\Delta F^\circ_y \ (700\,^\circ K) = +17.9 \text{ kcal}$$

$$\Delta F^\circ_y \ (1000\,^\circ K) = +17.2 \text{ kcal}$$

For cupric oxide, $m = n = 1$ and

$$\Delta F^\circ_y \ (700\,^\circ K) = +23.6 \text{ kcal}$$

$$\Delta F^\circ_y \ (1000\,^\circ K) = +24.0 \text{ kcal}$$

With such large positive standard free energies of formation, neither reactions can occur.

Nickel - The Ni (β) may form stable NiO; hence m = n = 1, and

$$\Delta F^\circ_y \text{ (700 °K)} = +4.2 \text{ kcal}$$

$$\Delta F^\circ_y \text{ (1000 °K)} = +4.1 \text{ kcal}$$

Therefore, the nickel does not reduce solid MoO_3 in this temperature range.

Tantalum - Tantalum may form Ta_2O_5, so m = 2 and n = 5, and

$$\Delta F^\circ_y \text{ (700 °K)} = -184 \text{ kcal}$$

$$\Delta F^\circ_y \text{ (1000 °K)} = -183 \text{ kcal}$$

Tantalum probably will reduce MoO_3 violently in this temperature range.

Tungsten - The stable oxide is WO_3, so m = 1 and n = 3, and

$$\Delta F^\circ_y \text{ (700 °K)} = -20.6 \text{ kcal}$$

$$\Delta F^\circ_y \text{ (1000 °K)} = -27.1 \text{ kcal}$$

Tungsten probably would reduce MoO_3 between 700 °K and 1000 °K.

Niobium - Niobium may form Nb_2O_4 and Nb_2O_5. When m = 2 and n = 4,

$$\Delta F^\circ_y \text{ (700 °K)} = -136 \text{ kcal}$$

$$\Delta F^\circ_y \text{ (1000 °K)} = -76.7 \text{ kcal}$$

When m = 2 and n = 5,

$$\Delta F^\circ_y \ (700\,^\circ K) = -150 \text{ kcal}$$

$$\Delta F^\circ_y \ (1000\,^\circ K) = -149 \text{ kcal}$$

Hence, niobium will reduce nickel, probably forming Nb_2O_5.

3. Reduction of Mo_3O_9 Vapor by Cu, Ni, Ta, W, and Nb

The standard free energy of the decomposition

$$Mo_3O_{9(g)} \rightleftarrows 3MoO_{2(s)} + \frac{3}{2}O_{2(g)} \qquad \Delta F^\circ_g$$

is given by

$$\Delta F^\circ_g(T) = 43,100 + 5.3\ T$$

The oxidation of the metal can be represented by the equation used in Section B:

$$mM_{(s)} + \frac{n}{2}O_{2(g)} \rightleftarrows M_mO_{n(s)}$$

with standard free energy ΔF°_x, and the oxidation-reduction process:

$$\frac{n}{3}MoO_{3(g)} + mM_{(s)} \rightleftarrows M_mO_{n(s)} + \frac{n}{3}Mo_{(s)}$$

with the standard free energy change;

$$\Delta F^\circ_z = \frac{n}{3}\Delta F^\circ_g + \Delta F^\circ_x$$

Assuming that the solid phases are immiscible, the equilibrium pressure of MoO_3 can be calculated from ΔF°_z:

$$P^{equil.}_{MoO_3} = e^{3\Delta F^\circ_z / nRT} = \exp\left\{\left[\Delta F^\circ_g + \frac{3\Delta F^\circ_x}{n}\right] \frac{1}{RT}\right\}$$

The reaction will proceed only if the $MoO_{3(g)}$ pressure is higher in the system than the calculated equilibrium pressure.

Copper - If cuprous oxide forms, m = 2, n = 1,

$$P^e_{MoO_3}(700\,^\circ K) = 1.7 \times 10^{-9} \text{ torr}$$

$$P^e_{MoO_3}(1000\,^\circ K) = 1.8 \times 10^{-2} \text{ torr}$$

and when cupric oxide forms, m = n = 1,

$$P^e_{MoO_3}(700\,^\circ K) = 4.0 \times 10^{-4} \text{ torr}$$

$$P^e_{MoO_3}(1000\,^\circ K) = 6.8 \times 10^{2} \text{ torr}$$

Solid MoO_3 has an equilibrium vapor pressure 10^{-7} torr at 700°K and 1 torr at 1000°K. So copper could reduce Mo_3O_9 vapor by forming Cu_2O.

Nickel - NiO is the most probable oxide, so m = n = 1,

$$P^e_{MoO_3}(700\,^\circ K) = 2.8 \times 10^{-22} \text{ torr}$$

$$P^e_{MoO_3}(1000\,^\circ K) = 2.9 \times 10^{-10} \text{ torr}$$

Solid MoO_3 has an equilibrium vapor pressure of 10^{-8} torr at 700°K and 10^{-2} torr at 1000°K; therefore nickel would reduct MoO_3 vapor in this temperature range.

Tantalum - Ta_2O_5 would be expected, so m = 2, n = 5.

$$P^e_{MoO_3} = 8.5 \times 10^{-61} \text{ torr}$$

$$P^e_{MoO_3} = 1.4 \times 10^{-37} \text{ torr}$$

Tantalum will reduce MoO_3 vapor.

Tungsten - WO_3 would be expected, so m = 1, n = 3.

$$P^e_{MoO_3} \ (700°K) = 1.2 \times 10^{-32} \text{ torr}$$

$$P^e_{MoO_3} \ (1000°K) = 4.7 \times 10^{-18} \text{ torr}$$

Tungsten probably would be oxidized by MoO_3 vapor in this temperature range.

Niobium - If the product is Nb_2O_4, m = 2, n = 4, and

$$P^e_{MoO_3} \ (700°K) = 3.8 \times 10^{-58} \text{ torr}$$

$$P^e_{MoO_3} \ (1000°K) = 1.4 \times 10^{-35} \text{ torr}$$

but when the product is Nb_2O_5, m = 2, n = 5,

$$P^{e}_{MoO_3} = 1.7 \times 10^{-54} \text{ torr}$$

$$P^{e}_{MoO_3} = 3.9 \times 10^{-33} \text{ torr}$$

Niobium could reduce MoO_3 vapor; and Nb_2O_4 would form at both 700°K and 1000°K.

4. Reduction of MoO_3 and Mo_3O_9 by Cesium

For the solid MoO_3 in the additive reservoir the reaction,

$$MoO_{3(s)} + 2Cs_{(g)} \rightleftarrows MoO_{2(s)} + Cs_2O_{(s)}$$

has to be considered. It is evident that cesium will not reduce MoO_3 if its pressure is low enough. Thus for any given MoO_3 reservoir temperature there is a maximum cesium reservoir temperature for which the reaction will not occur. Figure V-6 is the result of this calculation.

In the gas phase, the following reaction may occur:

$$Mo_3O_{9(g)} + 6Cs_{(g)} \rightleftarrows 3\,MoO_{2(s)} + 3Cs_2O_{(\ell)}$$

$$\Delta F^\circ = -298,270 - 69.09\ T \log T + 442.1\ T$$

$$P_{Mo_3O_9} \cdot P_{Cs}^{\,6} = \exp\left[\frac{\Delta F^\circ(T)}{RT}\right]$$

at T = 1000°K

$$P_{Mo_3O_9}\,(\text{torr}) = (9,700)\ P_{Cs}^{\,-6}$$

P_{Cs} (torr)	0.1	1.0	2	3	5	10
$P_{Mo_3O_9}$ (torr)	9.7×10^{9}	9.7×10^{3}	150	13	0.62	9.7×10^{-3}

Here, the equilibrium pressure of Mo_3O_9 is tabulated as a function of the cesium pressure. If the trimer pressure in the system is lower than this value, then no reduction takes place. If it is higher, the cesium vapor will reduce the excess trimer until this equilibrium pressure is established. So, if the additive reservoir temperature is $\sim$ 1000°K making the trimer pressure $\sim$ 1 torr, the cesium pressure must be smaller than 5 torr; otherwise reduction of Mo_3O_9 will take place in the gas phase.

It may be concluded, therefore, that for every given additive reservoir temperature, there exists a critical cesium pressure (critical cesium reservoir temperature) above which cesium would reduce the Mo_3O_9 vapor.

D. COMPATIBILITY TEST

The thermodynamic calculations concerning chemical reactions are useful, because they define the upper limit which can be achieved under optimum equilibrium conditions. However, both the products of reaction and the energies of reaction must be known; uncertainties in either will lead to error in the predictions. Furthermore, thermodynamics cannot be used to predict rates, and in practice many possible reactions seemingly do not occur because their rates are extremely slow. In order to supplement the MoO_3-material compatibility calculations above simple compatibility tests were run in vacuum. In these tests solid MoO_3 was placed in contact with several materials at 600°C for 60 hours. The materials tested were alumina, nickel, molybdenum, niobium and tantalum. The reaction products in each case were collected and analyzed crystallographically for molybdenum dioxide and trioxide. The results indicated that tantalum and niobium were quite reactive with solid MoO_3; the extent of interaction was less with molybdenum, and only slight attack was observed with nickel. The alumina appeared to be completely inert to MoO_3 under these conditions. In a separate test the compatibility of copper with MoO_3 was investigated. Between the temperatures 500°C and 600°C, MoO_3 interacted with copper metal, forming a liquid product. The data in Table V-1 indicate that no reduction of MoO_3 by copper should occur. However, a eutectic of Cu_2O and MoO_3 has been reported to form with a melting point at 535°C; therefore, physical dissolution of cuprous oxide can occur in this temperature range, which would considerably decrease its activity, so that ΔF becomes smaller, allowing the reaction to occur.

E. DIFFERENTIAL THERMAL ANALYSIS

A Fisher Model 260 Differential Thermo Analyzer was obtained to study the physical and chemical changes occurring with metal oxides as a function of temperature. The purpose of these measurements was to provide a semi-quantitative check on the thermodynamic calculations just discussed. Since most of the changes are accompanied by considerable enthalpy change, the energetics of these changes and the temperatures at which they occur can be determined by monitoring the temperature difference between the sample being examined and a thermally inert sample of similar heat capacity while both samples are heated at the same constant rate. This is accomplished with the Thermo Analyzer. The Thermo Analyzer is designed to carry out measurements in air as well as under inert atmosphere provided by argon or nitrogen gas flow through the furnace.

Finely powdered molybdenum trioxide was heated up to 1200°C with a constant heating rate of 10°C/min. Except for a broad endothermic peak due to the desorption of adsorbed water below 100°C, the only well defined peak was due to the melting of the MoO_3. The melting point thus obtained was 780°C for the sample. The same sample of MoO_3 was run again in the Thermo Analyzer between room temperature and 1200°C, and an identical thermogram was obtained. This observation indicates that molybdenum trioxide heated in air up to 1200°C suffers no significant physical or chemical change (except the slow sublimation which occurs at the higher temperatures), which is in agreement with the thermodynamic calculations.

Molybdenum trioxide was heated in slow-flowing argon at a rate of 10°C/min. Again, a well-defined endothermic peak indicated

the melting point, and no other peak has been observed. Then the same experiment was repeated with the sample after cooling it to room temperature. An identical thermogram was obtained; hence no significant decomposition occurs in the absence of oxygen.

When the mixture of molybdenum metal powder and molybdenum trioxide (2 moles/ 1 mole) was heated in argon, a broad exothermic peak beginning at 400 °C indicated the start of a slow exothermic reaction, possibly the heterogeneous reduction of MoO_3 by molybdenum. The melting point endothermic peak of MoO_3 was absent completely; no trioxide was left in any significant quantity after the reaction was completed.

$$MoO_3 + 2Mo = 3MoO_2$$

A small but sharp exothermic peak was observed at 500 °C, and a considerable increase in reaction rate was found around 800 °C, just above the melting point of MoO_3.

The mixture of copper powder and molybdenum trioxide was heated in argon at a rate of 10 °C/ minute, in order to investigate the interaction between MoO_3 and Cu observed during degassing experiments. According to thermodynamic calculations, no chemical reaction should take place below 700 °C. While pure copper shows only one small exothermic peak at 370 °C in addition to a well-defined desorption peak at low temperatures, the mixture produced numerous small peaks in addition to a well-defined endothermic peak at around 500 °C, signifying the existence of a eutectic in the Cu-MoO_3 system. Above 600 °C a broad exothermic peak has started, and the product obtained after the run was a crystalline black mass similar to that material obtained during degassing of MoO_3 in a copper tube.

The differential thermal analysis of certain systems, like cesium oxides, is a difficult problem. A specially designed sample holder is needed which can be evaluated to a high degree. A system capable of handling cesium has been built recently, and preliminary runs are being made. The usefulness of the differential thermal analysis is limited and it has to be complemented with mass spectrometry, especially when the species in the gas phase are of interest.

F. DIODE EXPERIMENTS

Four diode experiments were undertaken to study the behavior of MoO_3. Two of these were filamentary diodes of a new type designed to study the effects of MoO_3 on the work function of a tungsten emitter. The other two diodes were of a simple fixed-spacing type without guarding. These latter diodes were used to study the effects of MoO_3 on overall diode performance.

1. Filamentary Tubes

The filamentary diodes were designed to study work function changes due to additives both with and without cesium present. The first filamentary diode built contained both cesium and MoO_3. The purpose of this test was to observe the work function changes due to cesium and MoO_3 and to ascertain whether any reaction would occur between the Cs and MoO_3. Figure V-4 is a drawing of the tube' s design. An eight-pin ceramic lead-through was used for the electrical connections. The diode consisted of an emitter filament, three auxiliary .010"-diameter tungsten heater filaments parallel to the .005"-diameter tungsten emitter filament, two cylindrical guards, a cylindrical collector with an attached annular additive reservoir, the metal envelope, and an external copper tube to serve as the cesium reservoir. The auxiliary heater filaments were used to heat the additive reservoir by radiation. The temperature of the additive reservoir was read by means of a thermocouple.

Before the MoO_3 diode was assembled measurements were made on a test setup to determine how the auxiliary heaters would perform. The results of these tests indicated that additive reservoir

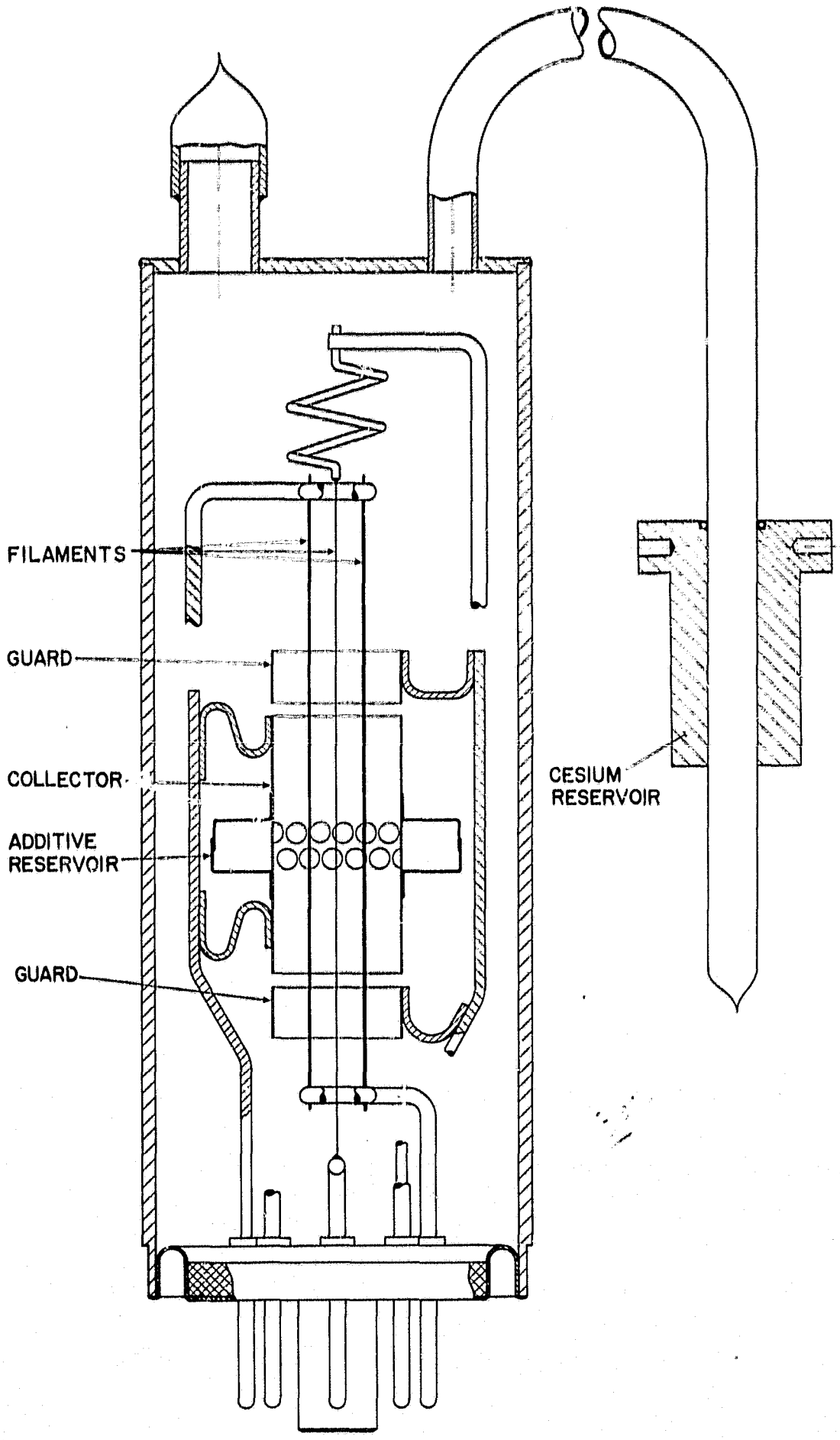


Figure V-4. Schematic of Cesium-Molybdenum Trioxide Filamentary Diode.

temperatures up to 700°C could be obtained. Also found from the test setup was the fact that the heater filaments affected the thermionic emission from the emitter filament only in that their emitted radiation influenced the emitter temperature, and these effects were easily corrected for by measuring the emitter filament resistance.

The diode was assembled with the MoO_3 in pellet form. Then the diode was outgassed at temperatures up to 600°C. External heaters were used to raise the envelope temperature to this value. Figure V-5 is a schematic diagram of the outgassing setup. The diode was evacuated through the outgassing tubulation by means of a vac-ion pump.

Once outgassing was c mpleted, the vac-ion line was pinched off and the cesium was distilled into its reservoir. This was carried out with the envelope and MoO_3 reservoir at an elevated temperature to prevent possible reaction between the cesium and the MoO_3. Figure V-6 indicates the maximum cesium reservoir temperature which can be held without a reaction between cesium vapor and solid MoO_3. For the cesiating temperature of 200°C this meant the MoO_3 temperature had to be more than 400°C. Once cesiating was completed, the remainder of the outgassing tube containing the glass cesium capsule was pinched off.

The first test to be run with the diode was to obtain the bare work function with the cesium reservoir cold. The result was a work function of 4.55 eV, which is in good agreement with previous results for similar tungsten filaments.

The test procedure followed after the initial bare work function measurements was as follows: First the additive temperature was

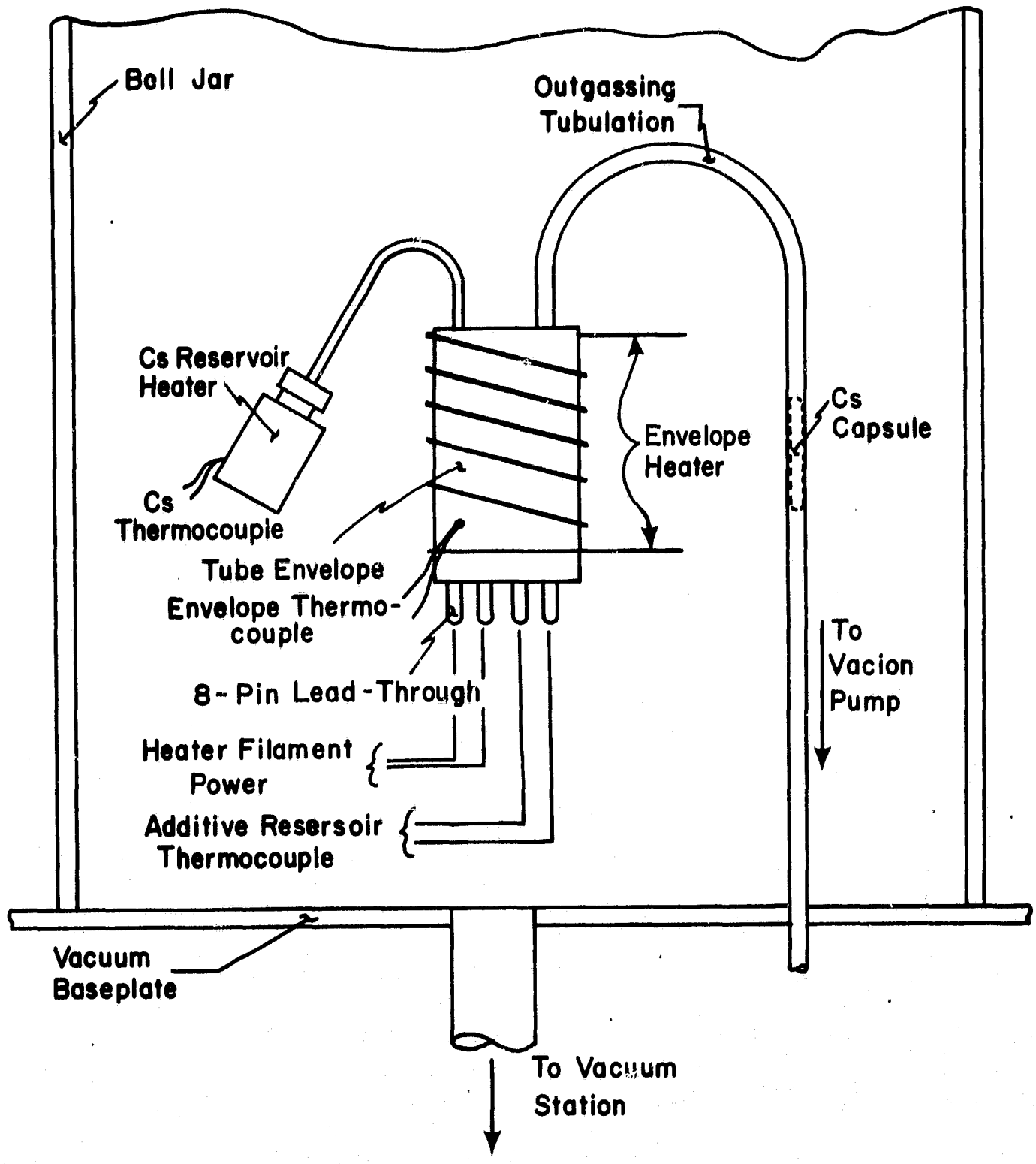


Figure V-5. Schematic Diagram of Filamentary Diode Outgassing Setup.

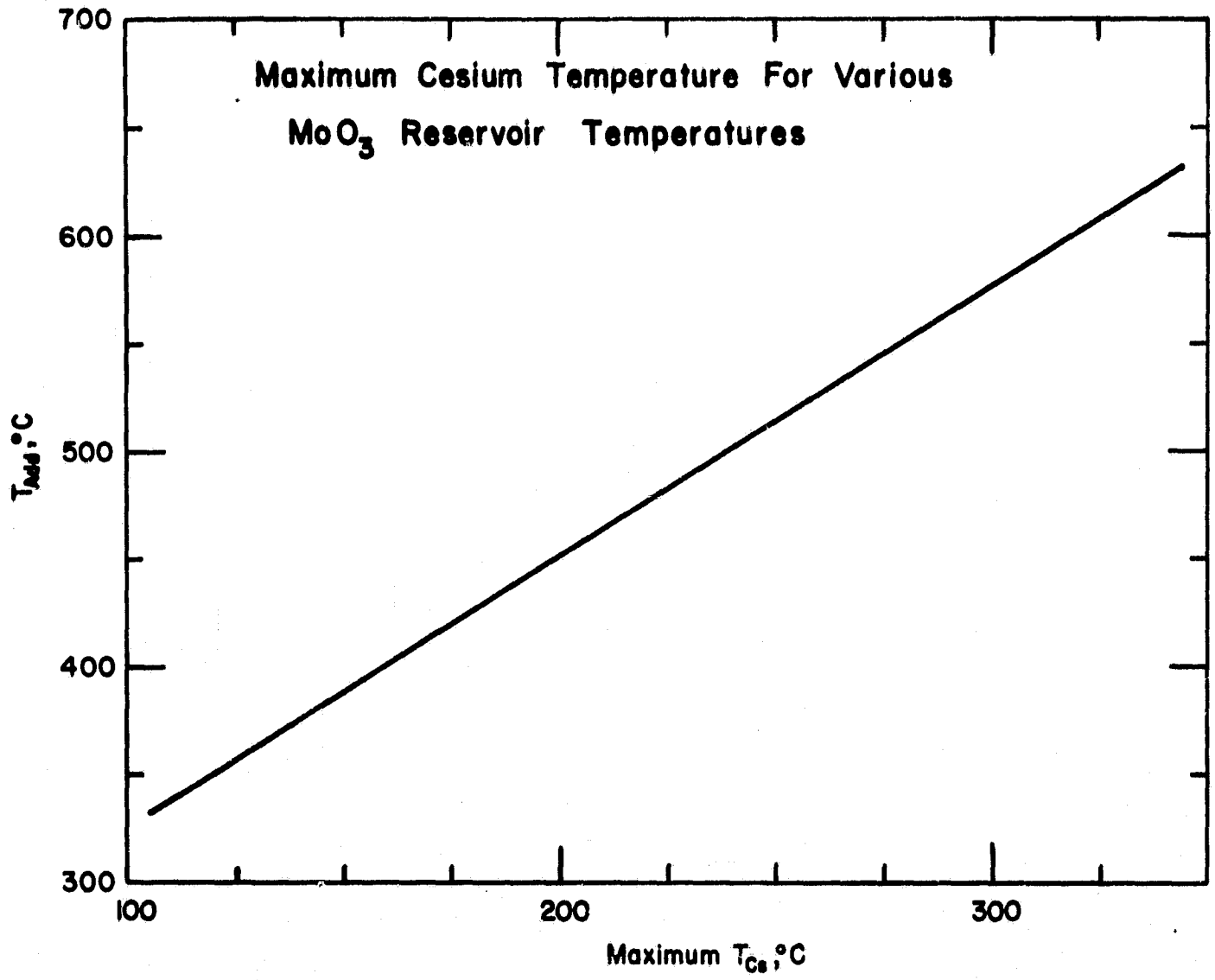


Figure V-6. Maximum Operating Temperatures for Cesium Reservoir.

raised, using the auxiliary heater filaments, to 550°C for periods up to 60 minutes, then additive work function measurements were made. After the work function had stabilized the cesium reservoir temperature was raised to 125°C and work function measurements again made, thus yielding cesium plus oxygen results. Measurements were also made with cesium only with a reservoir temperature of 125°C. All these results are shown in Figure V-7.

The reason why data was not obtained for temperatures below 1900°K emitter temperature was due to electrical leakage across the ceramic lead-through, which masked the emission current at lower temperatures. This leakage was worsened by the presence of the hot auxiliary filaments; therefore they could not be left on when measurements were made. This prevented obtaining steady-state additive data at 550°C as the additive reservoir cooled to about 450°C when the heater filaments were shut off. This temperature shifted slightly as the emitter temperature changed, but by no more than 20°C, which meant the additive temperature was controlled mainly by the envelope temperature when the auxiliary filaments were off.

The results of this experiment indicate that an oxygen effect was definitely present for an additive temperature of 450°C. Measurements made immediately after the auxiliary filaments were turned off showed a decreasing oxygen effect which soon stabilized. Thus this stable level must be associated with the 450°C additive temperature which was the equilibrium reservoir temperature with the heaters off. This temperature could not be raised due to an increase in the electrical leakage with increasing envelope temperature.

The data does not correspond well with the expected results for MoO_3 at 450°C. The effects of MoO_3 should be negligible as the oxygen pressure expected is less than 10^{-8} torr, an oxygen pressure which has little effect on the emitter work function at 2100°K. On the other hand, large changes have been obtained, in thermionic diodes, with Cs_2O in the range of 700°K additive temperature. Thus, the oxygen effect appears to have been caused by the presence of Cs_2O or a related cesium oxide. This conclusion was reinforced by the fact that after approximately 50 hours of operation the cesium pressure could no longer be controlled by changing the cesium reservoir temperature. On examining the diode when it was opened, cesium was found to be present in the MoO_3. Therefore, it appeared that some combination of molybdenum and cesium oxides had formed.

Because of the uncertainty in the above experiment a second filamentary diode was built to operate with MoO_3 alone. The design of the diode is shown in Figure V-8. This diode contained no internal reservoir or auxiliary heaters, and had one external reservoir for the MoO_3. A second tube leadsfrom the diode envelope to a Vac.-Ion pump which was always connected to the diode. The continuous operation of the pump prevented the build-up of oxygen in the diode, but meant that the experiment would not be in a strictly equilibrium condition. However, the pump could be used to measure the gas pressure in the diode. To prevent reaction between MoO_3 and the copper reservoir tube, the reservoir was lined with Al_2O_3, which does not react with MoO_3 up to at least 900°K. This was observed in the compatibility experiments mentioned previously.

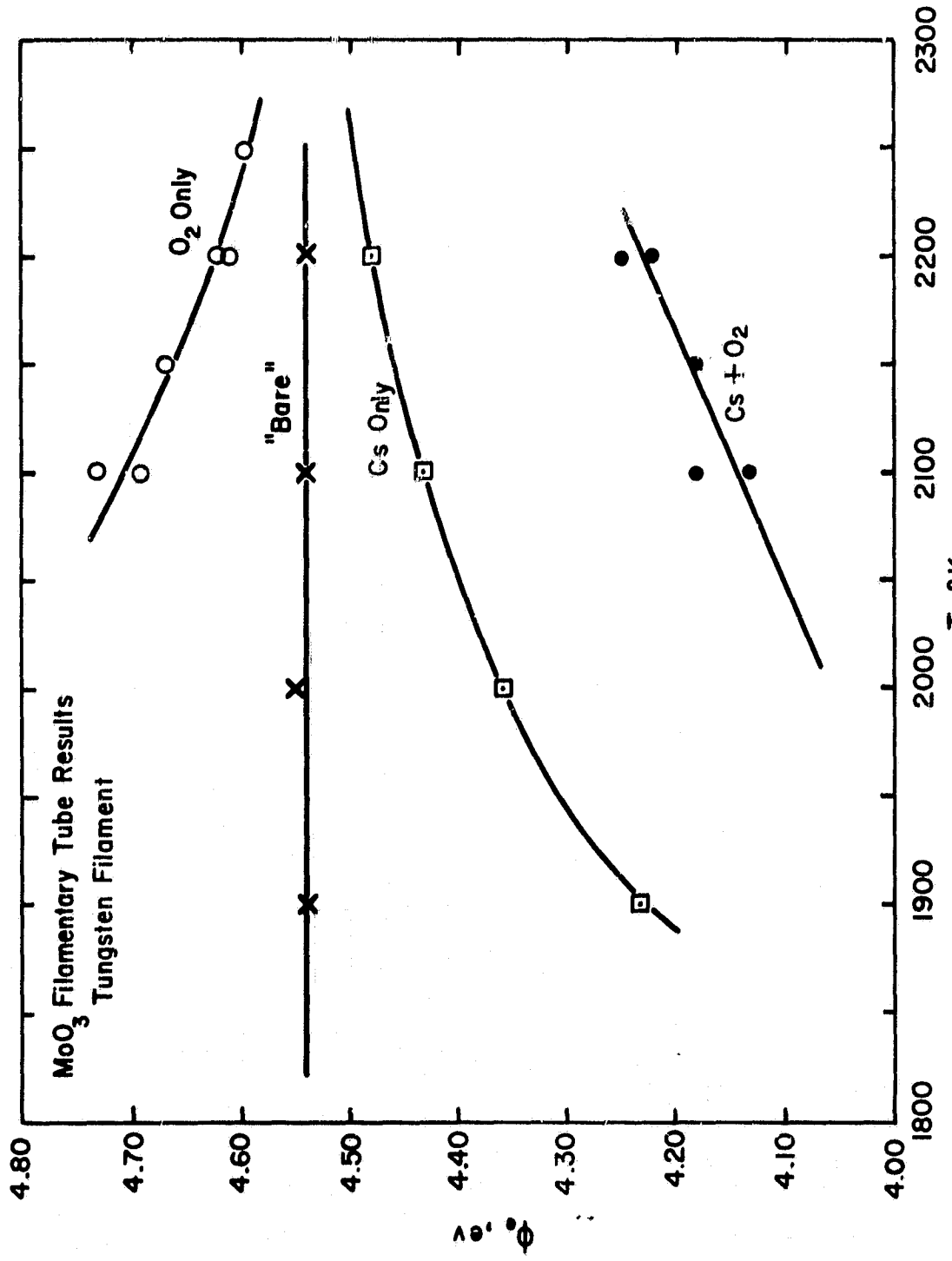


Figure V-7. Filamentary Diode Work Function Results for Bare, Cesium Only, Oxygen Only, and Cesium-Oxygen Conditions.

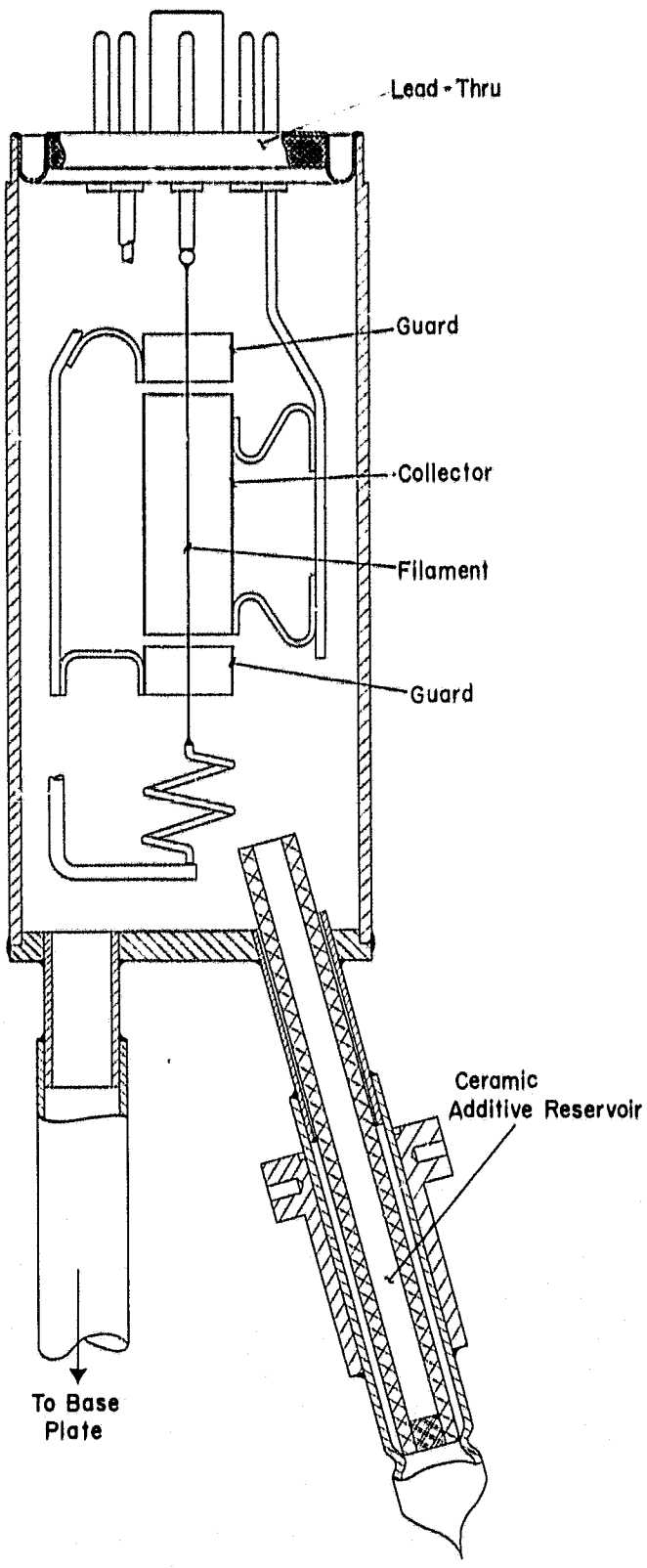


Figure V-8. Schematic of MoO_3 Filamentary Diode.

To prevent MoO_3 condensation on the envelope walls, the envelope had to be maintained at a high temperature, at or above the reservoir temperature. Besides preventing condensation of MoO_3 the high temperature prevented large amounts of oxygen from being released or adsorbed by the walls, which would mask the oxygen being released by decomposition of MoO_3 at the emitter.

As with the previous filamentary diode, this diode was thoroughly outgassed. The additive was outgassed at temperatures up to 300°C, while the envelope was held at temperatures up to 400°C. This outgassing lowered the residual oxygen pressure in the diode to approximately 10^{-8} torr. The diode and additive were not outgassed at higher temperatures in order to prevent possible reactions of the MoO_3. Since the pump was operating continuously, it was possible at each increase in additive or envelope temperature above the outgassing temperatures to allow the diode to outgas before data was obtained. Thus, data was obtained after a one- to two-day period of outgassing after each temperature increase.

Data was obtained following the above method of stabilizing the pressure for additive temperatures of 100, 400, 500, and 600°C. The first measurement at 100°C was to check the bare work function, which was found to be 4.55 eV, namely the same as the previous filamentary diode. The data at 400, 500 and 600°C was obtained with envelope temperatures of 600, 600 and 650°C, respectively. Figure V-9 indicates the results and compares them with results of Stickney's[1] work on polycrystalline tungsten filaments at known oxygen pressures. These curves can be used to interpret the results of the present experi-

ment in terms of oxygen pressure. The bare work function data (T_{MoO_3} = $T_{envelope}$ = 100°C) corresponded to the 10^{-9} torr oxygen pressure line, indicating the low-temperature background pressure of oxygen in the envelope. The figure also includes the pump pressure readings for the data. These readings were, of course, higher than the partial oxygen pressures found by comparing the data to Stickney's.

The results of the experiment were complicated by the transient changes in oxygen pressure following a temperature increase in the MoO_3 reservoir. This outgassing effect was minimized by waiting for the pressure to stabilize before measurements were made. There remained a steady oxygen effect dependent on the additive reservoir temperature, as the figure indicates. The difference in the slopes between the data and the constant-pressure data of Stickney indicates that the oxygen pressure increased with emitter temperature, the change in pressure being about the same as predicted in the thermodynamic analysis. The overall effect was much smaller than anticipated from the calculations, however, and indicated that the data used in the calculations needs to be improved. This low oxygen pressure also helps to explain the small changes observed in the following fixed-spacing diode results.

When the diode was cut open the additive reservoir contained a very small amount of MoO_3. The diode itself was heavily coated on all parts with MoO_2. In order to vaporize nearly all the MoO_3 from the reservoir the vapor pressure of MoO_3 must have been what was expected from published results. However, the presence of MoO_2 in the diode, which is a nonvolatile oxide, and the low oxygen pressure seen by the filament indicated that some reaction other than what was expected had occurred. Little MoO_3 had been reduced at the filament, the major reduction occurring at the much lower envelope temperature.

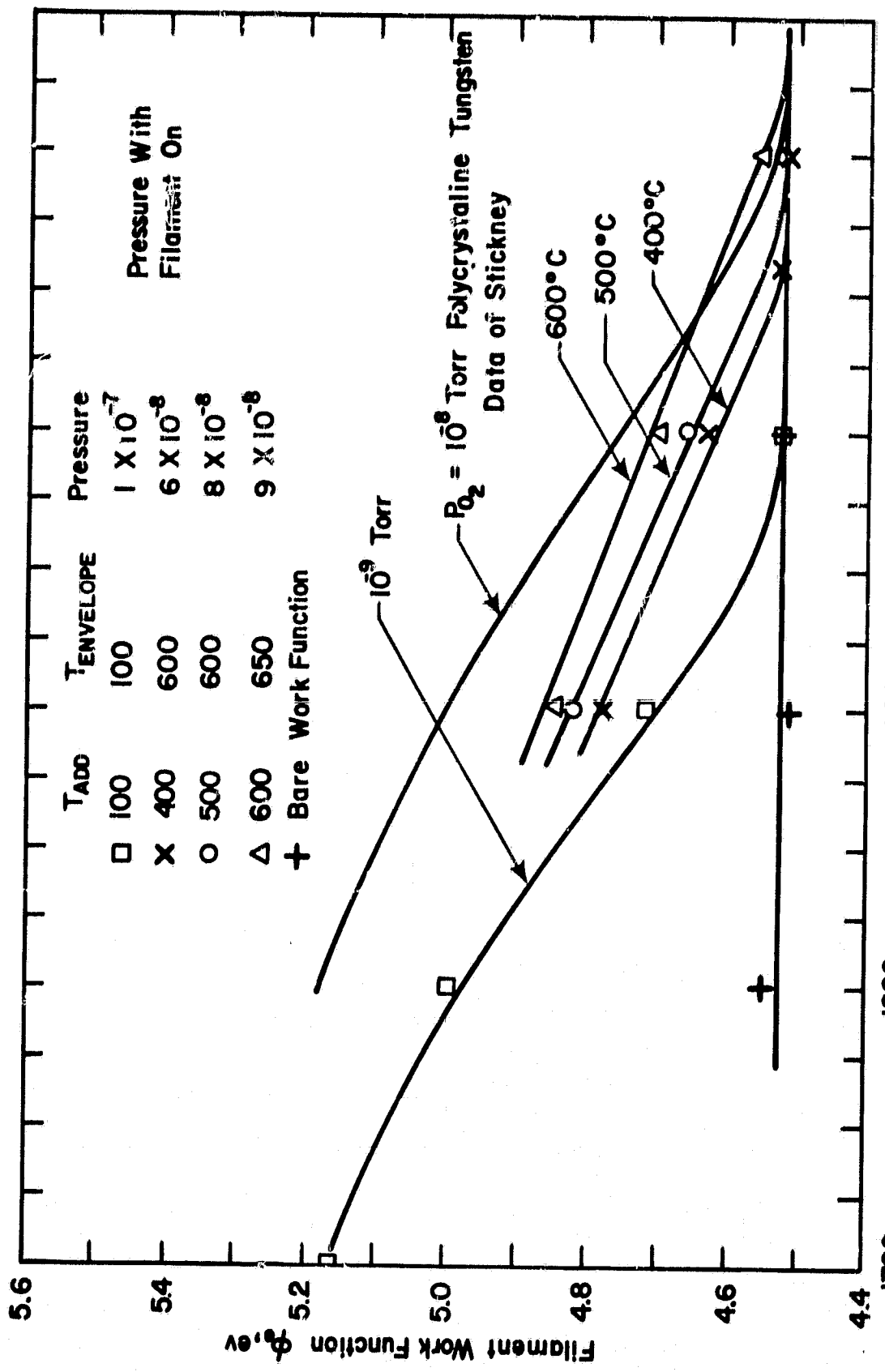


Figure V-9. Work Function Results of MoO_3 Filamentary Diode and Comparison to Stickney's Data.

2. Fixed-Spacing Converters

In conjunction with the filamentary diode experiments discussed above, two fixed-spacing diodes were operated with MoO_3 as an additive. These diodes were intended by investigate the influence of MoO_3 on the output of a thermionic converter. Due to the design of these diodes, that is, the proximity of the emitter sleeve and collector and the lack of a guard, meaningful work function measurements could not be obtained. Instead, changes in output were observed through changes in the envelopes of the current-voltage curves.

The design of the first diode tested is shown in Figure V-10. The diode includes a reservoir for the additive MoO_3. This reservoir was made of Cu tubing with a nickel tube connecting the reservoir to the diode. The additive was lead to the interelectrode space through six holes in the collector. These six holes were arranged to give a nearly uniform additive density throughout the interelectrode space. To allow easy diffusion of the additive in this space, the diode was designed to have an 8-mil spacing.

As the first test was performed with cesium alone, a means had to be devised to isolate the additive from the diode until it was required, for if MoO_3 in contact with cesium vapor is not held above a certain temperature it will be reduced by cesium. Figure V-6 above indicates that, for cesium a reservoir temperature of over 300°C the solid MoO_3 has to be over 600°C. However, the vapor pressure of MoO_3 is starting to become significant at 600°C. To avoid having to hold the MoO_3 at a high temperature, it was sealed in a molybdenum capsule, which was in turn placed in the copper additive reservoir as

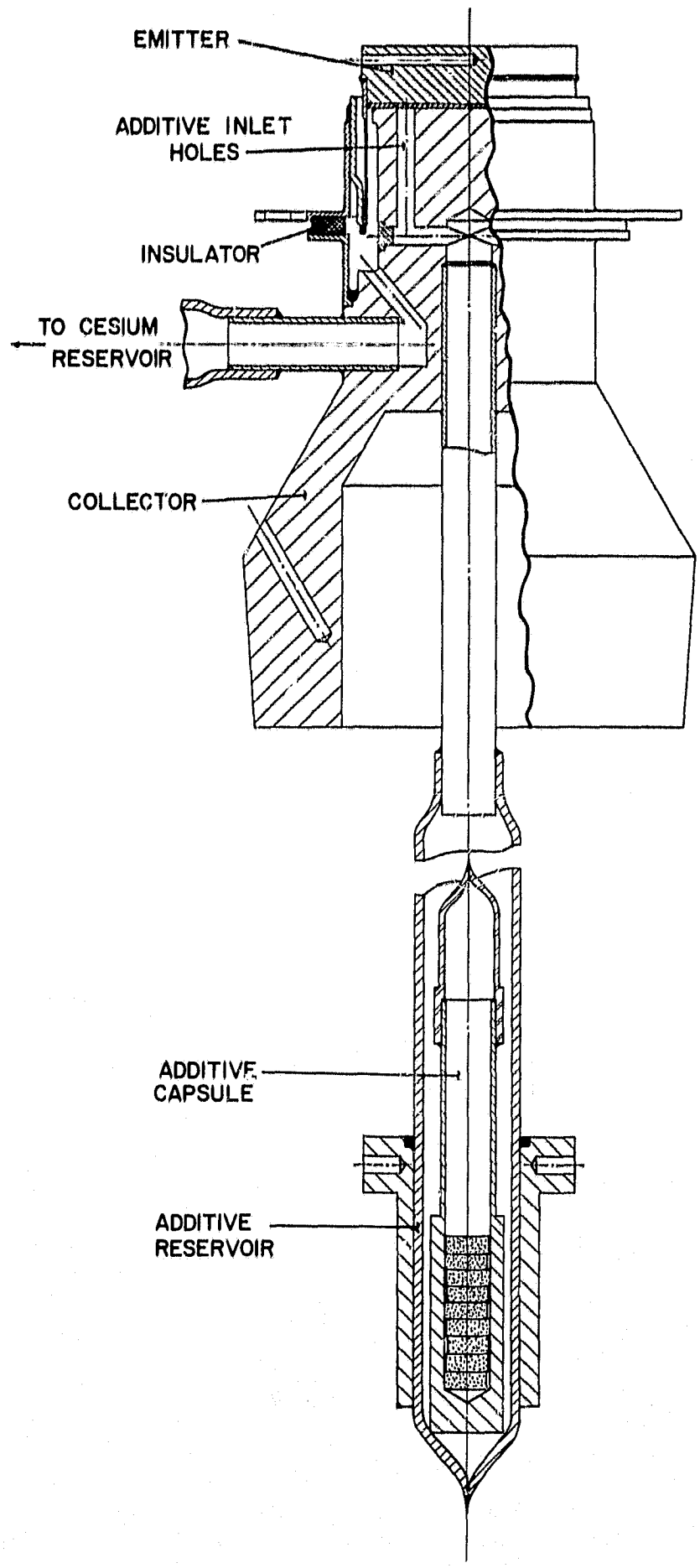


Figure V-10. Schematic of MoO_3 Fixed Spacing Diode with Mo Capsule.

Figure V-10 indicates. When the MoO_3 was desired the outer copper tube was pinched until the heat-treated molybdenum capsule cracked open. From this point on, the additive could enter the interelectrode space.

Prior to being assembled to the diode, the additive capsule was outgassed separately. This outgassing was done at temperatures up to 400°C. A temperature of 400°C was held for 48 hours. Once the capsule was outgassed it was installed into the diode and the entire converter was outgassed, after which the diode was cesiated and cesium data obtained.

After the cesium-only performance was completely documented the additive capsule was opened and the output of the converter was compared with the corresponding cesium-only data. Two typical comparisons are shown in Figures V-11 and V-12. As these figures show, there was a small additive effect; the cesium-pressure-optimized envelope moved to higher voltages by 0.1 volt. No additional effect could be obtained when the additive reservoir temperature was increased or decreased. The lack of sensitivity and the gradual disappearance of the 0.1-volt shift led to the conclusion that the initial change was due to a burst of oxygen supplied to the diode at the time the additive capsule was cracked, and that the MoO_3 was not contributing a steady additive effect.

The detailed thermodynamic calculations on the compatibility of MoO_3 with diode materials discussed previously indicated that MoO_3 would react with Mo at a high enough temperature. It was thought that this would only be a surface reaction. Examination of the additive capsule when the diode was opened, however, showed that all the MoO_3

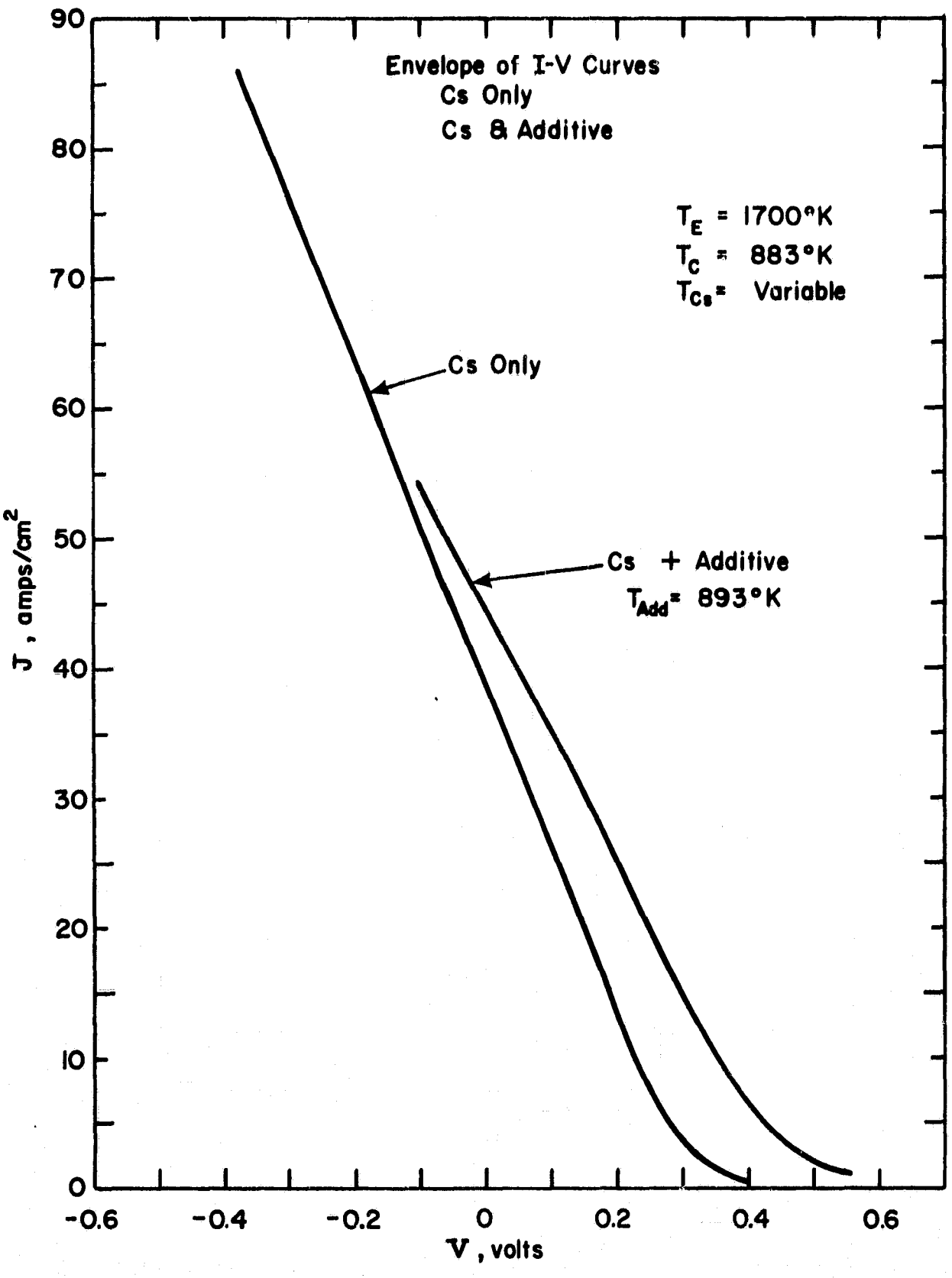


Figure V-11. Comparison of Envelopes for Cesium Only and Cesium Plus Additive Operation at T_E = 1700°K.

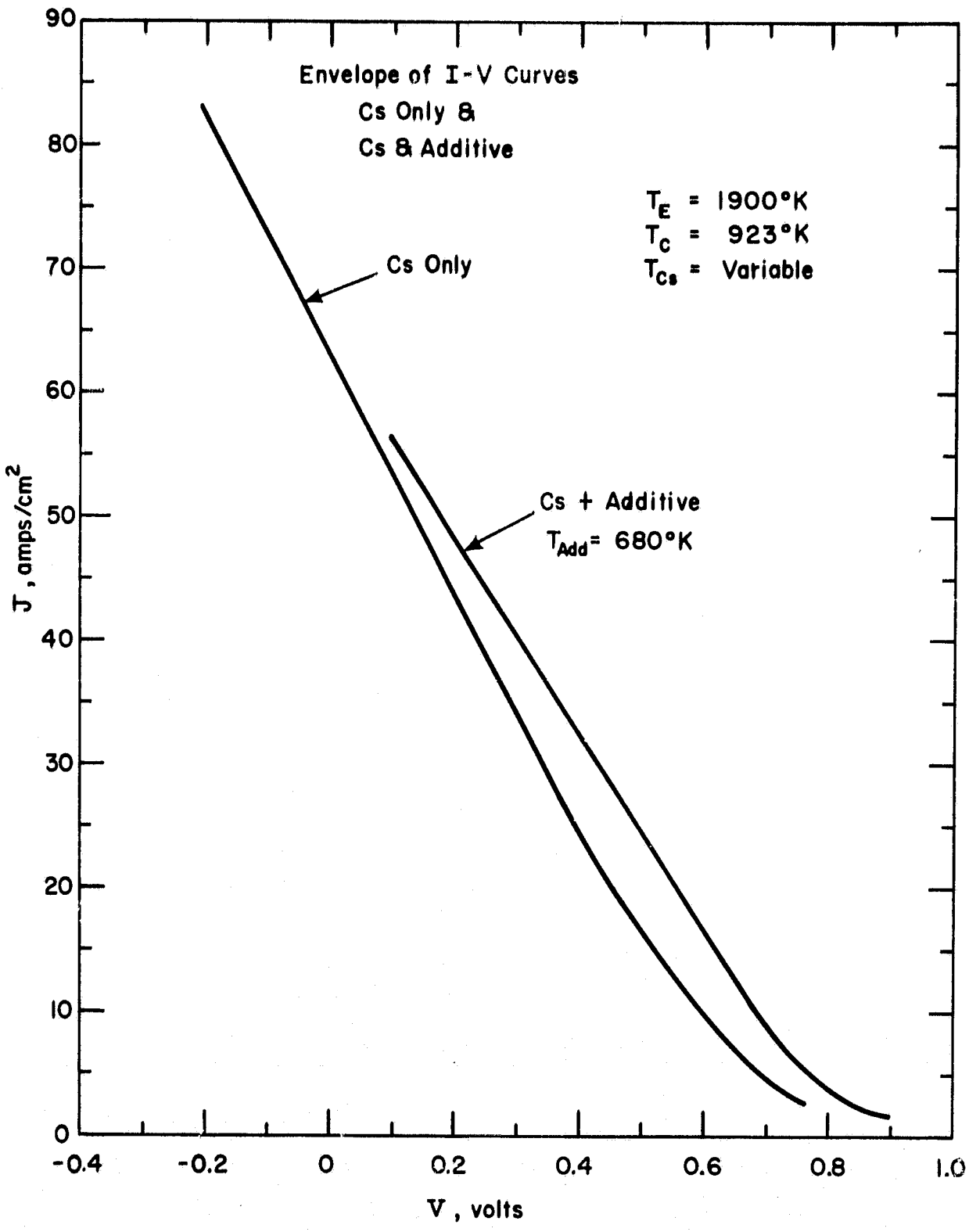


Figure V-12. Comparison of Envelopes for Cesium Only and Cesium Plus Additive Operation at T_E = 1900°K.

had been reduced to MoO_2 by the molybdenum metal. Thus, no MoO_3 was available as an additive, which explained the negative results obtained with this diode. The shift in envelopes indicated must have been due to oxygen in the capsule before it was cracked open, the MoO_3 having been reduced during the outgassing period.

To avoid the decomposition of MoO_3 in its reservoir or along the walls of the tubing leading to the interelectrode space, a second diode with an alumina reservoir was prepared. The compatibility tests reported above indicated that Al_2O_3 is compatible with MoO_3 at least up to 600°C. Thus the diode shown schematically in Figure V-13 with the entire additive reservoir lined with Al_2O_3 was assembled.

The disadvantage of this second diode was that the MoO_3 was always exposed to the cesium vapor in the diode. Therefore, the maximum cesium pressure conditions shown in Figure V-6 had to be followed at all times. However, it was hoped that the Al_2O_3-lined additive reservoir would avoid the problem of losing MoO_3 due to reaction with Mo.

This diode, like the previous one, had an interelectrode spacing of 8 mils. The cesium reservoir and tubulation were identical. The outgassing procedure, however, had to be changed. The additive was outgassed in the diode instead of separately. The diode and additive were heated together to 350°C and held for 100 hours while the additive outgassed. After this time the collector and emitter were raised to their normal outgassing temperatures while the additive was held to 350°C. After outgassing was completed, the diode was cesiated; this was done while holding the additive at an elevated

temperature. After cesiating, the diode testing was immediately started. Current-voltage curves were obtained for varying cesium and additive reservoir temperatures, at two emitter temperatures, 1700°K and 1900°K. The collector temperature was chosen to be near optimum at each emitter temperature. Because of the possible cesium-MoO_3 reaction at high cesium pressure, the number of current-voltage families was limited, except for additive temperatures above 600°C.

The results of testing the diode for over 100 hours showed little correlation between diode output and additive reservoir temperature. Figures V-14a and V-14b show the diode output for two additive temperatures and an emitter temperature of 1700°K. Figures V-15a and V-15b show results for the same additive temperatures and for an emitter temperature of 1900°K. The waiting time between changes in additive temperature was not standardized; it was varied six hours for Figure V-14 and three hours for Figure V-15.

Comparison of identical-condition I-V families throughout the diode testing period indicated a steady decline in output current. The maximum change after 100 hours of operation was equivalent to a change in cesium temperature of 5°C. This change occurred principally in the first 30 hours of operation.

The lack of response of the diode to changes in additive temperature indicated that either the MoO_3 did not volatilize or it had reacted to form a nonvolatile product. When the diode was dismantled it was found that some MoO_3 had reacted in its reservoir but that a substantial amount still existed. However, changes in the appearance of the emitter and collector indicated that very small amounts of MoO_3 had actually gotten to this region. It appeared, therefore, that MoO_3 had not volatilized as much as had been expected, although the reason was not apparent.

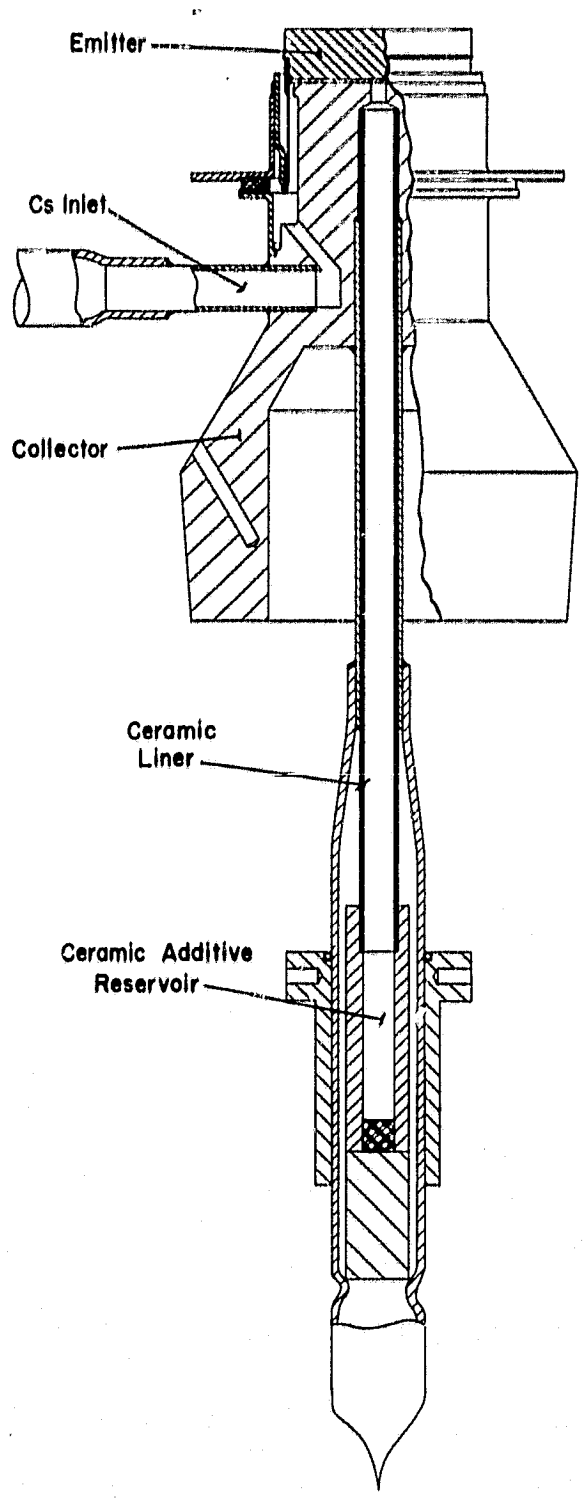


Figure V-13. Schematic of Fixed-Spacing Diode with MoO_3 Additive in Al_2O_3 Lined Reservoir.

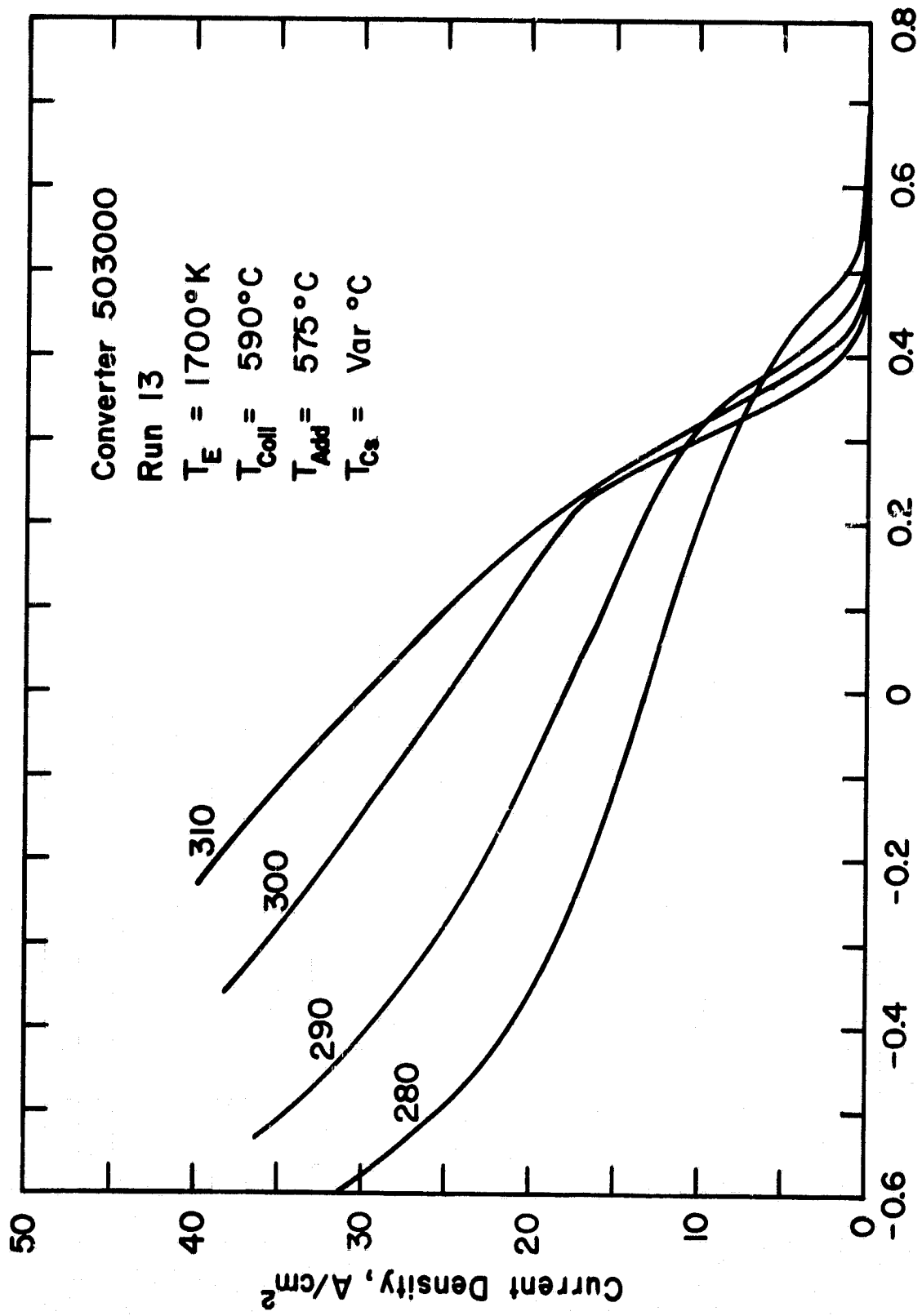


Figure V-14a. I-V Curves for Cesium-MoO_3 Operation.

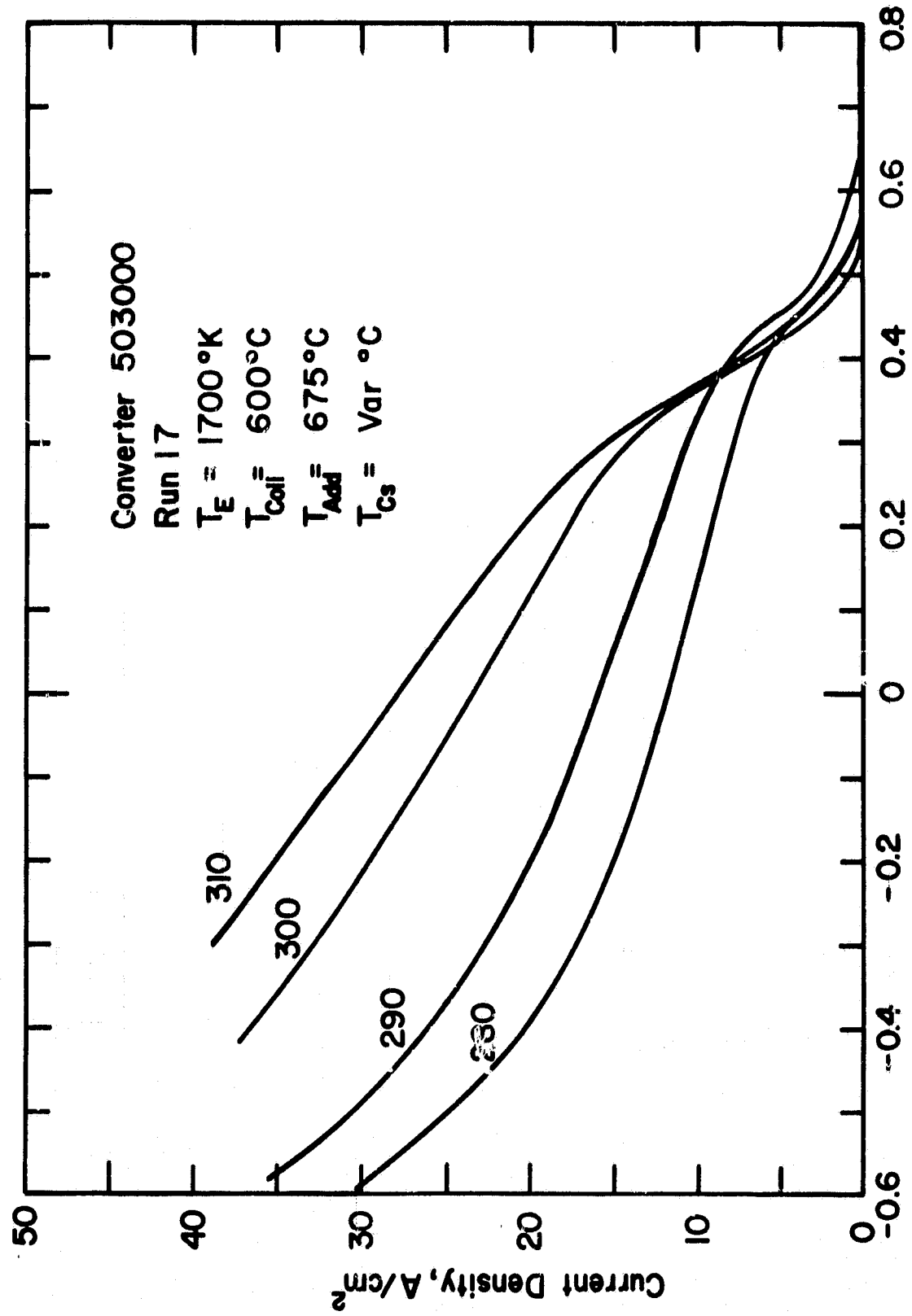


Figure V-14b. I-V Curves for Cesium-MoO_3 Operation.

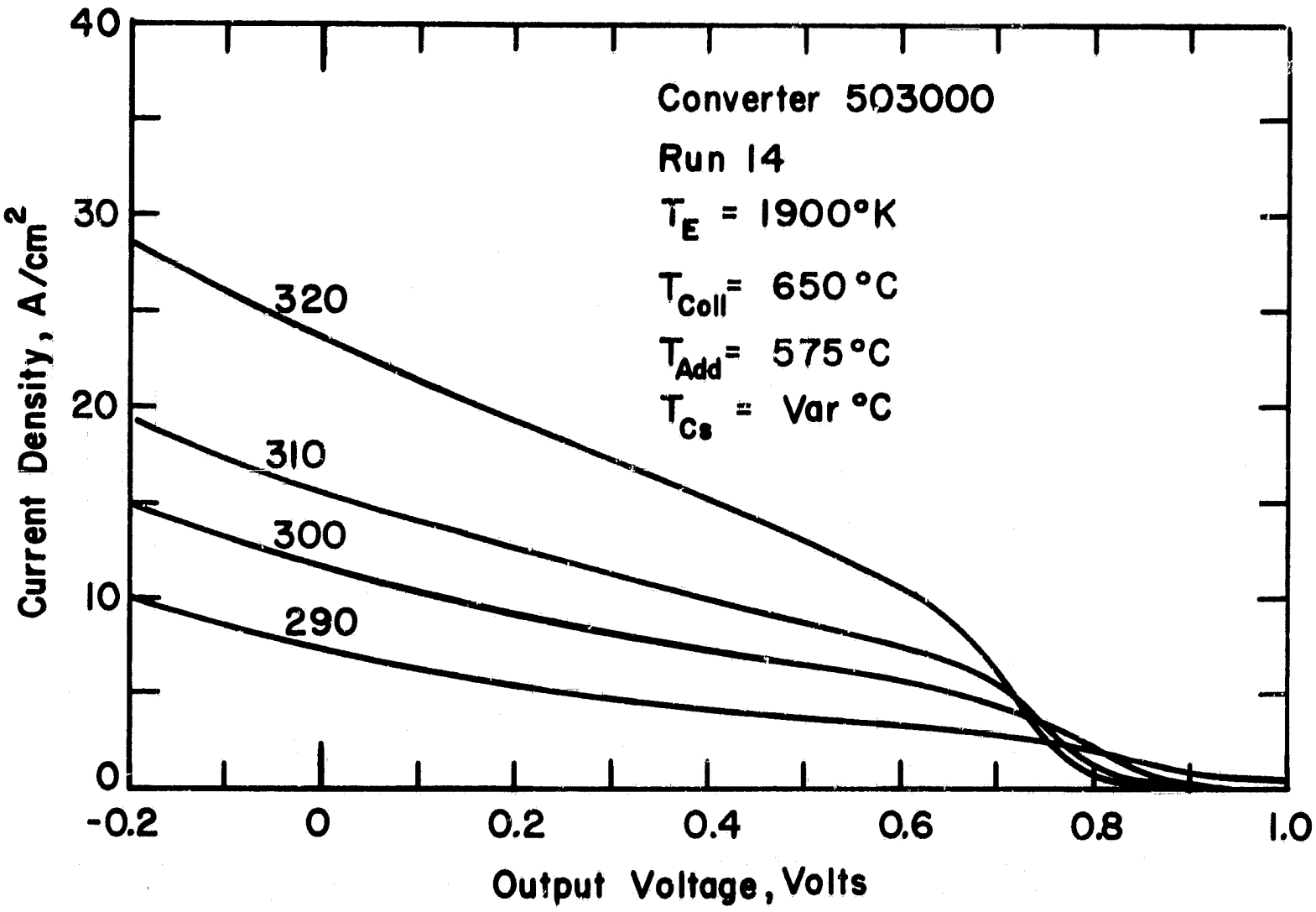


Figure V-15a. I-V Curves for Cesium-MoO_3 Operation.

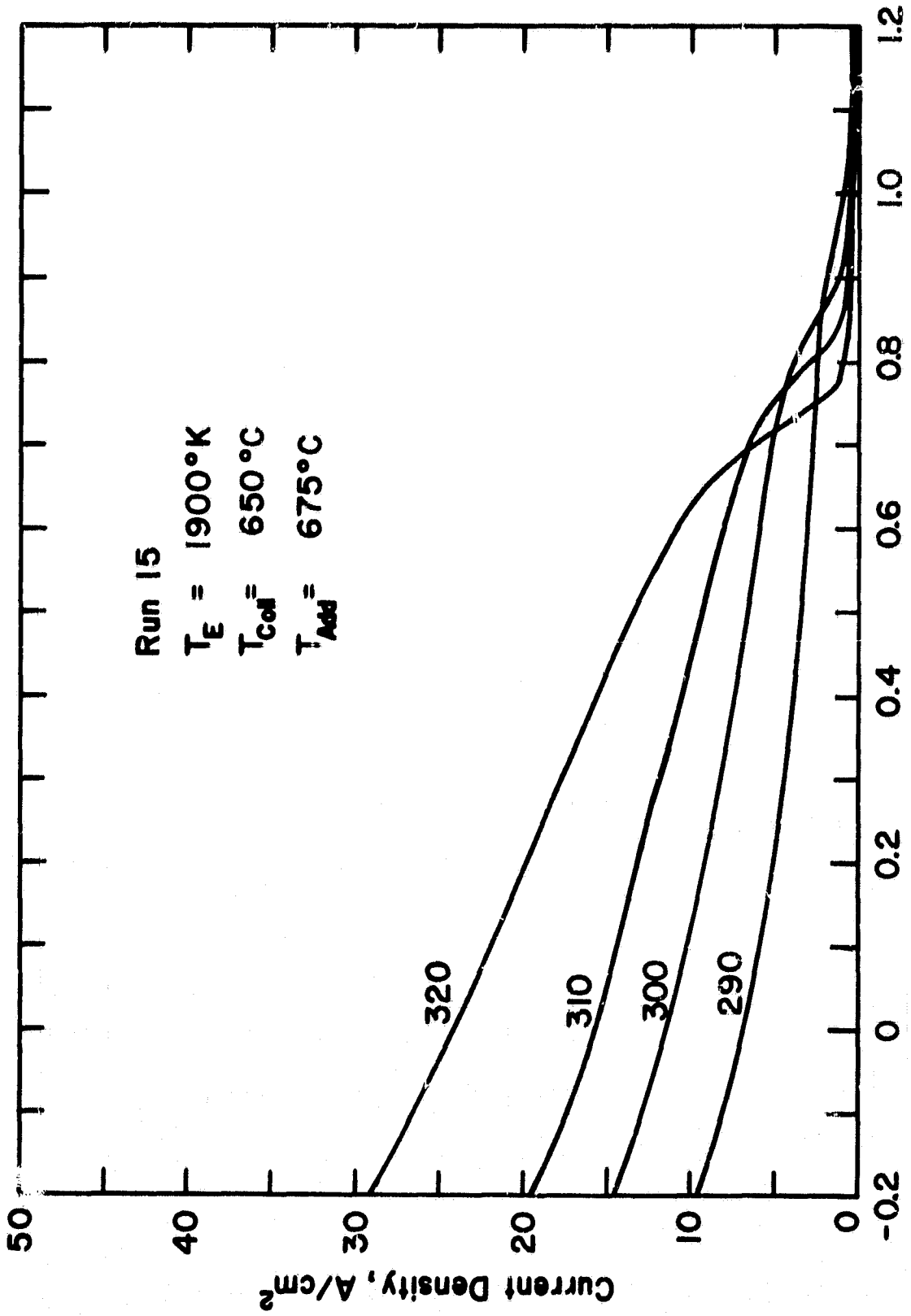


Figure V-15b. I-V Curves for Cesium-MoO_3 Operation.

G. CONCLUSIONS

The survey of the thermodynamic data indicated that uncertainties still exist in the value of many properties of MoO_3. The behavior of MoO_3 at temperatures above its melting point, 1068°K, and in the gaseous phase is not well documented. Thus, it is not possible to pin down the effects of MoO_3 in a thermionic converter without doing experimental studies with MoO_3 to observe the reactions. This type of study can be done with a mass spectrometer, and would clear up some of the problems encountered in the diode experiments reported. The two diode experiments (filamentary and converter) with alumina reservoirs are examples. Both experiments were similar, yet with cesium present, little volatilization of the MoO_3 occurred, whereas with MoO_3 alone, almost all the MoO_3 volatilized. Yet very little is known about MoO_3-Cs compounds, although some have been postulated. Therefore, the results of these experiments cannot be explained at this time.

The experimental work reported indicates that MoO_3 would provide oxygen to an emitter; however, problems such as the compatibility with cesium mentioned above complicate the use of this material considerably. The filamentary diode with MoO_3 yielded oxygen pressures which correspond to that expected for solid MoO_3 decomposing at the envelope temperature 600°C. However, this is also the pressure which should be observed when gaseous MoO_3 decomposes at the emitter; thus one cannot specify with certainty the source of oxygen in this experiment. The other experiments all suffered from some reaction between MoO_3 and other materials, either parts of the reservoir or cesium. The filamentary diode filled with cesium and

MoO_3 formed a volatile cesium oxide because the oxygen effect was observed at a low additive temperature. However, the fixed-spacing diode presumably did not act in the same manner. Evidently, a reaction with cesium produced one or more nonvolatile oxide reaction products.

REFERENCES FOR CHAPTER V

1. D. H. Killefer and A. Linz, Molybdenum Compounds, p. 36, Interscience Publ., (1952).

2. J. Feiser, Metall. U. Erz. 28, 297 (1931).

3. P. E. Blackburn, M. Hoch, and H. L. Johnston, J. Phys. Chem. 62 [7], 769 (1958).

4. Von R. Horbe, O. Knacke, and K. E. Prescher, Metall. J. Erz 14, 232 (1961).

5. J. Berkowitz, M. G. Inghram, and W. A. Chupka, J. Chem. Phys. 26 [4], 842 (1957).

6. E. A. Gulbransen, K. F. Andrew, and F. A. Brassart, J. Electrochem. Soc. 110, 242 (1963).

7. G. B. Barbi, J. Phys. Chem. 68, 1025 (1964).

8. Rapp, Trans. Metal. Soc. of AIME 227, 371 (1963).

9. W. A. Chupka, J. Chem. Phys. 26, 842 (1957).

10. A. N. Selikman, N. N. Gorowitsch, and T. J. Prosenkowa, A. anorg. Chem., USSR, 1, 632 (1956).

CHAPTER VI

ELECTROPOSITIVE ADDITIVES

F. Fraim, D. Lieb and E. Gyftopoulos

The work function of a metal surface is reduced when a fraction of the surface area is covered by an adsorbed monolayer of a more electropositive metal. This suggests that it may be possible to control the values of the electrode work functions of a diode converter by means of an electropositive vapor other than cesium, while the latter is being used for thermionic ion emission. Such diodes are usually called cesium diodes with electropositive vapors.

Under low-pressure conditions of operation, namely, when collisions in the interelectrode space are negligible, the performance of diodes with electropositive additives is ideal. However, for this performance, to be advantageous over that achieved by cesium-only diodes, the following conditions must be satisfied: (1) For a given emitter work function, the additive pressure must be small. (2) The emitter work function must be such that the low cesium pressure required for ideal performance is sufficient to yield the necessary positive ions for space-charge neutralization. (3) The value of the collector work function with the additive must be about 1.5 eV.

In the light of these conditions, consider the suitable electropositive additives. First, there are the monovalent electropositives, such as potassium, etc. These are not at all beneficial because they are less electropositive and have a smaller radius than cesium. Second, there are the bivalent electropositives, such as barium, calcium, etc.

These are less electropositive than cesium but, because they form a double bond on refractory metal surfaces, they are more effective adsorbates. A simple review of melting points and vapor pressure data on these elements indicates that they could easily satisfy requirements (1) and (2) above. Experiments have been performed with barium.[1] A major difficulty, however, arises with regard to requirement (3). For a specific illustration, consider barium as an additive, since the other bivalent elements have comparable or less desirable features. The required barium reservoir temperature for attainment of the desired emitter work function is about 1100°K. To avoid condensation of barium on the collector, the collector temperature must be slightly higher than that of the barium reservoir. At this value, the bariated work function is about 2.1 eV, which is very high for most practical purposes. Thus the performance of the diode with barium additive is not so high as one might expect because of the reasonably low emitter work function, the space charge neutralization, and the lack of collisions. On the basis of the melting points, the electronegativities, and the bare work functions of the other bivalent elements, one would expect even worse results when they are used as electropositive additives in diodes. It appears that pure bivalent electropositives in conjunction with pure refractory electrode surfaces are not beneficial. Similar comments can be made about trivalent electropositives. However, since these electropositives have not been previously studied with respect to their thermionic properties, it was felt that a preliminary study of a trivalent element might be worthwhile.

For this study ytterbium was selected as having the most favorable combination of vapor pressure (0.1 torr at 900°K) and work function

(2.8 eV). An experiment was performed using ytterbium in a fixed-spacing planar converter for the purpose of investigating its effects on the converter output in the unignited and ignited regions.

Because little was known of the outgassing characteristics of ytterbium (that is, the amount of dissolved gases the metal would release on being heated), the sample was outgassed separately in an initial experiment. It was placed in a copper tube which was connected to a sputter ion vacuum pump; then the temperature of the copper was slowly raised while the vacuum pressure was monitored to determine the amount of outgassing.

Only water vapor, which appeared at about 400°K, was present in the sample. The pressure then slowly decreased until, after 52 hours, the pressure was stable at 10^{-7} torr. At temperatures above about 700°K, an increase in pressure to a new stable value was noted. This was due to the vaporization of the Yb. At 800°K the vapor pressure is about 10^{-3} torr (see Ref. 2), but the pressure in the outgassing test at this temperature was only 10^{-6} torr. The cold walls present between the Yb and the vacuum pump condensed most of the Yb before it reached the pump, causing the low pressure. The fact that Yb had vaporized at 800°K (which was the highest temperature at which the Yb was held) was evidenced by the deposits of Yb found on the inner wall of the copper tube when it was examined at the end of the experiment.

After preliminary testing of the Yb sample was finished, it was transferred to the test converter. The diode (Figure VI-1) has a rhenium emitter and sleeve and a niobium body. The face of the collector is a thin molybdenum layer. The diode is equipped with two reservoirs made of copper tubing. The Cs reservoir connection

terminates in an orifice 10 mils in diameter, which prevents significant Yb distillation into the colder Cs reservoir at all but the highest Yb pressures (above 1 torr of Yb pressure the distillation would become significant). The converter was outgassed for 130 hours, with 12 hours of this time at the conditions T_E = 1900° K, T_C = 900° K, T_A = 620° K, T_{Cs} = 470° K. For the remainder of the time the emitter was held at about 1100° K with the collector and additive and cesium reservoirs at the above conditions.

After a preliminary Cs-only test to establish the validity of the diode structure, Yb vapor was driven into the interelectrode space by raising the additive reservoir temperature. At first no effect was observed, but as the collector temperature was increased from its initial value (920° K) to 1000° K, an increase in current appeared. However, this increase in current was not stable, and after 100 minutes the current density dropped to its initial value (Figure VI-2). These curves show that some Yb reached the collector during heating of the reservoir, but that its effect was small until the increased collector temperature released additional vapor into the interelectrode space. When the Yb condensed on the collector was exhausted, the curves dropped back to lower values. Stable equilibrium values for the J-V characteristics could not be obtained in this test. The results indicate, however, that Yb does affect the emitted current.

Figure VI-3 shows two J-V characteristics obtained under equilibrium conditions. An interesting feature of these curves is the double ignition observed at relatively large applied voltages. The higher-voltage ignition appears sensitive to the Yb pressure, while the lower one is not (compare Curves A and B). When the Yb reservoir

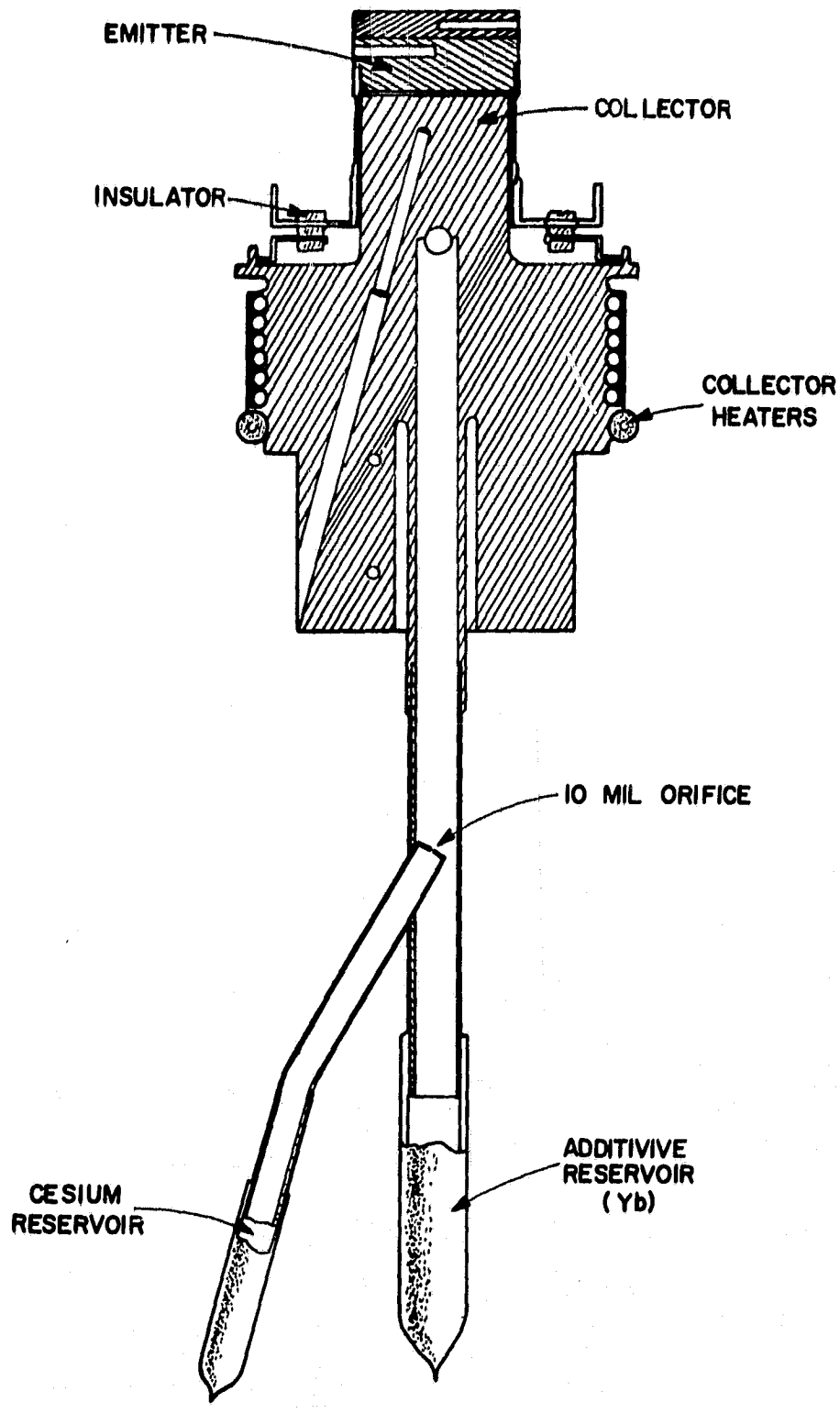


Figure VI-1. Schematic of Test Vehicle for Electropositive Additives.

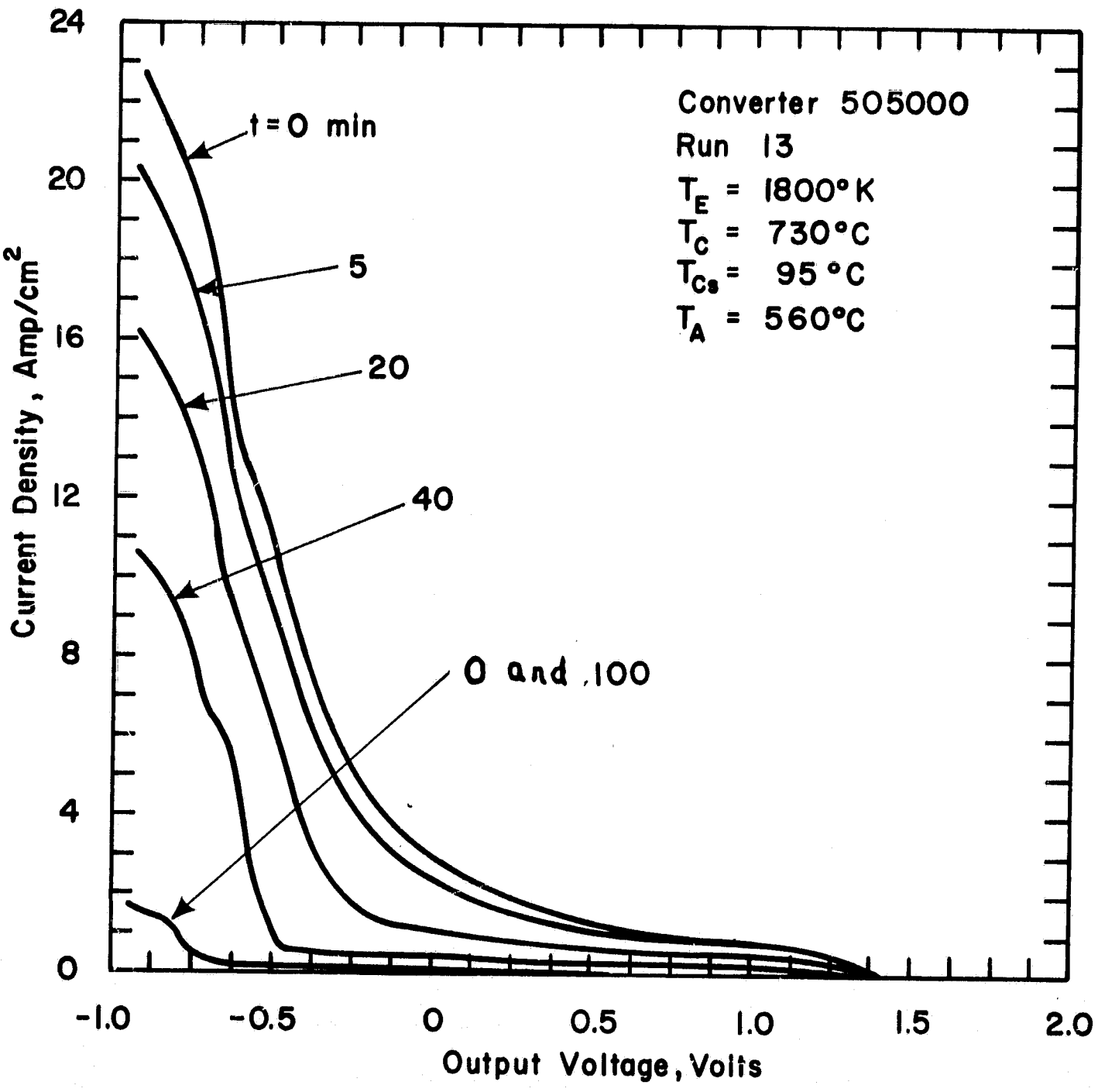


Figure VI-2. J-V Characteristics Showing the Transient Effects Following a Change in Collector Temperature.

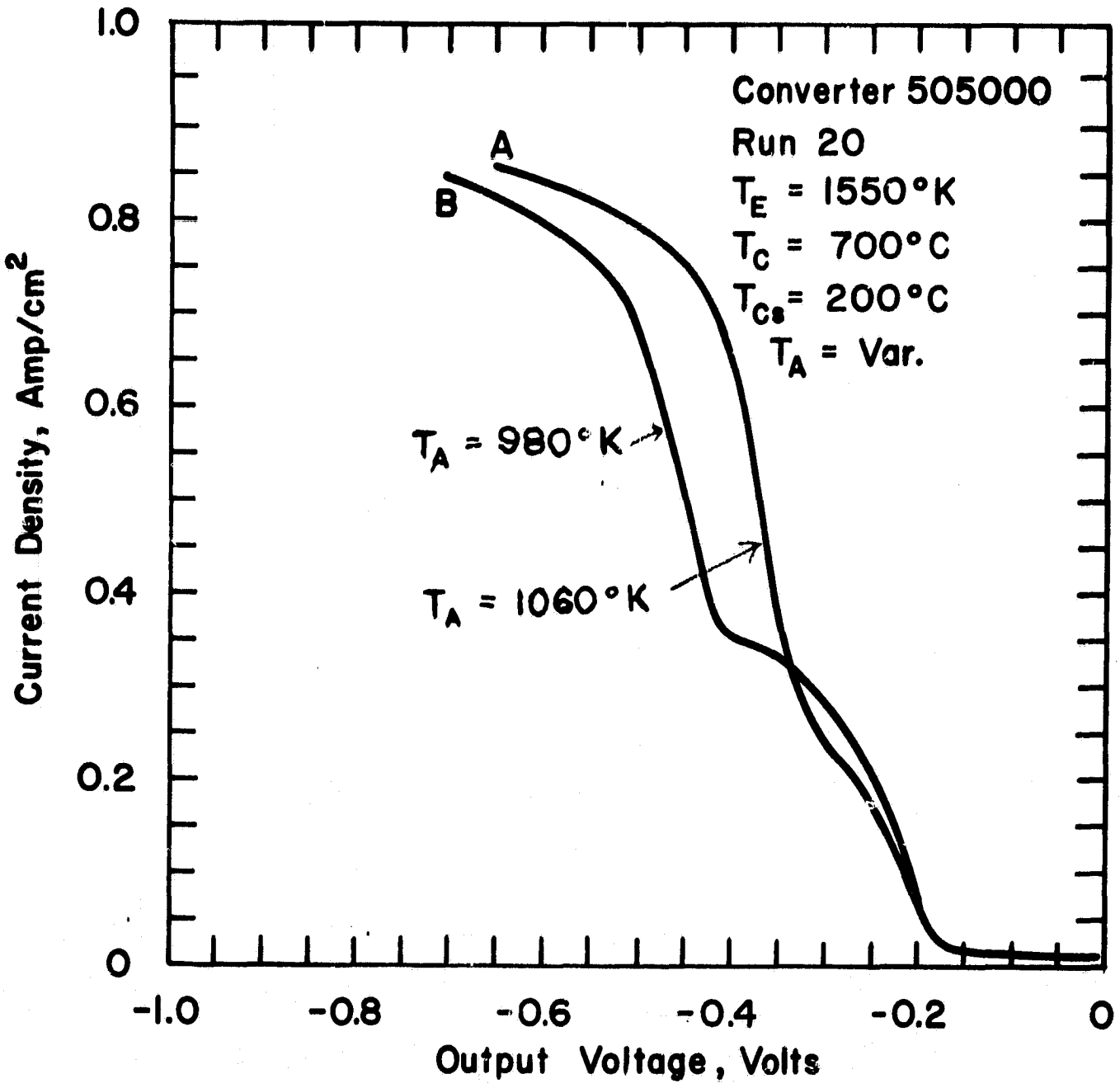


Figure VI-3. Comparison of J-V Curves at Different Yb Reservoir Temperatures.

temperature was lowered to about 500°K the second ignition disappeared.

The high reservoir temperature (1000 to 1100°K) required for the Yb (compared with the expected value of 800°K), together with the transient effect described above and shown in Figure VI-2, implies that there is a cold spot in the diode or reservoir tubing. Such a spot was found at the orifice of the Cs reservoir, and an additional heater was provided for this area. Unfortunately, an emitter-to-collector short developed in the diode, and testing was terminated.

The diode was then cut apart to determine the nature of the short and to determine whether any reactions with Yb had taken place. A grayish powdery metallic deposit was found on the collector surface. The shorting appeared to have taken place at several small projections having a brassy appearance. Spectrographic analysis at the deposit showed a Yb-Cu mixture with a slight predominance of the Cu. It was probably this Cu which caused the shorting. When the reservoir connection was opened a large plug of Yb was indeed found at the Cs reservoir orifice. In addition, brassy-looking shavings were found deposited on the Yb reservoir copper tubing. Analysis of the shavings again showed a Yb-Cu mixture, but with Yb predominating. Yb probably formed a eutectic at the high reservoir temperatures (1100°K).

These experiments show that Yb introduced into a thermionic converter will increase the apparent saturation currents observed at a particular Cs reservoir temperature. Difficulties were experienced because of reactions with the copper reservoir, and any further experiments should use another material for the reservoir. The Cu observed

on the collector is unexplained but could be the result of transport from the reservoir. No other unusual chemical or physical attack was observed in the converter. In view of the doubtful performance improvement to be expected and because of the difficulties with the copper reservoir, this study was not pursued further.

REFERENCES FOR CHAPTER VI

1. J. Psaroutharis, "Thermionic Energy Converter with Barium and Cesium Vapors," Thermionic Conversion Specialist Conference, Cleveland, Ohio, October 1964.

2. Vapor Pressure Curves of the Elements (Chart), Richard E. Honig, RCA Laboratories, Princeton, N.J., September 1962.

APPENDIX

CONVERTER PERFORMANCE WITH AND WITHOUT ADDITIVES

(See Section IV-E of Text)

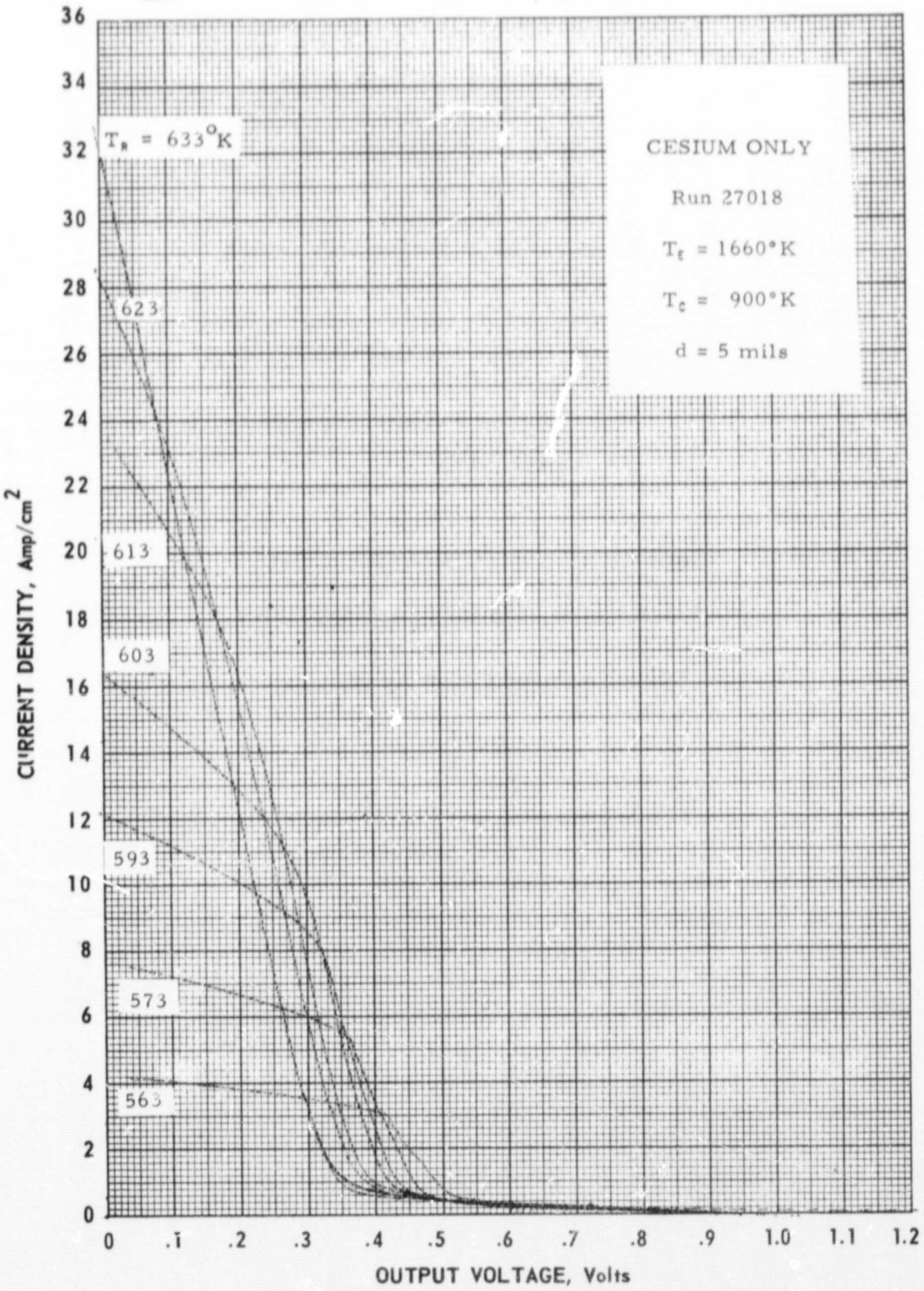


Figure A-1. Family of Volt-Ampere Characteristics at T_E = 1660°K and d = 5 mils for Cesium Only.

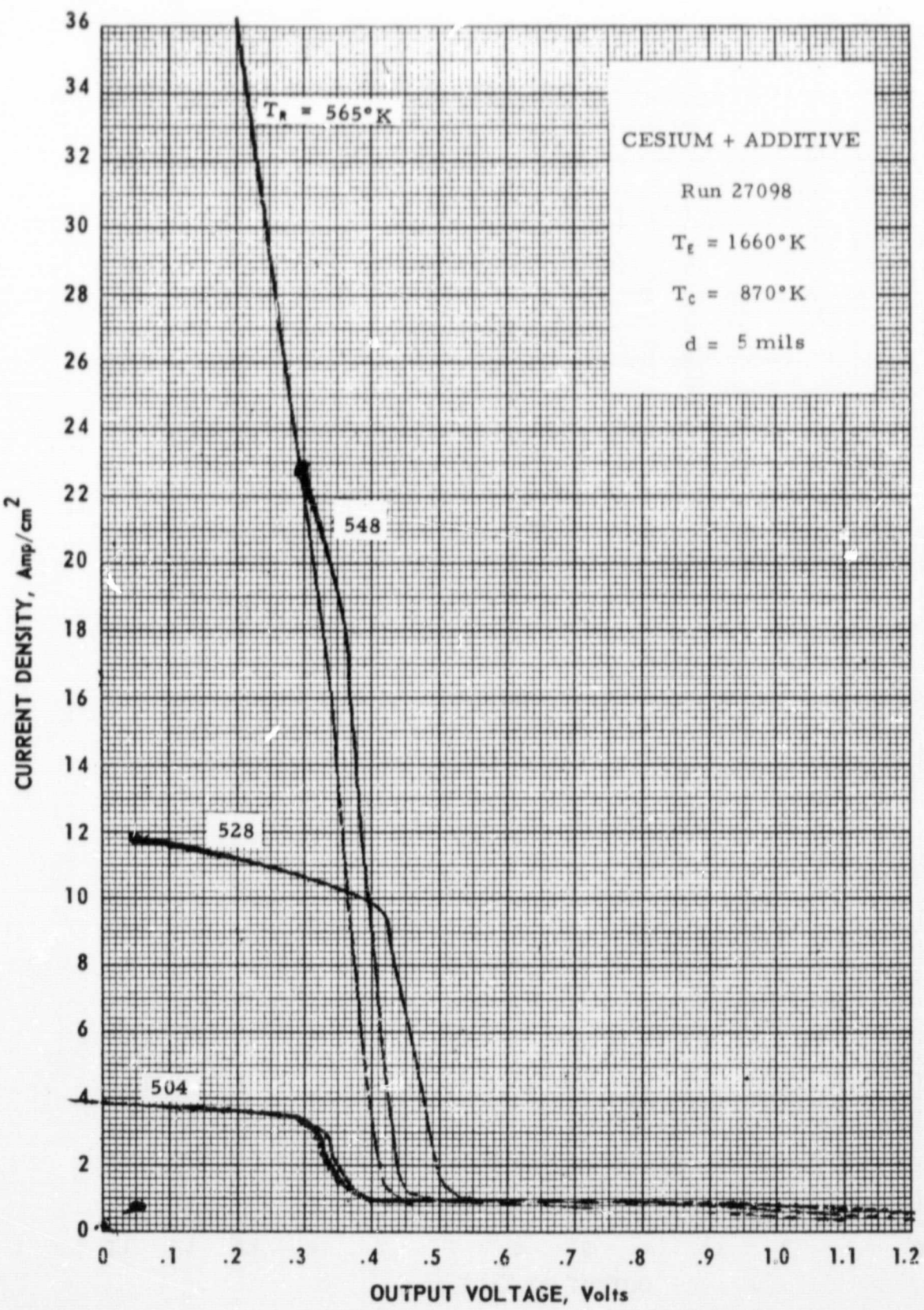


Figure A-2. Family of Volt-Ampere Characteristics at T_E = 1660°K and d = 5 mils for Cesium and Additive.

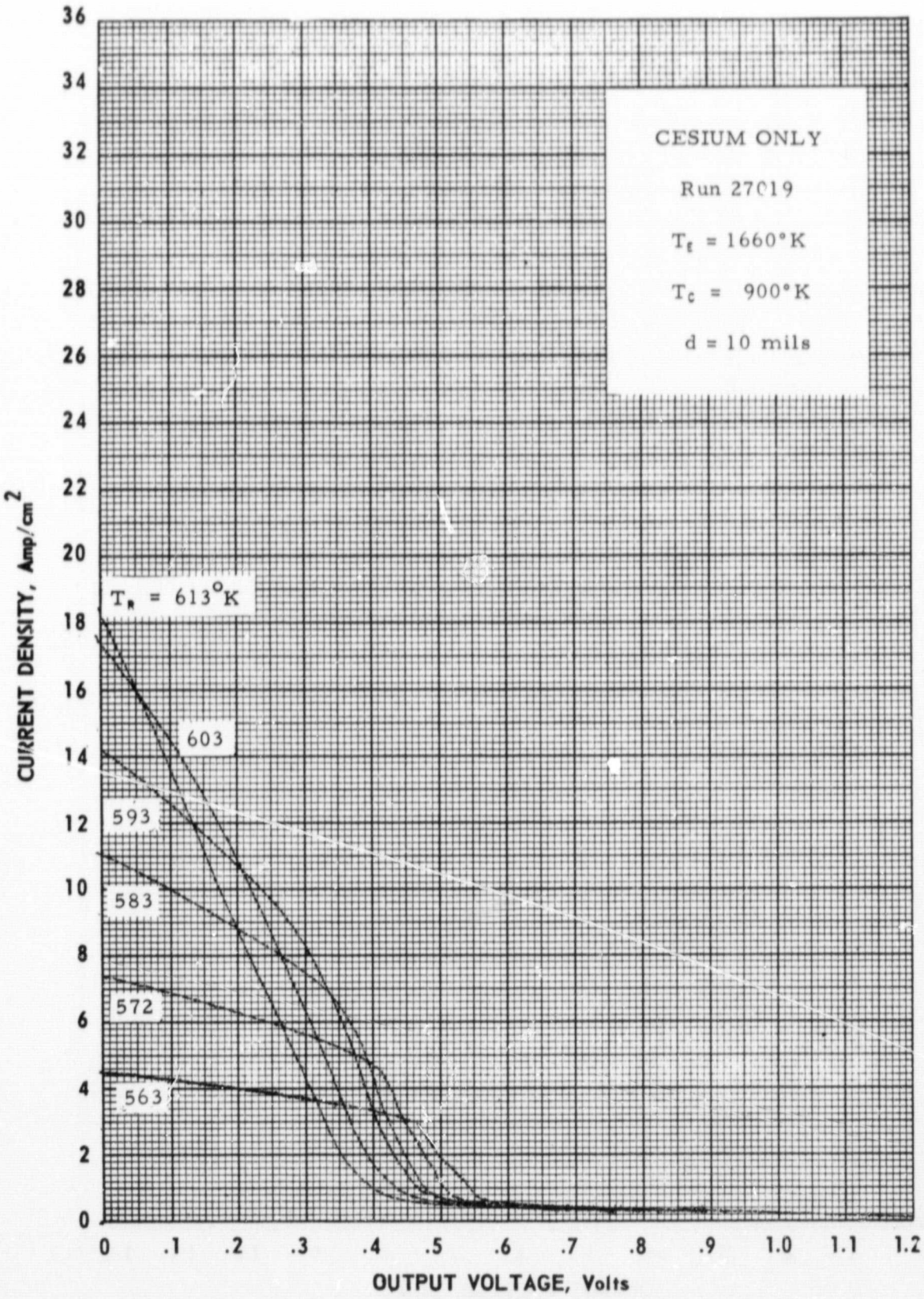


Figure A-3. Family of Volt-Ampere Characteristics at T_E = 1660°K and d = 10 mils for Cesium Only.

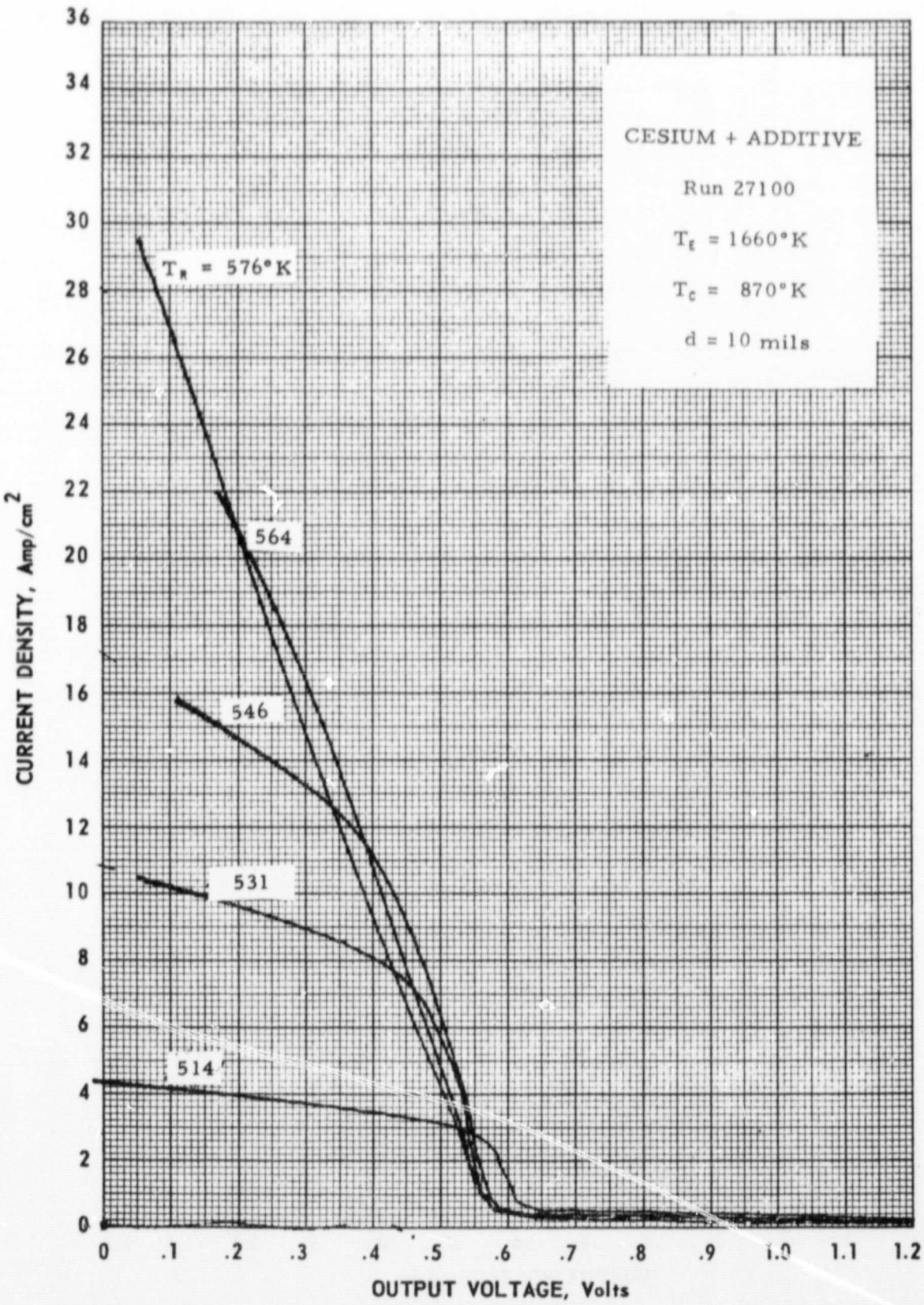


Figure A-4. Family of Volt-Ampere Characteristics at T_E = 1660°K and d = 10 mils for Cesium and Additive.

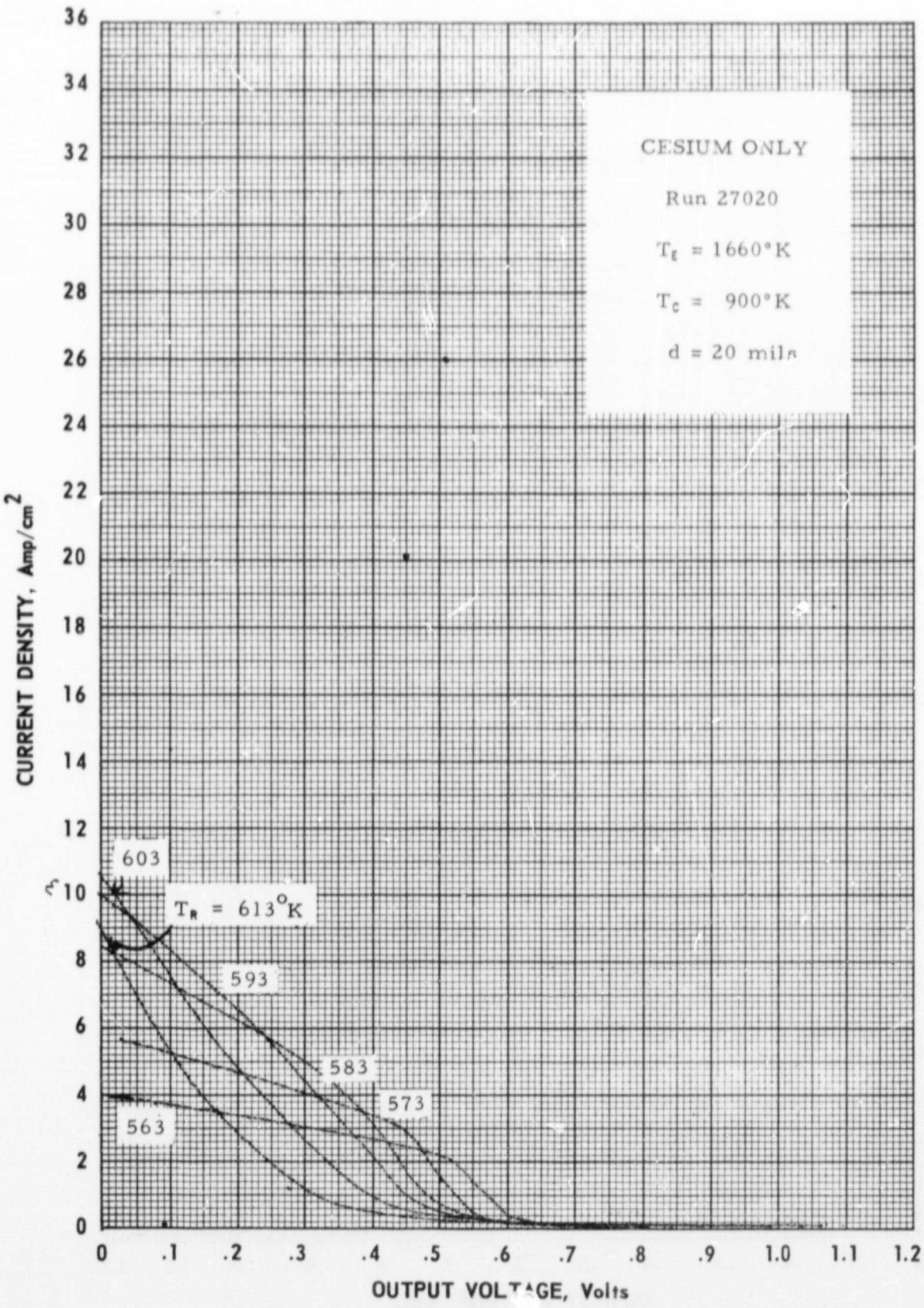


Figure A-5. Family of Volt-Ampere Characteristics at T_E = 1660°K and d = 20 mils for Cesium Only.

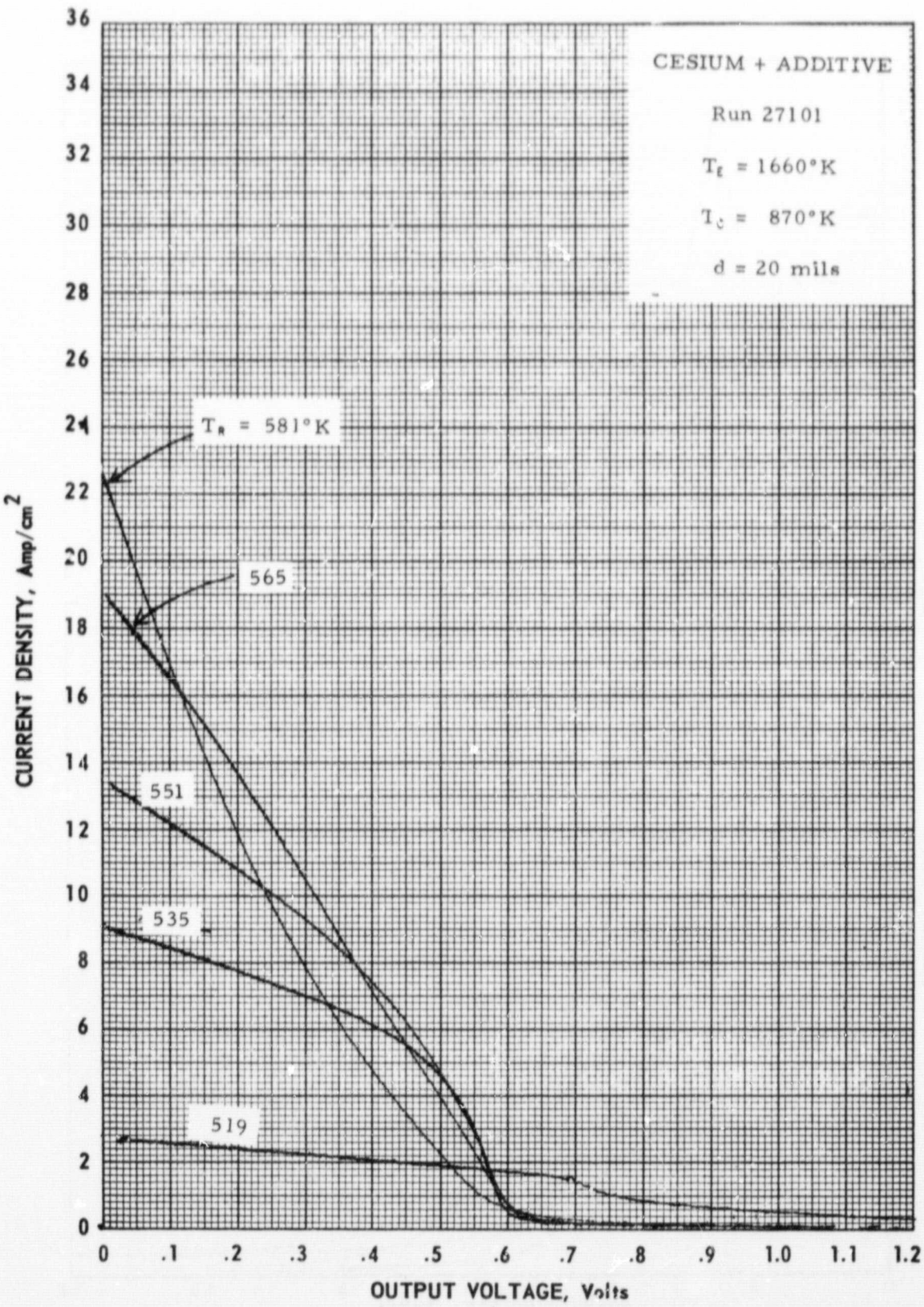


Figure A-6. Family of Volt-Ampere Characteristics at T_E = 1660°K and d = 20 mils for Cesium and Additive.

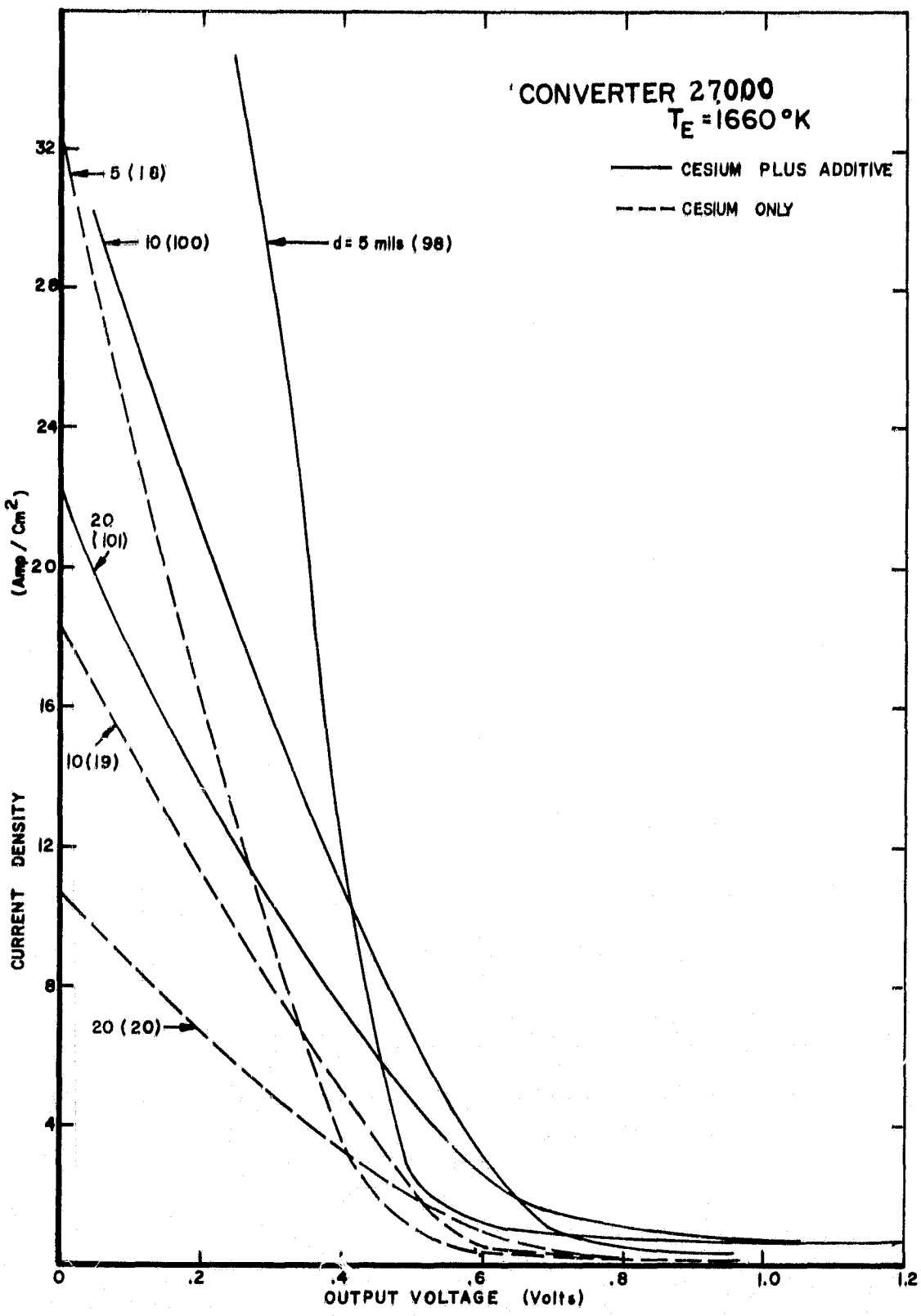


Figure A-7. Comparison of Cesium Envelopes With and Without Additive at T_E = 1660°K.

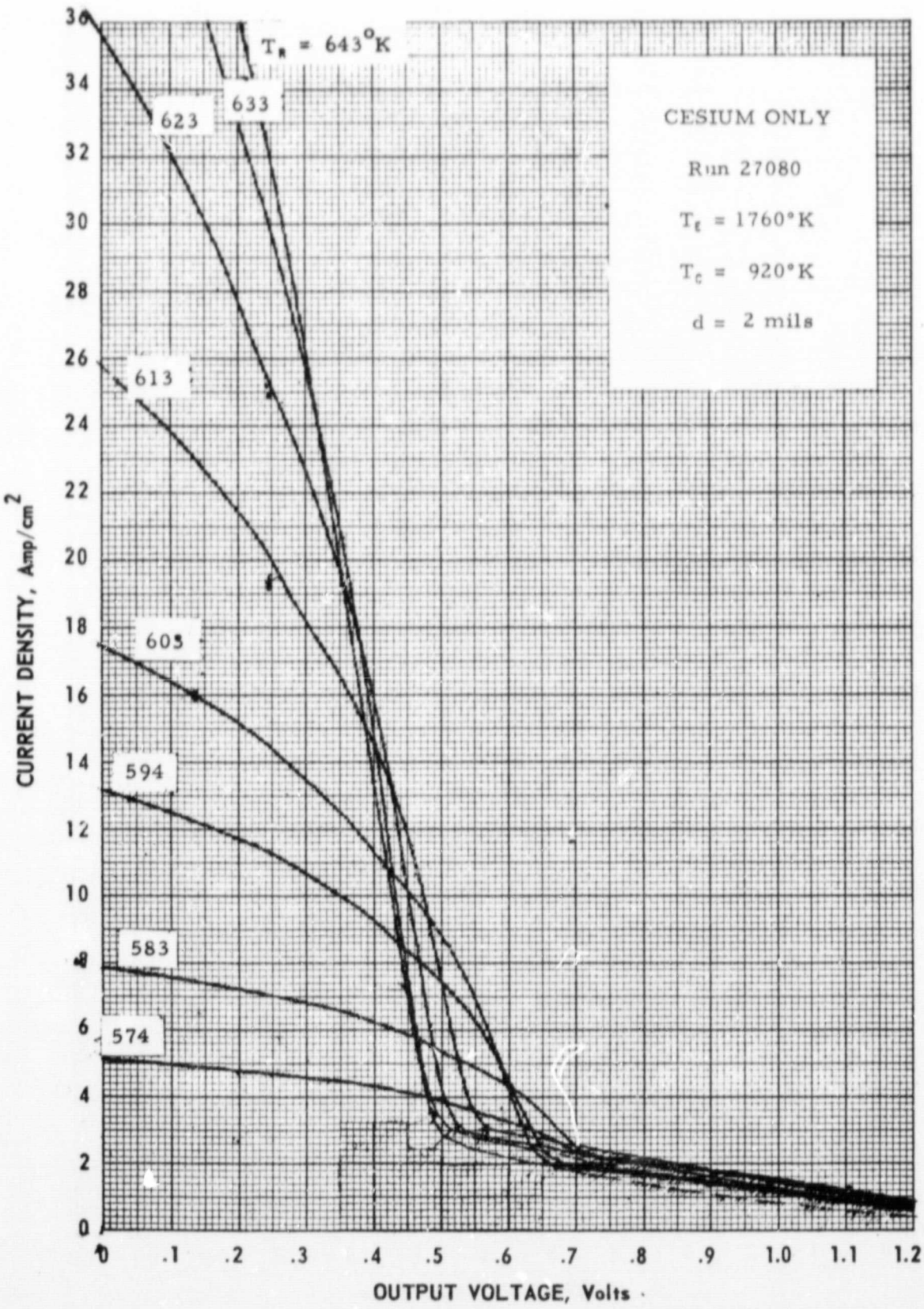


Figure A-8. Family of Volt-Ampere Characteristics at T_E = 1760°K and d = 2 mils for Cesium Only.

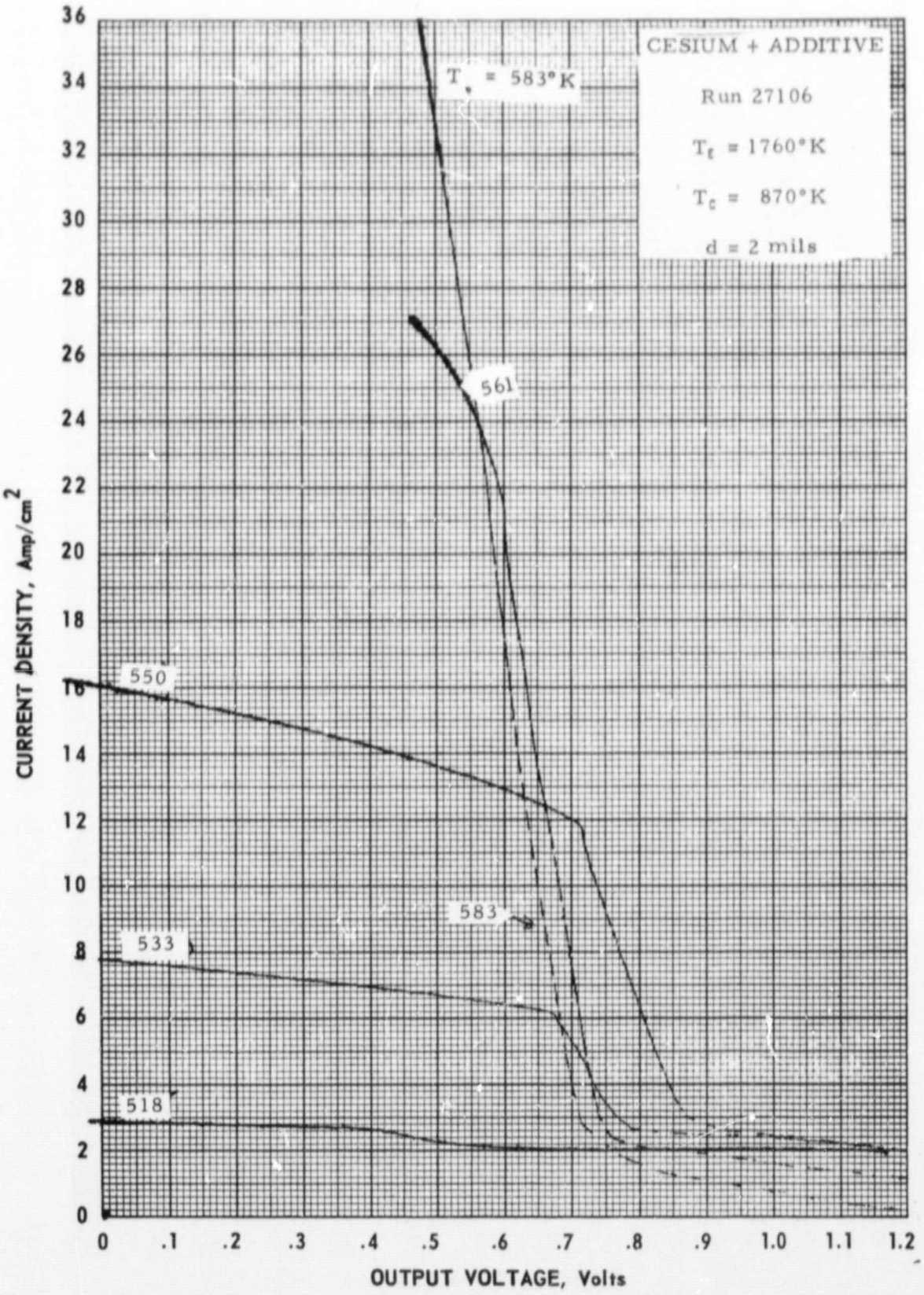


Figure A-9. Family of Volt-Ampere Characteristics at T_E = 1760°K and d = 2 mils for Cesium and Additive.

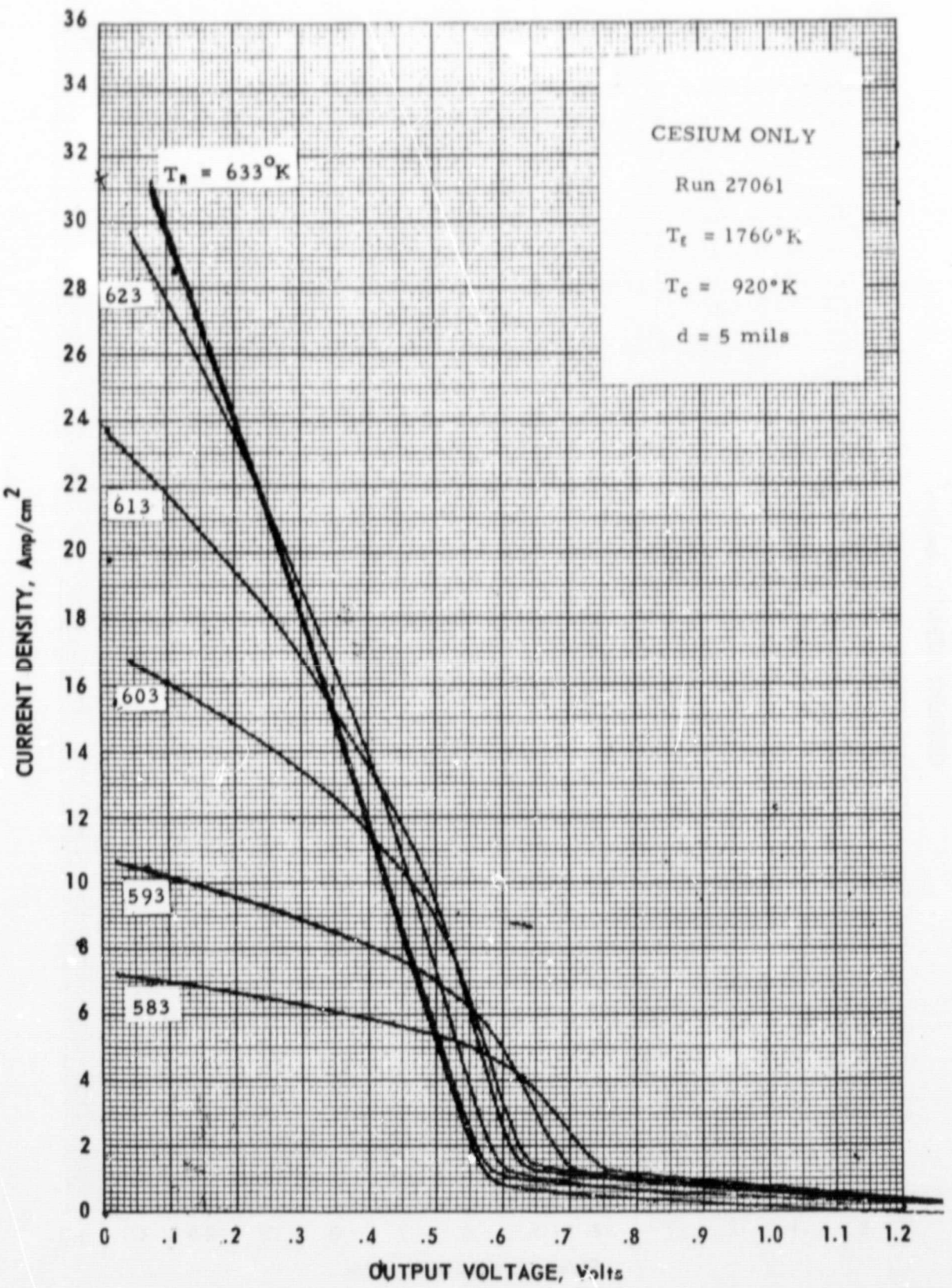


Figure A-10. Family of Volt-Ampere Characteristics at T_E = 1760°K and d = 5 mils for Cesium Only.

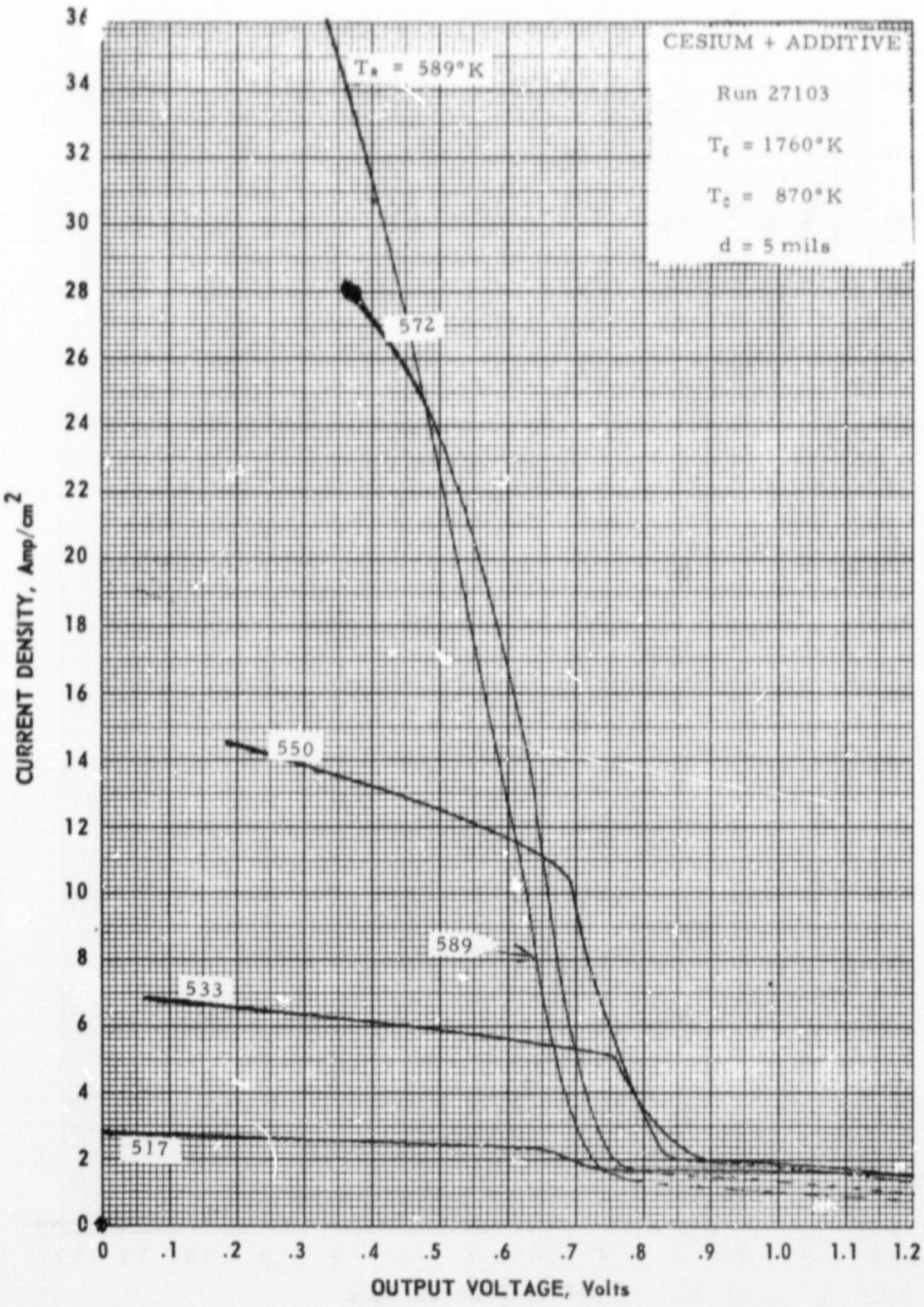


Figure A-11. Family of Volt-Ampere Characteristics at T_ε = 1760°K and d = 5 mils for Cesium and Additive.

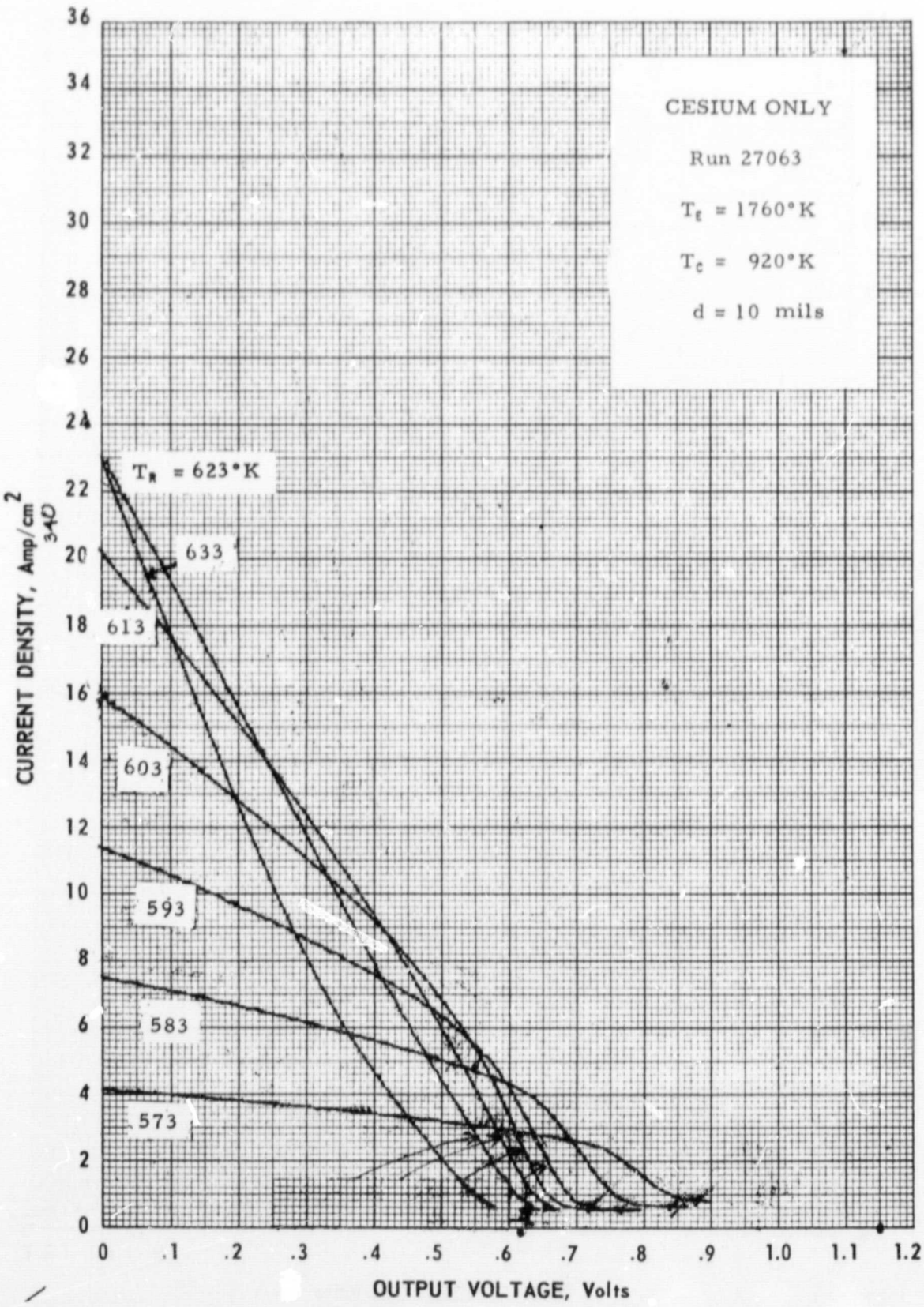


Figure A-12. Family of Volt-Ampere Characteristics at T_E = 1760°K and d = 10 mils for Cesium Only.

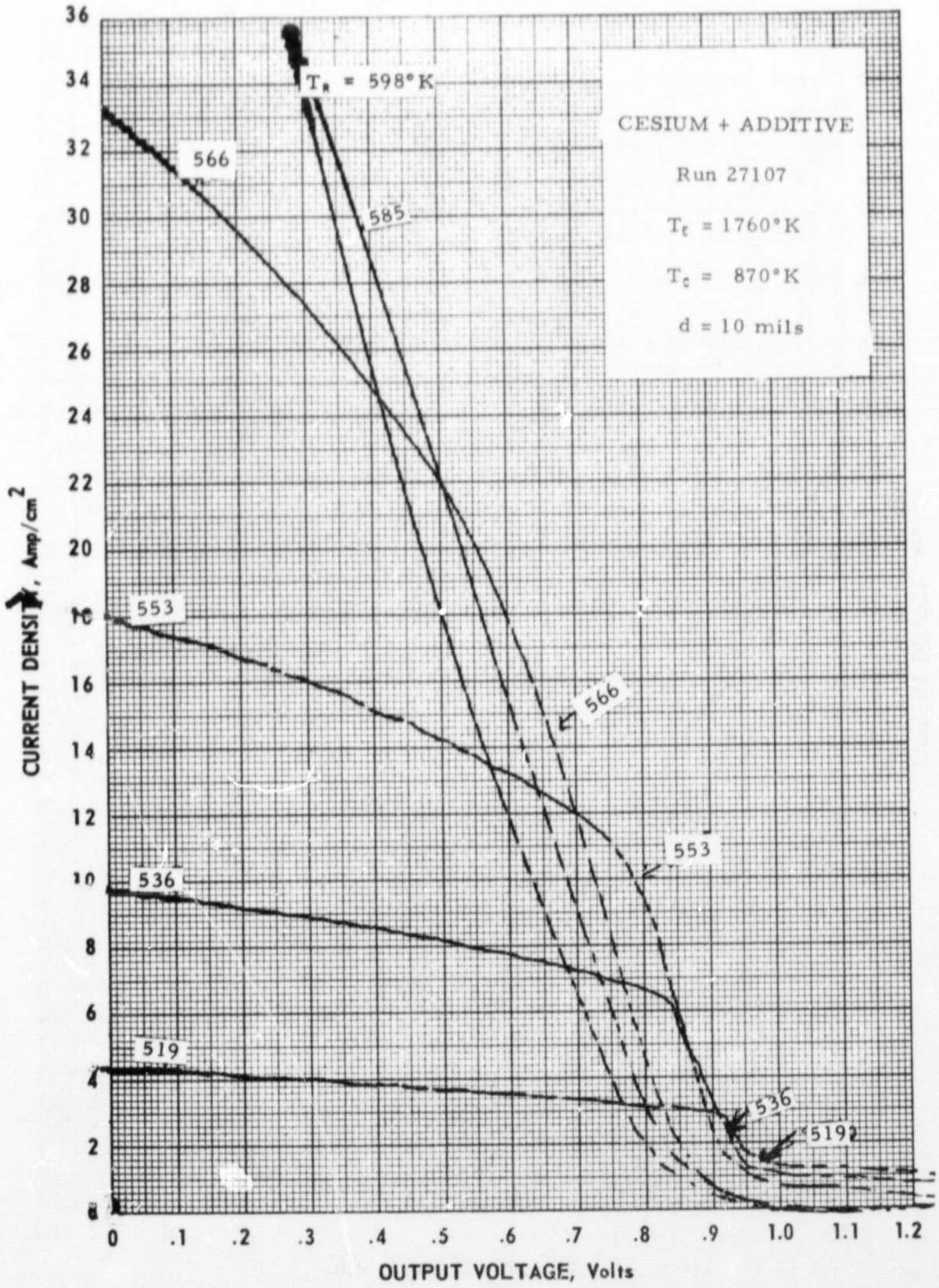


Figure A-13. Family of Volt-Ampere Characteristics at T_E = 1760°K and d = 10 mils for Cesium and Additive.

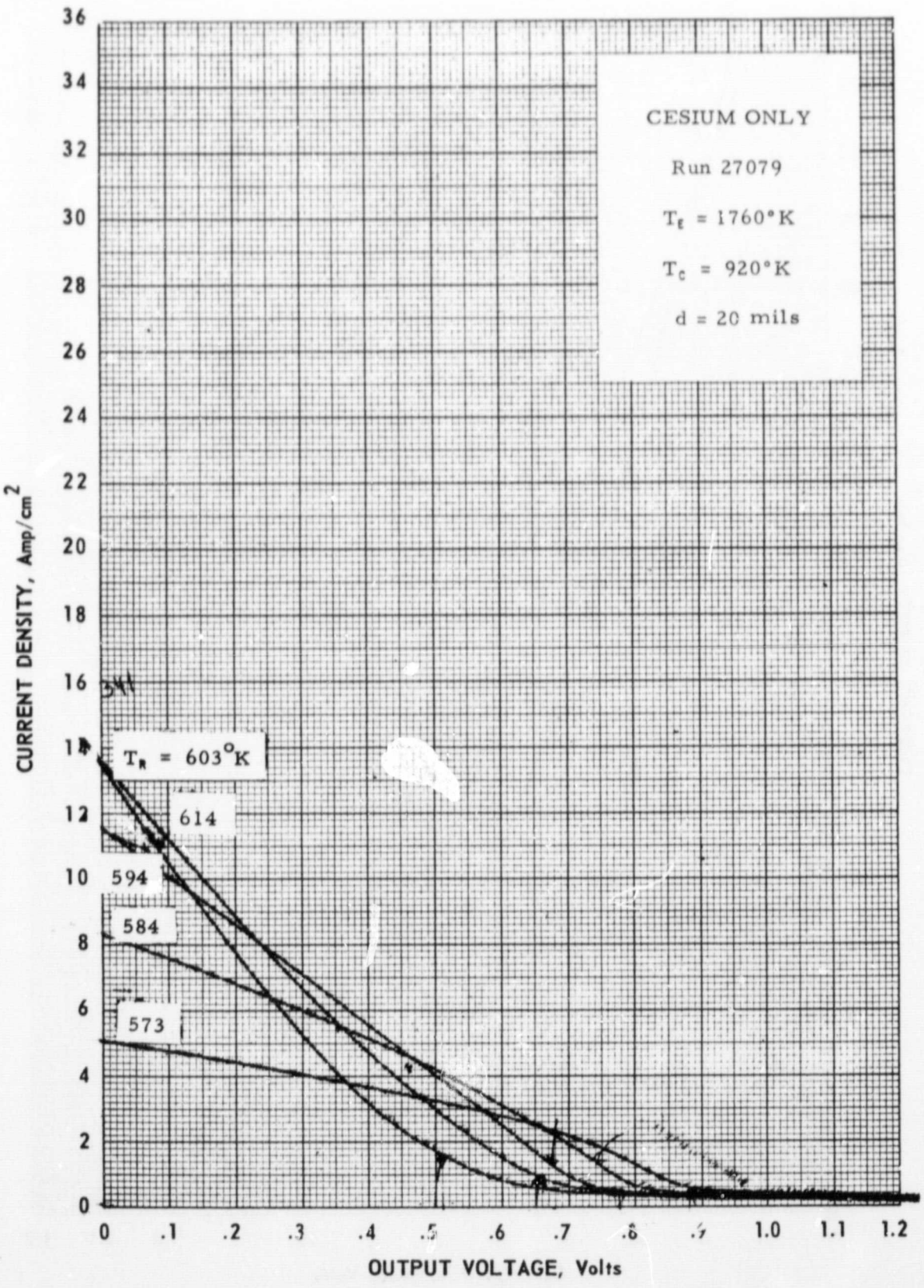


Figure A-14. Family of Volt-Ampere Characteristics at T_E = 1760°K and d = 20 mils for Cesium Only.

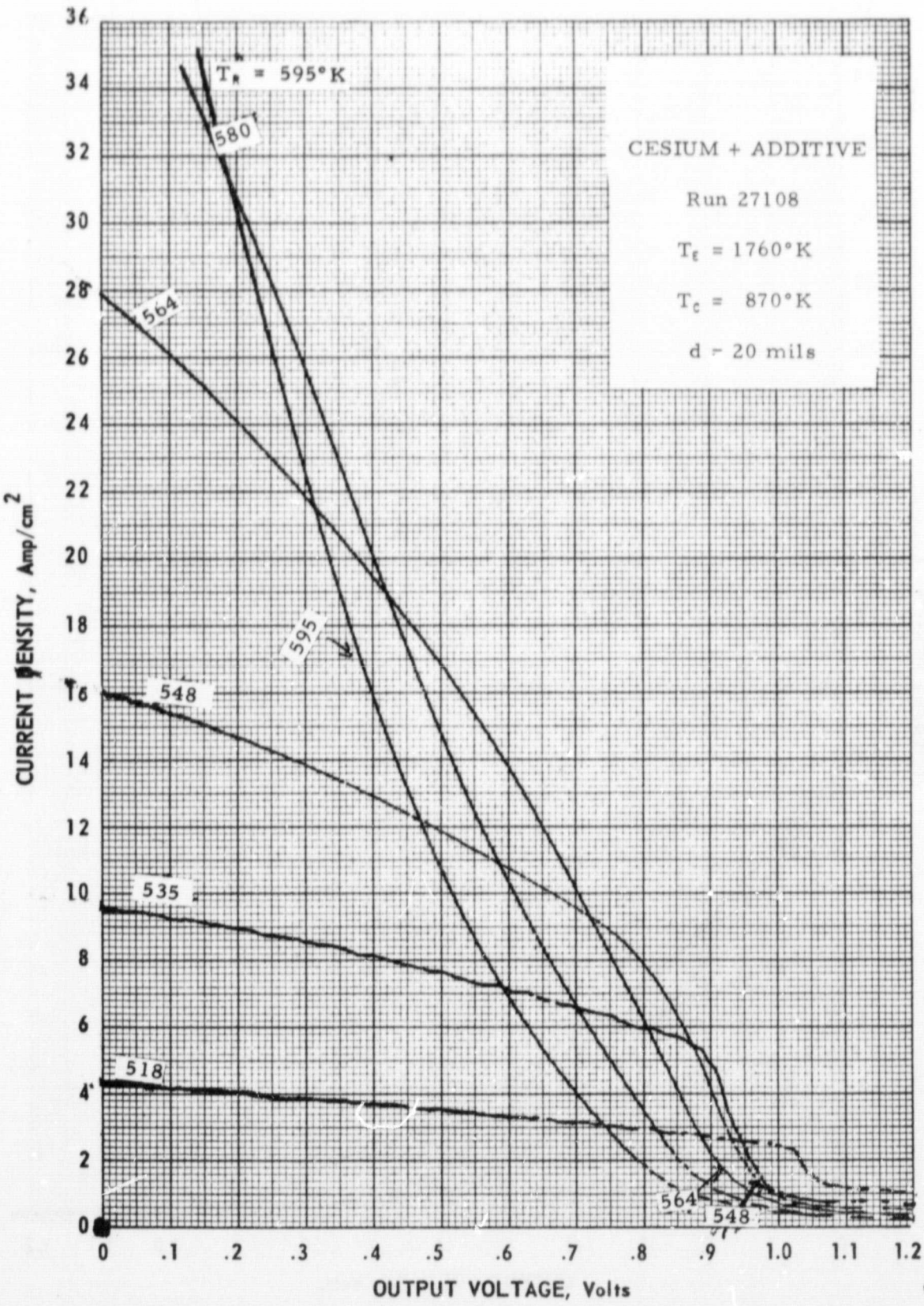


Figure A-15. Family of Volt-Ampere Characteristics at T_E = 1760°K and d = 20 mils for Cesium and Additive.

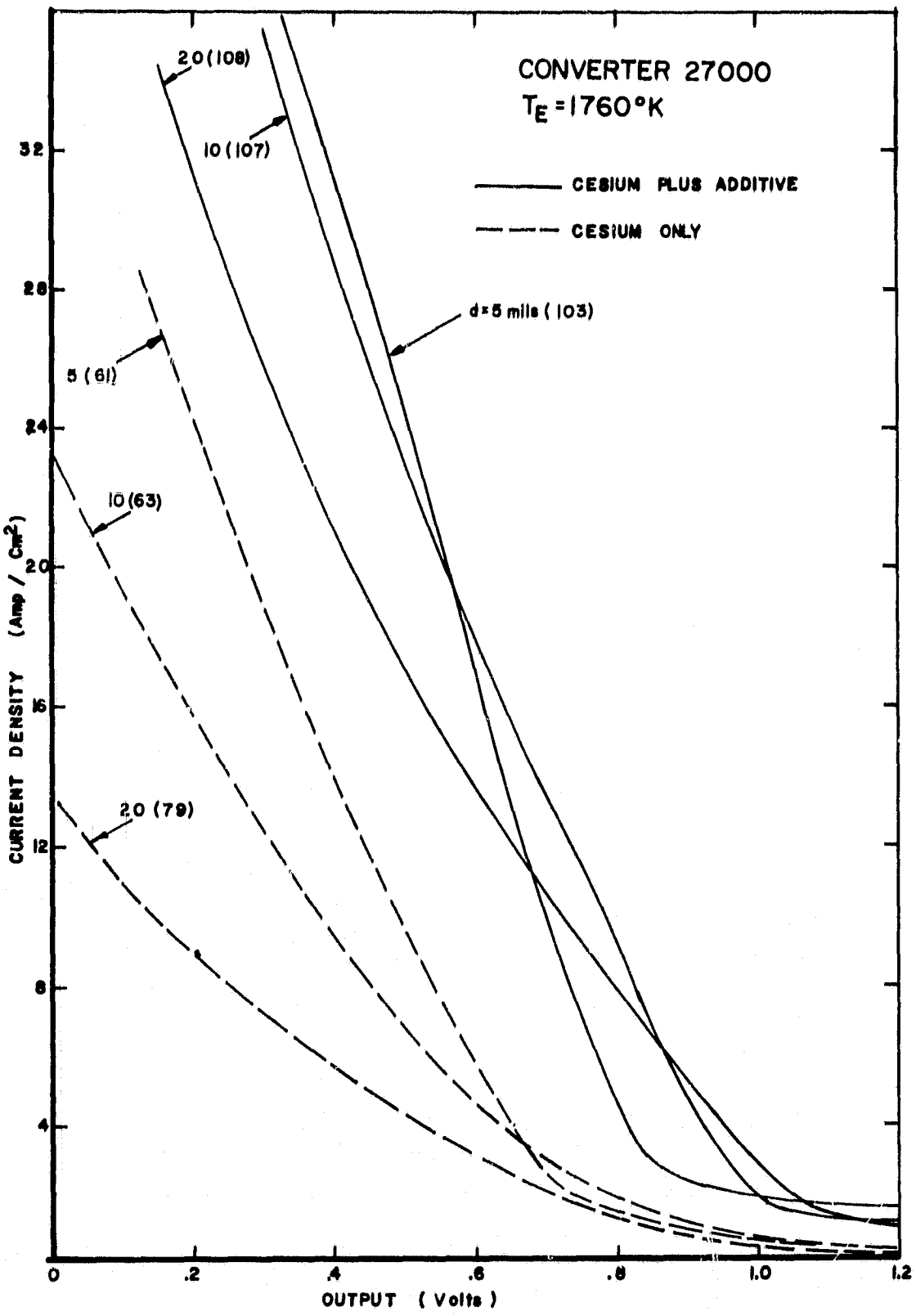


Figure A-16. Comparison of Cesium Envelopes With and Without Additive at T_E = 1760°K.